CALIFORNIA INSTITUTE OF TECHNOLOGY

EARTHQUAKE ENGINEERING RESEARCH LABORATORY

STOCHASTIC SYSTEM DESIGN AND APPLICATIONS TO STOCHASTICALLY ROBUST STRUCTURAL CONTROL

BY

ALEXANDROS TAFLANIDIS

REPORT NO. EERL 2007-05

PASADENA, CALIFORNIA

SEPTEMBER 2007

A REPORT ON RESEARCH SUPPORTED BY THE CALIFORNIA INSTITUTE OF TECHNOLOGY UNDER THE SUPERVISION OF JAMES L. BECK.

STOCHASTIC SYSTEM DESIGN AND APPLICATIONS TO STOCHASTICALLY ROBUST STRUCTURAL CONTROL

Thesis by

Alexandros Taflanidis

In Partial Fulfillment of the Requirements for the

degree of

Doctor of Philosophy

CALIFORNIA INSTITUTE OF TECHNOLOGY

Pasadena, California

2007

(Defended September 24, 2007)

Acknowledgements

I would like to firstly thank my advisor, James Beck, for his tireless mentoring throughout my stay at Caltech on both my research and my work as a teaching assistant. He has taught me to be a thorough scientist and a good instructor. I am extremely appreciative of his unwavering support and the amount of freedom he granted me for pursuing my own ideas. I hope we can continue our collaboration for many years to come.

Special thanks go to my good friend Jeff Scruggs for sharing his wisdom with me so patiently in my first two years at Caltech. His guidance has helped me tremendously in getting a better appreciation of the special needs of the structural control field. Similarly many thanks to my good friend and colleague Joseph (Sai-Hung) Cheung for his help on understanding stochastic simulation techniques and the time he always willingly offered for our research-related discussions.

Special gratitude goes to my ex-professors and advisors on my bachelor and Master Thesis, Demos Angelides and Georgios Manos, for their mentoring during those years and their support in my decision to pursue a Ph.D at Caltech. Additional thanks go to Professor Angelides for our close collaboration over the last few years in various research projects.

I would also like to thank the rest of my Ph.D committee members, Professor Joel Burdick, Professor Wilfred Iwan, and Professor Swaminathan Krishnan, for their insightful discussion and comments.

I have made a lot of good friends at Caltech and I would like to thank all of them for their support. Special thanks go to the famous lunch group: Nick Hudson, Michael Wolf, Moh El Naggar, Joseph Klamo, Kristo Kiecherbaum, Tim Chung, Sam Taira, Judith Mitrani, and of course to Ernie. You guys have made the long hours of graduate school pass quickly. I would also like to thank the SOPS soccer team for entrusting me with the captain position over the last couple of years and sharing with me many happy moments on the soccer field. Special thanks go to Sarah for sharing the last couple of years with me and providing support whenever I needed it.

Last but not least I would like to thank my family, especially my mother, for their unconditional love and support throughout the years.

This research was made possible, in part, through the fellowships provided by Harold Helwing, George Housner at Caltech, and the Greek Konstantinos Katseas fellowship. I am extremely grateful and honored to have received this funding.

Abstract

The knowledge about a planned system in engineering design applications is never complete. Often, a probabilistic quantification of the uncertainty arising from this missing information is warranted in order to efficiently incorporate our partial knowledge about the system and its environment into their respective models. In this framework, the design objective is typically related to the expected value of a system performance measure, such as reliability or expected life-cycle cost. This system design process is called *stochastic system design* and the associated design optimization problem *stochastic optimization*. In this thesis general stochastic system design problems are discussed. Application of this design approach to the specific field of structural control is considered for developing a robust-to-uncertainties nonlinear controller synthesis methodology.

Initially problems that involve relatively simple models are discussed. Analytical approximations, motivated by the simplicity of the models adopted, are discussed for evaluating the system performance and efficiently performing the stochastic optimization. Special focus is given in this setting on the design of control laws for linear structural systems with probabilistic model uncertainty, under stationary stochastic excitation. The analysis then shifts to complex systems, involving nonlinear models with high-dimensional uncertainties. To address this complexity in the model description stochastic simulation is suggested for evaluating the performance objectives. This simulation-based approach addresses adequately all important characteristics of the system but makes the associated design optimization challenging. A novel algorithm, called Stochastic Subset Optimization (SSO), is developed for efficiently exploring the sensitivity of the objective function to the design variables and iteratively identifying a subset of the original design space that has

high plausibility of containing the optimal design variables. An efficient two-stage framework for the stochastic optimization is then discussed combining SSO with some other stochastic search algorithm. Topics related to the combination of the two different stages for overall enhanced efficiency of the optimization process are discussed.

Applications to general structural design problems as well as structural control problems are finally considered. The design objectives in these problems are the reliability of the system and the life-cycle cost. For the latter case, instead of approximating the damages from future earthquakes in terms of the reliability of the structure, as typically performed in past research efforts, an accurate methodology is presented for estimating this cost; this methodology uses the nonlinear response of the structure under a given excitation to estimate the damages in a detailed, component level.

Contents

List of Figures

List of Tables

CHAPTER 1

Introduction

1.1 Stochastic System Design

In engineering design, the knowledge about a planned system is never complete. First, it is not known in advance which design will lead to the best system performance in terms of a specified metric; it is therefore desirable to optimize the performance measure over the space of design variables that define the set of acceptable designs. Second, modeling uncertainty arises because no mathematical model can capture perfectly the behavior of a real system and its environment. In practice, the designer chooses a model that he or she feels will adequately represent the behavior of the built system as well as its future excitation; however, there is always uncertainty about which values of the model parameters will give the best representation of the constructed system and its environment, so this parameter uncertainty should be quantified. Furthermore, whatever model is chosen, there will always be an uncertain prediction error between the model and system responses. For an efficient engineering design, all these uncertainties, associated with future excitation events, as well as the modeling of the system, must be explicitly accounted for.

A probability logic approach provides a rational and consistent framework for quantifying all aforementioned uncertainties (Cox 1961; Jaynes 2003). In this approach, probability can be interpreted as a means of describing the incomplete, i.e., missing, information about the system in consideration. This is established by characterizing the relative plausibility of

different properties of the system by a probability model which is implicitly conditioned on available knowledge. The specific probability model chosen represents the expected information gain based on the knowledge we have about the system; this gain is quantified in terms of the absolute or relative information entropy (Shannon 1948; Papadimitriou et al. 2000). In this context, choosing a probability model with the largest entropy is equivalent to incorporating the largest possible uncertainty into the system description, subject to the available information. For example, subject to specifications of the first and second moments (or, equivalently, expected value and variance) for a continuous variable that is restricted within some range, the most appropriate, in the aforementioned context, probability model selection is a truncated Gaussian probability density function; if no specification is made of the moments of the variable, then the most appropriate selection is a uniform probability density function. This knowledge-based interpretation of probability leads to a logical consideration of all system uncertainties without requiring the introduction of the non-rigorous concept of "inherent randomness" and, ultimately, to a powerful framework for formulating the design problem and performing the required optimization. In this work, this design process is called *stochastic system design*.

Applications of similar design approaches considering uncertainties have been presented in many areas, including transportation engineering, e.g., Sakawa et al. (2002); chemical engineering, e.g., Acevedo and Pitsikopoulos (1988), Gupta and Maranas (2000); telecommunications, e.g., Laguna (1998); energy scheduling, e.g., Morton (1996); control design, e.g., Wang and Stengel (2002); and finances, e.g., Kouwenberg and Zenios (2001). The state-of-the-art review by Sahinidis (2004) provides details about the optimization methods that have been suggested for identifying the optimal design configuration in such design applications. Most of these methods take advantage of some special characteristics of the class of problems addressed. This feature often limits their applicability to other types of robust-to-uncertainties design problems.

It should be noted that even though the theoretical ideas for design considering modeling uncertainties were introduced many decades ago, the computational cost associated with this design methodology—because of the complex coupling between system modeling, stochastic analysis, and optimization—has reduced the range of applications considered. Often the formulation of stochastic design problems is restricted by the available computational resources and the ability to perform the associated design optimization. For complex systems this has often dictated (a) use of mathematical models that do not adequately consider all characteristics of the true system behavior, or (b) adaptation of approximate techniques for evaluating their performance in a probabilistic setting. Recent advances in software and hardware computer technology have contributed to overcoming many of these restrictions and the general concept of stochastic system design is rapidly spreading to new types of applications.

In the current study the focus is primarily on the design of structural and mechanical systems. For these systems, stochastic design problems are usually related to the expected life-cycle cost of a system, or to its reliability, quantified in terms of the "failure" probability, i.e., the probability given all available information that the system will exhibit unacceptable performance. Many variants of such problems have been posed, typically expressed in one of the following three forms: (a) optimization of the system reliability given deterministic constraints, e.g., May and Beck (1998), Au (2005); (b) optimization of the cost of the structure given reliability constraints, e.g., Enevoldsen and Sorensen (1994), Vietor (1997); or (c) optimization of the expected life-cycle cost of the structure, e.g., Ang and Lee (2001). Approaches have been suggested for transforming the latter problem to one of the former two. This is established by approximating the cost related to future damages to the structure in terms of its failure probability (see, for example, Kong and Frangopol (2003)). In this setting, Reliability-Based Design Optimization (RBDO), i.e., design considering reliability measures in the objective function or the design constraints, has emerged as one of the standard tools for robust and cost-effective design of engineering systems (Moses 1977; Enevoldsen and Sorensen 1994; Sorensen et al. 1994).

In RBDO a particular source of difficulty is the high computational cost associated with a single reliability analysis. Even though relatively efficient algorithms have been recently developed for calculation of failure probabilities for complex systems (Au and Beck 2001a; Au and Beck 2001b; Schueller et al. 2004), each evaluation still requires a substantial computational effort, particularly for dynamic reliability problems. To reduce this computational effort, many specialized approaches have been proposed for reliability-based optimizations. These approaches include, for example, use of some proxy for the failure probability (e.g., reliability index obtained through first-order or second-order analysis, as, for example, in Enevoldsen and Sorensen (1994)), and response surface approximations to the limit state function defining the model's response for each design choice (e.g., Gasser and Schueller (1997)). Such specialized approaches may work satisfactorily under certain conditions, but are not proved to converge to the solution of the original design problem. This is particularly true for optimization problems that involve the reliability of the system as the objective function, rather than as constraint as commonly adopted in RBDO, because the sensitivity of the objective function to some design variables can be highly complex and not accurately described through approximate techniques.

In this thesis, general stochastic system design problems are discussed that involve as objective function the expected value of a system performance measure. Special attention is given to problems with reliability objectives, i.e., when the expected value corresponds to a failure probability. This class of problems, which belongs to RBDO, will be referred to herein as ROP (reliability objective problems). The analysis focuses on methods that are applicable to complex systems, involving, for example, nonlinear models with high-dimensional uncertainties and performance measures that cannot be analytically evaluated. These characteristics distinguish the design problems considered here from the typical applications of stochastic system design and make the associated optimization highly challenging.

Special attention is given to design problems involving structural control applications. Therefore, before outlining in more detail the goals and the plan of the thesis, the general characteristics of structural control design are briefly discussed.

1.2 Structural Control

Over the last three decades, there has been a growing interest in the application of control technologies for civil structures in order to reduce their dynamic response and to increase the system reliability with respect to future dynamic excitations, e.g., wind, earthquakes, sea waves. The extensive efforts of many researchers have yielded numerous manifestations of this idea, resulting in several distinct actuation strategies and controller designs. Several state-of-the-art reports (Housner et al. 1997; Spencer and Nagarajaiah 2003; Dyke 2005) provide a detailed survey.

1.2.1 Types of structural control systems

The most fundamental distinction between the different control systems in civil engineering is based on their energy requirements. The three major classes may be defined as follows:

Passive systems: do not require an external power source for operation and utilize the motion of the structure to develop dissipative local control forces. They represent, today, the biggest percentage of full-scale structural control implementations and include various types of mechanical devices, for example, viscoelastic dampers, tuned mass dampers, liquid column mass dampers, and friction dampers.

Active systems: require a large power source for operation of actuators which supply control force to the structure based on feedback from sensors that measure the excitation and/or the response of the structure. These forces may be used to both add and dissipate energy in the structure. The full-scale implementations of active systems for structural control applications, especially for aseismic design, have been limited.

Semi-active systems: also utilize the motion of the structure to develop dissipative control forces but they use feedback measurements to alter the characteristics of the dissipative mechanism in real time. The external power source requirements are orders of magnitude smaller than active systems or their dissipative capabilities. Different types of semi-active devices have been proposed for civil engineering structures, such as variable orifice dampers, variable friction dampers, variable stiffness devices, and controllable fluid dampers. Most of these devices dissipate energy through mechanical means.

Of these different classes active systems give the greatest improvement of the structural response under dynamic excitations. However, they possess great disadvantages in their significant power requirement, which for large structures are typically too big to be met with local supplies. This raises a question for practicality and also for reliability, since control in civil engineering applications aims at the protection of structures from extreme events (e.g., strong earthquakes, high winds, tidal waves) during which the electrical power grid is susceptible to destabilizations and blackouts. Because of this limitation of active systems, the focus of research has shifted to semi-active ones which have power requirements that can be satisfied by local supplies and at the same time allow, though in a limited range, for real-time force control, making them superior to passive systems (Symans and Constantinou 1999).

A recent promising development in the structural control area has been the application of regenerative force actuation (RFA) networks (Scruggs and Iwan 2005). RFA networks are an extension of semi-active technology in which mechanical energy is first converted to electrical energy, and is then dissipated in a controllable resistive network. They consist of an array of electromechanical actuators (Scruggs and Iwan 2003), each of which can be operated as a semi-active system, i.e., provide controllable dissipation (Figure 1.1(a)). These networks have a unique advantage in that if two or more devices are used to control a structure, their associated electronics may be connected so that electrical power can be transmitted from one actuator to another. Figure 1.1(b) illustrates these ideas. Thus, in

addition to providing local dissipation (as do semi-active devices), it is possible for an RFA network to transmit energy between remote locations in a structure. The network, as a whole, must always dissipate energy, which imposes a constraint on the system forcing capabilities and makes the synthesis of control laws challenging. Thus, like semi-active devices, the power required for operation of the electromechanical actuators in the RFA network is only that required for the sensing and intelligent controller systems, which, contrary to the requirements of fully-active systems, can be provided by a small local power supply. This feature makes them appropriate devices for structural control applications.

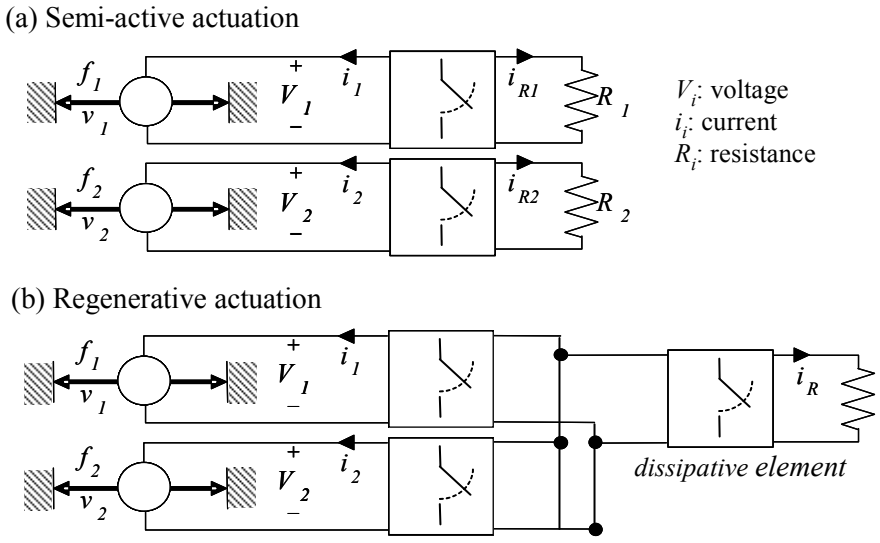

Figure 1.1: Illustration of (a) electromechanical actuators and (b) RFA network application (taken from Scruggs et al. 2007a)

It should finally be noted that semi-active devices and RFA network have an important physical limitation on the control forces they can achieve, arising from their dissipative characteristics. This introduces significant nonlinearities in the behavior of the controlled system. Similar physical constraints exist for most active actuators; in this case they correspond to a limitation of the maximum attainable control force. For large structures, where the required control forces for efficient reduction of unwanted structural vibrations

can be big, this limitation can be fairly important for the overall quality of the controlled system.

1.2.2 Controller design

In considering the application of advanced actuation technologies for structural control, one fundamental question is whether the versatility afforded by the technology justifies the associated increased cost and maintenance issues, beyond those of simpler passive systems? The answer to this question has as much to do with the feedback control law as it does with the physical limitations of the device's hardware. A high-quality control system requires that one designs the feedback controller with specific control objectives in mind, related to meaningful structural performance measures, while at the same time addressing actuator and system nonlinearities and the uncertainties in the system and excitation models. Note that because of the physical constraints for the actuators used in typical structural control applications, the usual stability-robustness issues in control system design do not apply to these problems. Thus, the performance of the controlled system is the only metric by which the quality of the control design should be judged.

Most of the research efforts on control law design for structural applications have been on extending linear control methodologies, primarily some variant of $\mathcal{H}_2$ control, to structural control problems. At the controller design stage potential nonlinearities regarding the structural and excitation models are either (a) neglected, for example in the context of the well known clipped-optimal control design for semi-active systems, e.g., Dyke et al. (1996), or (b) approximately considered through linearization techniques, e.g., Suhardjo and Kareem (2001), Erkus and Johnson (2006) (more details about these linearization techniques are provided in Section 7). To consider the nonlinearities arising from the limitations of the actuators, heuristic feedback controller design techniques have been suggested; methods such as hysteretic, dissipation-based, and energy-based approaches, e.g., Kim and Wang (1993), Gavin (2001), Zhang and Iwan (2002). These techniques have gained acceptance in part because they are natural extensions of passive structural response

control techniques. However, they do not lead to controllers which *directly* optimize meaningful global measures of dynamic structural performance, such as drifts, accelerations, etc. Ad-hoc methods (the popular "clipped-optimal" control for example) that do incorporate such global measures in the controller optimization have also been suggested. Typically, such controllers are designed in an iterative fashion, in which controller performance is qualitatively assessed for successive design iterations through simulation. For structural control applications with few actuators and one dominant mode, this approach is often sufficient to arrive at a satisfactory controller but still cannot, in general, guarantee any bound on the level of performance actually attained (Scruggs et al. 2007a). Recently, a simple controller synthesis methodology has been developed that can guarantee easily-computable upper bounds on the stochastic stationary performance for semi-active and regenerative systems (Scruggs 2007; Scruggs et al. 2007a; Scruggs et al. 2007b) as long as the dynamical system and excitation models are linear. Note that most aforementioned methodologies primarily focus on the mean square structural response and do not explicitly account for uncertainties in the system and excitation models.

Since the motivation, though, for the implementation of control technology to civil systems stems in many applications from the concept of system reliability, it stands to reason that the optimal strategy in structural control design should be that which maximizes reliability. Theoretical reliability-related control methods, such as $\mathcal{H}_\infty$, μ-synthesis (Dullerud and Paganini 1999) and the many offshoots of these, have become the standard tools in the design of feedback controllers that are robust to model uncertainty, where a compact set of possible models for the system is chosen. Information implying that some of the possible values of the model parameters are more probable than others is not explicitly treated. However, as discussed earlier, in most engineering applications, there is considerable knowledge about the relative plausibility of the parameter values, which can be quantified by assigning probability distribution functions to them. This observation has motivated a number of studies related to control applications for linear systems. The controller synthesis for robust stability and performance of linear controlled systems with parametric

probabilistic uncertainty was addressed in Wang and Stengel (2002), and the robust performance in Spencer et al. (1994). Monte Carlo simulation and FORM/SORM, respectively, have been used in these studies for the reliability evaluations but minor attention has been given on the complexity of the associated controller design optimization. The first-passage failure probability has also been used as a reliability performance objective for structural control applications; an approach originally proposed in May and Beck (1998) for systems with probabilistic parameter uncertainty and stochastic excitation, and further elaborated in Yuen and Beck (2003) and Scruggs et al. (2006). An upper bound for the first-passage failure probability has been used as a reliability measure in all these studies, calculated by neglecting the correlation between the different modes of system failure. For linear dynamical systems under stationary excitation that do not include uncertainty for the model parameters, reliability constraints have been applied in performance optimization based on covariance control design in Field and Bergman (1998). Note that all research efforts referenced in this paragraph have been restricted to linear controlled system models.

1.3 Overview of the Thesis

This thesis presents a stochastic system design approach for problems that are related mainly to earthquake engineering. Topics involving efficient system modeling, performance evaluation, and design optimization are discussed. Initially design problems that involve relatively simple models are addressed; analytical approximations are considered for the performance evaluation in these cases. Then the focus is shifted to design cases which might involve complex models for the system in consideration and its environment. The methods developed for studying these systems are intended to be general; specialized assumptions are avoided. To address the potential complexity in the model description, stochastic simulation is suggested for evaluating the system performance. This simulation-based approach allows for explicit consideration at the design stage of (a) nonlinearities in the models assumed for the system and its future excitation, and (b) complex failure modes. Applications of the general design approach to

the specific field of structural control are discussed for deriving a robust-to-uncertainties nonlinear controller design methodology. This design approach addresses the challenges discussed earlier related to control law synthesis for structural control applications.

Chapter 2 outlines the stochastic system design problem and discusses the challenges involved in the associated optimization process when stochastic simulation is used for evaluating the model performance. A probabilistic model for characterizing the system excitation in earthquake engineering applications is also developed. This model establishes a direct link between the probabilistic seismic hazard description of the structural site and future ground motions and can efficiently describe both the far-field and the near-field characteristics of the latter.

In Chapter 3 design problems are addressed that involve relatively simple models. Special focus is given on the design of control laws for linear structural systems with probabilistic model uncertainty, under stationary stochastic excitation. The focus is primarily on reliability-based synthesis. An analytical approach, motivated by the simplicity of the models adopted, is discussed for the design problem. This approach gives useful insight into the characteristics of the controller synthesis and allows for direct comparison to other design methods that have been proposed for such applications. An accurate analytical approximation for the first-passage failure probability is presented and questions are addressed related to stability, optimality, relationships to minimum variance synthesis, and appropriate characterization of robust-reliability for control applications in which model uncertainty is included. This chapter also contains an investigation of the influence of probabilistic quantification of model uncertainty on classical control approaches, such as $\mathcal{H}_2$ and multi-objective $\mathcal{H}_2$ designs.

Then the focus is shifted to design problems which might involve complex models. Chapters 4 and 5 discuss the design optimization problem when stochastic simulation methods are selected for evaluating the performance objective. In particular, Chapter 4

presents a novel algorithm, called Stochastic Subset Optimization (SSO), for efficiently exploring the sensitivity of the objective function to the design variables and iteratively identifying a subset of the original design space that has high plausibility of containing the optimal design variables. Statistical properties, appropriate stochastic simulation techniques for complex system models, and stopping criteria for the iterative approach are presented. An efficient two-stage framework for the stochastic optimization is then discussed in Chapter 5 by combining SSO with some other stochastic search algorithm. Topics related to these algorithms, as well as to the combination of the two different stages for overall enhanced efficiency and accuracy of the optimization process, are discussed.

Chapter 6 presents two applications for general structural design problems. The first considers the design of a base-isolation system for improving the reliability of a three-story building against near-field earthquakes. The efficiency of SSO and the suggested combined optimization framework are examined in detail in the context of this example. The second example discusses the retrofitting of a four-story structure with viscous dampers. The expected lifetime cost is adopted as the design objective in this case. Instead of approximating the damages from future earthquakes in terms of the reliability of the structure, as typically performed in RBDO problems, a comprehensive methodology is presented for estimating this cost; this methodology uses the nonlinear response of the structure under a given excitation to estimate the damages in a more-detailed, component level. Applications to two structural control problems are discussed in Chapter 7. The first considers the Benchmark Base Isolation Control problem proposed by the American Society of Civil Engineers (ASCE) and discusses the optimization of an RFA network for its protection against near-field ground motions. The second considers an offshore platform (Tension Leg Platform) in the North Sea and discusses the design of passive and active tuned mass dampers for improvement of its reliability in a random sea environment.

CHAPTER 2

Stochastic System Design: Theoretical Discussion

This chapter outlines initially the stochastic system design problem and presents the challenges involved in the associated optimization process when stochastic simulation is used for evaluating the model performance. The details of reliability-based performance evaluation are then discussed and the implementation of this general methodology to the specific field of structural control is introduced. Since the applications in this thesis focus primarily on earthquake engineering, a probabilistic excitation model for describing earthquake ground motions is also developed here. This stochastic ground motion model can efficiently represent both far-field and near-field characteristics of ground motions. This model has also been published in Taflanidis et al. (2007b).

2.1 General Problem

2.1.1 Stochastic system model

Consider a system that includes some controllable parameters that define the system design, referred to herein as design variables, $\boldsymbol{\varphi}=[\varphi_1,\varphi_2,...,\varphi_{n_\varphi}]\in\Phi\subset\mathbb{R}^{n_\varphi}$, where Φ denotes the bounded admissible design space. For simplicity a single model class, $\mathcal{M}$, is chosen to represent a system design and its environment (characterizing future excitations), though the ideas discussed here can be easily extended to cases where multiple model classes are considered (Muto and Beck 2007). In the latter case, the performance simply needs to be

averaged over the whole set of model classes using probabilistic weighting factors for each one that correspond to its relative plausibility. The model class $\mathcal{M}$ in this study represents the augmentation of the individual system, excitation, and performance evaluation models that the designer has chosen, as shown in Figure 2.1. The whole analysis is conditioned on the chosen model class $\mathcal{M}$. For notational simplicity this conditioning is not explicitly noted in the subsequent probability models for the system and its environment. Each model in the class is specified by a n_θ-dimensional vector $\boldsymbol{\theta}=[\theta_1,\theta_2,...,\theta_{n_\theta}]$ lying in $\Theta \subset \mathbb{R}^{n_\theta}$, the set of possible values for the model parameters. Because there is uncertainty in which model best represents the system behavior, a PDF (probability density function) $p(\boldsymbol{\theta}|\boldsymbol{\varphi})$, which incorporates our available prior knowledge about the system and its environment, is assigned to these parameters. The PDF $p(\boldsymbol{\theta}|\boldsymbol{\varphi})$ should be interpreted as a measure of the relative plausibility of the model defined by $\theta \in \Theta$ (Jaynes 2003); all probabilistic results are implicitly conditional on the chosen probability model for $p(\boldsymbol{\theta}|\boldsymbol{\varphi})$.

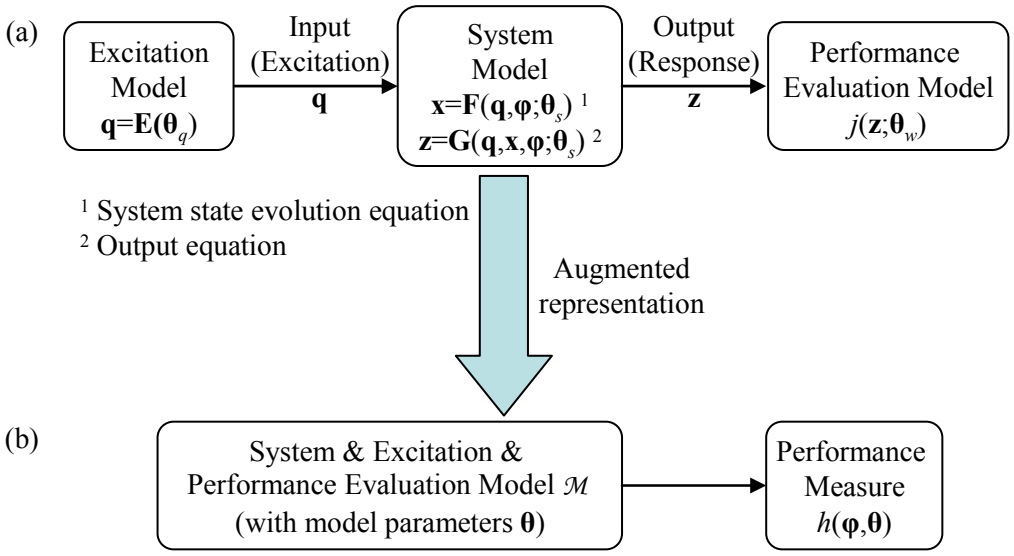

Figure 2.1: Representation of (a) initial and (b) augmented system model

The selection of the specific probability model for the model parameters, $p(\boldsymbol{\theta}|\boldsymbol{\varphi})$, should be based on the available prior knowledge about the anticipated behavior of the system and should not spuriously reduce the uncertainty corresponding to these parameters that is not

supported by this knowledge. Such knowledge may come from observations of similar systems. The principle of maximum information entropy (Jaynes 2003) can be used for quantifying in a logical manner this knowledge. The probability models that are chosen according to this principle express the maximal uncertainty about the values of the model parameters, given all prior information. If any other choice is made there should be strong grounds for the implied reduction in uncertainty in the modeling. Some examples have been discussed in Section 1.1. If data are available from the behavior of the actual system, then the additional information contained in them can be used to update the probability model $p(\boldsymbol{\theta}|\boldsymbol{\varphi})$ using a Bayesian statistical framework (Beck and Katafygiotis 1998; Beck and Au 2002; Muto and Beck 2007). In the case that more than one model class $\mathcal{M}$ is being considered as a candidate for the analytical system model, the information in the data can be also used to update the relative plausibility of the different model classes and possibly perform model class selection (Beck and Yuen 2004; Muto and Beck 2007).

With regard to the excitation model, the uncertainty in the model description may stem from (a) the representation of a sample realization of the system stochastic input, assuming that its characteristics (for example, spectral properties) are known, but additionally from (b) the incomplete knowledge about these characteristics related to anticipated future excitations. Typically, the first type is expressed by using a stochastic sequence, commonly a white-noise sequence, as input to the excitation model, and the second by assigning PDFs to the parameters defining the properties of this model. The uncertain model parameter vector for the excitation model, denoted $\boldsymbol{\theta}_q$ in Figure 2.1, expresses both these sources of uncertainty.

In this stochastic-modeling framework, nonparametric modeling uncertainties may be incorporated into the system description as a model prediction error, i.e., an error between the response of the actual system and that of the assumed model. The influence of such a prediction error can be taken into account at various levels with respect to the system model. For example, different prediction errors can be considered for each of the individual

components that comprise the augmented system model; that is, for those components that, in the modeling context, can be considered as (stochastically) independent. Alternatively, one single prediction error can be considered for the performance of the augmented system that combines the errors that may exist for all individual components. No matter how the influence of the model prediction error is incorporated into the augmented system model, the error itself can be modeled probabilistically as a random variable (Beck and Katafygiotis 1998) and can be augmented into $\boldsymbol{\theta}$ to form an uncertain parameter vector, comprised of both the uncertain model parameters and the model prediction error. The selection of the probability model for this error follows the same guidelines as discussed earlier for the other model parameters; the principle of maximum information entropy can be implemented for quantifying the available prior information. In most design problems, knowledge of only the mean value and the expected spread (variance) of the error is typically available. For such cases, the maximum entropy principle indicates that a Gaussian PDF should be selected for probabilistically characterizing the prediction error. In applications for which the errors associated with each independent system-model component are separately considered, the maximum entropy principle indicates that these errors should be modeled as uncorrelated variables.

2.1.2 Optimal stochastic system design

The favorability of different system designs, given the values of the system's model parameters, is evaluated by the function $h(\boldsymbol{\varphi},\boldsymbol{\theta}): \mathbb{R}^{n_\varphi} \mathrm{x} \mathbb{R}^{n_\theta} \rightarrow \mathbb{R}$, which corresponds to the performance measure of the system response. The convention that lower values of $h(\boldsymbol{\varphi},\boldsymbol{\theta})$ correspond to better performance is adopted herein. In the stochastic setting considered, the performance of the system may be expressed in terms of the *stochastic integral*:

$$E_{\boldsymbol{\theta}}[h(\boldsymbol{\varphi},\boldsymbol{\theta})] = \int_{\Theta} h(\boldsymbol{\varphi},\boldsymbol{\theta})\, p(\boldsymbol{\theta} \mid \boldsymbol{\varphi}) d\boldsymbol{\theta} \tag{2.1}$$

where $E_{\boldsymbol{\theta}}[.]$ denotes expectation with respect to the PDF for $\boldsymbol{\theta}$. Through appropriate definition of $h(\boldsymbol{\varphi},\boldsymbol{\theta})$ this performance objective can correspond to many different interpretations—for example, system reliability, as in (2.8) or (2.12), or expected life-cycle cost, as in (6.15). Equivalently, $h(\boldsymbol{\varphi},\boldsymbol{\theta})$ can be considered as a utility function (see, for example, Porter et al. (2004b)) that quantifies the preference for the different outputs of the system (response $\mathbf{z}$ in Figure 2.1).

In many engineering design applications the performance of the system has been traditionally interpreted in a deterministic framework, i.e., without quantifying the influence of the inherent uncertainty in the model properties. Application of the suggested stochastic design framework to these systems requires an extension of the deterministic performance quantification to a probabilistic one. This can be established in various ways. Two relatively straightforward choices are (a) the average value of the deterministic performance measure, or (b) the probability that the performance measure will not exceed some acceptable threshold (more details on how this probability is calculated are given in the next section). The corresponding designs will be characterized in this work as *average robustness* and *reliability robustness*, respectively. Which performance quantification is more appropriate depends on the nature of the performance measure and the characteristics of the design problem. The selection is ultimately related to the question of which is more important, regulation of performance on the average or of the performance that exceeds some specific threshold? A simple comparison between average and reliability robustness design will be presented in Section 3.7, in the context of the example considered there. Of course, one can specify different utility functions, for example a function that considers only performances that exceeds some acceptable threshold, as in the case of the reliability robustness, but additionally incorporates a relative weighing on how large the deviation from that threshold is (such a weighing does not exist for the reliability robustness design). The details for such a specification depend on the design application considered. All aforementioned approaches, simple or more complicated, will ultimately lead to a performance measure $h(\boldsymbol{\varphi},\boldsymbol{\theta})$ to be used in the proposed stochastic design framework.

The function in (2.1) corresponds, then, to the objective for a robust-to-uncertainties design. We then have the *optimal stochastic system design problem*:

$$\begin{aligned} &\text{minimize } E_{\boldsymbol{\theta}}[h(\boldsymbol{\varphi},\boldsymbol{\theta})] \\ &\text{subject to } \mathbf{f}_c(\boldsymbol{\varphi}) \geq 0 \end{aligned} \tag{2.2}$$

where $\mathbf{f}_c(\boldsymbol{\varphi})$ corresponds to a vector of constraints, which can be either deterministic or correspond to stochastic integrals (like the objective function). Such optimization problems, arising in decision making under uncertainty, are typically referred to as stochastic optimization or stochastic programming problems, e.g., Ruszczynski and Shapiro (2003), Marti (2005). A key difficulty in these problems is in dealing with an uncertainty space that is large and it frequently leads to a challenging evaluation of the multi-dimensional integral in (2.1). Optimization (2.2) may be further complicated by the presence of (i) design constraints that are also expressed as stochastic integrals, or (ii) integer design variables that model logical and other discrete design selections. In the current study the focus is primarily on problems that involve continuous design variables and deterministic constraints. Optimization (2.2) may be then equivalently formulated as the determination of:

$$\boldsymbol{\varphi}^* = \arg\min_{\boldsymbol{\varphi}\in\Phi} E_{\boldsymbol{\theta}}[h(\boldsymbol{\varphi},\boldsymbol{\theta})] \tag{2.3}$$

where the deterministic constraints are taken into account by appropriate definition of the admissible design space Φ.

2.1.3 Stochastic optimization

For optimization (2.3), the stochastic integral in (2.1) must be evaluated. For simple systems this integral may be sometimes efficiently calculated or at least analytically approximated, e.g., Marti 2005. Such stochastic system design problems will be discussed

in detail in Chapter 3. For complex systems, though, this is rarely true, and so the objective function can be typically estimated only by stochastic simulation techniques. In this setting, an unbiased estimate of the expected value in (2.1) can be obtained, for example, by direct Monte Carlo integration using a finite number, N, of random samples of $\boldsymbol{\theta}$, drawn from $p(\boldsymbol{\theta}|\boldsymbol{\varphi})$:

$$\hat{E}_{\boldsymbol{\theta},N}[h(\boldsymbol{\varphi},\boldsymbol{\Omega}_N)] = \frac{1}{N}\sum_{i=1}^{N} h(\boldsymbol{\varphi},\boldsymbol{\theta}_i) \tag{2.4}$$

where $\boldsymbol{\Omega}_N=[\boldsymbol{\theta}_1 \ldots \boldsymbol{\theta}_N]$ is the sample set of the model parameters with vector $\boldsymbol{\theta}_i$ denoting the sample of these parameters used in the i^{th} simulation. In this stochastic simulation-based setting, the system response can be evaluated through computer simulation, rather than approximated analytically. This allows for efficiently addressing nonlinearities of the system models and complex performance metrics.

The quality of the estimate (2.4) is quantified in terms of its coefficient of variation, denoted as c.o.v., which is defined as the ratio of the standard deviation of the estimate over its mean value and can be expressed by (Fishman 1996):

$$\begin{aligned} \text{c.o.v.} &= \frac{\Delta_u}{\sqrt{N}} = \frac{1}{\sqrt{N}}\sqrt{\frac{E_{\boldsymbol{\theta}}\left[\left(h(\boldsymbol{\varphi},\boldsymbol{\theta}) - E_{\boldsymbol{\theta}}[h(\boldsymbol{\varphi},\boldsymbol{\theta})]\right)^2\right]}{E_{\boldsymbol{\theta}}[h(\boldsymbol{\varphi},\boldsymbol{\theta})]^2}} \\ &\approx \frac{1}{\sqrt{N}}\frac{\sqrt{\frac{1}{N}\sum_{i=1}^{N}\left[h(\boldsymbol{\varphi},\boldsymbol{\theta}_i) - \hat{E}_{\boldsymbol{\theta},N}[h(\boldsymbol{\varphi},\boldsymbol{\Omega}_N)]\right]^2}}{\hat{E}_{\boldsymbol{\theta},N}[h(\boldsymbol{\varphi},\boldsymbol{\Omega}_N)]} \end{aligned} \tag{2.5}$$

where Δ_u is the unit coefficient of variation for the estimator in (2.4).

The estimate of $E_{\boldsymbol{\theta}}[h(\boldsymbol{\varphi},\boldsymbol{\theta})]$ in (2.4) involves an unavoidable error $e_N(\boldsymbol{\varphi},\boldsymbol{\Omega}_N)$ which is a function of both the sample set $\boldsymbol{\Omega}_N$ as well as the current system model configuration,

defined by the design variable selection $\boldsymbol{\varphi}$. The optimization in (2.3) is then approximated by:

$$\boldsymbol{\varphi}_N^{\,*} = \arg\min_{\boldsymbol{\varphi}\in\Phi} \hat{E}_{\boldsymbol{\theta}}[h(\boldsymbol{\varphi},\boldsymbol{\Omega}_N)] \quad . \tag{2.6}$$

If the stochastic simulation procedure is a consistent one, then as $N \to \infty$, $\hat{E}_{\boldsymbol{\theta},N}[h(\boldsymbol{\varphi},\boldsymbol{\Omega}_N)] \to E_{\boldsymbol{\theta}}[h(\boldsymbol{\varphi},\boldsymbol{\theta})]$ and $\boldsymbol{\varphi}_N^* \to \boldsymbol{\varphi}^*$ under mild regularity conditions for the optimization algorithms used (Ruszczynski and Shapiro 2003). The existence of the estimation error $e_N(\boldsymbol{\varphi},\boldsymbol{\Omega}_N)$, which may be considered as noise in the objective function, contrasts with classical deterministic optimization where it is assumed that one has perfect information. Optimization (2.6) is also closely related to the general field of simulation-based optimization (see, for example, Gosavi (2003)) since the objective function is obtained by means of a simulation-based approach.

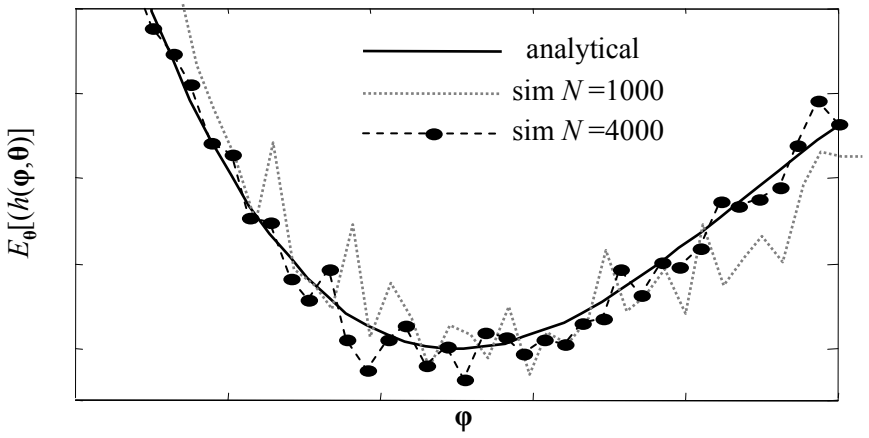

Figure 2.2: Comparison between analytical and simulation-based (sim) evaluation of an objective function

Figure 2.2 illustrates the difficulties associated with $e_N(\boldsymbol{\Omega}_N,\boldsymbol{\varphi})$. The curves corresponding to simulation-based evaluation of the objective function have non-smooth characteristics, a feature which makes application of gradient-based algorithms challenging. Also, the

estimated optimum depends on the exact influence of the estimation error, which is not the same for all evaluations; different runs of the algorithm might converge to different solutions, which do not necessarily correspond to the true optimum. Another source of difficulty, especially when complex system models are considered, is the high computational cost associated with the estimation in (2.4), since N system analyses must be performed for each objective function evaluation. Even though recent advanced stochastic optimization algorithms (see Chapter 5) can efficiently address the first two aforementioned problems, this latter one remains challenging for many engineering design applications. Specialized, approximate approaches have been proposed in various engineering fields for reduction of the computational cost (for example, for reliability-based optimal design problems as discussed earlier in Section 1.1). These approaches may work satisfactorily for certain applications, but typically cannot be proved to converge to the solution of the original design problem. For this reason such approaches are avoided in this current study. Optimization problem (2.6) is directly solved so that $\boldsymbol{\varphi}_N^* \approx \boldsymbol{\varphi}^*$.

An efficient framework, consisting of two stages, is presented in Chapter 5 for such optimizations. The first stage implements a novel approach, called Stochastic Subset Optimization (SSO), for efficiently exploring the sensitivity of the objective function to the design variables and iteratively identifying a subset of the original design space that has high plausibility of containing the optimal design variables. The SSO algorithm is discussed in detail in Chapter 4. The second stage of the proposed optimization framework adopts some appropriate stochastic optimization algorithm to pinpoint the optimal design variables using information from the first stage. Topics related to the combination of the two different stages for enhanced overall efficiency are discussed, for example by construction of importance sampling densities from the information available from SSO.

2.2 Reliability-Based Design

The reliability of the system reflects the plausibility of occurrence of unacceptable performance, based on all available information. Let $\mathbf{z} \in \mathbb{R}^{n_z}$ correspond to the system response vector, D_s be the region in $\mathbf{z}$ space that defines the acceptable system performance and $g(\boldsymbol{\varphi},\boldsymbol{\theta})$ be the limit state function that defines the system unacceptable performance, referred to as failure, with the convention that $g(\boldsymbol{\varphi},\boldsymbol{\theta}) \geq 0$ denotes the failure region in the $\boldsymbol{\theta}$ space. Note that the failure region can be determined either in terms of the response vector space or the model parameter vector $\boldsymbol{\theta}$, since the latter includes the performance evaluation and system input model parameters. The reliability of the system for specified design variables $\boldsymbol{\varphi}$ is quantified by the failure probability:

$$P_F(\boldsymbol{\varphi} \mid \Theta) = P\left(\mathbf{z} \notin D_s\right) = P\left(g(\boldsymbol{\varphi},\boldsymbol{\theta}) \geq 0\right) \tag{2.7}$$

where P denotes probability. System model uncertainties can be taken into account in this formulation by employing the idea of robust probability of failure (Papadimitriou et al. 2001). This probability is expressed as:

$$\begin{aligned} P_F(\boldsymbol{\varphi} \mid \Theta) &= E_{\boldsymbol{\theta}}[I_F(\boldsymbol{\varphi},\boldsymbol{\theta})] = \int_{\Theta} I_F(\boldsymbol{\varphi},\boldsymbol{\theta})\, p(\boldsymbol{\theta} \mid \boldsymbol{\varphi}) d\boldsymbol{\theta} \\ &= \int_{g(\boldsymbol{\varphi},\boldsymbol{\theta})\geq 0} p(\boldsymbol{\theta} \mid \boldsymbol{\varphi}) d\boldsymbol{\theta} = \int_{\Theta_f} p(\boldsymbol{\theta} \mid \boldsymbol{\varphi}) d\boldsymbol{\theta} \end{aligned} \tag{2.8}$$

where $I_F(\boldsymbol{\varphi},\boldsymbol{\theta})$ is the indicator function of failure, which is 1 if the system model that corresponds to $(\boldsymbol{\varphi},\boldsymbol{\theta})$ fails, i.e., its response departs from the acceptable performance set, and 0 if it does not, and Θ_f is the region in the Θ space that leads to unacceptable performance for the given design configuration and performance choices (system response and safe region definition). In (2.8) $\boldsymbol{\theta}$ represents the augmented uncertain parameter vector comprised of both the model parameters as well as the model prediction error (if one considered).

If direct Monte Carlo estimation is used for evaluation of the integral in (2.8) the c.o.v. in (2.5) may be further simplified to (Au and Beck 2001a):

$$\text{c.o.v.} \approx \sqrt{\frac{1-\hat{P}_F(\boldsymbol{\varphi}\,|\,\Theta)}{N\cdot\hat{P}_F(\boldsymbol{\varphi}\,|\,\Theta)}} \quad . \tag{2.9}$$

An equivalent expression can also be derived for the robust failure probability by explicitly considering the influence of the model prediction error between the responses of the actual system and the assumed model. Let $\tilde{g}(\boldsymbol{\varphi},\boldsymbol{\theta})$ be the limit state function defining the model's failure, and let the model prediction error, $\varepsilon(\boldsymbol{\varphi},\boldsymbol{\theta})$, be defined in such a way that the relationship

$$\varepsilon(\boldsymbol{\varphi},\boldsymbol{\theta}) = \tilde{g}(\boldsymbol{\varphi},\boldsymbol{\theta}) - g(\boldsymbol{\varphi},\boldsymbol{\theta}) \tag{2.10}$$

holds. In this context, and noting that $g(\boldsymbol{\varphi},\boldsymbol{\theta})>0$ corresponds to $\tilde{g}(\boldsymbol{\varphi},\boldsymbol{\theta}) > \varepsilon(\boldsymbol{\varphi},\boldsymbol{\theta})$, $P_F(\boldsymbol{\varphi}|\Theta)$ is transformed into:

$$\begin{aligned} P_F(\boldsymbol{\varphi}\,|\,\Theta) &= \int_{\Theta}\int_{-\infty}^{\infty} I_F(\boldsymbol{\varphi},\boldsymbol{\theta},\varepsilon)\,p(\boldsymbol{\theta}\,|\,\boldsymbol{\varphi})\,p(\varepsilon)\,d\varepsilon\,d\boldsymbol{\theta} = \int\int_{g(\boldsymbol{\varphi},\boldsymbol{\theta})>0} p(\boldsymbol{\theta}\,|\,\boldsymbol{\varphi})\,p(\varepsilon)\,d\varepsilon\,d\boldsymbol{\theta} \\ &= \int_{\Theta}\int_{\tilde{g}(\boldsymbol{\varphi},\boldsymbol{\theta})>\varepsilon} p(\boldsymbol{\theta}\,|\,\boldsymbol{\varphi})\,p(\varepsilon)\,d\varepsilon\,d\boldsymbol{\theta} = \int_{\Theta} p(\boldsymbol{\theta}\,|\,\boldsymbol{\varphi})\left[\int_{-\infty}^{\tilde{g}(\boldsymbol{\varphi},\boldsymbol{\theta})} p(\varepsilon)\,d\varepsilon\right] d\boldsymbol{\theta} \end{aligned} \tag{2.11}$$

where in this case the vector $\boldsymbol{\theta}$ corresponds solely to the uncertain parameters for the system and excitation model, i.e., excluding the model prediction error. The last integral (in brackets) in (2.11) can be analytically solved: it corresponds to $P_\varepsilon(\tilde{g}(\boldsymbol{\varphi},\boldsymbol{\theta}))$, where P_ε is the cumulative distribution function for the model prediction error ε conditioned on $(\boldsymbol{\varphi},\boldsymbol{\theta})$. The robust failure probability in (2.8) is then expressed by

$$P_F(\boldsymbol{\varphi}\,|\,\Theta) = E_{\boldsymbol{\theta}}[P_\varepsilon(\tilde{g}(\boldsymbol{\varphi},\boldsymbol{\theta}))] = \int_{\Theta} P_\varepsilon(\tilde{g}(\boldsymbol{\varphi},\boldsymbol{\theta}))\,p(\boldsymbol{\theta}\,|\,\boldsymbol{\varphi})\,d\boldsymbol{\theta} \quad . \tag{2.12}$$

Thus, the performance measure in optimal reliability problems corresponds either to (a) $h(\boldsymbol{\varphi},\boldsymbol{\theta})=I_F(\boldsymbol{\varphi},\boldsymbol{\theta})$ or (b) $h(\boldsymbol{\varphi},\boldsymbol{\theta})=P_\varepsilon(\tilde{g}(\boldsymbol{\varphi},\boldsymbol{\theta}))$, depending on which formulation is adopted, (2.8) or (2.12). The optimal reliability problem is formulated as

$$\boldsymbol{\varphi}^* = \arg\min_{\boldsymbol{\varphi}\in\Phi} P_F(\boldsymbol{\varphi} \mid \Theta) \quad . \tag{2.13}$$

Note that expressions similar to (2.12) may de developed by considering different characterizations for the influence of the model prediction error, for example, by taking it into account directly with respect to the model response, $\mathbf{z}$, as in Papadimitriou et al. (2001). Typically there is some form of equivalence between these different characterizations. For example, the definition of the limit state function along with relationship (2.10) leads automatically to a specific relationship between the assumed model and the actual system responses. Special care is needed so that the first definition leads to a realistic relationship in the latter case, in the context of the specific application and the probabilistic model considered for the prediction error.

2.3 Controlled System Design

A controlled system model is characterized by separate models for the system, excitation, sensors, and actuators, along with a control law. The control law is parameterized by some finite-dimensional vector. Such a parameterization may refer to explicit characteristics of the control law, for example to feedback or feedforward gains, or to the choice of "tuning knobs" for the controller design, for example to the weighting matrices in the setting of linear quadratic regulator or adaptive control designs (see, for example, Stengel (1994) or Krstic et al. (1995), respectively). The design variables, $\boldsymbol{\varphi}$, in this setting refer to these parameters of the control law, and the design space Φ to the compact set of feasible controller parameters. A schematic description is given in Figure 2.3.

This system can be easily represented in the augmented form of Figure 2.1. Thus the general stochastic system design formulation discussed earlier can be naturally extended to control applications to develop a robust-to-uncertainties nonlinear controller design methodology. The simulation-based methodology discussed earlier will contribute to *explicit* consideration of all important, linear or nonlinear, characteristics of the system model at the design stage, but will lead to a challenging controller optimization problem, especially for systems that include higher-order controllers with large dimensional parameter vectors. For controlled systems it is interesting to compare how the stochastic design approach compares to classical methodologies that have become the standard tools for controller synthesis. Some insight to this question will be given in Chapter 3. Because of their greater familiarity in the control literature, Chapter 3 will address the design of control laws for linear structural systems with probabilistic model uncertainty, under stationary stochastic excitation. An analytical approach, motivated by the simplicity of the models, will be discussed for this design problem that gives useful insight in the characteristics of the controller synthesis and allows for direct comparison to other controller design methods that have been proposed for such applications.

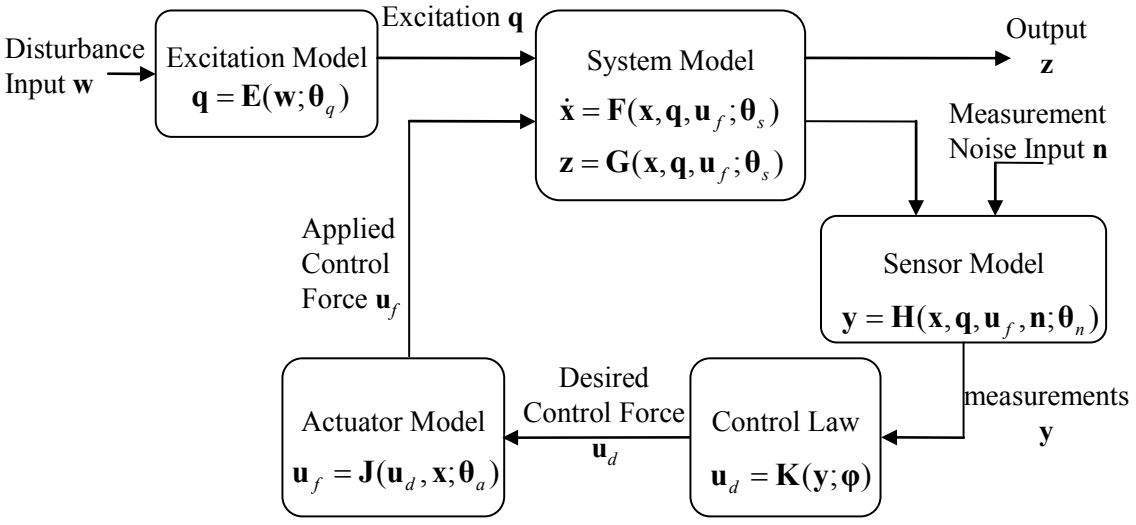

Figure 2.3: Representation of controlled system model

2.4 Probabilistic Seismic Ground Motion Model

The focus of the applications that are discussed in this study is on earthquake engineering. For this reason a probabilistic model for efficiently describing the stochastic excitation, i.e., the ground motion time history, needs to be developed. Contrary to methodologies that are based on linear or approximate system design approaches, for which such models have to be simple, the simulation-based approach discussed in the current study allows for consideration of more complicated descriptions for the ground motion. Two desirable characteristics for the models used for this purpose are: (i) parameters with well-defined physical meaning which can be treated in a realistic probabilistic framework and can be related to the seismic hazard for a specific site, and (ii) small computational effort to simulate a sample of the excitation (since a large number of simulations will be typically needed for the stochastic optimization). The model developed here is based on the methodologies presented by Mavroeidis and Papageorgiou (2003) and Boore (2003). These methodologies, which were initially intended for generating synthetic ground motions, are reinterpreted here to form a stochastic model for the earthquake excitation. The low-frequency (long period) and high-frequency components of the ground motion are independently modeled, according to these methodologies, and then combined to form the acceleration time history. Such an approach for stochastic modeling of ground motion has been initially discussed in Au and Beck (2001a). That methodology is extended here to address near-field characteristics of earthquake excitations.

2.4.1 High-frequency component

The fairly general, point source stochastic method is selected for modeling the higher-frequency (>0.1–0.2 Hz) component of ground motions. The stochastic method is based on a parametric description of the ground motion's radiation spectrum $A(f;M,r)$, which is expressed as a function of the frequency, f, for specific values of the earthquake magnitude, M, and epicentral distance, r. This spectrum consists of many factors which account for the spectral effects from the source (source spectrum) as well as propagation

through the earth's crust. The duration of the ground motion is addressed through an envelope function $e(t;M,r)$, which again depends on M and r. These frequency and time domain functions, $A(f;M,r)$ and $e(t;M,r)$, completely characterize the model. More details on them are provided in Appendix 2A. Particularly, the two-corner point-source model by Atkinson and Silva (2000) can be selected for the source spectrum because of its equivalence to finite fault models. This equivalence is important because of the desire to realistically describe near-fault motions and adaptation of a point-source model might not efficiently address the proximity of the site to the source (Mavroeidis and Papageorgiou 2003). The spectrum developed by Atkinson and Silva (2000) has been reported in their studies to efficiently address this characteristic.

The time-history (output) for a specific event magnitude, M, and source distance, r, is obtained according to this model by modulating a white-noise sequence $\mathbf{Z}_w$ (input) through the following steps: (i) the sequence $\mathbf{Z}_w$ is multiplied by the envelope function $e(t;M,r)$; (ii) this modified sequence is then transformed to the frequency domain; (iii) it is normalized by the square root of the mean square of the amplitude spectrum; (iv) the normalized sequence is multiplied by the radiation spectrum $A(f;M,r)$ and finally (v) it is transformed back to the time domain to yield the desired acceleration time history. This is the approach that was adopted in Au and Beck (2001a) for stochastic modeling of ground motions.

In the context of the model description discussed in Section 2.1 the model parameter vector is $\boldsymbol{\theta}_s=[M, r, \mathbf{Z}_w]$, composed of the seismological parameters, M and r, and the white-noise sequence $\mathbf{Z}_w$. The latter may be equivalently considered as the stochastic input to the model. The seismological parameters can be characterized by the probabilistic seismic hazard of the structural site, based on the location and size of the seismic faults. The uncertainty in moment magnitude M is typically modeled by the Gutenberg-Richter relationship (Kramer, 2003) truncated on some interval $[M_{min}, M_{max}]$ leading to a PDF:

$$p(M) = \frac{b_m \exp(-b_m \cdot M)}{\exp(-b_m \cdot M_{\min}) - \exp(-b_m \cdot M_{\max})} \tag{2.14}$$

with seismological parameter b_m chosen according to characteristics for the regional seismicity. The geometrical distribution (available knowledge) of the local faults in the specific application considered leads to a probabilistic characterization for the epicentral distance r (quantification of the missing information).

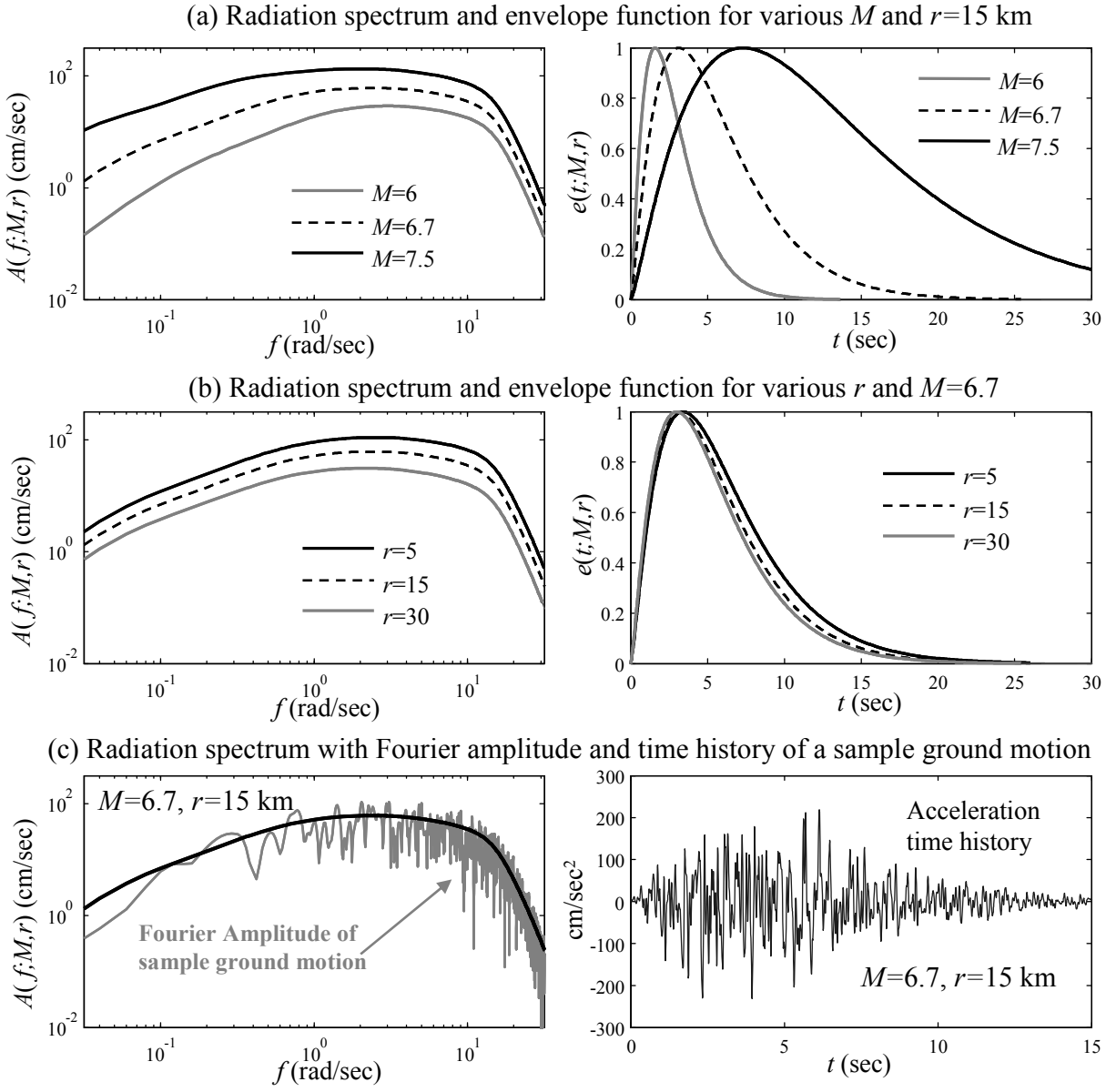

Figure 2.4: Radiation spectrum, envelope function, and sample excitation according to the stochastic ground motion method

Figure 2.4 shows functions $A(f;M,r)$ and $e(t;M,r)$ for different values of M and r. It can be seen that as the moment magnitude increases the duration of the envelope function also increases and the spectral amplitude becomes larger at all frequencies with a shift of dominant frequency content towards the lower-frequency regime. As the epicentral distance increases, the spectral amplitude decreases uniformly and the envelope function also decreases, but at a relatively smaller amount. Figure 2.4(c), includes the radiation spectrum $A(f;M,r)$ with the Fourier amplitude and the time history of a sample ground motion generated according to this model.

2.4.2 Low-frequency component

For describing the pulse characteristic of near-fault ground motions, the simple analytical model developed by Mavroeidis and Papageorgiou (2003) is selected. This model is based on an empirical description of near-fault ground motions and has been calibrated using actual near-field ground motion records from all over the world. According to it, the pulse component (due to forward directivity and permanent offset effects) of near-fault motions is described through the following expression for the ground motion velocity pulse:

$$V(t) = \frac{A_p}{2}\left[1+\cos\left(\frac{2\pi f_p}{\gamma_p}(t-t_o)\right)\right]\cos\left[2\pi f_p(t-t_o)+\nu_p\right],\ t\in\left[t_o-\frac{\gamma_p}{2f_p},t_o+\frac{\gamma_p}{2f_p}\right] \quad (2.15)$$
$$=0 \ \text{otherwise}$$

where A_p, f_p, ν_p, γ_p, and t_o describe the signal amplitude, prevailing frequency, phase angle, oscillatory character (i.e., number of half cycles), and time shift to specify the epoch of the envelope's peak, respectively. Note that all parameters have an unambiguous physical meaning. The selection of their values based on regional seismicity characteristics is addressed next.

In response to the recent realization of the importance of near-fault motions to the structural performance (Hall et al. 1995), a number of studies have been directed towards developing

predictive relationships (Somerville 1998; Alavi and Krawinkler 2000; Mavroeidis and Papageorgiou 2003; Bray and Rodriguez-Marek 2004) that may connect the pulse characteristics to the seismic hazard of a site. One of the main challenges in this process has been the small number of available earthquake records that exhibit near-fault characteristics, because of primarily the sparsity of instrumentation to capture near-fault motions in large events and secondarily the limitations of accelerometers, until recently, to accurately record the low-frequency component of ground motions. This feature has prohibited a complete understanding of the characteristics of near-fault motions and the implications they have for structural systems, which are still open research topics for both seismologists and engineers. Still, the studies referenced earlier establish predictive relationships for the period and the amplitude of near-fault pulses for seismological parameters that belong to some specific ranges; for example Bray and Rodriguez-Marek (2004) suggest that the relationships developed in their study should be used for magnitududes M>6. Use of the predictive relationships for different magnitude ranges should be avoided.

Most of these studies include no measure of the uncertainty associated with the predictions, and give a deterministic relationship for the pulse frequency and the peak ground velocity (PGV). For example the study by Somerville (1998) has suggested:

$$\begin{aligned} &\log_{10} f_{\mathrm{p}} = 3 - 0.5M_w \\ &\log_{10}\mathrm{PGV} = 0.5M_w - 1 - 0.5\log_{10}R \quad . \end{aligned} \tag{2.16}$$

In these expressions M_w is the seismic moment and R the closest distance from the fault. Both of these parameters can be calculated based on the values for the moment magnitude and the distance from the source (see Appendix 2A). A more recent study by Bray and Rodriguez-Marek (2004) takes into account the influence of local site conditions as well as the uncertainty in the predictions; this leads to a more appropriate characterization for probabilistic seismic hazard assessment. According to this recent study the mean values for the logarithms of the pulse period and the peak ground velocity of the ground motion are:

$$\ln(1/f_{\mathrm{p}}) = a_p + b_p M + \varepsilon_f$$
$$\ln \mathrm{PGV} = c_p + e_p M + g_p \ln(r^2 + d_p^2) + \varepsilon_v \tag{2.17}$$

with parameter values that are given in Table 2.1 (obtained through regression analysis) and prediction errors, ε_f and ε_p, respectively, which follow a Gaussian distribution with zero mean and standard deviation that are also presented Table 2.1.

Table 2.1 Parameters for predictive relationships for near-fault pulse characteristics

	Soil Conditions	a_p	b_p	-	-	Standard deviation for ε_f
Pulse Period	Rock	-8.60	1.32	-	-	0.40
	Soil	-5.60	0.93	-	-	0.58
	All motions	-6.37	1.03	-	-	0.57
	Soil Conditions	c_p	d_p	e_p	g_p	Standard deviation for ε_v
PGV	Rock	4.46	7.00	0.34	-0.58	0.39
	Soil	4.58	7.00	0.34	-0.57	0.49
	All motions	4.51	7.00	0.34	-0.57	0.49

It should be noted that significant differences exist between the predictive relationships suggested by different researchers (a more detailed comparison is discussed in Bray and Rodriguez-Marek (2004)), and that the uncertainty level reported in Bray and Rodriguez-Marek (2004) should be considered as high. These remarks indicate that our knowledge about the characteristics of near-fault motions is still limited. Since the description suggested in Bray and Rodriguez-Marek (2004) accounts for such limited knowledge, through a probabilistic characterization, it should be considered, at least at the current time, as the more appropriate one to use. According to that study, the logarithm of the pulse

period and the logarithm of the PGV are modeled as Gaussian random variables with conditional mean values as given in (2.17) and standard deviations as given in Table 2.1.

Regarding the rest of the parameters in (2.15): selection of t_o will be discussed in the next section; the phase angle and the number of half cycles cannot be associated with any fault characteristics that are known a priori (Mavroeidis and Papageorgiou 2003; Bray and Rodriguez-Marek 2004), but a probabilistic model for them can be chosen based on the values reported by Mavroeidis and Papageorgiou (2003) when calibrating their model to a database of near-fault ground motions. A uniform distribution on $[-\pi/2, \pi/2]$ for ν_p, and a Gaussian with mean 1.8 and standard deviation 0.3 for γ_p seem to be appropriate selections based on the results of the aforementioned study.

Finally, in the context of the model description discussed in Section 2.1 the model parameter vector for the near-fault pulse model in (2.15) is $\boldsymbol{\theta}_s=[M, r, \gamma_p, \nu_p, \varepsilon_f, \varepsilon_v]$, composed of the seismological parameters, M and r, and the pulse characteristics γ_p , ν_p, ε_f, and ε_v. If instead of the scaling of the pulse characteristics suggested by Bray and Rodriguez-Marek (2004), the study by Somerville (1998) is selected, then $\boldsymbol{\theta}_s=[M, r, \gamma_p, \nu_p]$.

2.4.3 Model of near-fault ground motions

The stochastic model for near-fault ground motions is finally established by combining the above two components. The model parameters consist of the seismological parameters M and r, the additional parameters for the velocity pulse, ν_p, γ_p, and possibly ε_f and ε_v, and the white noise sequence $\mathbf{Z}_w$. The following procedure, which is equivalent to the methodology in Mavroeidis and Papageorgiou (2003), describes the model:

(1) Apply the stochastic method to generate an acceleration time history.

(2) Generate a velocity time history for the near-field pulse using equation (2.15). The pulse is shifted in time to coincide with the peak of the envelope $e(t;M,r)$. This

defines the value of the time shift parameter t_o. Differentiate the velocity time series to obtain an acceleration time series.

(3) Calculate the Fourier transform of the acceleration time histories generated in steps 1 and 2.

(4) Subtract the Fourier amplitude of the time series generated in step 2 from the spectrum of the series generated in 1.

(5) Construct a synthetic acceleration time history so that its Fourier amplitude is the one calculated in step 4 and its Fourier phase coincides with the phase of the time history generated in step 2.

(6) Finally superimpose the time histories generated in steps 2 and step 5.

Figure 2.5 illustrate a synthetic near-fault ground motion sample for values M=6.7, r=5 km, γ_p=1.7, and v_p=π/6. Both the acceleration and velocity time histories of the synthetic ground-motion are presented. The difference between the ground motions generated by the stochastic method and the final time history are evident in this figure when looking at the velocity time history. This difference is attributed to the existence of the near-field pulse.

The model presented here provides a powerful tool for stochastic representation of ground motions that can characterize adequately both far-field and near-field characteristics of potential future earthquake excitations. The importance of this property has been illustrated clearly for stochastic design problems in Taflanidis et al. (2007b). In that study the stochastic design based on a ground motion model that addressed only far-field characteristics of ground motions (the model presented in Section 2.4.1) yielded significantly worse performance when evaluated over a suite of near-field earthquake records, compared to a design that was based on the probabilistic model discussed in this section. Also, the ground motion model suggested here can address the variability of future excitations by appropriate probabilistic description of the model parameters. As long as the

uncertainty about these model parameters is adequately described, the model can efficiently characterize future earthquake excitations. Still, one should acknowledge that the understanding we have of the near-field characteristics of earthquake ground motions is limited, especially when trying to predict them. Future research in improving this knowledge would greatly improve the efficiency of the modeling approach presented here.

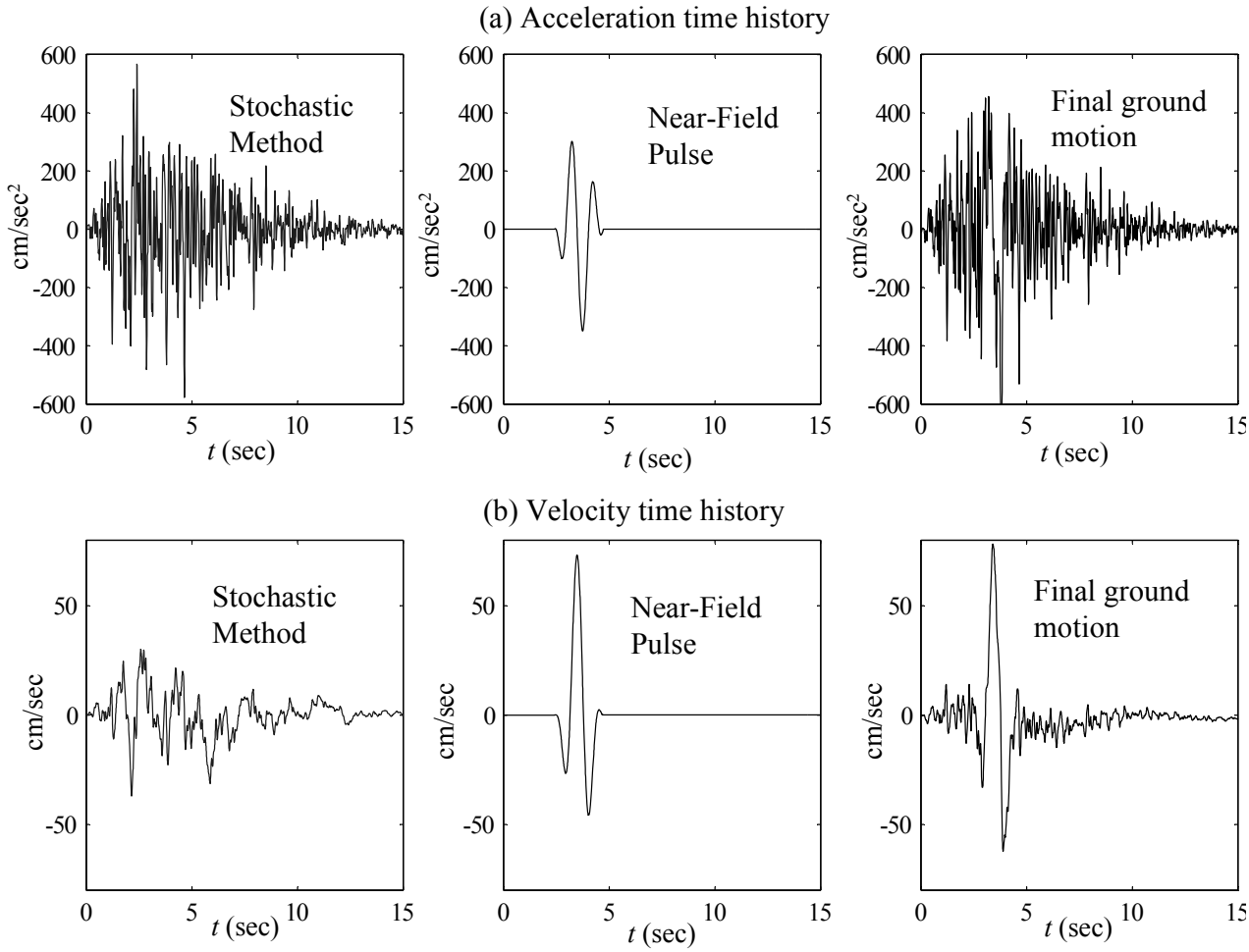

Figure 2.5: Sample near-fault ground motion: acceleration and velocity time histories

Appendix 2A: Characteristics of Amplitude Spectrum and Envelope Function for the Stochastic Method

A thorough review of the stochastic method for generation of synthetic ground motions is presented by Boore (2003). The characteristics for the functions $A(f;M,r)$ and $e(t;M,r)$ are briefly summarized here. The total spectrum $A(f;M,r)$ for the acceleration time history may be expressed as a product of the source, $E(f;M)$, path, $P(f;\mathrm{r})$, and site, $G(f)$, contributions:

$$A(f;M,r) = (2\pi f)^2 E(f;M) P(f;r) G(f) \quad . \tag{A2.1}$$

The source spectrum is given by:

$$E(f;M) = CM_w S(f;M) \text{ with } S(f;M) = \left[\frac{1-e}{1+\left(f/f_a\right)^2} + \frac{e}{1+\left(f/f_b\right)^2} \right] \tag{A2.2}$$

where the displacement source spectrum $S(f;\mathrm{M})$ described above is the two-corner point-source model developed by Atkinson and Silva (2000) for ground motions in California (see Boore (2003) for other choices for $S(f;\mathrm{M})$). For this spectrum the lower and upper frequencies and the weighing parameter are given, respectively, by

$$\begin{aligned} \log_{10} f_a &= 2.181 - 0.496M \\ \log_{10} f_b &= 2.41 - 0.408M \\ \log_{10} e &= 0.605 - 0.255M \quad . \end{aligned} \tag{A2.3}$$

In equation (A2.1) M_w is the seismic moment (in dyn-cm) which is connected to the moment magnitude by the relationship $\log_{10} M_w = 1.5(M+10.7)$. The constant C is given by $C = R_\Phi VF/(4\pi R_o \rho_s \beta_s)$, where R_Φ is the radiation pattern, usually averaged over a suitable range of azimuths and take off angles, $V = 1/\sqrt{2}$ represents the partition of total shear-wave velocity into horizontal components, $F = 2$ is the free surface amplification, ρ_s and β_s are the

density and shear-wave velocity in the vicinity of the source, and R_o is a reference distance, set to 1 km.

The path effect, $P(f;r)$, is given by the multiplication of the geometrical spreading and anelastic attenuation:

$$P(f;r) = Z(r)\exp\left[-\pi f \cdot R / \left(Q(f)\cdot c_Q\right)\right] \tag{A2.4}$$

where $Q(f)$ is a regional attenuation function, c_Q is the seismic velocity used in the determination of $Q(f)$, $Z(r)$ is the geometrical spreading function, and $R=[h^2+r^2]^{1/2}$ is the radial distance from the earthquake source to the site, with $\log_{10}h=0.15M-0.05$ (Atkinson and Silva 2000) representing a moment-dependent, nominal "pseudo-depth". The site effect, $G(f)$, is given by the multiplication of a high-frequency diminution $D(f)$ and an amplification factor $A_m(f)$, $G(f)=A_m(f)D(f)$. The diminution may be expressed by the k_o filter or the f_{max} filter, expressed respectively as:

$$D_1(f) = \exp(-\pi\kappa_o f),\ D_2(f) = \left[1+\left(f / f_{max}\right)^8\right]^{-1/2} \tag{A2.5}$$

or as a combination of both (Boore 2003). The amplification factor may be described through the empirical curves given in Boore and Joyner (1997).

Finally, the envelope function for the earthquake excitation is represented by

$$e(t;M,r) = a_t\left(t/t_n\right)^{b_t}\exp\left(-c_t(t/t_n)\right) \tag{A2.6}$$

where a_t, b_t and c_t are chosen so that $e(t;M,r)$ has a peak equal to unity when $t=\lambda_t t_n$, and $e(t;M,r)=\eta$ when $t=t_n$. The equations for these parameters are

$$b_t = -\lambda_t\ln(\eta_t)/[1+\lambda_t(\ln(\lambda_t)-1)],\ c_t = b_t/\lambda_t,\ a_t = [\exp(1)/\lambda_t]^{b_t}. \tag{A2.7}$$

The time t_n is given by $t_n=2T_w$ where T_w is the duration of the ground motion, expressed as a sum of a path dependent (typically chosen as $0.05R$) and a source dependent component (typically chosen as a fraction of $1/f_a$).

The parameters adopted in the applications considered in the current study for the $A(f;M,r)$ and $e(t;M,r)$ functions are: radiation pattern $R_{\Phi}=0.55$, rock density $\rho_s=2.8$ g/cm^3, and shear-wave velocity $\beta_s=c_Q=3.5$ km/sec; anelastic attenuation factor $Q(f)=180f^{0.45}$ (selected for the region of California according to Atkinson and Silva (2000) and geometrical spreading function $Z(R)=1/R$ for distances $R<40$ km and $Z(R)=1/40$ for distances $R>40$ km. The diminution is expressed through combination of both f_{max} and k_o filters with values $f_{max}=10$ rad/sec and $\kappa_o=0.03$. The latter selection is a compromise between regional estimates for California that typically range from about 0.02 to 0.04 (Atkinson and Silva 2000). Site amplification is chosen for generic rock sites (Boore and Joyner 1997). The parameters for the envelope function $e(t;M,r)$ are $\lambda_t=0.2$, $\eta_t=0.05$ (as suggested in Boore (2003)), and the duration is selected as $T_w=0.05R+0.5f_a$.

CHAPTER 3

Stochastic System Design: Linear Controlled Systems

This chapter discusses the design of control laws for time invariant, linear systems with probabilistic model uncertainty, under stationary stochastic excitation. The specific model and excitation choices are motivated by their familiarity in the control literature and the desire to compare the proposed stochastically-robust-to-uncertainties methodology to other standard controller synthesis approaches. Because of the linearity and stationarity assumptions, the system performance can be analytically evaluated. Contrary to simulation methods, this approach allows for efficient optimization and gives valuable insight into the theoretical characteristics of the problem. In terms of actuator characteristics, the linearity requirement restricts the design to control applications that are passive or active, or may be modeled as such for design purposes.

Initially the evaluation of stochastic integrals is discussed where the performance measure can be analytically calculated and corresponds to a smooth function, and the uncertain parameter vector is lower-dimensional; then an analytical approach is presented for approximation of the reliability of dynamical systems. Based on this theory the reliability-based design of linear controlled systems is discussed. Finally the extension of standard controller synthesis methods, such as $\mathcal{H}_2$ and multi-objective $\mathcal{H}_2$ designs, to account for probabilistic model uncertainty is discussed. The materials presented in this chapter have also been published in Taflanidis et al. (2006), Taflanidis, Scruggs et al. (2008), and Taflanidis et al. (2007a).

Note that the theoretical ideas discussed here can be extended to the design of any linear system under stationary excitation, i.e., not necessarily involving control implementation. Also, the evaluation of the stochastic integrals and the stochastic design methodology discussed in Section 3.2 can also be extended to any system, not necessarily corresponding to a linear model, which satisfies the relevant properties, that is, a smooth performance measure and lower-dimensional uncertain parameter vector. To avoid a lengthy presentation, the theory is developed in the context of controlled system design, since that corresponds to the primary motivation of the study.

The stochastic design methodology discussed in this chapter involves various types of optimization problems for which the objective corresponds to a nonlinear, non-convex, smooth function. The optimization in these problems is expressed with respect either to the uncertain model parameters or the design variables. The highly efficient optimization toolbox TOMLAB (Holmstrom et al. 2007) has been used for solving the optimization problems encountered in the current chapter. TOMLAB integrates many well-known optimization routines and has recently emerged as one of the most powerful computational packages for nonlinear optimizations. It also includes an efficient approach for multi-stage global nonlinear optimization (see algorithm "glccluster" in Holmstrom et al. (2007)) which has been preferred for the problems considered here.

3.1 Linear Time Invariant System Model

A linear, time-invariant, dynamic system in state-space subjected to stationary Gaussian excitation is considered to model the system behavior:

$$\begin{aligned} \dot{\mathbf{x}}(t) &= \mathbf{A}\mathbf{x}(t) + \mathbf{B}\mathbf{u}(t) + \mathbf{E}\mathbf{w}(t) \\ \mathbf{z}(t) &= \mathbf{C}\mathbf{x}(t) + \mathbf{D}\mathbf{u}(t) \\ \mathbf{y}(t) &= \mathbf{L}\mathbf{x}(t) \end{aligned} \tag{3.1}$$

where $\mathbf{x}(t) \in \mathbb{R}^{n_x}$ is the system state vector, composed of the structural states together with any ancillary states used to model sensor and actuator dynamics, spectral characteristics of the external excitation and so forth. Vector $\mathbf{u}(t) \in \mathbb{R}^{n_u}$ is composed of control forces that are assumed to be formulated based on a feedback vector $\mathbf{y}(t) \in \mathbb{R}^{n_y}$, which is linearly related to $\mathbf{x}(t)$ through the matrix $\mathbf{L}$. The performance of the controlled system is assessed through the favorability of the output response quantities $\mathbf{z}(t) \in \mathbb{R}^{n_z}$, which are assumed to be a linear combination of the state and control vectors. To simplify the performance evaluation a normalized output vector is assumed, given by:

$$\mathbf{z}_n(t) = \frac{1}{\gamma}\left(\mathbf{C}_n\mathbf{x}(t) + \mathbf{D}_n\mathbf{u}(t)\right);\ \mathbf{C}_n = \mathbf{NC},\ \mathbf{D}_n = \mathbf{ND} \tag{3.2}$$

where $\mathbf{N}$ is a diagonal matrix with elements the normalization factors for each response quantity and γ is a factor that uniformly scales the system response vector. The elements of this normalized vector correspond to the performance variables for the system. Disturbance input $\mathbf{w}(t) \in \mathbb{R}^{n_a}$ is a zero-mean Gaussian white-noise vector process with spectral intensity matrix $\mathbf{\Phi}_a$. It is used to model both input disturbances to the system as well as sensor and actuator noise. Control input $\mathbf{u}(t)$ is assumed to be a linear feedback function of the response measurements; i.e.,

$$\mathbf{u}(t) = \mathbf{K}(\boldsymbol{\varphi})\mathbf{y}(t) \tag{3.3}$$

where the free parameters in the feedback controller gain matrix $\mathbf{K}(\boldsymbol{\varphi}) \in \mathbb{R}^{n_u x n_y}$ constitute the design variables, which are chosen so as to yield favorable behavior for the performance variables $\mathbf{z}_n(t)$. For establishing the same terminology that is commonly adopted in feedback control design methodologies the feedback control gain will be represented in this, chapter as

$$\mathbf{K} = \mathbf{K}(\boldsymbol{\varphi}) : \boldsymbol{\varphi} \in \Phi \quad . \tag{3.4}$$

The subset of admissible gain matrices is denoted $\mathcal{K}$. For systems with active control devices, the admissible values of **K** are constrained by the requirement that they result in a stabilized closed-loop system. For systems with passive control devices (e.g.,, linear viscous dampers and springs), the "feedback data" **y**(*t*) consists of relative velocities (for dampers) and relative displacements (for springs), and **K** is constrained to be a diagonal, negative-semi-definite matrix. Controllers of the form (3.3) establish an instantaneous relationship between the feedback measurements at time *t*, and the resultant control forces **u**(*t*). However, the assumptions above implicitly allow for the consideration of dynamic controllers as well. This can be done by augmenting the state vector **x**(*t*) to include a desired number of controller states, and the augmentation of **y**(*t*) to include all these augmented states.

Under the stated conditions, the normalized output (3.2) of the closed loop system in (3.1) and (3.3) has a Gaussian distribution with zero mean and covariance matrix:

$$\boldsymbol{\Sigma}_{zz} = E\left[\mathbf{z}_n(t)\mathbf{z}_n^T(t)\right] = \frac{1}{\gamma^2}\left[\mathbf{C}_n + \mathbf{D}_n\mathbf{K}\mathbf{L}\right]\mathbf{P}\left[\mathbf{C}_n + \mathbf{D}_n\mathbf{K}\mathbf{L}\right]^T \tag{3.5}$$

where the state covariance matrix, $\mathbf{P}=E[\mathbf{x}(t)\mathbf{x}^T(t)]$, under stationary response is determined by the solution of the Lyapunov matrix equation:

$$\left[\mathbf{A} + \mathbf{B}\mathbf{K}\mathbf{L}\right]\mathbf{P} + \mathbf{P}\left[\mathbf{A} + \mathbf{B}\mathbf{K}\mathbf{L}\right]^T + \mathbf{E}\boldsymbol{\Phi}_a\mathbf{E}^T = \mathbf{0} \quad . \tag{3.6}$$

Thus, the uncertainty stemming from the stochastic input can be straightforwardly analytically propagated to the system output, in terms of the stationary performance. In Section 3.3 it will be demonstrated how this can also be established for the system reliability. Two measures commonly used for assessing this stationary performance of the

closed-loop system, which will be involved in the discussions in this chapter, are the $\mathcal{H}_2$ and generalized $\mathcal{H}_2$ metrics, defined respectively as:

$$J_2 = E\left[\mathbf{z}_n^T(t)\mathbf{z}_n(t)\right] = trace(\Sigma_{zz})$$
$$J_{g2} = \max_{1\le i\le n_z}\left(E\left[z_{n,i}^2(t)\right]\right) = \max_{1\le i\le n_z}\left(\Sigma_{zz}(i,i)\right) \tag{3.7}$$

where $E[]$ in these equations denotes expectation with respect to the stochastic disturbance input $\mathbf{w}(t)$. The controller synthesis approaches that adopt these measures as performance objectives are typically referred to as $\mathcal{H}_2$ and multi-objective $\mathcal{H}_2$ designs, respectively.

3.2 Estimation of Stochastic Integrals and Stochastic Optimization for Simple System Models

Frequent use is made in this chapter of stochastic integrals of the form:

$$E_{\boldsymbol{\theta}}[h(\mathbf{K},\boldsymbol{\theta})] = \int_{\Theta} h(\mathbf{K},\boldsymbol{\theta})\, p(\boldsymbol{\theta})\, d\boldsymbol{\theta} \tag{3.8}$$

where (i) the performance measure $h(\mathbf{K},\boldsymbol{\theta})$ can be analytically evaluated, rather than obtained through computer simulation, (ii) the dimension of the uncertain parameter vector, $\boldsymbol{\theta}$, is relatively small, and (iii) the integrand corresponds to a smooth function. The estimation of such integrals can be performed efficiently if all local maxima, or at least the global maximum, of the integrand can be identified, since it is expected that the bigger contribution to the integral will come from the region in Θ close to those maxima. Thus, evaluation of the integral in these regions leads to estimation of (3.8). Two different methods are presented next for this estimation; one based on an asymptotic approximation, and the other based on stochastic simulation. The requirements about the analytical form, the smoothness of the function $h(\mathbf{K},\boldsymbol{\theta})$ and the dimension of the uncertain parameter vector are related to efficient numerical optimization for identification of the maxima of the

integrand. For problems for which these requirements do not hold, the methods discussed here, though theoretically correct, involve large computational cost and should be avoided. Instead, the general methodology discussed in the next two chapters should be preferred.

3.2.1 Asymptotic approximation

For the estimation of stochastic integrals like the one in (3.8), Papadimitriou et al. (1997) derived an analytical approximation, which is based on Laplace's asymptotic method and which entails fitting a Gaussian distribution to the integrand at its global maximum denoted, $\boldsymbol{\theta}^*$. The integral is approximately:

$$\int_{\Theta} h(\mathbf{K},\boldsymbol{\theta})\, p(\boldsymbol{\theta}) d\boldsymbol{\theta} \cong (2\pi)^{n_\theta/2} \frac{h(\mathbf{K},\boldsymbol{\theta}^*)\, p(\boldsymbol{\theta}^*)}{\sqrt{\det\left\{\mathbf{H}_s(\mathbf{K},\boldsymbol{\theta}^*)\right\}}} \tag{3.9}$$

where $\mathbf{H}_s(\boldsymbol{\theta}^*) = -\nabla_{\boldsymbol{\theta}}\nabla_{\boldsymbol{\theta}} s\big|_{\boldsymbol{\theta}=\boldsymbol{\theta}^*}$ is the negative of the Hessian matrix of $s(\boldsymbol{\theta})$, evaluated at $\boldsymbol{\theta}^*$, where s is the log of the integrand:

$$s(\boldsymbol{\theta}) = \log p\left(\boldsymbol{\theta}\right) + \log h(\mathbf{K},\boldsymbol{\theta}) \quad . \tag{3.10}$$

The expression in (3.9) is a reasonable approximation for the case where the integrand is concentrated in a single region in Θ, with one maximum. However, in many cases there may be many prominent local maxima, called design points. In such cases, a better approximation can be obtained by conducting asymptotic expansions like (3.9) at each design point, with the integral in (3.8) then approximated as the summation of these expansions (Au et al. 1999). The identification, though, of all design points and the calculation of all second-order derivative information can be a time consuming task when the space of the uncertain parameters is large.

The accuracy of the estimation in (3.9) depends on the (a) estimation error related to the asymptotic characteristic of the approximation, and (b) the error in identifying the exact location of the local minima and evaluating the Hessian matrix at these points. The latter error can be important when analytical forms are not available for the first- and second-order derivatives of the integrand with respect to $\boldsymbol{\theta}$. In such cases numerical differentiation is needed for obtaining the relevant information, a task which is often numerically unstable and typically computationally expensive. This characteristic can reduce the accuracy of the asymptotic approximation in (3.9).

3.2.2 Stochastic simulation

Stochastic simulation using Importance Sampling techniques may be used as an alternative to evaluate integrals like the one in (3.8), when at least one design point is known (Au and Beck 1999). For such an implementation, N samples, $\boldsymbol{\theta}_k, k = 1,...,N,$ are randomly drawn from a user-prescribed distribution $p_{is}(\boldsymbol{\theta})$, called the *importance sampling distribution*. Then, the integral in (3.8) is simplified using the Law of Large Numbers as follows:

$$\int_{\Theta} h(\mathbf{K},\boldsymbol{\theta})\, p(\boldsymbol{\theta}) d\boldsymbol{\theta} = \int_{\Theta} h(\mathbf{K},\boldsymbol{\theta}) \frac{p(\boldsymbol{\theta})}{p_{is}(\boldsymbol{\theta})} p_{is}(\boldsymbol{\theta}) d\boldsymbol{\theta} \approx \frac{1}{N} \sum_{k=1}^{N} h(\mathbf{K},\boldsymbol{\theta}_k) \frac{p(\boldsymbol{\theta}_k)}{p_{is}(\boldsymbol{\theta}_k)} \quad . \tag{3.11}$$

It was shown in Au et al. (1999) that even for cases where multiple design points exist, (3.11) yields a good approximation of (3.8) if $p_{is}(\boldsymbol{\theta})$ is chosen such that its peak is near the design point corresponding to the global maximum of the integrand, and has a spread larger than that of $p(\boldsymbol{\theta})$. High accuracy in identification of the location of the design points is not required in this methodology. The computational effort for evaluation of the stochastic integral using this stochastic simulation approach will be typically larger than the asymptotic approximation (3.9) but this method gives a more robust estimate of the stochastic integral, independent of the existence of multiple design points, the accuracy of the identification of these points, and of the second-order derivative information.

3.2.3 Stochastic optimization

The two methods discussed previously for evaluation of stochastic integrals can be implemented for estimating the performance objective and efficiently performing the associated design optimization for stochastic design problems.

If the asymptotic approximation is used, then the stochastic programming problem is solved by the simultaneous optimization for all the design points and the optimal design variables. The efficiency of this approach depends on the accuracy of the asymptotic approximation, particularly close to the optimal solution. If the accuracy is high or the approximation yields a consistent estimation error, then the identification of the optimal design configuration will be accurate. Unfortunately, though, the accuracy of the asymptotic approximation cannot be typically known a priori. On the other hand the stochastic simulation approach is characterized by greater robustness and can lead to more reliable identification of the optimal solution, though at a greater computational cost. This approach suffers additionally from the existence of an estimation error as discussed in Section 2.1. The technique of selecting Common Random Numbers (Spall 2003) for the random samples in (3.11) may be implemented for reducing the variance of different estimates and thus increasing the computational efficiency of the optimization algorithm used. Sections 5.1 and 5.2 provide more details on this topic. Alternatively a two-stage approach can be applied for the stochastic optimization, where the asymptotic approximation is used initially to converge to an approximate optimal solution, and then the stochastic simulation approach is adopted in order to verify the optimality of the candidate solution and, if needed, identify the truly optimal design configuration

Note, finally, that both the methods considered here for evaluation of the stochastic integral require the identification of the design points of the integrand. In the context of a stochastic optimization algorithm, the location of the design points at the current iteration of the optimization algorithm can be used as initial guesses for subsequent iterations. If the design

configurations compared between the different iterations are not far away from each other this approach is expected to yield a significant improvement in computational efficiency.

3.3 Reliability Calculation for Linear Dynamic Systems

The reliability performance of the system described in Section 3.1 is related to the probability that the trajectory for $\mathbf{z}_n(t)$ will remain inside a hyper-cubic safe region $D_s \subset \mathbb{R}^{n_z}$ defined as:

$$D_s = \left\{ \mathbf{z}_n(t) \in \mathbb{R}^{n_z} : \left| z_{ni}(t) \right| < 1, \forall i = 1,...,n_z \right\} \tag{3.12}$$

over some time duration $t \in [0,T]$ chosen to correspond to the duration of the event causing the dynamic excitation of the system. Note that matrices $\mathbf{C}_n$ and $\mathbf{D}_n$ in (3.2), and consequently vector $\mathbf{z}_n$, can be scaled (normalized) arbitrarily so that the above hypercube can be used to represent failures with arbitrary thresholds. The scalar parameter γ is used to uniformly vary the relationship of $\mathbf{z}_n$ to the failure thresholds. The normalization of the system response was chosen so that the failure region is defined as a hyper-cube. Figure 3.1(a) shows an example of D_s for a three-dimensional space.

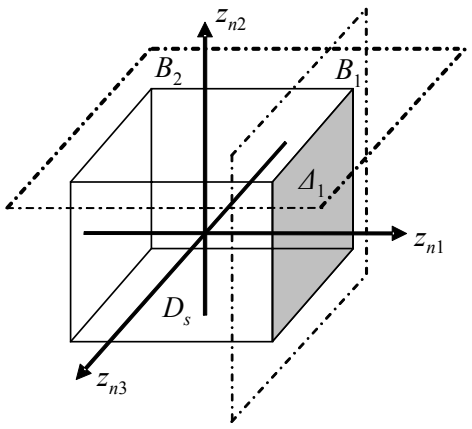

Figure 3.1: Three-dimensional example of failure surfaces

The probability of failure $P_F(\mathbf{K}|T)$ associated with design configuration corresponding to $\mathbf{K}$ is defined as:

$$P_F(\mathbf{K}\,|\,T) = P\left(\mathbf{z}_n(t) \notin D_s \text{ for some } t \in [0,T]\right) \quad . \tag{3.13}$$

For a given problem, the evaluation of P_F is conditioned on prior knowledge or assumptions of the system model in (3.1). In particular, if a nominal model is used for a system, i.e., all parameters in the state space representation are treated as known, then the only uncertainty in the system model stems from the random input $\mathbf{w}(t)$. As discussed in Section 3.1, this uncertainty can be analytically propagated for the stationary system response. It will be illustrated next how this leads to a relatively simple approximation for the system reliability. On the other hand, if there is uncertainty in some or all of the model parameters in (3.1), then this introduces additional uncertainty regarding the statistics of the system response, and consequently affects P_F.

3.3.1 Systems with known parameters

Let S_D be the boundary of the safe region D_s. Then the probability of failure, calculated as the probability of first passage across S_D, equals:

$$P_F(\mathbf{K}\,|\,T) = 1 - \exp\left(-\int_0^T n_{\mathbf{z}}^+(\mathbf{K},t)\mathrm{d}t\right) \tag{3.14}$$

where the hazard function $n_{\mathbf{z}}^+(\mathbf{K},t)$ is the mean out-crossing rate of the boundary S_D, conditioned on no previous out-crossing having occurred (Taflanidis and Beck 2005); i.e.,

$$n_{\mathbf{z}}^+(\mathbf{K},\mathrm{t}) = \lim_{\Delta t \to 0} \frac{E[\text{number of out-crossings in } [t,t+\Delta t] \mid \text{no out-crossings in } [0,t]]}{\Delta t} \quad . \tag{3.15}$$

In this analysis, it will be assumed that the time duration T is large enough, compared to the system's dynamics, so that the system response statistics can be assumed to be stationary throughout the interval $t \in [0,T]$. Under stationarity, the conditional mean out-crossing rate may be *approximated* to have a constant value (Taflanidis and Beck 2006a), which will be denoted by $\nu_{\mathbf{z}}^{+}(\mathbf{K}) = \lim_{t\to\infty} n_{\mathbf{z}}^{+}(\mathbf{K},t)$. Thus, the probability of failure is given by:

$$P_F(\mathbf{K}\,|\,T) = 1 - \exp\left(-\nu_{\mathbf{z}}^{+}(\mathbf{K})T\right) \quad . \tag{3.16}$$

For a vector process the mean out-crossing rate in (3.16) may be calculated by considering out-crossings perpendicular to the boundary as discussed in Belyaev (1968). Let B_i denote the pair of hyper-planes corresponding to failure mode i, as shown in Figure 3.1(a). Let Δ_i be the hyper-polygon corresponding to the (n_z-1)-dimensional intersection of S_D and B_i. Then $\nu_{\mathbf{z}}^{+}$ may be expressed as a sum of the out-crossing rates corresponding to each failure mode i. Let $\mathbf{n}_i$ be the unit outward normal vector at the boundary, such that $z_{ni} = \mathbf{n}_i^T \mathbf{z}_n$, and let $\mathbf{o}_i$ be the orthogonal component of $\mathbf{z}_n$, such that $\mathbf{o}_i = \mathbf{z}_n - z_{ni}\,\mathbf{n}_i$. The out-crossing rate may then be approximated as (Taflanidis and Beck 2005):

$$\nu_{\mathbf{z}}^{+}(\mathbf{K}) \approx \sum_{i=1}^{n_z} \nu_{z_i}^{+} \theta_{z_i} \lambda_{z_i} \quad . \tag{3.17}$$

This out-crossing rate is a multiplication for each failure mode of three factors: Rice's unconditional out-crossing rate $\nu_{z_i}^{+}$, a correlation weighting factor θ_{z_i}, and a correction factor λ_{z_i}, which are each described below.

Unconditional mean out-crossing rate: In (3.17), the product $\nu_{z_i}^{+}\theta_{z_i}$ is an approximation to the unconditional mean out-crossing rate perpendicular to the boundary B_i. First, consider

$\nu_{z_i}^+$, which corresponds to Rice's unconditional out-crossing rate for the scalar process z_i for the double barrier $|z_i| = 1$ (Rice 1944; Rice 1945):

$$\nu_{z_i}^+ = \frac{\sigma_{\dot{z}_i}}{\pi\sigma_{z_i}} \exp\left\{-\frac{1}{2\sigma_{z_i}^{\ 2}}\right\} \tag{3.18}$$

where $\sigma_{z_i}^2$ and $\sigma_{\dot{z}_i}^2$ are the stationary variances for z_{ni} and $\dot{z}_{ni}$. This component accounts for out-crossing over the entire pair of hyper planes B_i. The calculation of the variances in (3.18) is straightforward. According to the discussion in Section 3.1 the variance $\sigma_{z_i}^2$ is:

$$\sigma_{z_i}^2 = \frac{1}{\gamma^2}\mathbf{n}_i^T\left[\mathbf{C}_n + \mathbf{D}_n\mathbf{KL}\right]\mathbf{\Phi}\left[\mathbf{C}_n + \mathbf{D}_n\mathbf{KL}\right]^T\mathbf{n}_i \quad . \tag{3.19}$$

A restriction must be imposed in order for $\sigma_{\dot{z}_i}^2$ to be finite. Note that:

$$\dot{\mathbf{z}}_n(t) = \frac{1}{\gamma}\left(\mathbf{C}_n + \mathbf{D}_n\mathbf{KL}\right)\left(\mathbf{A} + \mathbf{BKL}\right)\mathbf{x}(t) + \frac{1}{\gamma}\left(\mathbf{C}_n + \mathbf{D}_n\mathbf{KL}\right)\mathbf{E}\mathbf{w}(t) \tag{3.20}$$

and that $\mathbf{w}(t)$ is white noise (and so has infinite variance). It follows that for the problem to be well-posed:

$$\left(\mathbf{C}_n + \mathbf{D}_n\mathbf{KL}\right)\mathbf{E} = 0 \Rightarrow \left(\mathbf{C} + \mathbf{DKL}\right)\mathbf{E} = 0, \quad \forall\mathbf{K} \in \mathcal{K} \quad . \tag{3.21}$$

This restriction is equivalent to the requirement that the response vector $\mathbf{z}_n(t)$ be differentiable. Given that (3.21) holds:

$$\sigma_{\dot{z}_i}^2 = \frac{1}{\gamma^2}\mathbf{n}_i^T\left[\mathbf{C}_n + \mathbf{D}_n\mathbf{KL}\right]\left[\mathbf{A} + \mathbf{BKL}\right]\mathbf{\Phi}\left[\mathbf{A} + \mathbf{BKL}\right]^T\left[\mathbf{C}_n + \mathbf{D}_n\mathbf{KL}\right]^T\mathbf{n}_i \quad . \tag{3.22}$$

If performance variables need to be used that do not satisfy (3.21), the problem may be circumvented by using filtered estimates of the variables instead of the actual variables. A low-pass filter, with bandwidth higher than the frequency range for which the dynamics of the system are important, should be chosen. This way (3.21) can be satisfied and the introduction of the filter does not alter the important dynamic characteristics of the performance variables. Such a filter can be augmented in the state-space representation, as discussed earlier.

Next, consider the correlation weighting factor θ_{z_i}, which is equal to

$$\theta_{z_i} = P\left[\mathbf{o}_i \in \Delta_i \,||\, z_{ni} \models 1\right] = \int_{\Delta_i} p\left(\mathbf{o}_i \,|\, |\, z_{ni} \models 1\right) d\mathbf{o}_i \quad . \tag{3.23}$$

This (n_Z–1)-dimensional integral takes into account the correlation between failure events on different planar surfaces of S_D. For n_z=2, Figure 3.2 illustrates this concept. Both trajectories in the figure correspond to "failure" for $z_{n1}(t)$, but for the gray trajectory, failure of z_{n2} precedes failure of z_{n1} and so its failure is already accounted for as an out-crossing of z_{n2}=1. Rice's out-crossing rate does not distinguish between these two instances of out-crossing on the z_{n1}=1 hyper plane, and the correlation weighting factors θ_{z_i} are introduced in (3.17) to account for this.

For the evaluation of this multi-dimensional integral, note first that the probability density $p\left(\mathbf{o}_i \,|\, |\, z_{ni} \models 1\right)$ is Gaussian with mean and covariance matrix which are algebraically related to $\mathbf{\Sigma}_{zz}$ (Johnson and Wichern 2002):

$$\begin{aligned} E\left[\mathbf{o}_i \,|\, z_{ni} = 1\right] &= \mathbf{\Sigma}_{\mathbf{o}_i z_{ni}} \left(\sigma_{z_i}{}^2\right)^{-1} \\ Var[\mathbf{o}_i \,|\, z_{ni}] &= \mathbf{\Sigma}_{\mathbf{o}_i \mathbf{o}_i} - \mathbf{K}_{\mathbf{o}_i z_{ni}} \left(\sigma_{z_i}{}^2\right)^{-1} \mathbf{K}_{\mathbf{o}_i z_{ni}}{}^T \end{aligned} \tag{3.24}$$

where $\boldsymbol{\Sigma}_{\mathbf{o}_i\mathbf{o}_i} = E\left[\mathbf{o}_i\mathbf{o}_i^T\right]$ and $\boldsymbol{\Sigma}_{\mathbf{o}_i z_{ni}} = E\left[\mathbf{o}_i z_{ni}\right]$ are simply block elements of matrix $\boldsymbol{\Sigma}_{zz}$. Straightforward numerical integration of (3.23) is only efficient when $n_z \leq 3$, since the time required for such numerical integration increases exponentially with the dimension of the integral. For larger n_z, stochastic simulation can be used to evaluate. For jointly Gaussian processes and hyper-cubic regions, Genz (1992) has introduced a series of three transformations that reduce significantly the computational effort needed for Monte Carlo integration. The algorithm proposed in Genz (1992) is used in this study for the calculation of this integral. Note that we are mainly interested in larger values for this probability integral. It is expected that if the correlation weighting factor is small on some hyper plane B_i, then the corresponding failure rate will also be small which implies that the dominant failure rates will be weighted by large values of the multivariate integral. This feature enables us to obtain good absolute accuracy without too much computational effort in the Monte Carlo integration according to Genz's procedure.

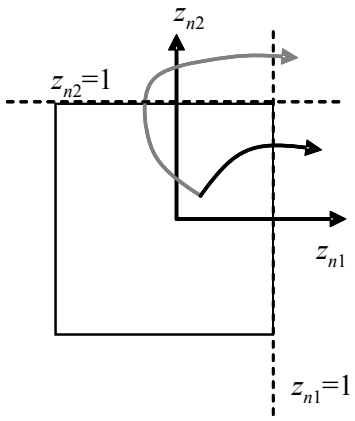

Figure 3.2: Spatial correlation between failures of performance variables z_1 and z_2

Correction for conditional out-crossing rate: Last, consider λ_{z_i}. This temporal correction factor λ_{z_i} is an adjustment to account for the conditioning of the out-crossing rate $\nu_{\mathbf{z}}^{+}$ on the absence of prior out-crossings, as in (3.15). Neglecting this correction factor is equivalent to assuming a Poisson process approximation for the out-crossing events (i.e.,

independence between out-crossings) and this assumption may not be justified for narrow-band systems, or for small failure thresholds (Lutes and Sarkani 1997), as illustrated on Figure 3.3. For the narrowband response in Figure 3.3(a), the occurrence of an out-crossing failure event establishes a high probability for a subsequent out-crossing, one period later. For the response in Figure 3.3(b), the failure threshold is so small that the system fails with a frequency on the same order as the dominant time constants of the system response, thus establishing high temporal correlation between one failure and the next.

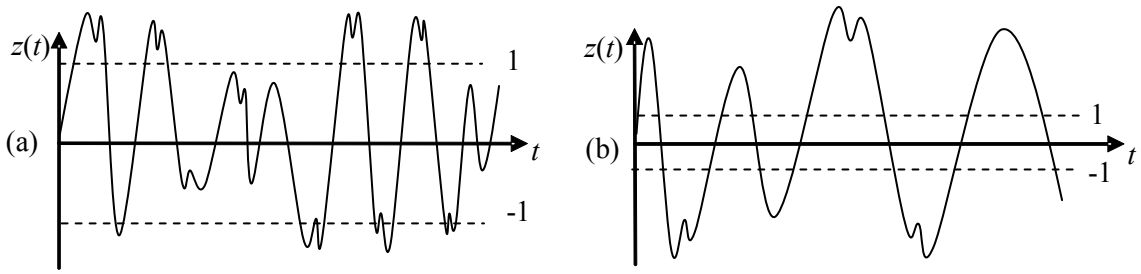

Figure 3.3: Cases for which the Poisson approximation to out-crossing times is not a good model

In general, it is impossible to calculate λ_{z_i} analytically. Many semi-empirical approximations exist for this correction factor (Vanmarcke 1975; Winterstein and Cornell 1985; Taflanidis and Beck 2005). The report by Taflanidis and Beck (2005) provides a thorough presentation. It is demonstrated in that study that the selection should be based on the bandwidth characteristics of the dynamical system. For brevity, only the approximation by Taflanidis and Beck (2005) is presented here, which has been shown to exhibit a great deal of flexibility with respect to the dynamic system bandwidth characteristics:

$$\lambda_{z_i} \approx \frac{1-\exp\left\{-q^{0.6}\left(\frac{2}{\sqrt{\pi}}\right)^{0.1}\frac{\sqrt{2}}{\sigma_{z_i}}\right\}}{1-\exp\left(-1/\left(2\sigma_{z_i}{}^2\right)\right)}, \quad q=\frac{\sigma_{z_i}^5}{4\pi I_{ce} I_{cv}} \tag{3.25}$$

where for a process with spectral density $S_{z_i z_i}$:

$$I_{cv} = \int_{-\infty}^{\infty} |\omega| S_{z_i z_i}(\omega) d\omega, \; I_{ce} = \int_{-\infty}^{\infty} S_{z_i z_i}^2(\omega) d\omega \quad . \tag{3.26}$$

These two integrals may be numerically evaluated by substituting the spectral density $S_{z_i z_i}$ for the equivalent expression $\mathbf{H}_{z_i}(\omega)\mathbf{\Phi}\mathbf{H}_{z_i}(\omega)^*$ where $\mathbf{H}_{z_i}(\omega)$ is the transfer function matrix for z_{ni}. The frequency range over which the dynamics of the structural system are important is partitioned at desired points and the frequency response is obtained (using for example the Control System Toolbox of MATLAB). The one-dimensional integrals in (3.26) are numerically calculated using the trapezoidal rule. Good accuracy may be obtained with a relatively small number of points.

3.3.2 System including model uncertainty

For systems that involve probabilistic model uncertainty the robust probability of failure may be evaluated using the total probability theorem:

$$\begin{aligned} P_F\left(\mathbf{K} \mid T, \Theta\right) &= \int_{\Theta} P_F\left(\mathbf{K} \mid T, \boldsymbol{\theta}\right) p(\boldsymbol{\theta}) d\boldsymbol{\theta} \\ &= 1 - \int_{\Theta} p(\boldsymbol{\theta}) \exp\left(-\nu_{\mathbf{z}}^{+}\left(\mathbf{K} \mid \boldsymbol{\theta}\right) T\right) d\boldsymbol{\theta} = 1 - E_{\boldsymbol{\theta}}\left[\exp\left(-\nu_{\mathbf{z}}^{+}\left(\mathbf{K} \mid \boldsymbol{\theta}\right) T\right)\right] \end{aligned} \tag{3.27}$$

where $P_F(\mathbf{K}|T,\boldsymbol{\theta})$ corresponds to the probability of failure given the values of the model parameters and is calculated as described in the previous section. The evaluation of the integral in (3.27) must in general be performed numerically; this is nontrivial if the dimension of $\boldsymbol{\theta}$ is not small (say, more than 3). The two methods presented in Section 3.2 may be used for this purpose. Numerical issues pertaining to such an evaluation are discussed next.

The asymptotic approximation for the integral in (3.27) requires an optimization for the maxima of the log of the integrand which in this case corresponds to

$$s(\boldsymbol{\theta}) = \log p(\boldsymbol{\theta}) - \nu_z^+ \left(\mathbf{K} \mid \boldsymbol{\theta}\right) T \tag{3.28}$$

and it also requires the calculation of the Hessian matrix of $s(\boldsymbol{\theta})$ at those points. The importance sampling method requires an optimization for finding the design points of the integrand. The expression for the objective function in both cases involves the out-crossing rate which included two factors that may only be evaluated numerically: the out-crossing correction factor λ_{z_i}, and the correlation weighting factor θ_{z_i}. Analytical expressions for the gradient vector, needed for any efficient optimization algorithm, and the Hessian matrix, needed by some optimization algorithms and always for the asymptotic approximation to the reliability integral, cannot be derived, so numerical differentiation is the only possibility. Moreover, the calculation of the correlation weighting factor is performed in a computationally efficient manner through an algorithm based on Monte Carlo simulation. Because of the latter feature, even though satisfactory accuracy may be obtained with a relatively small number of samples, the computational cost for the accuracy needed in order to estimate the gradient vector and the Hessian matrix of $s(\boldsymbol{\theta})$ is high. The required one or two steps of numerical differentiation for the calculation of the gradient and especially the Hessian is a potentially unstable numerical process and requires high accuracy—or at least a consistent estimation error—for the calculation of $s(\boldsymbol{\theta})$. The required number of Monte Carlo samples in Genz's procedure for obtaining the desired accuracy for the estimation of $s(\boldsymbol{\theta})$ is prohibitive for applications to systems in higher dimensions. Instead, an approach using the same random numbers in the Monte Carlo algorithm when evaluating $s(\boldsymbol{\theta})$ to calculate the first- and second-order derivatives of $s(\boldsymbol{\theta})$ is adopted. This selection, provided that the number of samples is sufficient, yields a result with consistent estimation error which allows for an accurate calculation of the gradient and Hessian. A detailed theoretical discussion about use of common random numbers is provided in Chapter 5. It is understandable that the influence of numerical errors is going to

be larger for larger dimensions of the uncertain parameters and the number of samples for the Monte Carlo integration should be chosen accordingly.

For the calculation of the reliability integral by stochastic simulation with the use of importance sampling, the accuracy needed for Genz's procedure for the estimation of the out-crossing rate $\nu_{\mathbf{z}}^{+}\left(\mathbf{K}\,|\,\boldsymbol{\theta}_k\right)$ at each sample $\boldsymbol{\theta}_k$ is not high. We are interested in the value of the integral and not for the value of the out-crossing rate $\nu_{\mathbf{z}}^{+}\left(\mathbf{K}\,|\,\boldsymbol{\theta}_k\right)$, and thus calculating the latter with high accuracy is unnecessary. The estimation error induced by the smaller accuracy should average to a small number for the calculation over the whole sample space of the $\boldsymbol{\theta}_k$s. Also the design point for the importance sampling distribution need not be calculated to high accuracy.

3.3.3 Accuracy and efficiency of the analytical approximation

The accuracy and efficiency of the analytical approximation presented in the previous two sections has been examined in detail in Taflanidis and Beck (2005) and Taflanidis and Beck (2006a) for dynamical systems with a range of different characteristics. The examples considered there show that the accuracy of the approximation is high and that the error introduced by the approximation, though it cannot be analytically estimated, does not influence the efficiency of the reliability evaluation in most applications because (i) either it is small or (ii) it produces consistent estimation errors in the calculated failure probabilities. The latter is especially important for reliability-based optimization applications. For evaluation of the reliability assuming a nominal model, the computational efficiency was reported to depend strongly on the dimension of the output because the correlation between failure events at different parts of the boundary is accounted for by a multivariate integral with dimension one less than that of the output. For medium or high level of accuracy, the relationship to the output dimension was demonstrated to be almost linear, but for higher levels, exponential. However accuracy requirements that correspond to the latter case do not typically appear in the context of stochastic system design applications.

For systems with model uncertainty the asymptotic approximation around the design points of the integrand has been shown to have computational cost and estimation error that increase with the size of the uncertain parameters and the output of the system (Taflanidis and Beck 2006a). When both are high, this cost is significant and the estimation error can be large. For cases where at least one dimension is kept low, the asymptotic approximation has been shown to give a computationally efficient estimation. The computational effort for evaluation of the reliability integral using stochastic simulation with importance sampling was shown to be larger but this method was proven to give robust estimation independent of the level of uncertainty, the existence of multiple design points, the level of failure probability, and the dimension of the space of uncertain parameters. Thus, it should be preferred when the accuracy of the asymptotic approximation cannot be guaranteed to be small.

3.4 Nominal Reliability-Based Controller Design

The computationally-efficient methodology discussed in the previous chapter for approximating the first-passage failure probability of a linear system, is applied now for investigating the design of controllers that maximize system reliability. The reliability-optimal controller $\mathbf{K}^*$ for a given T is the one which minimizes P_F; i.e.,

$$\mathbf{K}^* = \arg\min_{\mathbf{K}\in\mathcal{K}} P_F(\mathbf{K} \mid T, \Theta) \tag{3.29}$$

where P_F under stationary conditions is calculated as described in the previous section.

As discussed earlier the evaluation of P_F depends on prior knowledge for the model parameters. The design methodology that considers a probabilistic description for these parameters is defined as the robust reliability-based design. In this context, the design adopting a nominal system description, i.e., assuming the model parameters are known, will be mentioned as nominal design. The robust design is going to be discussed in the

following two sections. In the current section the design adopting a nominal system description is addressed. In this case the probability of failure is given by (3.16) with out-crossing rate calculated using (3.17). The optimization described by (3.29) is equivalent to the minimization of the stationary out-crossing rate $\nu_{\mathbf{z}}^{+}$, and the dependence on the time duration T vanishes,

$$\mathbf{K}^{*} = \arg\min_{\mathbf{K}\in\mathcal{K}} \left(1 - \exp\left(-\nu_{\mathbf{z}}^{+}(\mathbf{K})T\right)\right) = \arg\min_{\mathbf{K}\in\mathcal{K}} \left(\nu_{\mathbf{z}}^{+}(\mathbf{K})\right) \quad . \tag{3.30}$$

3.4.1 Sensitivity of optimal controllers to the out-crossing rate components

From a control optimization point of view, Rice's out-crossing rate, ν_{z_i}, is the principal component of $\nu_{\mathbf{z}}^{+}$ since it is directly related to the "failure events," i.e., the out-crossing of each barrier B_i. This rate is a product of $\exp\{-1/(2\sigma_{z_i}^2)\}$, which increases with σ_{z_i} (i.e., with the probability mass in the tails of the distribution), and $\sigma_{\dot{z}_i} / \sigma_{z_i}$, which increases with the bandwidth of z_i (Lutes and Sarkani 1997). These two components signify competing objectives of variance and bandwidth reduction for z_i. However, the sensitivity of $\nu_{\mathbf{z}}^{+}$ to changes in σ_{z_i} is much greater than to the bandwidth, because the variance enters into the equation as an exponential. Thus, the influence of the bandwidth component on the overall objective is only a primary influence if there are controller gains $\mathbf{K}\in\mathcal{K}$ which drastically alter the bandwidth without also resulting in frequent failures. In practice, the limitations in actuator capabilities that are typical of many civil engineering problems yield only a limited ability of the control gain **K** to modify the bandwidth of the system, without also resulting in high failure rates for force-related failure modes, such as shear forces, accelerations, and actuator force saturations. Thus, the exponential-weighted variance is typically the component of $\nu_{\mathbf{z}}^{+}$ most relevant to the control optimization; a feature which indicates a relationship of reliability-based design to minimum-variance design methods (such as $\mathcal{H}_2$ and multi-objective $\mathcal{H}_2$ designs). Note that the exponential weighting gives

greater importance for control optimization to performance variables with larger variances; characteristic which indicates a closer connection to multi-objective $\mathcal{H}_2$ design rather than $\mathcal{H}_2$ design.

Next, consider the correlation weighting factor θ_{z_i}. The importance of this factor in finding the optimum gain is potentially significant because it accounts for correlation between different failure modes. For example, if failure mode 1 is only likely to occur if failure mode 2 has already occurred, then the statistics of failure mode 1 do not significantly affect P_F. Consequently, the assumption of uncorrelated failure events (equivalent to assuming $\theta_{z_i} = 1,\ \forall i$), may lead to departure from the true optimum. The degree to which θ_{z_i} is relevant depends very much on the dynamic characteristics of the system, the chosen response quantities z_i, and their corresponding failure thresholds. In Taflanidis and Beck (2005), it has been demonstrated to be of significance in a number of examples.

The influence of λ_{z_i} is generally less significant for control optimization. As discussed, this factor is important for problems involving narrow-band systems, or cases where even the optimal $\mathbf{K}^*$ results in frequent failures. In most civil engineering applications the latter is not a major concern because of the way in which "failure" is typically interpreted, i.e., it corresponds to rare events. As noted in Taflanidis and Beck (2005), λ_{z_i} mainly adjusts for very low damping in the system and, as the application of control tends to greatly increase the damping, this has the effect of greatly reducing the overall influence of this factor in the neighborhood of $\mathbf{K}^*$.

3.4.2 Optimization considerations

The optimization problem (3.30) involves a non-linear objective function which has components, the correlation weighting factors $\gamma_{z_i},\ \forall i$, that are estimated through an algorithm based on Monte Carlo integration. The technique of selecting Common Random

Numbers (Spall 2003) for the random samples in the Monte Carlo integration that is used in successive evaluations of the out-crossing rate, may be implemented for reducing the variance of the estimate and improving the efficiency of the optimization algorithm used. Identification of the global minimum of this non-convex optimization problem may be performed by any appropriate algorithm selected for this purpose. As discussed earlier, the time required for accurate evaluation of the objective function in this optimization increases exponentially with the dimension of the output vector primarily because of the need to calculate the correlation weighting factors through Monte Carlo integration for each component of that vector. For improving the computational efficiency of the controller optimization, performance variables that, based on engineering judgment, will not have influential statistics for any **K** in the admissible controller space should not be included in the output.

Based on the discussion of the previous section, the out-crossing rate may be treated, for control optimization purposes, as a weighted sum of exponentials involving the reciprocal of the variances of each performance variable. Uniform scaling of these variances, i.e., change of γ, alters the sensitivity of the out-crossing rate to each one of them. It was shown in Taflanidis and Beck (2005) that such a scaling does not influence significantly any other factors of the out-crossing rate, i.e., does not influence the weighting coefficients of the sum. It is obvious then, that the optimum gain depends on the exact values of the failure thresholds and not simply their ratio and that this dependence is primarily governed by the sensitivity to the reciprocal of the variances $\sigma_{z_i}^2$. It is interesting to note that for $\gamma \to \infty$, which means $\sigma_{z_i}^2 \to 0,\ \forall i$, the largest variance dominates the sensitivity of the out-crossing rate to each of the performance variables and $\mathbf{K}^*$ converges to the gain that minimizes this variance. As the thresholds uniformly increase, there is a reduction in the importance of the less frequent "failure" events, i.e., the events that have smaller variances. Ultimately, the selection for the exact values of the failure thresholds should be based on engineering judgment for the acceptable safety or serviceability limit states of the dynamical system.

3.4.3 Stability of reliability-optimal controllers

Reliability-optimal controllers do not inherently guarantee stability of a system. For example if the entire system state space is not detectable from the output vector **z** for a given **K**, then it is possible that a controller which optimizes reliability for these outputs may destabilize the system. However, the stability of the controlled system may be enforced by appropriately constraining the space of admissible controllers $\mathcal{K}$ to the set of stabilizing controllers. Of course, for passive control systems this constraint arises naturally from the requirement that the control forces be dissipative. For active systems the constraint must be enforced explicitly.

3.4.4 Relationship to optimal minimum variance controllers

The optimization (3.30) requires a computationally-efficient means of evaluating P_F, which must be evaluated repeatedly in the optimization process as the domain $\mathcal{K}$ is searched for the optimal $\mathbf{K}^*$. Because of this complexity, it is important that this problem be motivated by placing it in contrast with other, more straight-forward optimal control problems discussed in the literature. As discussed earlier a relationship between reliability-based design and minimum-variance synthesis methods is expected, primarily with multi-objective $\mathcal{H}_2$ design, which is described by the optimization:

$$\mathbf{K}^* = \arg\min_{\mathbf{K}\in\mathcal{K}} \left\{ \max_{1\le i\le n_z} \left\{ \sigma_{z_i}^2 \right\} \right\} \quad . \tag{3.31}$$

While in general a nonconvex optimization, this problem has received significant attention over several decades, and very efficient "convexifying" methods have been developed for its solution with the use of Linear Matrix Inequalities (Boyd et al. 1994). Because the probability distributions for z_i in stationary response are zero-mean Gaussian distributions, optimization of the second moment implies the optimization of all higher-order moments. It follows that the above optimization also yields the $\mathbf{K}\in\mathcal{K}$ with the optimal lower bound on

the uniform rate of exponential decay for these probability distributions. In other words, it yields the controller which produces the distributions with the least "probability mass in the tails." On the surface, it might appear that this optimization would yield a controller which is reliability-optimal. After all, if the distributions for the components of **z** are optimized to minimize their tail mass, then so long as $\sigma_{z_i} << 1$, $\forall i$, the probability of $|z_i(t)| > 1$ is also minimized. However, a simple example illustrates that significant differences may exist between the two synthesis methods.

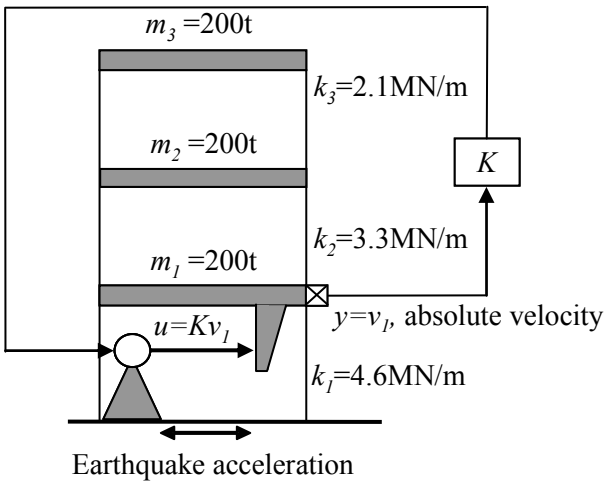

Figure 3.4: Structural model

As an example, consider an ideal 3-story shear building as shown in Figure 3.4. Modal damping of 2% is assumed. An ideal active actuator between the ground and first floor implements the familiar skyhook control law $u(t) = Kv_1(t)$, where $v_1(t)$ is the absolute velocity of the ground floor, and K is the control gain. The performance variables $\mathbf{z}_n(t)$ are taken as the vector $\mathbf{d}(t)$ of inter-story drifts, and the vector $\mathbf{a}(t)$ of absolute story accelerations. Their failure thresholds are chosen as 0.03 m and 2.65 g, respectively. Thus,

$$\mathbf{z}_n(t) = \frac{1}{\gamma}\left[\frac{1}{0.03m}\mathbf{d}^T(t) \quad \frac{1}{2.65g}\mathbf{a}^T(t)\right]^T \quad . \tag{3.32}$$

The earthquake excitation model chosen is the stationary response of a modified Kanai-Tajimi filter (Clough and Penzien 1993). Note that since the applications considered here are restricted to linear augmented system models, the ground-motion model presented in Section 2.4 would be inappropriate. The simpler Kanai-Tajimi filter is preferred for this purpose. The transfer function for this filter is

$$H(s) = \frac{2\zeta_g \omega_g s + \omega_g^2}{(s^2 + 2\zeta_g \omega_g s + \omega_g^2)} \frac{1}{(s + \omega_v)} \tag{3.33}$$

with ω_g=2 Hz, ζ_g=0.5, and ω_v=15 Hz. In order to satisfy (3.21) for the absolute acceleration responses, a high-frequency pole ω_v has been introduced compared to the traditional form of the Kanai-Tajimi filter. The RMS intensity of the input is selected as 0.2g. Formulating the system and excitation models in state space form and developing the augmented linear system model as in (3.1) is relatively straightforward and omitted here. Taflanidis and Beck (2005) provide a detailed discussion in augmentation characteristics for dynamical systems.

The reliability-optimal and multi-objective $\mathcal{H}_2$-optimal controllers are denoted $K^*_{P_F}$ and $K^*_{m\mathcal{H}_2}$, respectively, and their respective out-crossing rates are denoted ν_{P_F} and $\nu_{m\mathcal{H}_2}$, respectively. Ratios $K^*_{m\mathcal{H}_2}/K^*_{P_F}$ and $\nu_{m\mathcal{H}_2}/\nu_{P_F}$ are shown in Figure 3.5(a) for different values of γ. Values of $\nu_{m\mathcal{H}_2}/\nu_{P_F}$ are shown for both the analytical approximation discussed above, as well as the actual values obtained through stochastic simulation. The highly-efficient algorithm Importance Sampling Efficient Estimation (Au and Beck, 2001b) has been used for the simulation data. Figure 3.5(b) shows ν_{P_F}, and Figure 3.5(c) the associated P_F for T=10s, which is roughly 30 natural periods of the structure. As $\gamma \to \infty$, $K^*_{P_F}$ and $K^*_{m\mathcal{H}_2}$ converge, as do ν_{P_F} and $\nu_{m\mathcal{H}_2}$. This result agrees with the discussion presented earlier. However, the corresponding values of P_F at which this convergence becomes apparent represent extremely rare events that are typically of no engineering

interest, with failure probabilities below 10^{-8}. For ranges of γ that correspond to more interesting threshold definitions for reliability purposes, there is a significant difference between $K^*_{P_F}$ and $K^*_{m\mathcal{H}_2}$, as well as their associated reliabilities. For the value of γ=1, which corresponds to the nominal definition of the failure thresholds, the ratio of performance is 1.25 and the corresponding probability of failure 0.01.

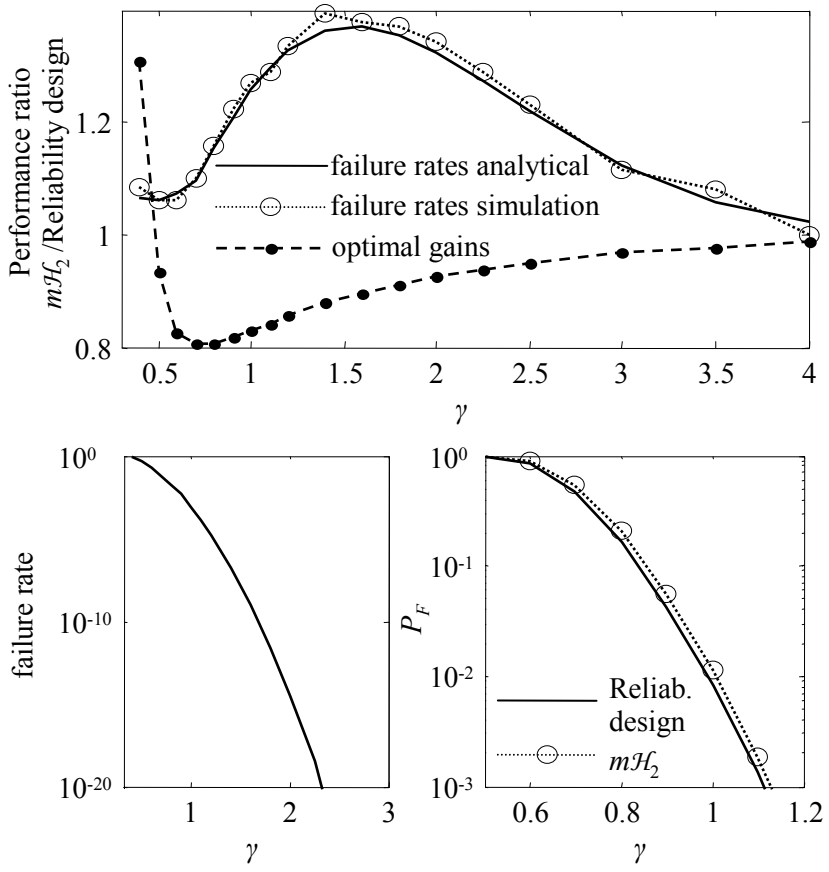

Figure 3.5: Comparison between optimal multi-objective $\mathcal{H}_2$ and reliability designs

The differences between optimal multi-objective $\mathcal{H}_2$ and reliability controllers reported here stem from the fact that optimizing the upper bound on the variances of the components of the response vector does not necessarily correspond to optimal reliability design with respect to the joint distribution of the whole vector. Multi-objective $\mathcal{H}_2$ design ultimately fails to take into account any correlation between the performance variables. How

important the difference between the two designs is depends on the behavior of the dynamical system around the regions of $K^*_{P_F}$ and $K^*_{m\mathcal{H}_2}$ gains. If the outputs are highly correlated, which corresponds to $\theta_{z_i} \approx 0$ for all response quantities apart from the dominant one (meaning the one that corresponds to the largest variance $\sigma^2_{z_i}$), optimal reliability and multi-objective $\mathcal{H}_2$ controllers will be close. This will also be true if there is a significant difference in the variances between the dominant performance variable and all others that are uncorrelated from it, i.e., correspond to non-negligible θ_{z_i}, in the neighborhoods near the optimal $K^*_{P_F}$ and $K^*_{m\mathcal{H}_2}$ gains. On the other hand, the difference between the above two designs may be significant when there are response quantities that have only a small degree of correlation and comparable stationary characteristics, i.e., comparable variances, in the neighborhoods of interest. The discussion motivates the further development of reliability-based structural control design.

A similar comparison between reliability controllers and $\mathcal{H}_2$ controllers is illustrated in Figure 3.6. Note that $\mathcal{H}_2$ optimal controllers minimize the mean variance of the response vector contrary to multi-objective $\mathcal{H}_2$ optimal controllers that minimize the maximum variance. The $\mathcal{H}_2$ design which is described by the optimization:

$$\mathbf{K}^* = \arg\min_{\mathbf{K}\in\mathcal{K}} \sum_{i=1}^{n_z} \sigma^2_{z_i} \quad . \tag{3.34}$$

For full-order controllers the $\mathcal{H}_2$ synthesis method may be implemented either by solving two Ricatti equations or by using Linear Matrix Inequalities (Dullerud and Paganini 1999). For reduced-order controllers, the problem may be approached by the use of LMIs (Iwasaki et al. 1994; Iwasaki and Skelton 1995).

The results in Figure 3.6 illustrate a bigger difference, as expected, between optimal $\mathcal{H}_2$ and reliability controllers, compared to the difference the latter and optimal multi-objective $\mathcal{H}_2$

controllers. $\mathcal{H}_2$ design does not take into account any correlation between the performance variables and does not emphasize the importance of the tails of the distribution for each performance variable; rather, it looks at the stationary performance of the response vector on the average. Thus, the departure from reliability objectives is expected to be larger for this synthesis method. As the scaling parameter γ increases, that is as the performance evaluation focuses more on rare events, the difference between the two design methods compared here becomes larger. This discussion brings forward an important topic: that $\mathcal{H}_2$ design, which is the approach selected in most civil engineering control applications, yields a significantly sub-optimal reliability performance, especially when this performance is related to large acceptable bounds. If the control implementation's purpose is to increase the system reliability then this popular design approach should be avoided!

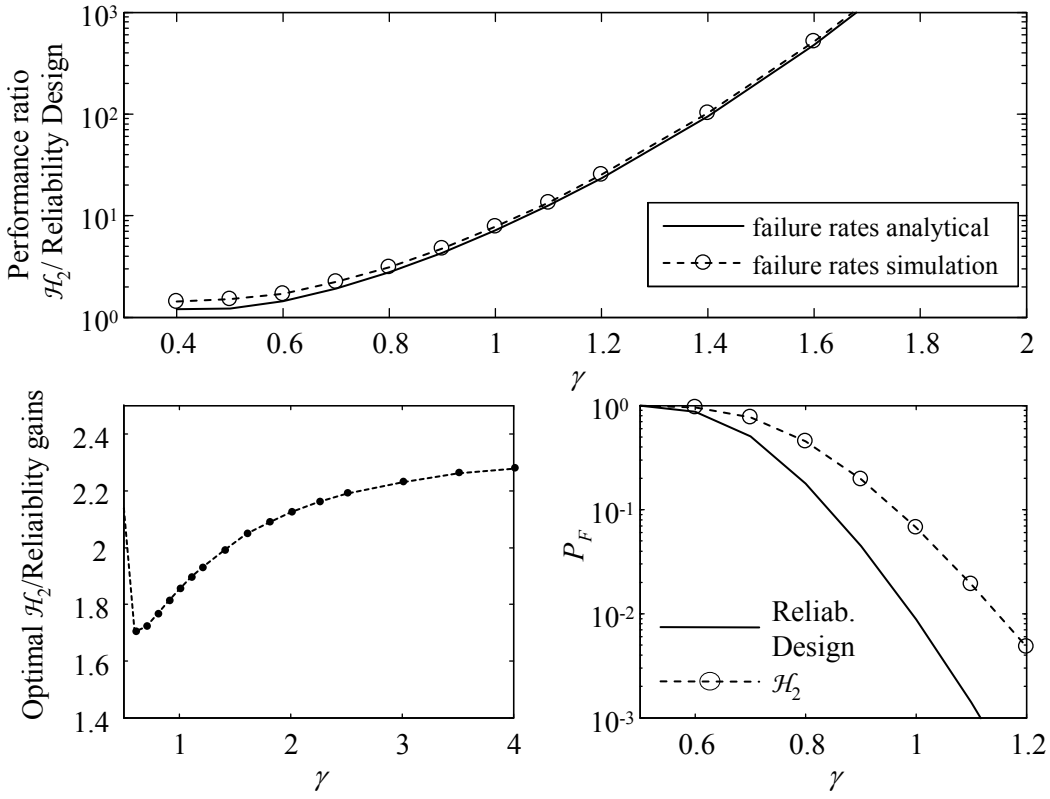

Figure 3.6: Comparison between optimal $\mathcal{H}_2$ and reliability designs

The example considered here also illustrates the importance of the exact selection of the failure threshold, i.e., the influence of the scaling factor γ. Note that the optimal gain for multi-objective $\mathcal{H}_2$ control is independent of the scaling of these thresholds (it is a homogenous problem). Thus, the ratio of the optimal gains corresponding to reliability and multi-objective $\mathcal{H}_2$ designs, as presented in Figure 3.5(a), is indicative of the sensitivity of the optimal gain for reliability-based design to the scaling of the failure thresholds. It is obvious that this sensitivity is significant.

3.5 Robust-Reliability Design with Fixed Time Duration

In the presence of parametric model uncertainty and using expression (3.27) for the robust failure probability, the robust reliability optimal controller in (3.29) may be expressed as

$$\mathbf{K}^* = \arg\min_{\mathbf{K}\in\mathcal{K}} \left(P_F\left(\mathbf{K} \mid T, \Theta\right)\right) = \arg\max_{\mathbf{K}\in\mathcal{K}} \left(\int_{\Theta} p(\boldsymbol{\theta}) \exp\left(-\nu_{\mathbf{z}}^{+}\left(\mathbf{K} \mid \boldsymbol{\theta}\right) T\right) d\boldsymbol{\theta}\right) \quad . \tag{3.35}$$

Assume that the asymptotic approximation, with only one design point, is a justifiable approximation for the reliability integral. Then the solution to the optimization above may be approximately solved by the simultaneous optimization of the optimal control gain $\mathbf{K}^*$ and the design point $\boldsymbol{\theta}^*$. To characterize this approximate solution, first define $\sigma_{\theta_i}^2$, i =1,…h as the eigenvalues of the Hessian matrix $\mathbf{H}_s(\mathbf{K},\boldsymbol{\theta}^*)$; i.e., the principal variances of the fitted Gaussian distribution for $s(\mathbf{K},\boldsymbol{\theta})$. Then the approximate solution to the optimal control problem can be expressed as the following simultaneous optimization of $\mathbf{K}$ and $\boldsymbol{\theta}$:

$$\begin{aligned} \mathbf{K}^* &= \arg\min_{\mathbf{K}\in\mathcal{K}} \left\{ \nu_{\mathbf{z}}^{+}(\mathbf{K} \mid \boldsymbol{\theta}^*) T - \log p(\boldsymbol{\theta}^*) + \sum_{i=1}^{h} \log \sigma_{\theta_i}(\mathbf{K}, \boldsymbol{\theta}^*) \right\} \\ \boldsymbol{\theta}^* &= \arg\min_{\boldsymbol{\theta}\in\Theta} \left\{ \nu_{\mathbf{z}}^{+}(\mathbf{K}^* \mid \boldsymbol{\theta}) T - \log p(\boldsymbol{\theta}) \right\} \quad . \end{aligned} \tag{3.36}$$

The agreement between the optimization problems described by (3.35) and (3.36) depends on the accuracy and consistency of the asymptotic approximation in the neighborhood of the optimal solution. If the asymptotic approximation describes sufficiently the main features of the reliability integral and yields a result with a consistent estimation error, then the optimal solutions will be close. In any case this approximation is useful for theoretical comparisons and can serve as an initial approach to a potentially suboptimal gain, which can later be improved by using more accurate, but also more computationally, expensive methods to calculate the reliability integral, for example, stochastic simulation with importance sampling. Most other comments made earlier for the case with no model uncertainty apply also here. In particular, stability conditions must be enforced for all model parameters $\boldsymbol{\theta}$ in the uncertain parameter space.

Contrary to the certain parameter case, the choice of the time duration, T, influences the design optimization. Note that this duration can be interpreted as the time horizon considered in the optimal reliability control problem. To further characterize this influence, a Taylor series expansion is implemented for (3.27), giving:

$$P_F\left(\mathbf{K}\,|\,T,\Theta\right)=-\sum_{j=1}^{\infty}\frac{\left(-T\right)^j}{j!}E_{\boldsymbol{\theta}}\left[\left(\nu_{\mathbf{z}}^{+}\left(\mathbf{K}\,|\,\boldsymbol{\theta}\right)\right)^j\right] \quad . \tag{3.37}$$

The robust-reliability optimal controller is therefore:

$$\mathbf{K}^{*}=\arg\min_{\mathbf{K}\in\mathcal{K}}\left(-\sum_{j=1}^{\infty}\frac{\left(-T\right)^j}{j!}E_{\boldsymbol{\theta}}\left[\left(\nu_{\mathbf{z}}^{+}\left(\mathbf{K}\,|\,\boldsymbol{\theta}\right)\right)^j\right]\right) \quad . \tag{3.38}$$

Thus, robust reliability design weighs the mean value of ν_z^+ (obtained for j=1 in the last infinite sum) against its higher-order moments over the uncertain parameter space, Θ. Time duration T enters the problem as a sensitivity parameter which defines the relative importance of the higher-order statistics.

3.5.1 Short time durations

For $T \to 0$, the reliability optimal controller in (3.38) may be approximated by retaining only the first element of the infinite series in (3.38):

$$\mathbf{K}^* |_{T\to 0} \approx \arg\min_{\mathbf{K}\in\mathcal{K}} \left(E_\Theta \left[\left(\nu_{\mathbf{z}}^+ \left(\mathbf{K} \,|\, \boldsymbol{\theta} \right) \right) \right] \right) \quad . \tag{3.39}$$

Thus, for small time durations, the optimal robust-reliability controller is the one that minimizes the expected value of the out-crossing rate, evaluated over the uncertain parameter space, without considering the higher-order statistics. As $\nu_{\mathbf{z}}^+ T$ increases the higher-order moments become important. The size of T for which the higher-order moments becomes significant depends on the value of the out-crossing rate $\nu_{\mathbf{z}}^+$. Smaller values of $\nu_{\mathbf{z}}^+$ correspond to bigger differences between the moments of different order, and thus to larger values of T for which the higher-order statistics become important in the controller optimization. For time durations for which $\nu_{\mathbf{z}}^+ \left(\mathbf{K} \,|\, \boldsymbol{\theta} \right) T << 1$, the reliability optimal controller may be approximated by truncating only the first few elements of the Taylor series in (3.38).

3.5.2 Infinite time durations

For duration $T \to \infty$, every controller inevitably fails with probability 1. But for civil engineering applications focusing on dynamic response due to earthquakes or wind response, infinite duration is not a realistic case. It is nonetheless instructive to ascertain the nature of $\mathbf{K}^*$ obtained by this limiting case, because it gives some intuition to the consequence of assigning an excessively large time horizon in the optimal control problem. Expression (3.38) provides no insight into the characteristics of reliability controllers in this case. Instead, the expression (3.36) can be used. To simplify the discussion, assume here that for all $\boldsymbol{\theta} \in \Theta$ and all $\mathbf{K} \in \mathcal{K}$, $\nu_{\mathbf{z}}^+ (\mathbf{K} \,|\, \boldsymbol{\theta}) > \delta_\varepsilon$, for δ_ε finite. In other words, assume that

there is no combination of uncertain parameters and control gain which yields infinitesimally small out-crossing rates. In this case, optimization (3.36) is equivalent to:

$$\begin{aligned} \mathbf{K}^*\big|_{T\to\infty} &= \arg\min_{\mathbf{K}\in\mathcal{K}} \left\{ \nu_{\mathbf{z}}^+(\mathbf{K}\,|\,\boldsymbol{\theta}^*) \right\} \\ \boldsymbol{\theta}^*\big|_{T\to\infty} &= \arg\min_{\boldsymbol{\theta}\in\Theta} \left\{ \nu_{\mathbf{z}}^+(\mathbf{K}^*\,|\,\boldsymbol{\theta}) \right\} \quad . \end{aligned} \tag{3.40}$$

Thus, the controller optimization seeks to improve the dynamic performance in regions of the model parameters for which the out-crossing rate is small. This design goal is in contrast to the usual objectives of robust design, as it focuses on regions of the uncertain parameter space for which regulation of the response is not so important, i.e., the out-crossing rate is small, without regard to the plausibility of the models that these regions represent. One could, perhaps, view this outcome as occurring because failure is so likely for all $\boldsymbol{\theta}\in\Theta$ that the optimization concentrates on the value of $\boldsymbol{\theta}$ that provides the "last, best hope" of preventing failure, irrespective of the likelihood of this parameter vector.

The above reasoning does bring to the fore an important point. One does not make a controller design more robust to modeling uncertainty by increasing the time duration over which performance is evaluated. However, a time duration which is too small effectively ignores higher moments in the distribution of $\nu_{\mathbf{z}}^+$ which arise due to parameter uncertainty. The choice of T must therefore be made with some care. The next section illustrates one way to do this, by treating T itself as an uncertain parameter.

3.6 Robust-Reliability Design with Uncertain Time Durations

The time duration T should be taken as the duration of the dynamic excitation, such as that due to a seismic event or wind storm (depending on the purpose of the control system), suggesting that it be treated as an uncertain parameter. A reasonable probability distribution for T is the exponential distribution; i.e.,

$$p(T)=\begin{cases}\dfrac{1}{\overline{T}}\exp\left(-\dfrac{T}{\overline{T}}\right) & T>0\\ 0 & T\le 0\end{cases} \tag{3.41}$$

where its expected value $E[T]=\overline{T}$. The robust probability of failure is then

$$P_F\left(\mathbf{K}\,|\,\overline{T},\Theta\right)=\int_{\Theta}\int_0^{\infty}P_F\left(\mathbf{K}\,|\,T,\boldsymbol{\theta}\right)p(\boldsymbol{\theta})p(T)dTd\boldsymbol{\theta}=1-\int_{\Theta}\frac{p(\boldsymbol{\theta})}{\nu_{\mathbf{z}}^{+}\left(\mathbf{K}\,|\,\boldsymbol{\theta}\right)\overline{T}+1}d\boldsymbol{\theta}\quad . \tag{3.42}$$

Using the asymptotic approximation and following similar steps as previously, the reliability-optimal controller may be found by the simultaneous optimization:

$$\begin{aligned}\mathbf{K}^{*}&=\arg\min_{\mathbf{K}\in\mathcal{K}}\left\{\frac{1+\nu_{\mathbf{z}}^{+}\left(\mathbf{K}\,|\,\boldsymbol{\theta}^{*}\right)\overline{T}}{p(\boldsymbol{\theta}^{*})}\sqrt{\det\left\{\mathbf{M}\left(\mathbf{K},\boldsymbol{\theta}^{*}\right)\right\}}\right\}\\ \boldsymbol{\theta}^{*}&=\arg\min_{\boldsymbol{\theta}\in\Theta}\left\{\frac{1+\nu_{\mathbf{z}}^{+}\left(\mathbf{K}^{*}\,|\,\boldsymbol{\theta}\right)\overline{T}}{p(\boldsymbol{\theta})}\right\}\end{aligned} \tag{3.43}$$

where matrix $\mathbf{M}$ is

$$\mathbf{M}\left(\mathbf{K},\boldsymbol{\theta}\right)=-\nabla_{\boldsymbol{\theta}}\nabla_{\boldsymbol{\theta}}^{T}\log\left\{\frac{p(\boldsymbol{\theta})}{1+\nu_{\mathbf{z}}^{+}\left(\mathbf{K}\,|\,\boldsymbol{\theta}\right)\overline{T}}\right\}\quad . \tag{3.44}$$

With this probabilistic treatment of T, we can still consider small- and large-time-duration cases, as was done for deterministic T in the previous section. However, now, it is with respect to the expected time duration $\overline{T}$ that these asymptotic cases are investigated. In the short-time-duration case, the conclusions are similar. However the infinite-time-duration case turns out to be quite different.

3.6.1 Short mean time durations

For small $\overline{T}$, a Taylor series expansion can be used in the same manner as in the previous section, to arrive at a simpler optimization. Consider that if $\nu_{\mathbf{z}}^{+}\overline{T} < 1 \; \forall \boldsymbol{\theta} \in \Theta$, $\frac{1}{\nu_{\mathbf{z}}^{+}\overline{T}+1} = \sum_{j=0}^{\infty}\left(-\nu_{\mathbf{z}}^{+}\overline{T}\right)^{j}$. Thus,(3.42) can be expanded as:

$$P_F\left(\mathbf{K} \mid \overline{T}, \Theta\right) = -\sum_{j=1}^{\infty}\left(-\overline{T}\right)^{j} E_{\boldsymbol{\theta}}\left[\left(\nu_{\mathbf{z}}^{+}\left(\mathbf{K} \mid \boldsymbol{\theta}\right)\right)^{j}\right] \quad . \tag{3.45}$$

If we further assume that $\overline{T} \to 0$, only the *first* moment of the out-crossing rate is important and the optimal robust-reliability controller is the one that minimizes the mean out-crossing rate over the uncertain parameters space.

$$\mathbf{K}^{*}\mid_{\overline{T}\to 0} = \arg\min_{\mathbf{K}\in\mathcal{K}}\left\{E_{\Theta}\left[\left(\nu_{\mathbf{z}}^{+}\left(\mathbf{K} \mid \boldsymbol{\theta}\right)\right)\right]\right\} \quad . \tag{3.46}$$

This optimization is identical to (3.39) for deterministic short-time durations. This is not surprising, because T is being treated as probabilistic with an arbitrarily-narrow distribution, thus converging to the case of deterministic $T \to 0$.

3.6.2 Infinite mean time durations

A more interesting case is where $\overline{T} \to \infty$. Consider that if $\nu_{\mathbf{z}}^{+}\overline{T} > 1 \; \forall \boldsymbol{\theta} \in \Theta$, $\frac{1}{\nu_{\mathbf{z}}^{+}\overline{T}+1} = -\sum_{j=1}^{\infty}\left(-\nu_{\mathbf{z}}^{+}\overline{T}\right)^{-j}$. Thus, (3.42) can be expanded as

$$P_F\left(\mathbf{K} \mid \overline{T}, \Theta\right) = 1 + \sum_{j=1}^{\infty}\left(-\overline{T}\right)^{-j} E_{\boldsymbol{\theta}}\left[\left(\nu_{\mathbf{z}}^{+}\left(\mathbf{K} \mid \boldsymbol{\theta}\right)\right)^{-j}\right] \quad . \tag{3.47}$$

The robust reliability-optimal controller can then be approximated by retaining only the first two terms of the infinite series:

$$\begin{aligned}\mathbf{K}^* &= \arg\max_{\mathbf{K}\in\mathcal{K}} \left\{ -\sum_{j=1}^{\infty} \left(-\overline{T}\right)^{-j} E_{\boldsymbol{\theta}}\left[\left(\nu_{\mathbf{z}}^{+}\left(\mathbf{K}\,|\,\boldsymbol{\theta}\right)\right)^{-j} \right] \right\} \\ &\approx \arg\max_{\mathbf{K}\in\mathcal{K}} \left\{ E_{\boldsymbol{\theta}}\left[\nu_{\mathbf{z}}^{+}\left(\mathbf{K}\,|\,\boldsymbol{\theta}\right)^{-1} \right] - \overline{T}^{-1} E_{\boldsymbol{\theta}}\left[\nu_{\mathbf{z}}^{+}\left(\mathbf{K}\,|\,\boldsymbol{\theta}\right)^{-2} \right] \right\} \quad .\end{aligned} \tag{3.48}$$

Also, if $\nu_{\mathbf{z}}^{+}\overline{T} >> 1$, it becomes a justifiable approximation to retain only the *first* term of the Taylor expansion in (3.47). In this case (3.48), becomes

$$\mathbf{K}^*\big|_{\overline{T}\to\infty} = \arg\max_{\mathbf{K}\in\mathcal{K}} \left\{ E_{\Theta}\left[\nu_{\mathbf{z}}^{+}\left(\mathbf{K}\,|\,\boldsymbol{\theta}\right)^{-1} \right] \right\} \quad . \tag{3.49}$$

This expression has a very intuitive interpretation. It is straight-forward to show that, for a given $\boldsymbol{\theta}\in\Theta$, the quantity $\nu_{\mathbf{z}}^{+}(\mathbf{K}\,|\,\boldsymbol{\theta})^{-1}$ is the expected (i.e., average) time duration *between* out-crossings in stationary response. Unlike the interpretation of the previous section, this interpretation of "infinite-duration" reliability-optimal control yields a useful result. The idea of maximizing the expected time between out-crossings is a very sensible design strategy. The above development illustrates that this idea does indeed have a connection to reliability-based control problem.

3.6.3 Illustrative example for robust reliability design

The extension of the structural control example discussed earlier for the case that there is some uncertainty in the model parameters is considered here. In most civil engineering applications, significant uncertainty is associated with the excitation model. The bandwidth ω_g and the RMS intensity of the acceleration input a_{RMS} are parameterized in this study as $\omega_g=\theta_f \cdot 2\text{Hz}$ and $a_{RMS}=\theta_R \cdot 0.2\text{g}$, respectively, with the parameters θ_f and θ_R modeled to be independent Gaussian variables with mean value one and coefficient of variation 20% and

10%, respectively. The case considering uncertainties only for the stochastic excitation model is referred to as uncertain case 1 (UC1). We also consider uncertain case 2 (UC2) that additionally includes uncertainty in the values of the inter-story stiffnesses $k_i = \hat{k}_i \theta_{s,i}$, *i=1,2,3,* where the $\hat{k}_i$ are the most probable values, given in Figure 3.4, and $\{\theta_{s,i}\}$ are correlated Gaussian random variables with mean value one and covariance matrix with elements:

$$E\left[\left(\theta_{s,i} - \hat{\theta}_{s,i}\right)\left(\theta_{s,j} - \hat{\theta}_{s,j}\right)\right] = \left(\sigma_\theta\right)^2 \exp\left[-\left(j-i\right)^2 / 2^2\right] \tag{3.50}$$

where σ_θ=0.2 is the standard deviation for each component $\theta_{s,i}$.

The probability of failure is presented for two different assumptions related to the duration of the excitation: (a) using a fixed value of *T*, denoted "Deterministic *T*", and (b) treating *T* as an uncertain parameter with exponential PDF and mean value $\overline{T}$, denoted "Uncertain *T*". The sensitivity of the design to the selection of the time duration and the benefits of including model uncertainty in the control system design are investigated here. For notational convenience, $\overline{T}$ is denoted simply by *T* to give a common label for cases (a) and (b) on the horizontal axis in the following figures. In Figure 3.7, the probability of failure under optimal robust designs and the optimal gain normalized with respect to the nominal reliability optimal gain is plotted for increasing values of *T*. Figure 3.8 presents the statistics for the out-crossing rate over the uncertain parameter space under optimal design for the "Deterministic *T*" assumption.

It should be noted, first, that UC2 involves larger uncertainty in the model description. This is expected to decrease the overall efficiency of the control application since it is more difficult to regulate the response of the system in the whole uncertain space, Θ. That is why the probability of failure and the statistics of the out-crossing rate under optimal design are

significantly larger for UC2. As the time duration, T, increases, the probability of failure increases at an exponential rate, as expected.

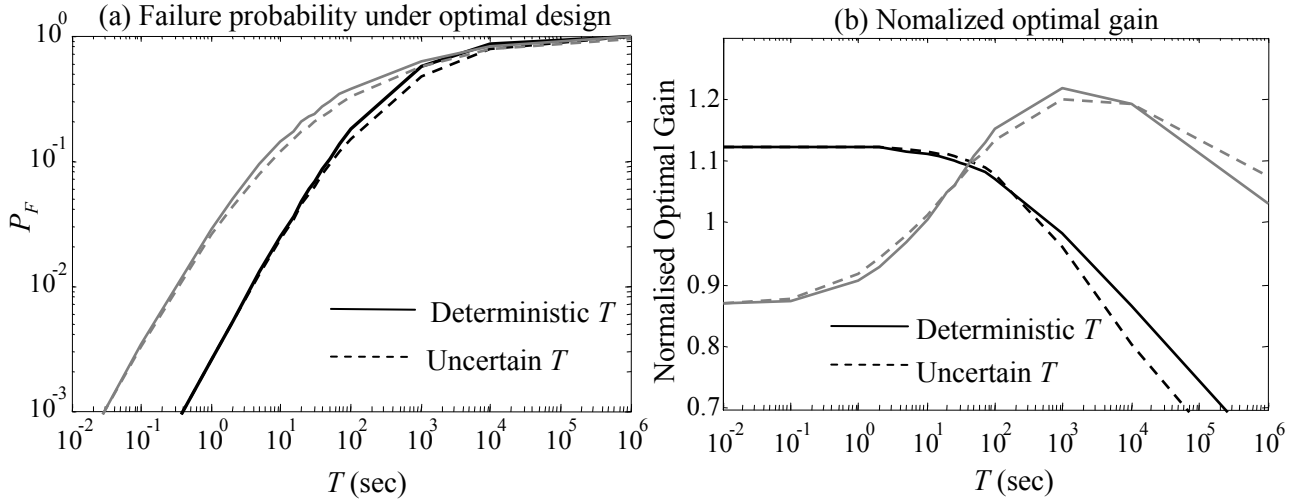

Figure 3.7: (a) Probability of failure under optimal robust-reliability design and (b) normalized optimal gain for UC1(black curves) and UC2 (grey curves)

The variation of T influences additionally the optimal gain and the relative importance of the statistics of the out-crossing rate under optimal design. Except for small time durations, there is some sensitivity of the optimal gain to the value of T. For small T, the probability of failure equals the expected value of the out-crossing rate over the uncertain parameter space and the optimal reliability controller is the one that minimizes this expected value, independent of the value of T. No sensitivity of the design to the value of T exists for this range. As the time duration increases, the higher moments of the out-crossing rate contribute more to the objective function and the reliability design exhibits sensitivity to the value of T. The expected value of the out-crossing rate no longer corresponds to a minimum under optimal design and the characteristics of the other statistics of this out-crossing rate also change. Since the out-crossing rate for UC2 is larger, the value of T for which this change in the design sensitivity occurs is smaller. The difference in the magnitude of the out-crossing rate also influences the relative importance of its statistics in the optimization. For UC1, the second moment is more important in the controller

optimization for either medium or large values of T. The same pattern does not apply to UC2. For large values of T, the second moment is no longer dominant in the controller design. Of course, it should be noted that the trade-off, under optimal design, between the higher order statistics of the out-crossing rate is in general complex and not simply determined by the first three moments for large values of T. The information presented here, though, is sufficient for a general understanding of the trend.

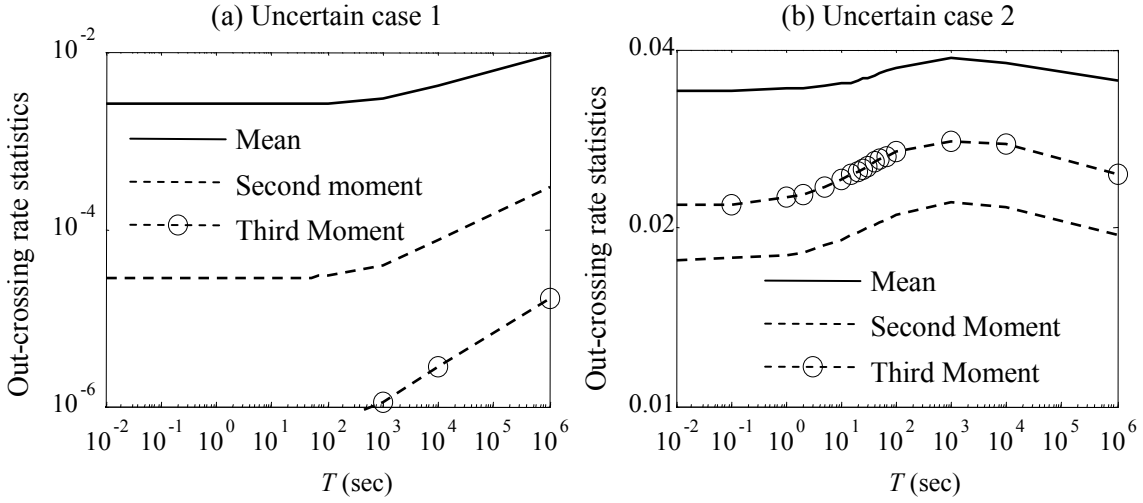

Figure 3.8: Statistics of the out-crossing rate over the uncertain parameter space for optimal robust reliability controller assuming deterministic time duration T for (a) UC1 and (b) UC2

Comparing now the "Deterministic T" and "Uncertain T" cases, it is evident, based on either the calculated reliability or the optimal controller gain in Figure 3.7, that only a small difference exists between them. This verifies the close relationship of the two objective functions in (3.35) and (3.42), discussed previously. This close relationship and the small sensitivity of the control system optimal gain to the exact value of T show that the expected duration of the excitation is an appropriate value to select for the time duration.

Figure 3.7(b) may also be used to obtain information on the difference between the robust and nominal reliability designs since the normalization of the optimal gain for the robust

design has been performed with respect to the nominal optimal gain, which is not affected by the value of T. Such a comparison is better depicted in Figure 3.9, which presents the percentile improvement in reliability performance of the robust design over the nominal one for increasing values of T. The performance improvement in this figure (y-axis) is defined as the ratio of the difference of the failure probabilities corresponding to the nominal and robust designs respectively (performance difference), over the performance (failure probability) of the robust design. Based on this figure, it is evident that there is a considerable improvement in the performance, in the context of the example considered, when the model uncertainty is included in the control system design. For UC2, this improvement is in general smaller because of the smaller overall efficiency of the control application, as discussed earlier.

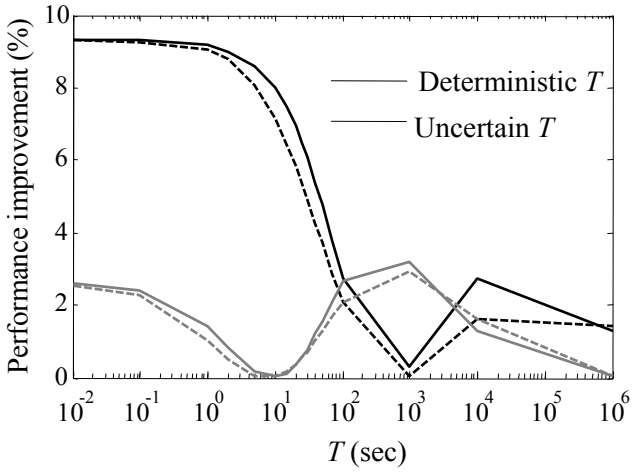

Figure 3.9: Percentile improvement in reliability performance under robust design compared to the nominal design for UC1(black curves) and UC2 (grey curves)

3.7 Probabilistic Robustness for Minimum Variance Control Design

The concept of probabilistically robust controller design is extended in this section to different performance characterizations. Let $J(\mathbf{K},\boldsymbol{\theta})$ denote the deterministic performance measure used to evaluate the behavior of the controlled system, given the values of the model parameters, with the convention again that smaller values for $J(\mathbf{K},\boldsymbol{\theta})$ correspond to

more favorable response. As discussed in Section 2.1, application of the stochastic design framework requires extension of the deterministic performance quantification to a probabilistic one. The two concepts for stochastic system design considered here are (a) the average robustness (AR) and the reliability robustness (RR). The probabilistic performance is expressed, respectively, as the expected value of $J(\mathbf{K},\boldsymbol{\theta})$ over the uncertain parameters, $E_{\boldsymbol{\theta}}[J(\mathbf{K},\boldsymbol{\theta})]$, and the probability that the behavior of the system will exceed some acceptable bound b, $P_{J>b}(\mathbf{K})$. These performance objectives are given by:

$$\begin{aligned} &\text{(a)AR}: \; E[J(\mathrm{K},\boldsymbol{\theta})] = \int_{\Theta} J(\mathbf{K},\boldsymbol{\theta}) p(\boldsymbol{\theta}) d\theta \\ &\text{(b)RR}: P_{J>b}(\mathbf{K}) = E[I_b(\mathbf{K},\boldsymbol{\theta})] = \int_{\Theta} I_b(\mathbf{K},\boldsymbol{\theta}) p(\boldsymbol{\theta}) d\theta \end{aligned} \tag{3.51}$$

where the indicator function I_b=1 if the system behavior is unacceptable, i.e., $J(\mathbf{K},\boldsymbol{\theta})>b$, and I_b=0 if not. The control design approach that uses the latter probabilistic quantification is also referred to as stochastic robustness; see, for example, Wang and Stengel (2002). This approach is directly related to the general notion of system reliability; that is why we have selected the term reliability robustness to characterize it. Finally, the robust controller is given by the optimization

$$\mathbf{K}^* = \arg\min_{\mathbf{K}\in\mathcal{K}} \int_{\boldsymbol{\theta}} h(\mathbf{K},\boldsymbol{\theta}) p(\boldsymbol{\theta}) d\boldsymbol{\theta} \tag{3.52}$$

with the performance measure, $h(\mathbf{K},\boldsymbol{\theta})$, selected either as $J(\mathbf{K},\boldsymbol{\theta})$ or $I_b(\mathbf{K},\boldsymbol{\theta})$ depending on the probabilistic formulation adopted. The evaluation of the first stochastic integral in (3.51) can be performed by the methods described in Section 3.2. The second one, though, cannot be evaluated by those methods because the performance measure is a non-smooth function. This stochastic integral, and the associated optimization problem, can be solved by the methodologies discussed in the following two chapters.

Which of the two probabilistic performance quantifications in (3.51) is more appropriate for control design is directly related to the nature of the metric $J(\mathbf{K},\boldsymbol{\theta})$ and the criteria

adopted in the design, i.e., which objective is more important, regulation of the average performance or the performance that exceeds acceptable bounds? The two different quadratic metrics given by (3.7), the $\mathcal{H}_2$ and the multi-objective $\mathcal{H}_2$ (m$\mathcal{H}_2$) performance, are considered here for the controlled system with specified model parameters. In a probabilistic setting, the most appropriate quantification for the $\mathcal{H}_2$ performance is AR, since the $\mathcal{H}_2$ metric is related to the average response of the system. Such quantification has been discussed also in Boers et al. (1997) and Boers (2002). The first study presented a theoretical investigation and showed that the associated design problem is well-posed. The second discussed necessary and sufficient conditions for the optimal feedback gain but did not address issues related to the estimation of the associated stochastic integrals; it was rather restricted to simple applications for the characterization of the parametric model uncertainty, for which the calculation of these integrals is trivial. For the m$\mathcal{H}_2$ performance both probabilistic quantifications could be appropriate depending on the application, but RR seems in general to be a better choice since the m$\mathcal{H}_2$ metric describes better the extreme response, rather than the mean one. The probabilistic characterization of the m$\mathcal{H}_2$ performance does not seem to have received any special attention in the control literature.

Apart from the probabilistically robust-to-model uncertainty approaches, the worst-case scenario design (denoted WC), a notion closer to the classical interpretation of robust feedback design, is also considered. In this case the optimal controller is designed by minimizing the maximum of the response metric for model parameters $\boldsymbol{\theta}$ belonging in a compact set Θ_c:

$$\mathbf{K}^* = \arg\min_{\mathbf{K}\in\mathcal{K}} \left(\max_{\boldsymbol{\theta}\in\Theta_c} J(\mathbf{K},\boldsymbol{\theta}) \right) \quad . \tag{3.53}$$

For some special cases of performance measures and characterizations of Θ_c this controller synthesis problem can be solved using LMIs, see, for example, Friedman et al. (1995). In

the current study this problem is approached by means of a nonlinear min-max optimization using, as stated earlier, the TOMLAB optimization toolbox.

The structural control example considered in Sections 3.4 and 3.6 is revisited here to illustrate some basic principles related to the concept of probabilistically robust controller synthesis. For the nominal system and for γ=1 the optimal performance for the two quadratic metrics considered is: for $\mathcal{H}_2$ 0.179 and for m$\mathcal{H}_2$ 0.0571. The model parameters that are assumed to have some level of uncertainty are the excitation characteristics θ_f and θ_R and the structural parameters $\{\theta_{s,i}\}$. Two different levels of uncertainty and two different distributions (Gaussian and Uniform) for the model parameters are assumed, leading to the following four cases with respect to the probabilistic models adopted:

Case 1, denoted as G1: all parameters follow Gaussian distributions. θ_f and θ_R follow independent distributions with mean value one and standard deviation 0.1 and 0.05, respectively. $\{\theta_{s,i}\}$ are assumed to be correlated Gaussian random variables with mean value one and covariance matrix elements as given in (3.50), with σ_θ=0.1.

Case 2, denoted as G2: same as Case 1 but with double the standard deviation for all model parameters. This case corresponds to greater variation of the model parameters with respect to their mean value, that is, to a higher level of uncertainty.

Case 3, denoted U1: all parameters follow a uniform distribution inside a compact set $\Theta_{c,1}$, which is defined as $\theta_f \in [0.9, 1.1]$, $\theta_R \in [0.9, 1.1]$, $\theta_{s,i} \in [0.9, 1.1]$. This selection corresponds to the same mean value and a half-spread equal to one standard deviation with respect to the uncertainty in Case 1. The uncertainty level is, thus, comparable to G1.

Case 4, denoted U2: same as Case 2 but with double the half-spread. The uncertainty level for this case is comparable to G2.

These four cases correspond, ultimately, to different prior knowledge for the model parameter values in terms of both the quality and the level of uncertainty. The worst case design is considered for sets $\Theta_{c,1}$ and $\Theta_{c,2}$; the corresponding performance metrics are denoted by WC1 and WC2, respectively. For the RR performance objective the threshold b is considered as a scaling of the optimal nominal performance $b=0.0571\gamma_b$, where 0.0571 is the optimal m$\mathcal{H}_2$ performance for the nominal system and γ_b is the scaling factor that defines the acceptable performance bound relative to that optimal performance. For better comparison when presenting the results the control gain is normalized with respect to the optimal m$\mathcal{H}_2$ gain for the nominal system. Also to better guide the discussion only the results that were deemed interesting are presented.

3.7.1 Average robustness for $\mathcal{H}_2$ performance

The variation of AR, WC, and nominal $\mathcal{H}_2$ performance with respect to the feedback gain is presented in Figure 3.10. Each curve in the figure represents different performance quantification. The minimum of each curve corresponds to the optimal design according to that performance quantification, i.e., metric. The efficiency of other control synthesis methods with respect to that metric should be judged by comparison to the optimal performance attained at that point. The curves related for AR and WC performance also differentiate between the various cases considered for the parametric model uncertainty.

The difference in the optimal gains as well as in the established performance between the various feedback selections is clearly illustrated in Figure 3.10. The results indicate the importance of adopting a probabilistic characterization for model uncertainty compared to the nominal design (Figure 3.10(a)); this importance is bigger for the cases that correspond to greater uncertainty level. Very small differences exist between cases G1 and U1 (which correspond to the same level of uncertainty but different distributions for the model parameters); this shows that the AR $\mathcal{H}_2$ performance, and therefore design, are relatively insensitive to the specific probability distributions of the parametric model uncertainty. The

comparison in Figure 3.10(b) shows potential differences in attainable performance and optimal gains between AR and WC designs. These differences are bigger when the set Θ_c considered for the possible values for the model parameters is bigger and indicates that the worst-case design approach is not appropriate when additional information about these values is available (quantified here by assigning PDFs to them) and the metric used is related to the average performance of the system.

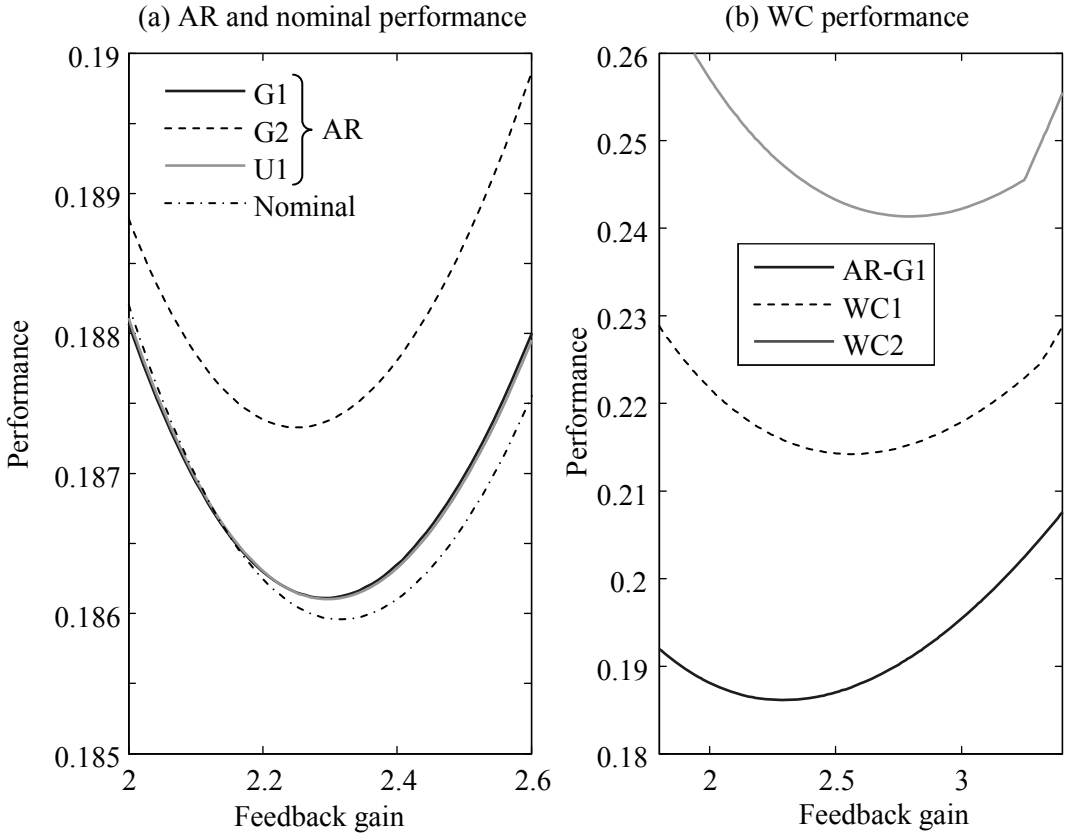

Figure 3.10: Nominal, average, and worst case $\mathcal{H}_2$ performance for variations of the feedback gain

3.7.2 Average and reliability robustness for m$\mathcal{H}_2$ performance

The variation of AR, WC, and nominal m$\mathcal{H}_2$ performance with respect to the feedback gain is presented in Figure 3.11. The presentation is similar to that in Figure 3.10. The results in

this figure verify most of the earlier comments made for the AR performance and design with respect to the $\mathcal{H}_2$ metric.

The results for the RR design are illustrated in Figure 3.12, Figure 3.13, and Figure 3.14. Figure 3.12 includes the optimal gain and the corresponding optimal performance for variation of the threshold γ_b. Increase of the threshold is equivalent to defining the unacceptable performance as corresponding to rare events (it leads to reduction of the probability of failure). Note that the WC approach in the setting considered here (worst case performance considering variations of the model parameters away from their nominal values) can be also interpreted as corresponding to design focusing on rare events.

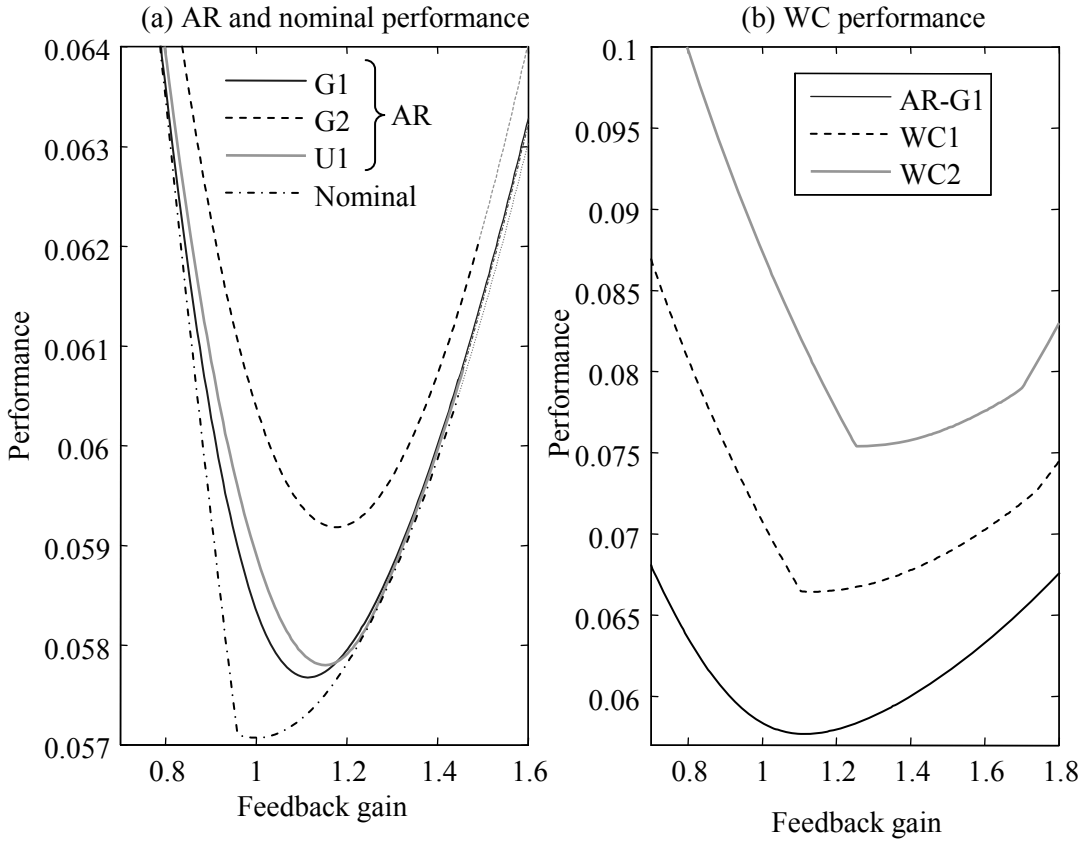

Figure 3.11: Nominal, average, and worst case m$\mathcal{H}_2$ performance for variations of the feedback gain

Figure 3.13 shows the variation of the RR performance with respect to the feedback gain for U1 and four different selections of the acceptable performance threshold for RR. The RR performance is shown in terms of both the failure probability (left plot) as well as of the normalized performance (right plot). The normalization in the latter case is performed with respect to the probability of failure corresponding to the optimal design. The optimal controller selection for Nominal, AR, WC1, and WC2 designs are also included in these plots for direct comparison (correspond to vertical lines). Figure 3.14 presents similar results, but for the model uncertainty corresponding to case G1.

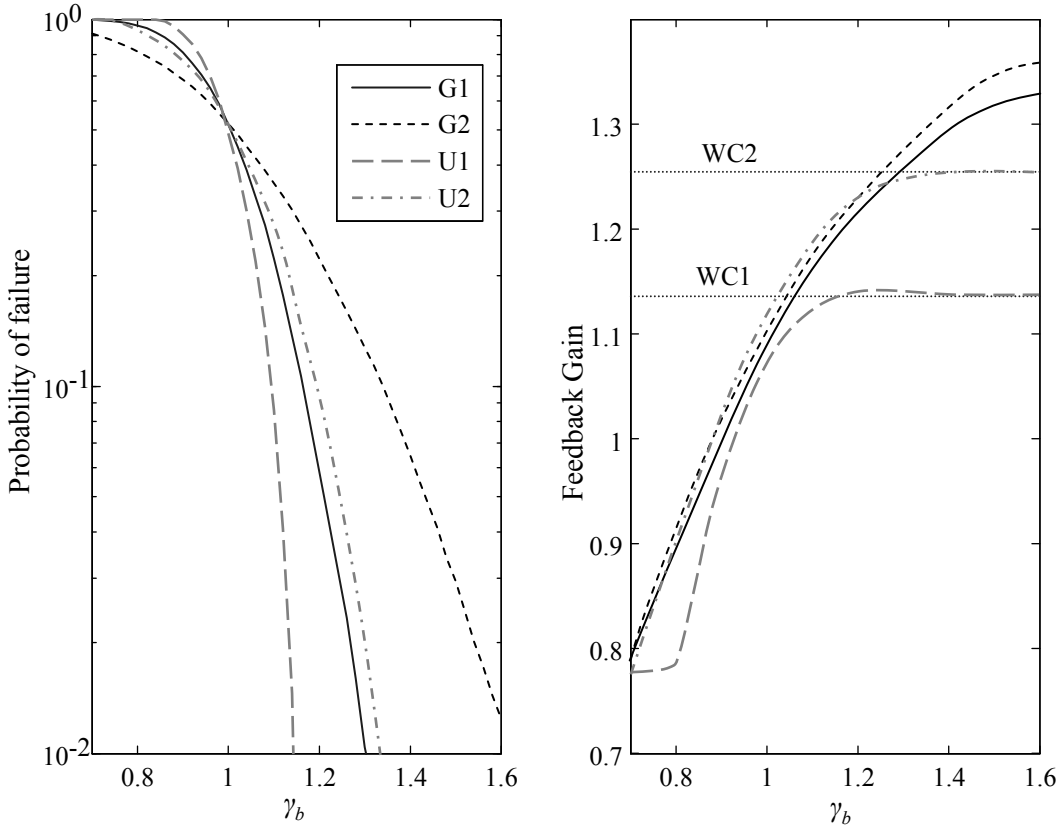

Figure 3.12: (a) Probability of failure under optimal design and (b) corresponding optimal gain for RR design for variation of the acceptable performance threshold. Horizontal lines in plot (b) correspond to optimal gain for WC design methods

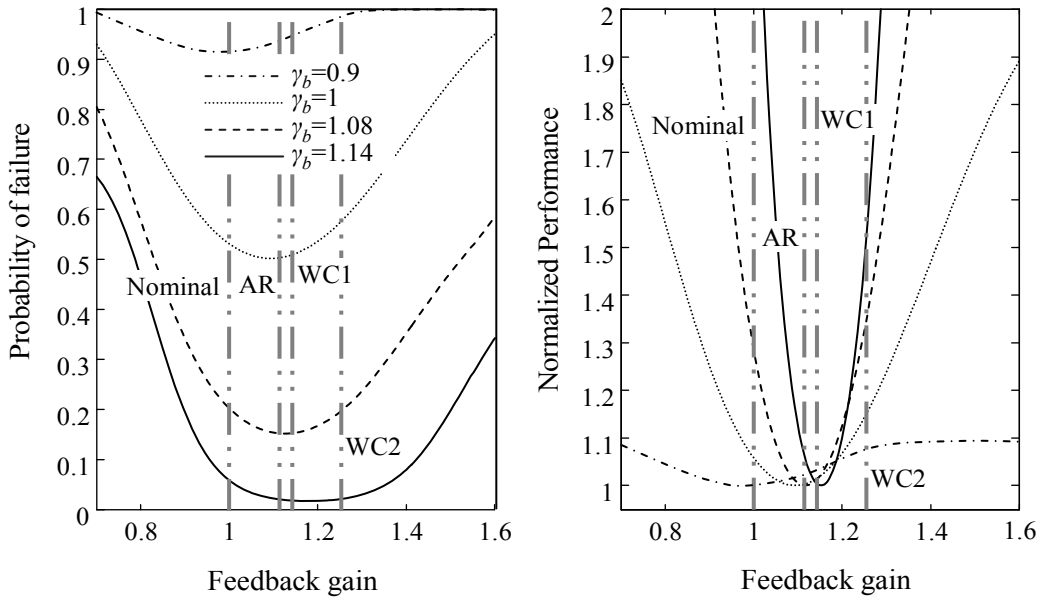

Figure 3.13: RR performance for variation of the feedback gain for U1 case for model uncertainty. Vertical lines correspond to optimal controller for other synthesis methods

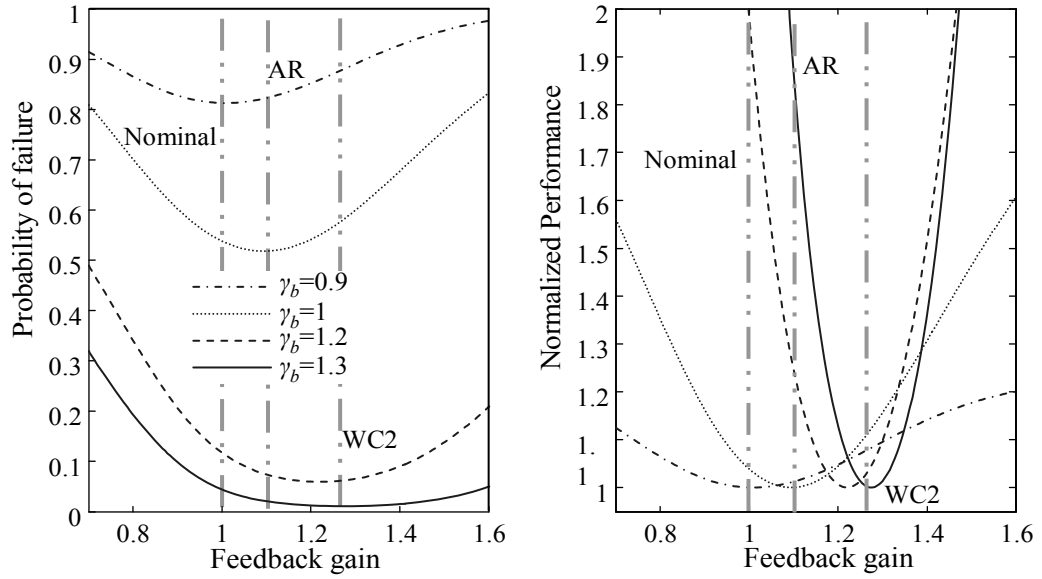

Figure 3.14: RR performance for variation of the feedback gain for G1 case for model uncertainty. Vertical lines correspond to optimal controller for other synthesis methods

The results in Figure 3.11, Figure 3.12, Figure 3.13, and Figure 3.14 indicate, again, the importance of adopting a probabilistic characterization for model uncertainty compared to the nominal design. This importance is greater for reliability-based quantification of the probabilistic performance, especially when the focus is on rare events. The comparison to the robust WC design shows also differences in attainable performance. These differences are, as expected, smaller for the performance quantification that focuses on rare events, that is, RR performance, and larger thresholds for the acceptable response.

With respect to the RR design (Figure 3.12, Figure 3.13, and Figure 3.14), it is evident that as the threshold for acceptable performance increases, the optimal design configuration moves further away from the nominal and the AR designs and it gets closer to a worst-case scenario design approach. Also the sensitivity of the normalized performance objective around that optimal configuration becomes larger. This latter characteristic is obvious when comparing the normalized performances (right plot in Figure 3.13 and Figure 3.14) and leads to an important implication: for designs problems for which the focus is on rare events, i.e., larger thresholds that determine acceptable system performance, the benefits from using an explicit reliability-based design approach are greater, compared to the designs that consider the nominal or the average performance. The explanation is simple: as the threshold increases, the regions in the model parameter space, Θ, that (a) lead to unacceptable performance and (b) have non-negligible probability for the model parameters $p(\boldsymbol{\theta})$, become smaller. Since in reliability context it is only important to regulate the performance in these small regions, the optimal controller can be quite different than the AR one, which focuses on the performance on the average inside Θ, or the nominal one, which only considers the nominal model parameter values. This will occur if these regions are different than the regions for the model parameter values that are important for the other designs, and ultimately depends on the characteristics of the uncertainty model used; that is, to the extent of the designers information about the true system. Additionally, as the threshold increases the comparative effectiveness of the optimal controller becomes greater, because it is easier to regulate the performance in the smaller regions in the model

parameter space that are important for the system reliability. This leads to the greater sensitivity, as mentioned earlier. All these patterns discussed here agree also with the behavior identified in Subsection 3.4.4. In that case the uncertainty referred solely to the stochastic input.

Note that for the U1 and U2 cases the space for the values of the model parameters, Θ, is, respectively, equivalent to the sets, $\Theta_{c,1}$ and $\Theta_{c,2}$, that are considered in the WC1 and WC2 designs. That is why as the threshold for the RR design becomes larger: the optimal design configuration converges asymptotically to the corresponding one for the worst-case design. For G1 and G2 this is not true since the model parameters can, with non-zero probability, have values that lay outside $\Theta_{c,1}$ or $\Theta_{c,2}$.

Another interesting discussion of these results is associated to the comparison between the different probability models for the uncertainty quantification. Comparing cases G1 and U1, or G2 and U2, (which correspond to a similar level of uncertainty but different distributions for the model parameters, that is, to different information entropies), it is evident that small differences exist between the AR performances, but they are larger between the RR performances. Additionally the differences between the AR m$\mathcal{H}_2$ performances, though small, are bigger than the differences when discussing in terms of the AR $\mathcal{H}_2$ performance (Section 3.7.1). This indicates that some small sensitivity exists to the specific probability distributions of the parametric model uncertainty for the m$\mathcal{H}_2$ performance for average robustness quantification. For the reliability robustness quantification a significant sensitivity exists. The level of uncertainty has some influence on the design, especially for the reliability-based performance quantification. For larger uncertainty levels, it is more difficult to regulate the performance in the whole model parameter space; this leads to larger failure probabilities (compare for example the performance between G1 and G2). Differences in optimal gain are reported only for large thresholds. It is interesting to note that for γ_b equal to 1, that is, a threshold for the acceptable performance equal to the optimal nominal performance, there are minimal

differences between the 4 different designs in terms of either the optimal gain or the corresponding performance level (failure probability). Also the optimal gains in this case are close to the nominal optimal gain and the optimal AR gain; this means that there is an equivalence of the performance quantification between all these design methods.

One final comparison is warranted between the two different probabilistic performance quantifications, the AR and the RR: The connection between them, in this example, depends strongly on the definition of acceptable performance. If the focus is on rare events then these design objectives have significantly different characteristics and corresponding optimal design configurations. These remarks illustrate that important differences may exist between the two objectives. Thus, the designer needs to exercise some level of caution when defining the performance measure in the stochastic design framework.

3.8 Concluding Remarks

The robust-to-model-uncertainty controller design for linear systems was addressed in this chapter. Both (i) reliability-based design and (ii) incorporation of measures of probabilistic robustness to classical linear control methodologies were discussed. For a system under stationary stochastic excitation it was demonstrated that the difference in the optimal design configuration between reliability-based design and minimum variance design, even for a model with simple dynamics and control law, can be important. Even though the reliability-based controller design involves a challenging, non-convex, nonlinear optimization, the potential improvement of the system's reliability over other synthesis methods may justify the extra computational effort. Additionally, controllers optimized by explicitly considering modeling uncertainties were demonstrated to yield considerable improvement in performance compared to controllers optimized using only a nominal model, or the usual control robustness notion of worst-case scenario design. This, again, justifies the additional computational cost that is involved in the design process when including probabilistic descriptions for model uncertainty. Also, significant differences were shown in the design characteristics between the concepts of average robustness and reliability robustness for

quantifying the stochastic performance, particularly when the focus of the latter is on rare events. The reliability robustness was shown to have a strong sensitivity to the level of uncertainty considered and a small sensitivity to the specific probability distribution functions used to quantify the missing information about the system. The average robustness was reported to be insensitive to both of these characteristics.

It should be noted that the research presented here for extending the ideas of probabilistic robustness to classical control methodologies represents only a first step towards systematic stochastic design of feedback controllers. The analysis was based on solving nonlinear optimization problems, which can be a quite challenging task when higher-order dynamic controllers are considered. A more thorough analytical approach is warranted, if possible, to allow for in-depth theoretical comparisons and for extension of the design methodology to complex controller structures. Certain simplifications with respect to the probability models for the parametric uncertainty could be employed as a first step for developing these approaches.

In terms of the suggested stochastic system design approach, the methodologies considered in this chapter exploit the characteristics of the design problem to simplify the calculation of the performance objective and solve the stochastic programming problem. For systems that do not fulfill the necessary properties for applying these design approaches, approximation techniques may be adopted. The study by Taflanidis, Beck and Angelides (2007) provides an interesting example related to the reliability-based design of Liquid Column Mass Dampers (LCMDs). The response of LCMDs involves a nonlinear damping term. Statistical linearization was suggested in that study for framing an equivalent linear system and implementing the reliability-based design methodology considered in Sections 3.3 and 3.4. It was shown in that paper that this approach is sufficient when the focus is only on the response of the structural system, but cannot be extended to design problems for which the reliability of the damper response needs to be also considered. This is attributed to the limitation of traditional statistical linearization techniques to describe

reliability-based characteristics (Roberts and Spanos 2003). This discussion illustrates that special attention is always needed for extending specialized techniques to systems for which all desired properties do not explicitly hold.

In the following chapters a direct approach is discussed for complex stochastic design problems. This approach is not based on adaptation of any approximation technique. Rather, a simulation-based methodology is suggested for the evaluation of the system performance.

CHAPTER 4

Stochastic Subset Optimization

In Chapter 3 a computationally efficient approach to stochastic design was discussed for problems for which the system performance can be analytically evaluated, the uncertain parameter vector is low dimensional, and the integrand in the stochastic integral corresponds to a smooth function. These characteristics allow for efficient approximation of the stochastic integrals and make the associated design optimization less challenging. At the same time they impose restrictions on the applicability of the proposed design methodology. At this point the focus is turned to stochastic design for complex systems. For such systems the aforementioned properties cannot be guaranteed, unless specialized approximate approaches are adopted for modeling the physical system or evaluating its response. But when such approaches are involved there is typically no guarantee that the design optimization leads to a favorable design configuration in terms of the actual system. Contrary, a simulation-based approach for evaluating the system model response and the associated stochastic integrals allow for efficient analysis of complex systems, with no need to implement specialized or approximate techniques.

Chapters 4 and 5 address the design optimization problem when stochastic simulation is used for evaluating the performance objective. The current chapter presents a novel algorithm, called Stochastic Subset Optimization (SSO), for efficiently exploring the sensitivity of the optimization objective to the design variables, and iteratively identifying a subset of the original design space that has high plausibility of containing the optimal

design variables. Statistical properties, appropriate stochastic simulation techniques for complex system models, and stopping criteria for the iterative approach are presented. An efficient two-stage framework for the stochastic optimization is then discussed in the next chapter, in which SSO is combined with some other stochastic search algorithm. In Chapters 4 and 5 only theoretical characteristics are presented. Numerical examples related to the suggested framework are discussed in detail in Chapter 6.

The development of SSO has been also published in Taflanidis and Beck (2006b, 2007a, 2007b).

4.1 Stochastic Subset Optimization

Consider, initially, the modified positive function, $h_s(\boldsymbol{\varphi},\boldsymbol{\theta}) : \mathbb{R}^{n_\varphi} \mathrm{x} \mathbb{R}^{n_\theta} \rightarrow \mathbb{R}^+$, as:

$$h_s(\boldsymbol{\varphi},\boldsymbol{\theta}) = h(\boldsymbol{\varphi},\boldsymbol{\theta}) - s \quad \text{where} \quad s < \min_{\boldsymbol{\varphi},\boldsymbol{\theta}} h(\boldsymbol{\varphi},\boldsymbol{\theta}) \tag{4.1}$$

and note that $E_{\boldsymbol{\theta}}[h_s(\boldsymbol{\varphi},\boldsymbol{\theta})] = E_{\boldsymbol{\theta}}[h(\boldsymbol{\varphi},\boldsymbol{\theta})] - s$. Since the two expected values differ only by a constant, optimization of the expected value of $h(.)$ is equivalent, in terms of the optimal design choice, to optimization for the expected value for $h_s(.)$. In the SSO setting we focus on the latter optimization.

4.1.1 Augmented problem

The basic idea in SSO is the formulation of an augmented problem, a general concept initially discussed in Au (2005) for reliability-based design problems, where the design variables are artificially considered as uncertain with distribution $p(\boldsymbol{\varphi})$ over the design space Φ. In the setting of this augmented stochastic design problem, define the auxiliary PDF:

$$\pi(\boldsymbol{\varphi},\boldsymbol{\theta}) = \frac{h_s(\boldsymbol{\varphi},\boldsymbol{\theta})\, p(\boldsymbol{\varphi},\boldsymbol{\theta})}{E_{\boldsymbol{\varphi},\boldsymbol{\theta}}[h_s(\boldsymbol{\varphi},\boldsymbol{\theta})]} \propto h_s(\boldsymbol{\varphi},\boldsymbol{\theta})\, p(\boldsymbol{\varphi},\boldsymbol{\theta}) \tag{4.2}$$

where $p(\boldsymbol{\varphi},\boldsymbol{\theta})=p(\boldsymbol{\varphi})p(\boldsymbol{\theta}|\boldsymbol{\varphi})$. The normalizing constant in the denominator is defined as:

$$E_{\boldsymbol{\varphi},\boldsymbol{\theta}}[h_s(\boldsymbol{\varphi},\boldsymbol{\theta})] = \int_{\Phi}\int_{\Theta} h_s(\boldsymbol{\varphi},\boldsymbol{\theta})\, p(\boldsymbol{\varphi},\boldsymbol{\theta}) d\boldsymbol{\theta} d\boldsymbol{\varphi} \tag{4.3}$$

and corresponds to the expected value of the performance measure in the augmented uncertain space. This expected value is not explicitly needed, but it can be obtained though stochastic simulation, which leads to an expression similar to (2.4) but with the pair [$\boldsymbol{\varphi}$, $\boldsymbol{\theta}$] defining the uncertain parameters. The transformation of the performance measure in (4.1) may be necessary to ensure that $\pi(\boldsymbol{\varphi},\boldsymbol{\theta})\geq 0$. For many stochastic design problems $h(\boldsymbol{\varphi},\boldsymbol{\theta})\geq 0$ and the transformation in (4.1) is unnecessary.

In terms of the auxiliary PDF, the objective function, $E_{\boldsymbol{\theta}}[h_s(\boldsymbol{\varphi},\boldsymbol{\theta})]$, can be expressed as:

$$E_{\boldsymbol{\theta}}[h_s(\boldsymbol{\varphi},\boldsymbol{\theta})] = \frac{\pi(\boldsymbol{\varphi})}{p(\boldsymbol{\varphi})} E_{\boldsymbol{\varphi},\boldsymbol{\theta}}[h_s(\boldsymbol{\varphi},\boldsymbol{\theta})] \tag{4.4}$$

where the marginal PDF $\pi(\boldsymbol{\varphi})$ is equal to:

$$\pi(\boldsymbol{\varphi}) = \int_{\Theta} \pi(\boldsymbol{\varphi},\boldsymbol{\theta}) d\boldsymbol{\theta} \quad . \tag{4.5}$$

Define, now:

$$J(\boldsymbol{\varphi}) = \frac{E_{\boldsymbol{\theta}}[h_s(\boldsymbol{\varphi},\boldsymbol{\theta})]}{E_{\boldsymbol{\varphi},\boldsymbol{\theta}}[h_s(\boldsymbol{\varphi},\boldsymbol{\theta})]} = \frac{\pi(\boldsymbol{\varphi})}{p(\boldsymbol{\varphi})} \quad . \tag{4.6}$$

Since $E_{\boldsymbol{\varphi},\boldsymbol{\theta}}[h_s(\boldsymbol{\varphi},\boldsymbol{\theta})]$ can be viewed simply as a normalizing constant, minimization of $E_{\boldsymbol{\theta}}[h_s(\boldsymbol{\varphi},\boldsymbol{\theta})]$ is equivalent to the minimization of $J(\boldsymbol{\varphi})$. For this purpose the marginal PDF

$\pi(\boldsymbol{\varphi})$ in the numerator of $J(\boldsymbol{\varphi})$ must be evaluated. Samples of this PDF can be obtained through stochastic simulation techniques. Appendix 4A briefly discusses two appropriate sampling algorithms, one using a direct approach to Monte Carlo (MC) simulation and one using Markov Chain Monte Carlo (MCMC) simulation. These algorithms will give sample pairs $[\boldsymbol{\varphi},\boldsymbol{\theta}]$ that are distributed according to the joint distribution $\pi(\boldsymbol{\varphi},\boldsymbol{\theta})$. Their $\boldsymbol{\varphi}$ component corresponds to samples from the marginal distribution $\pi(\boldsymbol{\varphi})$. SSO is based on exploiting the information in these samples

4.1.2 Subset analysis

Analytical approximations of $\pi(\boldsymbol{\varphi})$ based on the samples for $\boldsymbol{\varphi}$, was performed efficiently in Ching and Hsieh (2007), using the maximum entropy method for optimizations with reliability constraints, where the relationship of the probability of failure to the design variables was almost linear. Extension to optimization problems involving a stochastic integral as the objective function may be more challenging. The maximum entropy method corresponds, ultimately, to a polynomial approximation to $\log(\pi(\boldsymbol{\varphi}))$. Experience indicates that for challenging problems, including, for example, cases where the dimension n_φ is not small or the sensitivity for a design variable is complex, such approximations may be problematic. Alternative methods for estimating $\pi(\boldsymbol{\varphi})$ are kernel density estimators and histograms, as discussed in Au (2005). The first choice, though, may lead to spurious noise in the PDF that is difficult to interpret and the second can only be efficiently implemented if the dimension of the design parameter vector is small (e.g., not larger than two). In the SSO framework, such approximation of $\pi(\boldsymbol{\varphi})$ is avoided. The sensitivity analysis is performed by looking at the average value of $J(\boldsymbol{\varphi})$ over any subset of the design space $I \subset \Phi$, denoted by $H(I)$:

$$H(I) \triangleq \frac{\int_I J(\boldsymbol{\varphi}) d\boldsymbol{\varphi}}{V_I} \propto \frac{\int_I E_{\boldsymbol{\theta}}[h_s(\boldsymbol{\varphi},\boldsymbol{\theta})] d\boldsymbol{\varphi}}{V_I} \quad . \tag{4.7}$$

This term is also proportional, ignoring normalization constants, to the average value of the objective function in set I. To simplify the evaluation of $H(I)$, a uniform distribution is chosen for $p(\boldsymbol{\varphi})$. Note that $p(\boldsymbol{\varphi})$ does not reflect the uncertainty in $\boldsymbol{\varphi}$ but is simply a device for formulating the augmented problem, and thus can be selected according to convenience. Finally, $H(I)$ and an estimate of it based on the samples from $\pi(\boldsymbol{\varphi})$ obtained as described previously, are given, respectively, by:

$$H(I) = \frac{V_\Phi}{V_I} \int_I \pi(\boldsymbol{\varphi}) d\boldsymbol{\varphi} \tag{4.8}$$

$$\hat{H}(I) = \frac{N_I / V_I}{N_\Phi / V_\Phi} \tag{4.9}$$

where N_I and N_Φ denote the number of samples from $\pi(\boldsymbol{\varphi})$ belonging to the sets I and Φ, respectively, and V_I and V_Φ the volume of sets I and Φ, respectively. The estimate for $H(I)$ is equal to the ratio of the volume density of samples from $\pi(\boldsymbol{\varphi})$ in sets I and Φ. The coefficient of variation (c.o.v.) for this estimate depends on the simulation technique used for obtaining the samples from $\pi(\boldsymbol{\varphi})$. For a broad class of sampling algorithms this c.o.v. may be expressed as:

$$\text{c.o.v. } \hat{H}(I) = \sqrt{\frac{1 - P(\boldsymbol{\varphi} \in I)}{N \cdot P(\boldsymbol{\varphi} \in I)}} \approx \sqrt{\frac{1 - N_I / N_\Phi}{N \cdot N_I / N_\Phi}} \tag{4.10}$$

where

$$P(\boldsymbol{\varphi} \in I) \triangleq \int_I \pi(\boldsymbol{\varphi}) d\boldsymbol{\varphi} \approx N_I / N_\Phi \tag{4.11}$$

and $N = N_\Phi/(1+\gamma_s)$, $\gamma_s \geq 0$, is the effective number of independent samples. If direct Monte Carlo techniques are used then $\gamma_s = 0$, but if Markov Chain Monte Carlo (MCMC) sampling

is selected then $\gamma_s>0$, because of the correlation of the generated samples. Ultimately, the value of γ_s depends on the characteristics of the algorithm used. For example Au and Beck, (2003) provide for a formula for γ_s when the Metropolis-Hasting algorithm is used.

For the uniform PDF for $p(\boldsymbol{\varphi})$, note that $H(\Phi)=1$, the integral in (4.3) is equal to the average value in Φ of the objective function, $E_{\boldsymbol{\theta}}[h_s(\boldsymbol{\varphi},\boldsymbol{\theta})]$, and $H(I)$ is equal to the ratio:

$$H(I)=\frac{\int_I E_{\boldsymbol{\theta}}[h_s(\boldsymbol{\varphi},\boldsymbol{\theta})]d\boldsymbol{\varphi}/V_I}{\int_\Phi E_{\boldsymbol{\theta}}[h_s(\boldsymbol{\varphi},\boldsymbol{\theta})]d\boldsymbol{\varphi}/V_\Phi} \tag{4.12}$$

where the integrals in the numerator and denominator correspond to the average value of the objective function in sets I and Φ, respectively. Thus $H(I)$ expresses the average relative sensitivity of $E_{\boldsymbol{\theta}}[h_s(\boldsymbol{\varphi},\boldsymbol{\theta})]$ to $\boldsymbol{\varphi}$ within the set $I\subset\Phi$. Greater sensitivity, i.e., bigger contrast in the average value (volume density) of the objective function, corresponds to smaller values for $H(I)$.

A similar ratio, that will be used later on, is the ratio of the integrals for the objective function:

$$R(I)=\frac{\int_I E_{\boldsymbol{\theta}}[h_s(\boldsymbol{\varphi},\boldsymbol{\theta})]d\boldsymbol{\varphi}}{\int_\Phi E_{\boldsymbol{\theta}}[h_s(\boldsymbol{\varphi},\boldsymbol{\theta})]d\boldsymbol{\varphi}}=\frac{\int_I J(\boldsymbol{\varphi})d\boldsymbol{\varphi}}{\int_\Phi J(\boldsymbol{\varphi})d\boldsymbol{\varphi}} \quad . \tag{4.13}$$

An estimate for this ratio, using the samples from $\pi(\boldsymbol{\varphi})$ is:

$$\hat{R}(I)=\frac{N_I}{N_\Phi} \quad . \tag{4.14}$$

4.1.3 Deterministic subset optimization

Consider a set of admissible subsets A in Φ that have some predetermined shape and some size constraint, for example, related to the set volume, and define the *deterministic subset optimization*:

$$I^* = \arg\min_{I \in A} H(I) \quad . \tag{4.15}$$

Optimization (4.15) identifies the set that gives the smallest average value of $J(\boldsymbol{\varphi})$ (or equivalently $E_{\boldsymbol{\theta}}[h_s(\boldsymbol{\varphi},\boldsymbol{\theta})]$) within the class of admissible subsets A. If set A is properly chosen, for example, if its shape is "close" to the contours of $E_{\boldsymbol{\theta}}[h_s(\boldsymbol{\varphi},\boldsymbol{\theta})]$ in the vicinity of $\boldsymbol{\varphi}^*$, then $\boldsymbol{\varphi}^* \in I^*$ for the optimization in (4.15). The following argument illustrates this point.

Let the admissible subsets be defined as $A=\{I \subset \Phi : V_I = V_o\}$ and let I_ε be the region bounded by the level surface:

$$\mathcal{D}I_\varepsilon = \{\boldsymbol{\varphi} \in \Phi : (1+\varepsilon_l) J(\boldsymbol{\varphi}^*) = J(\boldsymbol{\varphi})\} \quad . \tag{4.16}$$

In some neighborhood of $\boldsymbol{\varphi}^*$, i.e., for some $\varepsilon_l \in (0,\varepsilon_m)$, the level surfaces $\mathcal{D}I_\varepsilon$ will be closed sets confining a simply connected subset I_ε. If $J(\boldsymbol{\varphi})$ is convex in the neighborhood of I_ε, then the volume V_{I_ε} will be a monotonically increasing function of ε, so if V_o is sufficiently small, $\exists\, e \in (0,\varepsilon_m)$ such that $V_{I_e} = V_o$. If, additionally, $V_o \to 0$ then $I_e \to \boldsymbol{\varphi}^*$. As V_o increases it is expected, since V_{I_ε} is monotonically increasing, that:

$$I_e = I^* = \arg\min_{I \in A} H(I) \quad . \tag{4.17}$$

Since $\boldsymbol{\varphi}^* \in I_e$ this means that $\boldsymbol{\varphi}^* \in I^*$.

4.1.4 Stochastic subset optimization

In the setting of the augmented stochastic problem and based on the estimate in (4.8), optimization (4.15) is approximately equal to the following *stochastic subset optimization*:

$$\hat{I} = \arg\min_{I \in A} \hat{H}(I) = \arg\min_{I \in A} \frac{N_I}{V_I} \tag{4.18}$$

which involves identification of the set $I \in A$ that contains the smallest volume density N_I/V_I of samples. Note that the computational cost for obtaining the samples needed for this optimization is comparable to the cost required for a single evaluation of the objective function in (2.4), depending on how many samples are simulated and the details of the algorithm used.

It was argued before that if A is properly chosen, then, with respect to the optimization in (4.15) for I^*, the optimum design variables $\boldsymbol{\varphi}^* \in I^*$. This argument is not necessarily true for the optimization in (4.18) because only estimates of $H(I)$ are used. $\hat{I}$ is simply the set, within the admissible subsets A, that has the largest likelihood, in terms of the information available through the obtained samples, of including $\boldsymbol{\varphi}^*$. This likelihood defines the quality of the identification and ultimately depends on $H(I)$; taking into account the fact that the average value of $E_{\boldsymbol{\theta}}[h_s(\boldsymbol{\varphi},\boldsymbol{\theta})]$ in the neighborhood of the optimal solution is the smallest in Φ, it is evident (see equation (4.12)) that smaller values of $H(\hat{I})$ correspond to greater plausibility for the set $\hat{I}$ to include $\boldsymbol{\varphi}^*$. Since only estimates of $H(\hat{I})$ are available in the stochastic identification, the quality depends, ultimately, on both (a) the estimate $\hat{H}(\hat{I})$ and (b) its coefficient of variation (defining the accuracy of that estimate). Large values for $\hat{H}(\hat{I})$, i.e., close to 1, correspond to a density for the failed samples that approximates a uniform distribution in Φ and indicate that the identified set $\hat{I}$ has lower likelihood of containing $\boldsymbol{\varphi}^*$. The c.o.v. for $\hat{H}(\hat{I})$ defines its accuracy. Smaller values for the c.o.v.

correspond to higher accuracy and, in the end, to greater plausibility for the set $\hat{I}$ to include $\boldsymbol{\varphi}^*$. Both the value for $\hat{H}(\hat{I})$ and its c.o.v. should be taken into account when evaluating the quality of the identification.

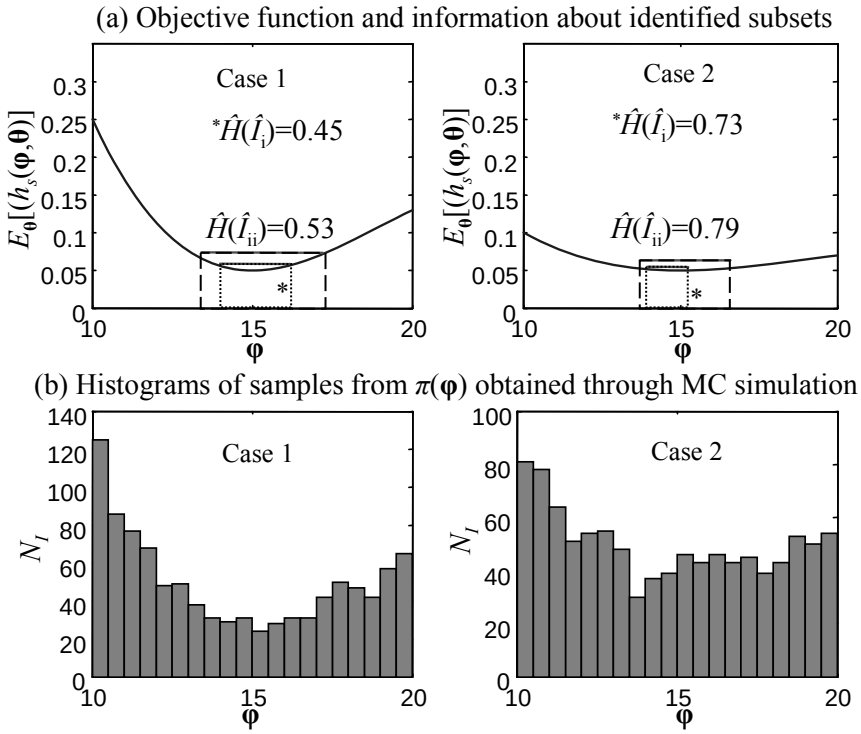

Figure 4.1: Example for the quality of identification for two cases

Figure 4.1 illustrates these concepts for a one-dimensional design-space problem. Part (a) includes the objective function and Part (b) the histograms of the samples for $\boldsymbol{\varphi}$ from $\pi(\boldsymbol{\varphi},\boldsymbol{\theta})$ using a direct Monte Carlo sampling approach with N_Φ=1000. The identified subsets according to (4.18) are shown in Figure 4.1(a) along with the corresponding estimate $\hat{H}(\hat{I})$. A characterization of admissible subsets is selected for this example that guarantees a specific level of the c.o.v. for $\hat{H}(I)$ (see (4.10)): $A_r = \{I \subset \Phi : N_I / N_\Phi = \rho\}$. Two classes are considered for the admissible subsets, corresponding to two different values for the constraint ρ: (i) ρ=0.1 and (ii) ρ=0.2. The first choice leads to a greater restriction for the

size of admissible sets, since a smaller number of samples are required within the identified set. The c.o.v. for the first class is 0.095 and for the second 0.063 for standard MCS. Two different cases are presented. For all cases, the optimal design choice corresponds to $\boldsymbol{\varphi}^*$=15. Case 1 has larger sensitivity with respect to the average value for the objective function compared to the second case. For this reason better quality of identification is established for this case: the value of the estimate $\hat{H}(\hat{I})$ is smaller when comparing the same classes of admissible subsets between the different cases. The distribution of the failed samples in the histograms in Figure 4.1(b) provides a visual verification of this characteristic: a region for $\boldsymbol{\varphi}^*$ can be identified more clearly for Case 1, whereas the distribution Case 2 approaches uniform near $\boldsymbol{\varphi}^*$. Comparing, now, the two classes of admissible subsets (i) and (ii), we see that the first class leads, as expected, to identification of a smaller size subset; this subset is characterized by a smaller $\hat{H}(\hat{I})$ but at the same time higher c.o.v. (smaller accuracy) for that estimate. These two features represent opposite characteristics for the quality of identification. More detailed discussion on the influence of the size of the admissible subsets to the SSO efficiency is provided in the next section.

4.1.5 Iterative approach

The relative size of the admissible subsets I define (a) the resolution of $\boldsymbol{\varphi}^*$ and (b) the accuracy information about $\hat{H}(I)$ that is extracted from the samples from $\pi(\boldsymbol{\varphi})$. Selecting smaller size for the admissible sets leads to better resolution for $\boldsymbol{\varphi}^*$. At the same time, though, this selection leads to smaller values for the ratio N_I/N_Φ (since smaller number of samples are included in smaller sets) and thus it increases the c.o.v. (reduces accuracy) of the estimation, as seen from (4.10). In order to maintain the same quality for the estimate, the effective number of independent samples must be increased, which means that more simulations must be performed. Since we are interested in subsets in Φ with small average value, the required number of simulations to gather accurate information for subsets with small size is large, i.e., a small percentage of the simulated samples fall in these subsets. These characteristics are clearly illustrated in Figure 4.1. In the examples presented in the

figure, the number of simulation samples must be 2.25 times larger for class (i) in order to get same accuracy of estimation for both classes of admissible subsets.

To account for this characteristic and to increase the efficiency of the identification process, an iterative approach can be adopted. At iteration k, additional samples in $\hat{I}_{k-1}$ (where $\hat{I}_0 = \mathbf{\Phi}$) that are distributed according to $\pi(\boldsymbol{\varphi})$ are obtained. A region $\hat{I}_k \subset \hat{I}_{k-1}$ for the optimal design parameters is then identified as above. The quality of the identification is improved by applying such an iterative scheme, since the ratio of the samples in $\hat{I}_{k-1}$ to the one in $\hat{I}_k$ is larger than the equivalent ratio when comparing $\hat{I}_k$ and the original design space Φ. The samples $[\boldsymbol{\varphi},\boldsymbol{\theta}]$ available from the previous iteration, whose $\boldsymbol{\varphi}$ component lies inside set $\hat{I}_{k-1}$, can be exploited for improving the efficiency of the sampling process. In terms of the algorithms described in Appendix 4A this may be established, for example, by (a) forming better proposal PDFs or (b) using the samples already available as seeds for MCMC simulation.

4.1.6 Influence of dimension of design variables

This iterative approach of SSO leads to a favorable feature for the computational cost of the algorithm with respect to the dimension of the search space (number of design variables, n_φ). For a specific reduction δ_k of the size (volume) of the search space in some step of the set identification:

$$\delta_k = \frac{V_{\hat{I}_k}}{V_{\hat{I}_{k-1}}} \tag{4.19}$$

the corresponding average size reduction per design variable is $\sqrt[n_\varphi]{\delta_k}$. This means that if the identification was performed in one step, the logarithmic average size reduction per variable would be inversely proportional to the dimension of the search space n_φ (assuming

δ_k remains the same). In the suggested iterative approach though, in n_{iter} iterations the average size reduction per design variables, is:

$$\sqrt[n_\varphi]{\prod_{k=1}^{n_{iter}} \delta_k} = \left(\sqrt[n_\varphi]{\delta_{mean}{}^{n_{iter}}} \right) = \left(\delta_{mean} \right)^{n_{iter}/n_\varphi} \tag{4.20}$$

where

$$\delta_{mean} = \sqrt[n_{iter}]{\prod_{k=1}^{n_{iter}} \delta_k} \tag{4.21}$$

is the geometric mean of the volume reductions over all of the iterations (note that if $\delta_k=\delta$, then $\delta_{mean}=\delta$). Thus, for the same average total size reduction over all design variables (left-hand side of equation (4.20)), the number of required iterations is proportional to the dimension of the design space (look at the exponent in the right-hand side of equation (4.20)), assuming that the mean reduction of the volume over all iterations, δ_{mean}, is comparable. This argument shows that the efficiency of SSO decreases linearly with the dimension of the design space, so SSO should be considered appropriate for problems that involve a large number of design variables.

4.1.7 Sensitivity to the model parameters

The SSO setting can be also used to obtain information about the sensitivity of the performance of the system to the model parameters. The concept is similar to the sensitivity analysis for the design variables as was described in Section 4.1.1; the samples from $\pi(\boldsymbol{\varphi},\boldsymbol{\theta})$ are projected in this case to the space of the model parameters Θ. The distribution of these samples compared to the prior distribution $p(\boldsymbol{\theta})$ expresses the sensitivity of the performance measure to the specific model parameters; bigger discrepancies between the distributions indicate greater importance of the corresponding model parameters in affecting the system performance. This can be also performed for each model parameter separately or for some selected group of the model parameters. This analysis will also illustrate the correlation

between the model parameters with respect to the system response. Such information is important for understanding the influence of the model parameters on the system model performance and can be exploited in various ways, for example for establishing importance sampling densities as will be discussed in Section 5.2.

4.1.8 Details for reliability objective problem

When SSO is implemented for ROP, selection of $I_F(\boldsymbol{\varphi},\boldsymbol{\theta})$ as the performance measure is beneficial because it simplifies the task of simulating samples from $\pi(\boldsymbol{\varphi},\boldsymbol{\theta})$. In this case these samples correspond simply to *failed samples*, i.e., samples that lead to failure of the system ($I_F(\boldsymbol{\varphi},\boldsymbol{\theta})=1$), and the auxiliary PDF $\pi(\boldsymbol{\varphi},\boldsymbol{\theta})$ is simply the PDF for the augmented uncertain parameter vector conditioned on failure of the system, i.e., $p(\boldsymbol{\varphi},\boldsymbol{\theta}|F)$. Similarly, the marginal $\pi(\boldsymbol{\varphi})$ corresponds to $p(\boldsymbol{\varphi}|F)$. The equation (4.4) for the objective function (probability of failure) in the context of the augmented design problem is simply an expression of Bayes' theorem:

$$P(F \mid \boldsymbol{\varphi}) = \frac{p(\boldsymbol{\varphi} \mid F)}{p(\boldsymbol{\varphi})} P(F) \tag{4.22}$$

where $P(F \mid \boldsymbol{\varphi}) \triangleq P_F(\boldsymbol{\varphi} \mid \Theta)$ and $P(F)$ is the failure probability in the augmented design problem, defined, similarly to (4.3), as:

$$P(F) = \int_{\Phi} \int_{\Theta} I(\boldsymbol{\varphi},\boldsymbol{\theta}) p(\boldsymbol{\varphi},\boldsymbol{\theta}) d\boldsymbol{\theta} d\boldsymbol{\varphi} \quad . \tag{4.23}$$

Monte Carlo simulation can be used for simulating samples from $p(\boldsymbol{\varphi}|F)$ at the first stage of the SSO algorithm. For design problems that involve small failure probabilities this approach may be inefficient because $1/P(F)$ trials are needed on the average in order to simulate one failed sample. Other stochastic simulation methods, such as Subset Simulation (Au and Beck 2001b) should be preferred in such cases. For subsequent iterations of SSO,

MCMC simulation should be chosen, preferably using the modified Metropolis-Hastings algorithm (see discussion in Appendix 4A) which is appropriate for problems with high-dimensional uncertainties. This approach is more efficient than restarting the sampling process after the identification of each new subset, i.e., using MCS. Since subsets are identified that are progressively closer to the optimal solution, and thus are characterized by smaller $P(F)$, the latter approach would involve an increasing computational cost for simulating the same number of samples from the target distribution $p(\boldsymbol{\varphi},\boldsymbol{\theta}|F)$ in set $\hat{I}_{k-1}$. In the MCMC approach, all samples simulated follow the distribution $p(\boldsymbol{\varphi},\boldsymbol{\theta}|F)$. Note that in the proposed iterative identification, the conditional samples populate gradually from a region with high probability content towards a region of low probability content in the design space, a concept similar to Subset Simulation (Au and Beck 2001a).

The $\boldsymbol{\theta}$ component of the simulated failed samples correspond to the conditional PDFs $p(\boldsymbol{\theta}|F)$ and ultimately answer the question: what is expected to happen when the system fails? Application of Bayes's theorem leads to an expression similar to (4.22), but with the design variables $\boldsymbol{\varphi}$ substituted by the model parameters $\boldsymbol{\theta}$. This shows that the marginal pdf $p(\theta_i|F)$ for the uncertain parameter θ_i, when compared to the marginal PDF $p(\theta_i)$, indicates how important the corresponding uncertain parameter is in affecting the system failure. This is similar to the ideas discussed in Au and Beck (2003) in the context of Subset Simulation.

4.2 Implementation Issues and Guidelines

In this section implementation topics related to the stochastic sampling from $\pi(\boldsymbol{\varphi},\boldsymbol{\theta})$ and the subset identification described by (4.18) are discussed for the SSO algorithm.

4.2.1 Characterization and normalization of search space

For notational simplicity, the updated search space for the design variables at the current stage of SSO is denotes as S. For the first iteration of SSO, $\Phi=S$, and for the k^{th} iteration

S=$\hat{I}_{k\text{-}1}$. The volume of this space is denoted by V_s and the number of samples in it N_s. Two different cases are discussed in detail for S: (i) a hyper-rectangle with no rotation relative to the Cartesian space, corresponding to a box-bounded search space on each design variable separately, and (ii) a hyper-ellipse, defined respectively as:

$$\begin{aligned} S_1 &: \ \left\| \mathbf{R}_d \left(\boldsymbol{\varphi} - \boldsymbol{\varphi}_o \right) \right\|_\infty = 1 \\ S_2 &: \ \left(\boldsymbol{\varphi} - \boldsymbol{\varphi}_o \right)^T \mathbf{A}_d \left(\boldsymbol{\varphi} - \boldsymbol{\varphi}_o \right) = 1 \end{aligned} \tag{4.24}$$

where $\boldsymbol{\varphi}_o \in \mathbb{R}^{n_\varphi}$ is the center of search space, $\mathbf{R}_d \in \mathbb{R}^{n_\varphi x n_\varphi}$ is a diagonal matrix with elements the reciprocals of the half-length of the search space for each design variable, $\|.\|_\infty$ corresponds to the infinity vector norm, and $\mathrm{A}_d \in \mathbb{R}^{n_\varphi x n_\varphi}$ is a positive-definite symmetric matrix. Another possible case not investigated here is the extension of the definition of hyper-rectangles to take into account possible rotations; this can be established by introduction of a rotational transformation with respect to each pair of hyper-planes.

Cases for which the initial design space Φ has a different shape than these two candidates can be addressed by selecting S_1 (or S_2) as a superset of Φ. A penalty term can then be used to describe the objective function for the region S_1-Φ, so that:

$$h_S(\boldsymbol{\varphi}, \boldsymbol{\theta}) = \begin{cases} h_S(\boldsymbol{\varphi}, \boldsymbol{\theta}) & \text{if } \boldsymbol{\varphi} \in \Phi \\ h_s(\boldsymbol{\varphi}, \boldsymbol{\theta}) + \lambda_s & \text{if } \boldsymbol{\varphi} \notin \Phi \end{cases} \text{ where } \lambda_s \geq \max_{\boldsymbol{\varphi} \in \Phi, \boldsymbol{\theta} \in \Theta} h_s(\boldsymbol{\varphi}, \boldsymbol{\theta}) \quad . \tag{4.25}$$

Figure 4.2 illustrates this idea. Such penalty techniques may be also used to take into account complex constraints in formulation (2.2), when this cannot be easily established by appropriate selection of Φ.

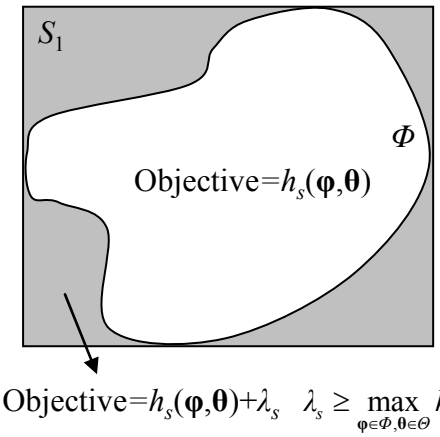

Figure 4.2: Adjustment of initial search space

The volumes of sets S_1 and S_2 in (4.24) which are needed in the SSO setting are, respectively:

$$V_{S_1} = 2^{n_\varphi} \det(A^{-1}),\ V_{S_2} = \frac{\pi^{n_\varphi/2}}{\Gamma\left(n_\varphi/2+1\right)} \det(\mathbf{A}_d^{-1}) \tag{4.26}$$

where $\Gamma(.)$ corresponds to the Gamma-function.

A normalization of the search space S is also considered. This normalization can increase (see discussion later) the efficiency of the subset optimization within S, needed for SSO, and can be established using a simple linear coordinate transformation:

$$\mathbf{x} = \mathbf{C}_d\left(\boldsymbol{\varphi} - \boldsymbol{\varphi}_o\right) \quad . \tag{4.27}$$

For S_1 $\mathbf{C}_d$=$\mathbf{R}_d$ and for S_2 $\mathbf{C}_d$ is an upper triangular matrix corresponding to the Cholesky decomposition of $\mathbf{A}_d$, that is, $\mathbf{C}_d^T\mathbf{C}_d$=$\mathbf{A}_d$. The normalized search space will be denoted by $\mathcal{X}$. The two sets in (4.24) are then transformed to a hyper-cube with half-length 1 and a unit radius hyper-sphere, respectively:

$$\begin{aligned} &\mathcal{X}_1 :\ \left\|\mathbf{x}\right\|_\infty = 1 \\ &\mathcal{X}_2 :\ \mathbf{x}^T\mathbf{x} = 1 \quad . \end{aligned} \tag{4.28}$$

In spherical coordinates, set $\mathcal{X}_2$ is described simply by r_c=1, where r_c corresponds to the radial coordinate. Since this description is simpler than the quadratic expression in (4.28) it is expected that use of a spherical coordinate system, instead of a Cartesian one, will be sometimes advantageous when the search space is $\mathcal{X}_2$ (or equivalently S_2). Some details pertaining to the transformations between spherical and Cartesian coordinates are given in Appendix 4B. Note, finally, that since the probability distribution of $\boldsymbol{\varphi}$ is uniform in S the same applies for the probability distribution for $\mathbf{x}$ in $\mathcal{X}$ (because the coordinate transformation is linear).

4.2.2 Selection of admissible subsets

Proper selection of the geometrical shape and size of the admissible sets is important for the efficiency of SSO. The geometrical shape should be chosen so that the challenging, non-smooth (see discussion later) optimization (4.18) can be efficiently solved while the sensitivity of the objective function to each design variable is fully explored. For example, the suggested hyper-rectangle or hyper-ellipse are appropriate choices for the shape of admissible subsets, depending also on the shape of the initial design space Φ. Note that the difference in size (volume) between Φ and the largest possible subset $I \subset \Phi$ should not be large. If this property does not hold, then the size reduction in the first iteration of SSO will necessarily have to be at least as big as this volume difference, feature which might reduce the quality of the SSO identification in the first iteration. This problem may be circumvented by appropriate adjustment of the design space, Φ, based on the desired shapes for the class of admissible subsets. For example, a superset Φ_{sup} that has shape similar to one of the admissible subsets, and circumscribes the desired design set Φ can be selected as initial search space for the optimal system configuration. As mentioned above, two choices for shapes or admissible subsets are considered herein: hyper-rectangles

without any rotation relative to the canonical Cartesian space and hyper-ellipses. For notational convenience the first class is simply referred to as hyper-rectangles.

The size of admissible subsets, now, is related to the quality of identification as discussed earlier. Selection of this size can be determined, for example, by incorporating a constraint for either (i) the volume ratio $\delta=V_I/V_S$ or (ii) the number of samples ratio $\rho=N_I/N_S$. The first choice cannot be directly related to any of the measures of quality of identification; thus proper selection of δ is not straightforward, though personal experience indicates that δ close to 0.25 is, in general, an appropriate option. The second choice allows for directly controlling the coefficient of variation and thus one of the parameters influencing the quality of identification. This selection was used for the subset identifications in Figure 4.1 and is discussed in more detail here.

The optimization in (4.18) adopting the latter characterization of admissible subsets corresponds to identification of the subset that has the smallest estimated $\hat{H}(\hat{I})$ within this class of subsets that guarantee a specific level of accuracy for that estimate:

$$\begin{aligned} &\hat{I} = \arg\min_{I \in A_\rho} N_I / V_I \\ &A_\rho = \left\{ I \subset S : \rho = N_I / N_S \right\} \quad . \end{aligned} \tag{4.29}$$

Note that according to (4.13) and (4.14), the ratio N_I/N_S is equal to an estimate for the ratio of the integral of objective function in sets I and S, respectively. Thus, another interpretation of the optimization in (4.29) is that it is equivalent to identification of the set that has the smallest estimated average value within the class of subsets that have a specific estimated integral:

$$\begin{aligned} &\hat{I} = \arg\min_{I \in A_\rho} \hat{H}(I) \\ &A_\rho = \left\{ I \subset S : \rho = \hat{R}(I) \right\} \quad . \end{aligned} \tag{4.30}$$

This interpretation indicates that for cases with smaller sensitivity around $\boldsymbol{\varphi}^*$, smaller size subsets I are identified since the admissible sets that satisfy the constraint for the $\hat{R}(I)$ ratio will be smaller. This characteristic is also evident in Figure 4.1 when comparing the two different cases (left and right plot). Let δ_k defined in (4.19) denote the size reduction at each step of the algorithm in the SSO iterative approach suggested. As the SSO iterative algorithm evolves, regions with smaller sensitivity, i.e., closer to the optimal value, are approached. According to the previous argument, this leads to identification of smaller size subsets; thus δ_k is a decreasing sequence. Since $\hat{H}(\hat{I})$ is equal to the ration ρ/δ_k the discussion here verifies that for cases with larger sensitivity to the objective function the value of $\hat{H}(\hat{I})$ is smaller, and indicates that $\{\hat{H}(\hat{I}_k)\}$ is expected to be an increasing sequence.

The volume (size) of the admissible subsets in the identification scheme (4.29) is adaptively chosen so that the ratio of samples in the identified set is equal to ρ. The choice of the value for ρ affects the efficiency of the identification. If ρ is large, a fewer number of samples is required for the same level of accuracy (c.o.v. in (4.10)). However, a large value of ρ means that the size of the identified subsets will decrease slowly (larger size sets are identified), requiring more steps to converge to the optimal solution. The choice of the constraint ρ is a trade-off between the number of samples required in each step and the number of steps required to converge to the optimal design choice. In the applications we have investigated so far it was found that choosing ρ=0.1–0.2 yields good efficiency. An adaptive scheme can also be applied: smaller values of ρ may be selected in the first iterations of SSO when the sensitivity of the design problem is large and so the values of $\hat{H}(\hat{I})$ small. As the algorithm converges to the optimal design configuration, $\hat{H}(\hat{I})$ increases and larger values of ρ can be chosen to decrease the c.o.v. of $\hat{H}(\hat{I})$ and thus improve the identification quality.

4.2.3 Identification of the optimal subsets

Another important issue for the efficiency of SSO is the identification of the optimal sets within the class of admissible subsets selected, i.e., optimization (4.18). Typically the cost associated with this optimization is significantly smaller than the cost of the stochastic simulation needed for generating the samples from $\pi(\boldsymbol{\varphi})$. Thus the computational efficiency of SSO is primarily determined by the efficiency of the stochastic simulation stage, not optimization (4.18). Still, the correct identification of the optimal subset within the search space has elementary importance for SSO; if the optimization cannot be accurately performed then the whole algorithm is inefficient.

A fundamental remark regarding this optimization is that the position in the search space of a set $I \in A$ and the number of sample points in it is non-continuous. Thus, only methods appropriate for non-smooth optimization problems, such as genetic algorithms or direct search methods (see Pardalos and Resende (2002) for more details), can be applied for the identification in consideration. The computational cost associated with these methods depends on (a) the number of parameters, n_A, needed to characterize the subsets and (b) the description of the admissible values for these parameters. The number of parameters is determined by the dimension of the design variables, n_φ, and the shape selected for the admissible subsets; for example, for hyper-rectangles (with no rotation) it is $n_A=2n_\varphi$ and for hyper-ellipses $n_A=2n_\varphi+n_\varphi(n_\varphi-1)/2$. Increase of n_A typically leads to an exponential increase of the computational cost associated with genetic algorithms or direct search methods. The characterization of the admissible values for the parameters that define the subsets depends on the analytical formula that has been selected for the mathematical representation of the subsets, as well as on the shape of the space $\mathcal{X}$. To illustrate this principle, consider the characterization of the center $\mathbf{x}_o$ of a hyper-ellipse inside $\mathcal{X}$ that corresponds to one of the two classes described by (4.28). If $\mathcal{X}$ is a hyper-cube with length two ($\mathcal{X}_1$) then $\boldsymbol{\varphi}_o$ should be described in Cartesian coordinates with the simple linear constraint $|x_{o,i}|<1 \ \forall\, i$, defining the admissible values for $\mathbf{x}_o$. If instead $\mathcal{X}$ is a hyper-rectangle ($\mathcal{X}_2$), then $\mathbf{x}_o$ should be described

in spherical coordinates, because this selection leads to a simple linear constraint for the admissible values for $\mathbf{x}_o$, that is, $r_c<1$. If a Cartesian coordinate system were selected in the latter case, then a nonlinear constraint would be involved, that is, $\mathbf{x}_o^T\mathbf{x}_o<1$, and the characterization of the admissible values for $\mathbf{x}_o$ would be inefficient for large n_φ. The inefficiency here means that many candidate selections for $\mathbf{x}_o$ will not satisfy the desired nonlinear constraint. This argument illustrates also the merits of establishing a normalization of the search space S, as discussed easier; this normalization allows for a more efficient parametric characterization of sets within this space.

Related to optimization problem (4.18), note additionally that the evaluation of the objective function and the constraint involve typically small computational effort; they simply consist of counting the number of samples within the subset, calculating the volume of the set, and checking that $I \subset S$. For choice of admissible subsets as hyper-rectangles these tasks are relatively straightforward. Appendix 4C discusses some relevant topics associated with these tasks for selection of the admissible subsets as hyper-ellipses.

This whole discussion shows that optimization (4.18) can be efficiently solved if an appropriate algorithm is available and, additionally, the admissible subsets are appropriately parameterized. Because of the significance of the optimization in the efficiency of SSO, special attention is warranted to guarantee that the identification is accurate. A simpler characterization of the admissible subsets should be preferred (for example, hyper-rectangles) when there is doubt about the reliability of the optimization process if more complex characterizations were chosen.

4.2.4 Characteristics for MCMC simulation

As discussed earlier, the cost of the stochastic simulation stage, needed for generating the samples from $\pi(\boldsymbol{\varphi})$, determines the effectiveness of SSO. This is particularly true for design problems involving complex system models for which the computational burden for a single evaluation of the model response, typically through computer simulation, is

significant. The cost associated with this sampling stage of SSO may be decreased by efficient application of MCMC simulation. This efficiency depends significantly on the quality of the selected proposal PDFs for the generated Markov Chains. Various studies exist that discuss appropriate selections for these PDFs depending on the characteristics of the problem; see for example Roberts et al. (1997), Roberts and Rosenthal (2001), Au and Beck (2003), Robert and Casella (2004). The proposal PDFs for the design variables $\boldsymbol{\varphi}$, whose prior distribution $p(\boldsymbol{\varphi})$ is uniform in Φ, are only addressed here. The discussion here is also applicable if the normalized coordinate system is used.

For *local random walk* a PDF centered at the current sample, with spread 70% of the dimension of the current subset S at each direction, is suggested for the proposal PDF for $\boldsymbol{\varphi}$. This is a proposal PDF that is easy to sample from and still approximates the form of $\pi(\boldsymbol{\varphi})$, which is expected to look like a convex function with small sensitivity as the identification converges to a set near the optimal design variables. A *global uniform proposal* PDF could also be chosen for $\boldsymbol{\varphi}$. Such a global proposal PDF avoids rejecting samples due to their $\boldsymbol{\varphi}$ component, in the candidate sampling step, falling outside the given search space S, which can occur with a local uniform PDF and which increases the correlation in the generated Markov Chain. As the SSO algorithm evolves and regions with small sensitivity are approached, this global proposal converges to the target distribution, $\pi(\boldsymbol{\varphi})$; this characteristic is expected to lead to increase of the efficiency of the MCMC at these later stages. This increase of efficiency is directly related to increase of the number of effective samples for the same number of total simulated samples and thus to a decrease of the c.o.v. (4.10). Since $\hat{H}(\hat{I})$ is expected to increase in these later stages, this decrease of the c.o.v. contributes significantly in maintaining a good level of quality for the optimal subset identification, i.e., partially counterbalances the quality deterioration generated by the larger values of $\hat{H}(\hat{I})$.

A final question related to these suggestions for proposal PDFs for $\boldsymbol{\varphi}$ that should be answered is how they can be effectively applied when the normalized search space is a

hyper-sphere (χ_2). In this case it is easier to perform the sampling in spherical coordinates. Using the Jacobian transformation in (B4.3), a uniform probability distribution for $\boldsymbol{\varphi}$, and thus for $\mathbf{x}$, corresponds to the following distributions for the spherical coordinates:

$$p(r_c) = \frac{r_c^{n-1}}{n},\ p(\psi_i) = \frac{\sin^{n_\varphi - 1 - i}(\psi_i)}{\int_0^\pi \sin^{n_\varphi - 1 - i}(\psi_i)\, d\psi_i}\ i = 1 : n_\varphi - 2,\ \ p(\psi_{n_\varphi - 1}) = \frac{1}{2\pi} \quad . \tag{4.31}$$

Generation of samples according to these distributions is straightforward (see, for example, Katafygiotis and Cheung (2002)).

4.2.5 Updating function h_s

Another way to improve the efficiency of the SSO is to continually update $h_s(\boldsymbol{\varphi},\boldsymbol{\theta})$ in (4.1) by re-defining s:

$$h_{s,k}(\boldsymbol{\varphi},\boldsymbol{\theta}) = h(\boldsymbol{\varphi},\boldsymbol{\theta}) - s_k \quad \text{where} \quad s_k = \min_{\boldsymbol{\varphi} \in \hat{I}_k, \boldsymbol{\theta}} h(\boldsymbol{\varphi},\boldsymbol{\theta}) \quad . \tag{4.32}$$

Figure 4.3 illustrates this concept. For choice $h_{s,2}(\boldsymbol{\varphi},\boldsymbol{\theta})$, which corresponds to a larger value of s, the sensitivity of the objective function, in the SSO setting, is larger and a candidate region for the optimal choice is more easily discernible (better quality is established) based on samples from $\pi(\boldsymbol{\varphi})$. If $h_s(\boldsymbol{\varphi},\boldsymbol{\theta})$ is reformulated, though, the ancillary density $\pi(\boldsymbol{\varphi},\boldsymbol{\theta})$ changes and the samples from the previous iteration cannot provide useful information for the next iteration unless the previous and the next loss functions $h_s(\boldsymbol{\varphi},\boldsymbol{\theta})$ are similar. For cases where the sensitivity of the objective function is small, our experience indicates that the re-formulation of the loss function can be beneficial (assuming that s can be set to a larger value). When the sensitivity is quite high, though, it is preferable to keep the same function and use the samples available to improve the efficiency when generating new ones.

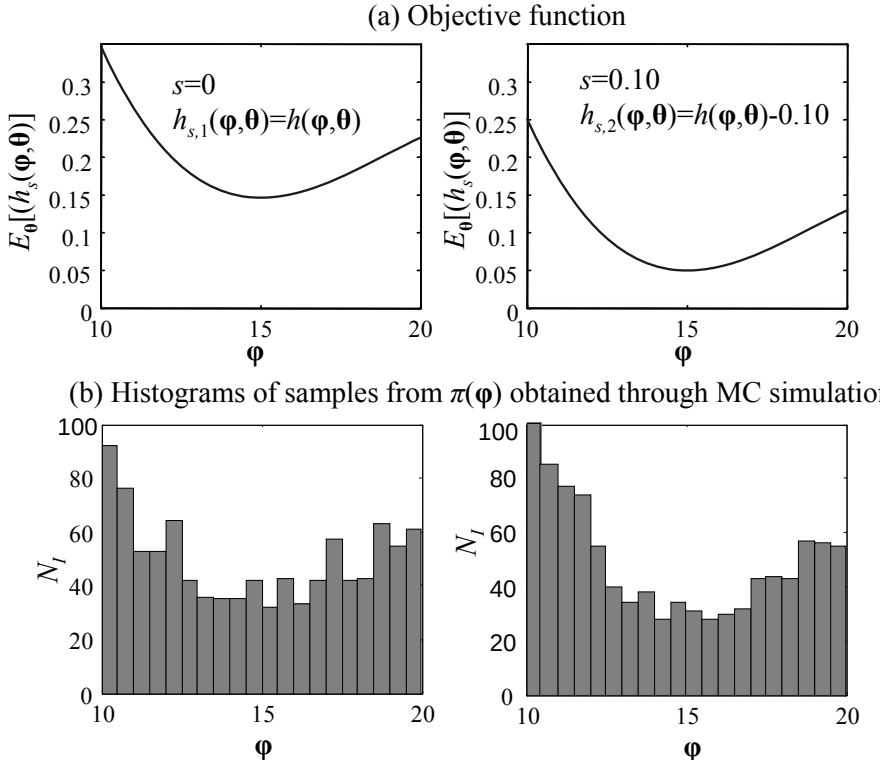

Figure 4.3: Influence of selection of *s* in SSO

4.3 Stochastic Subset Optimization Algorithm

The SSO algorithm is summarized as follows (Figure 4.4 and Figure 4.5 illustrate some important steps for selection of admissible subsets either as hyper-rectangles or hyper-ellipses):

Initialization: Define the bounded design space Φ, and the desired geometrical shape for the subsets I. Decide on the desired number of samples N and on the value for the constraint ρ.

Step k: Use some sampling procedure, such as MC simulation for the 1st step and MCMC simulation for subsequent steps, in order to simulate N samples (or effective samples) from $\pi(\boldsymbol{\varphi},\boldsymbol{\theta})$ inside the subset $\hat{I}_{k\text{-}1}$. Identify subset $\hat{I}_k$ as:

$$\hat{I}_k = \arg\min_{I \in A_{\rho,k}} N_I / V_I, \quad A_{\rho,k} = \left\{ I \subset \hat{I}_{k-1} : \rho = N_I / N \right\} \quad . \tag{4.33}$$

Keep only the $N_{\hat{I}_k}$ samples whose **φ** component belongs to the subset $\hat{I}_k$ (exploit these samples in the next step).

Stopping criteria: At each step, estimate ratio:

$$\hat{H}(\hat{I}_k) = \frac{N_{\hat{I}_k}}{N_{\hat{I}_{k-1}}} \frac{V_{\hat{I}_{k-1}}}{V_{\hat{I}_k}} \tag{4.34}$$

and its coefficient of variation according to the simulation algorithm used. Based on these two quantities and the desired quality of the identification (see next chapter), decide on whether to (a) stop (or even increase *N* to obtain better accuracy information about $\hat{H}(\hat{I}_k)$) or (b) proceed to step *k*+1.

Figure 4.4 also demonstrates the dependence of the quality of the identification on $\hat{H}(\hat{I}_k)$ for a two-dimensional example. This ratio expresses the difference in volume density of the samples inside and outside the identified set $\hat{I}_k$. In the first iteration, this difference is clearly visible. As SSO evolves and converges to subsets with smaller sensitivity to the objective function, the difference becomes smaller, and by the last iteration (Figure 4.4(f)), it is difficult to visually discriminate which region in the set has smaller volume density of failed samples. This corresponds to a decrease in the quality of the identification. It is also clear that as the identification process in SSO evolves, the reduction in the size of the identified subsets becomes larger, and that the value of $\hat{H}(\hat{I}_k)$ constantly increases. These patterns verify the theoretical discussion presented in Section 4.2.2, assuming that as the SSO identification progresses, regions of the design space with smaller sensitivity to the objective function are approached.

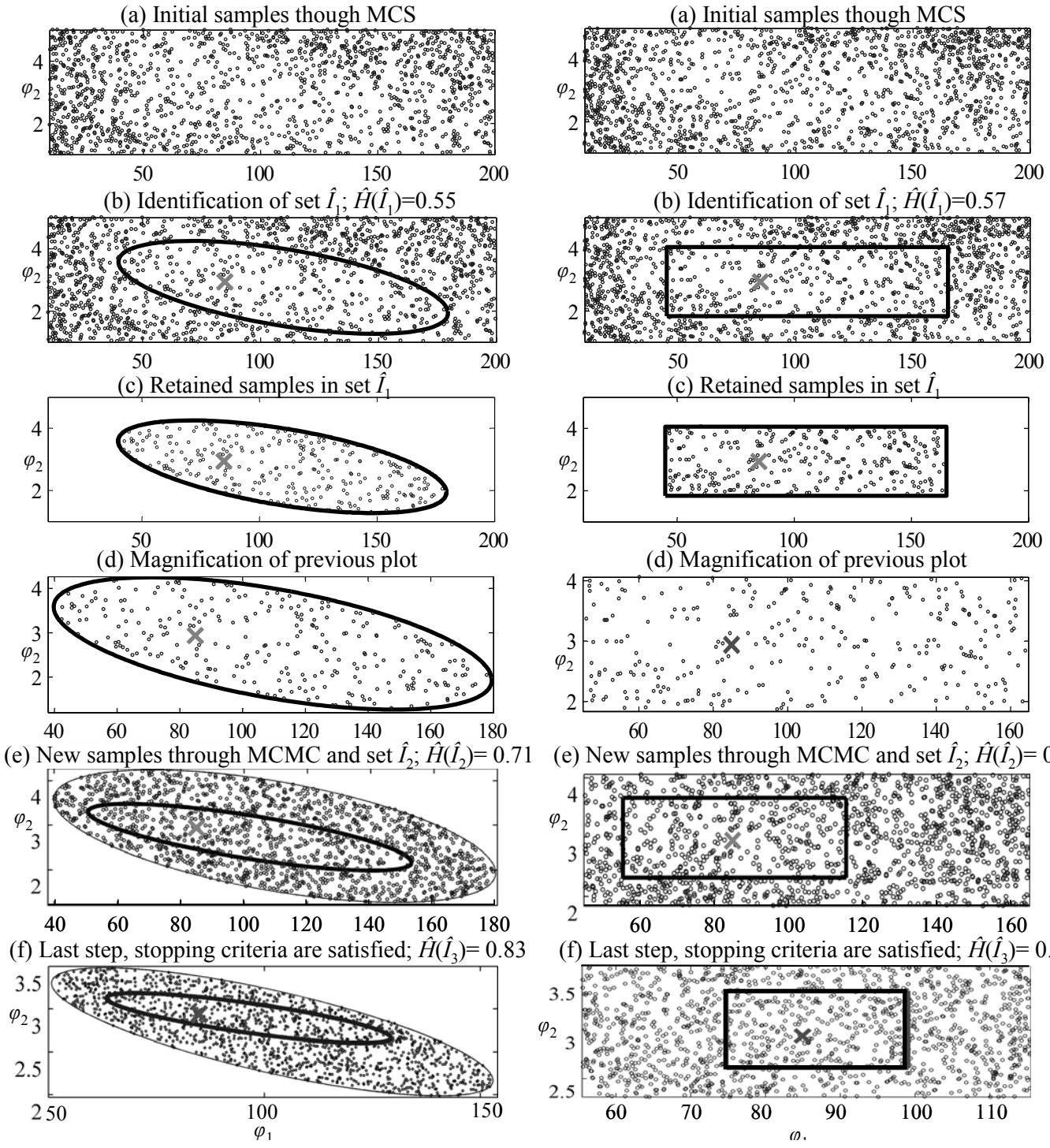

Figure 4.4: An illustrative example for the SSO algorithm for selection of admissible subsets as hyper-ellipses (left) or hyper-rectangles (right)

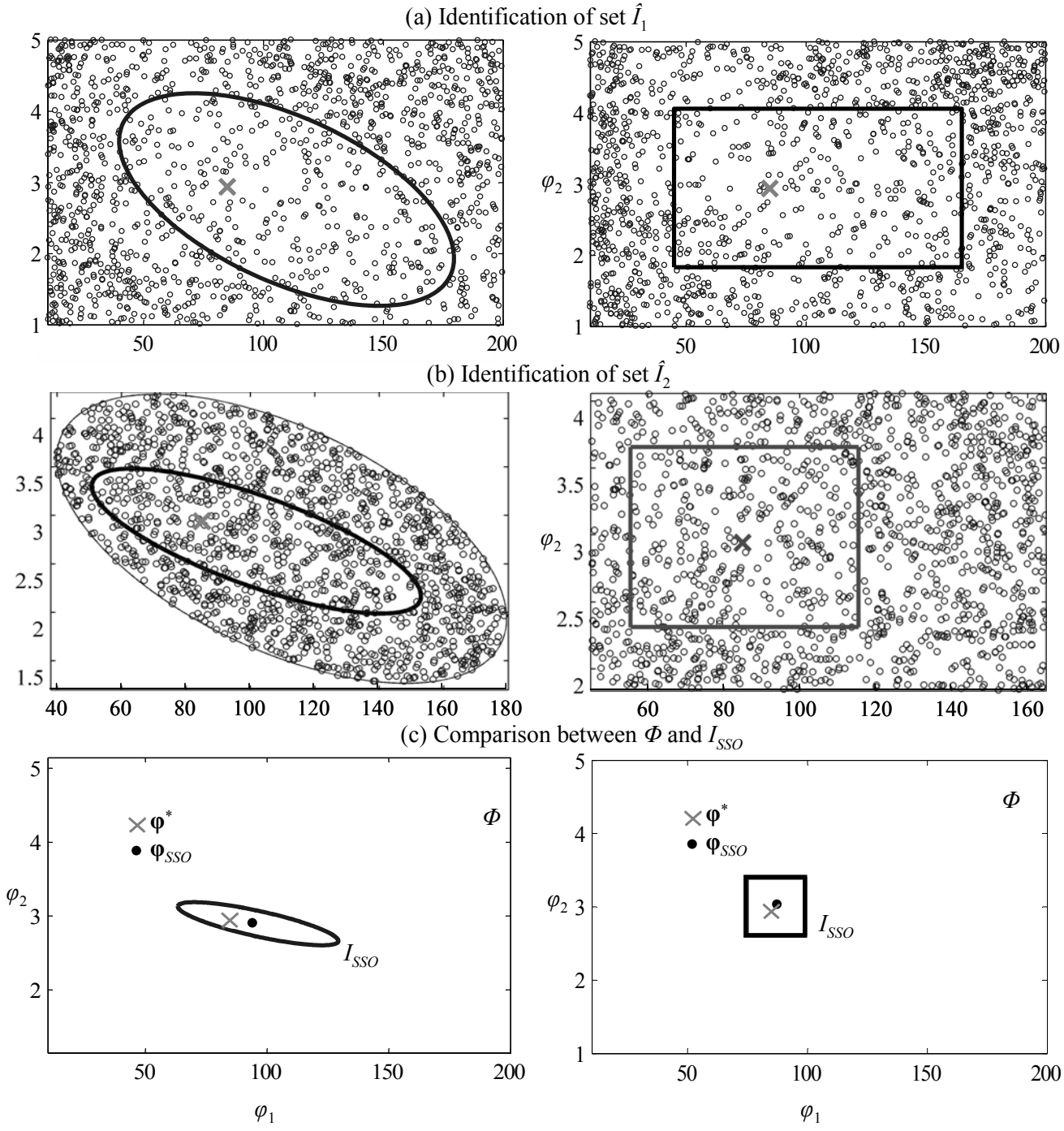

Figure 4.5: Some important steps for the SSO algorithm for selection of admissible subsets as hyper-ellipses (left) or hyper-rectangles (right)

4.4 Convergence Properties of Stochastic Subset Optimization

The SSO algorithm described in this chapter, will adaptively converge to a relatively small sub-region for the optimal design variables $\boldsymbol{\varphi}^*$ within the original design space. The size of this sub-region depends on the sensitivity of the objective function around the optimal point. If that sensitivity is large then SSO will ultimately converge to a "small" set I_{sso}, satisfying at the same time the accuracy requirements that make it highly likely that $\boldsymbol{\varphi}^*$ is in I_{sso}. The center point of this set, denoted herein as $\boldsymbol{\varphi}_{SSO}$, gives the estimate for the optimal design variables. Additionally SSO gives information about the local behavior of the objective function. As long as the shape of the admissible subsets is close to the contours of the objective function near the optimal design point, the subset identified in the last stage of SSO provides a good estimate for these contours. For improving the accuracy of this estimate, it might be desirable to increase the number of samples N, in the last iteration of SSO, in order to obtain more information for $\pi(\boldsymbol{\varphi})$. Also, selection of the shape of admissible subsets as hyper-ellipses should be more appropriate for this purpose, since the contours of the objective function are expected to fit better to hyper-elliptical shapes near the optimal design point. The comparison in Figure 4.5 between the two different classes of admissible subsets makes this remark obvious.

In cases, though, that the sensitivity of the objective function around the optimal point is not large enough, convergence to a small subset might be problematic and will require increasing the number of samples in order to satisfy the requirement for the quality of identification. Another important issue related to the identification in such cases is that there is no measure of the quality of the identified solution (i.e., how close $\boldsymbol{\varphi}_{SSO}$ is to $\boldsymbol{\varphi}^*$) that can be directly established through the SSO results. If the identification is performed multiple times, the c.o.v. of $\{\hat{E}_{\boldsymbol{\theta}}[h(\boldsymbol{\varphi}_{SSO,i},\boldsymbol{\theta})]\}$ could be considered a good candidate for characterizing this quality. This might not be always a good measure though. For example, if the choice for admissible subsets is inappropriate for the problem considered, it could be the case that consistent results are obtained for $\boldsymbol{\varphi}_{SSO}$ (small c.o.v.) that are far from the

optimal design choice $\boldsymbol{\varphi}^*$. Also, this approach involves higher computational cost because of the need to perform the identification multiple times. For such cases, it could be more computationally efficient (instead of increasing N in SSO and performing the identification multiple times) and more accurate (in terms of identifying the true optimum), to combine SSO with some other optimization algorithm for pinpointing $\boldsymbol{\varphi}^*$. A discussion of topics related to such algorithms as well as a complete framework for stochastic optimization will be presented in the next chapter. Numerical examples pertaining to the efficiency of SSO, as well as the combined optimization framework are presented in Chapter 6.

Appendix 4A: Sampling Techniques

Two algorithms that can be used for simulating samples from $\pi(\boldsymbol{\varphi},\boldsymbol{\theta})$ are discussed here:

Algorithm 1: accept-reject method, which can be considered a direct Monte Carlo approach. First, choose an appropriate proposal PDF $f(\boldsymbol{\varphi},\boldsymbol{\theta})$ and then generate a sequence of independent samples as follows:

(1) Randomly simulate candidate sample $[\boldsymbol{\varphi}_c, \boldsymbol{\theta}_c]$ from $f(\boldsymbol{\varphi},\boldsymbol{\theta})$ and u from uniform (0,1).

(2) Accept $[\boldsymbol{\varphi},\boldsymbol{\theta}]=[\boldsymbol{\varphi}_c,\boldsymbol{\theta}_c]$ if

$$h_s(\boldsymbol{\varphi}_c,\boldsymbol{\theta}_c)\frac{p(\boldsymbol{\varphi}_c,\boldsymbol{\theta}_c)}{Mf(\boldsymbol{\varphi}_c,\boldsymbol{\theta}_c)} > u, \text{ where } M > \max_{\boldsymbol{\varphi},\boldsymbol{\theta}} h_s(\boldsymbol{\varphi},\boldsymbol{\theta})\frac{p(\boldsymbol{\varphi},\boldsymbol{\theta})}{f(\boldsymbol{\varphi},\boldsymbol{\theta})} \quad . \tag{A4.1}$$

(3) Return to (1) otherwise.

Algorithm 2: Metropolis-Hastings algorithm, which belongs to Markov Chain Monte Carlo methods (MCMC) and is expressed through the iterative form:

(1) Randomly simulate a candidate sample $[\tilde{\boldsymbol{\varphi}}_{k+1},\tilde{\boldsymbol{\theta}}_{k+1}]$ from a proposal PDF $q(\tilde{\boldsymbol{\varphi}}_{k+1},\tilde{\boldsymbol{\theta}}_{k+1}|\boldsymbol{\varphi}_k,\boldsymbol{\theta}_k)$.

(2) Compute acceptance ratio:

$$r_{k+1} = \frac{h_s(\tilde{\boldsymbol{\varphi}}_{k+1},\tilde{\boldsymbol{\theta}}_{k+1},)\,p(\tilde{\boldsymbol{\varphi}}_{k+1},\tilde{\boldsymbol{\theta}}_{k+1},)q(\boldsymbol{\varphi}_k,\boldsymbol{\theta}_k \mid \tilde{\boldsymbol{\varphi}}_{k+1},\tilde{\boldsymbol{\theta}}_{k+1})}{h_s(\boldsymbol{\varphi}_{k+1},\boldsymbol{\theta}_{k+1},)\,p(\boldsymbol{\varphi}_{k+1},\boldsymbol{\theta}_{k+1},)q(\tilde{\boldsymbol{\varphi}}_{k+1},\tilde{\boldsymbol{\theta}}_{k+1} \mid \boldsymbol{\varphi}_k,\boldsymbol{\theta}_k)} \quad . \tag{A4.2}$$

(3) Simulate u from uniform (0,1) and set

$$[\boldsymbol{\varphi}_{k+1},\boldsymbol{\theta}_{k+1}] = \begin{cases} [\tilde{\boldsymbol{\varphi}}_{k+1},\tilde{\boldsymbol{\theta}}_{k+1}] \text{ if } r_{k+1} \geq u \\ [\boldsymbol{\varphi}_k,\boldsymbol{\theta}_k] \text{ otherwise} \end{cases} \quad . \tag{A4.3}$$

In this case the samples are correlated (the next sample depends on the previous one) but follow the target distribution after a burn-in period, i.e., after the Markov chain reaches stationarity. The algorithm is particularly efficient when samples that follow the target distribution are already available, since then no burn-in period is needed. Assume, in this setting, that there are N_a samples $[\boldsymbol{\varphi},\boldsymbol{\theta}]$ and a total $N>N_a$ are desired. Starting from each of the N_a original samples, $[N/N_a]$ samples are generated by the above process. Since the initial samples are distributed according to $\pi(\boldsymbol{\varphi},\boldsymbol{\theta})$, the Markov Chain generated in this way is always in its stationary state and all samples simulated follow the target distribution. Note that knowledge of the normalizing constant in the denominator of $\pi(\boldsymbol{\varphi},\boldsymbol{\theta})$ is not needed for any of the two algorithms.

The efficiency of both these sampling algorithms depends on the proposal PDFs $f(\boldsymbol{\varphi},\boldsymbol{\theta})$ and $q(\boldsymbol{\varphi},\boldsymbol{\theta})$. These PDFs should be chosen to closely resemble $h_s(\boldsymbol{\varphi},\boldsymbol{\theta})p(\boldsymbol{\varphi},\boldsymbol{\theta})$ and still be easy to sample from. If the first feature is established then the efficiency of the algorithm is high. For Metropolis-Hastings, the proposal PDFs can either be global (independent), i.e., $q(.)=q(\tilde{\boldsymbol{\varphi}}_{k+1},\tilde{\boldsymbol{\theta}}_{k+1})$, or establish a local random walk, i.e., $q=q(\tilde{\boldsymbol{\varphi}}_{k+1},\tilde{\boldsymbol{\theta}}_{k+1}|\boldsymbol{\varphi}_k,\boldsymbol{\theta}_k)$ (see Roberts and Rosenthal (2004) for more detailed discussion). In the latter case, the spread of the proposal PDFs is particularly important because it affects the size of the region covered by the Markov Chain samples (Roberts and Rosenthal 2001). Excessively large spread may

reduce the acceptance rate, increasing the number of repeated samples and thus slowing down convergence and create correlation between samples. On the other hand, small spread does not allow for efficient investigation of the whole region of the uncertain parameters and creates correlation between samples because of their proximity.

If the dimension of the uncertain parameter vector is high, a typical characteristic for dynamic problems where the excitation is modeled using a white-noise sequence $\mathbf{Z}_w$, the efficiency of the MCMC simulation process might be reduced (Au and Beck 2001a) because high correlation might exist between the current and the next chain state. For ROP the modified Metropolis-Hastings algorithm, discussed in detail in Au and Beck (2003), can be used in these cases (assuming that the performance measure is described by the indicator function). The modified algorithm differs from the original in the way that the candidate state is generated in steps 1 and 2. In the modified version the parameters in the uncertain parameter vector are divided into groups and steps 1 and 2 are applied for each group separately. A detailed discussion on grouping of uncertain parameters, choice of proposal PDFs, along with some other key issues for efficient MCMC simulation is presented in Au and Beck (2003). For general stochastic design problems the modified version of the Metropolis Hastings algorithm cannot be used; a global PDF should be chosen in this case for parameters that individually do not significantly influence the objective function, but have significant influence only when viewed as a group. The white-noise sequence in dynamic problems typically belongs to this category.

Appendix 4B: Relationship between Cartesian and Spherical Coordinates

The position of a point in the Euclidean $\mathbb{R}^{n_\varphi}$ space using a Cartesian coordinate system is determined by vector $\mathbf{x} \in \mathbb{R}^{n_\varphi}$. Using a spherical coordinate system this position is determined by the radial coordinate $r_c \in \mathbb{R}$ and the angular coordinates ψ_i, i=1,...,n_φ-1. The

last angular coordinate has range 2π and all the others have range π. The transformation from the spherical coordinate system to the Cartesian is:

$$\begin{aligned} x_1 &= r_c \cos\psi_1 \\ x_2 &= r_c \sin\psi_1 \cos\psi_2 \\ &... \\ x_{n_\varphi} &= r_c \sin\psi_1 \sin\psi_2 ... \cos\psi_{n_\varphi - 1} \end{aligned} \tag{B4.1}$$

while the inverse transformation is:

$$\begin{aligned} r_c &= \sqrt{\mathbf{x}^T \mathbf{x}} \\ \tan\psi_{n_\varphi - 1} &= \frac{x_{n_\varphi}}{x_{n_\varphi - 1}}, \quad \tan\psi_{n_\varphi - 2} = \frac{\sqrt{x_{n_\varphi}^2 + x_{n_\varphi - 1}^2}}{x_{n_\varphi - 2}} \\ &... \\ \tan\psi_1 &= \frac{\sqrt{x_{n_\varphi}^2 + x_{n_\varphi - 1}^2 + ... + x_2^2}}{x_{n_\varphi - 2}} \end{aligned} \quad . \tag{B4.2}$$

The Jacobian of the latter transformation is given by:

$$\left| \frac{\partial x_t}{\partial (r, \psi_i)} \right| = r_c^{n_\varphi - 1} \sin^{n_\varphi - 2}(\psi_1) \sin^{n_\varphi - 3}(\psi_2) ... \sin\left(\psi_{n_\varphi - 2}\right) \quad . \tag{B4.3}$$

Appendix 4C: Details for Characterization of Admissible Subsets as Hyper-Ellipses

In this appendix, some details are discussed pertaining to the selection of hyper-ellipses as admissible subsets $I \subset \mathcal{X}$. The analytical representation of such ellipses is:

$$\left(\mathbf{x} - \mathbf{x}_o\right)^T \mathbf{M}_d \left(\mathbf{x} - \mathbf{x}_o\right) = 1 \tag{C4.1}$$

where $\mathbf{M}_d \in \mathbb{R}^{n_\varphi x n_\varphi}$ is a positive-definite symmetric matrix, and $\mathbf{x}_o \in \mathbb{R}^{n_\varphi}$ is the center of the ellipse. If $\mathcal{X}$ is a hyper-rectangle ($\mathcal{X}_1$) then $\mathbf{x}_o$ should be described in Cartesian coordinates with admissible values given by $|x_{o,i}|<1 \ \forall i$. If $\mathcal{X}$ is a hyper-ellipse ($\mathcal{X}_2$), then $\mathbf{x}_o$ should be described in spherical coordinates with admissible values given by $r<1$. The matrix $\mathbf{M}_n$ can be efficiently parameterized as

$$\mathbf{M}_d^{-1} = \mathbf{D}_d^{1/2}\mathbf{B}_d\mathbf{D}_d^{1/2} \tag{C4.2}$$

where $\mathbf{D}_d$ is a diagonal matrix and $\mathbf{B}_d$ is a positive definite, symmetric matrix with unit values in the diagonal and off-diagonal terms that are less than 1. The values of the elements of $\mathbf{D}_d$ are related to the half-length of the ellipse in each principal orthogonal direction, thus these elements should be smaller than 1. The positive definite property for $\mathbf{B}_d$ must be incorporated into the characterization as an explicit nonlinear constraint; it corresponds to a requirement that all eigenvalues of $\mathbf{B}_d$ are positive. Another such nonlinear constraint must be used for the property $I \subset \mathcal{X}$. The equivalent analytical characterization for this requirement depends on the shape of the search space. It is discussed next for both the hyper-cubes and hyper-ellipses described in (4.28).

4.1C Subset relationship for hyper-ellipses within hyper-cube

An analytical expression for checking $I \subset \mathcal{X}_1$ is derived next when I is given by (C4.1) and $\mathcal{X}_1$ by $\|\mathbf{x}\|_\infty = 1$. Let $\mathbf{C}_n$ denote the upper triangular, invertible, matrix corresponding to the Cholesky decomposition for $\mathbf{M}_d$, then the coordinate transformation:

$$\mathbf{y} = \mathbf{C}_n\left(\mathbf{x} - \mathbf{x}_o\right) \tag{C4.3}$$

transforms the ellipse in (C4.1) to a unit radius hyper-sphere $\mathbf{y}^T\mathbf{y}=1$. The boundary surface of the hyper-cube in the transformed space is given by the intersection of the pair of hyper-planes:

$$\pm 1 = C_n^{-1}\mathbf{y} + \mathbf{x}_o \quad . \tag{C4.4}$$

If $\mathbf{C}_n^{-1} = \mathbf{T}$ then the minimum distance of these pair of hyper-planes from the origin of the transformed space is:

$$\min_i \left\{ \min \left(\frac{1-\mathbf{x}_o}{\sqrt{\sum_{j=1}^{n_\varphi} T_{ij}^2}}, \frac{1+\mathbf{x}_o}{\sqrt{\sum_{j=1}^{n_\varphi} T_{ij}^2}} \right) \right\} \quad . \tag{C4.5}$$

If that distance is greater than 1 then in the transformed space the hyper-sphere is within the intersection of the hyper-planes, which means $I \subset \chi_1$.

4.2C Subset relationship for hyper-ellipses within hyper-sphere

Next, the analytical expression for checking $I \subset \chi_2$ is investigated, where χ_2 is characterized as r_c<1. This will be satisfied if the maximum distance of the ellipse (C4.1) from the origin is smaller than 1. This maximum distance is given by the optimization problem:

$$\begin{aligned} &\max\ g(\mathbf{x}) = \mathbf{x}^T\mathbf{x} \\ &\text{subject to } \left(\mathbf{x}-\mathbf{x}_o\right)^T \mathbf{M}_d \left(\mathbf{x}-\mathbf{x}_o\right) = 1 \quad . \end{aligned} \tag{C4.6}$$

Introducing lagrange multiplier λ, consider the augmented problem:

$$f(\mathbf{x},\lambda) = \mathbf{x}^T\mathbf{x} - \lambda\left(\mathbf{x}-\mathbf{x}_o\right)^T \mathbf{M}_d \left(\mathbf{x}-\mathbf{x}_o\right) \quad . \tag{C4.7}$$

The first-order optimality conditions for all of the local extrema, give:

$$\nabla_{\mathbf{x}} f(\mathbf{x},\lambda) = 0 \Rightarrow \lambda\mathbf{M}_d\left(\mathbf{x}-\mathbf{x}_o\right) = \mathbf{x} \Rightarrow \left(\lambda\mathbf{M}_d - \mathbf{I}\right)\mathbf{x} = \lambda\mathbf{M}_d\mathbf{x}_o \tag{C4.8}$$

$$\frac{df(\mathbf{x},\lambda)}{d\lambda} = 0 \Rightarrow \left(\mathbf{x}-\mathbf{x}_o\right)^T \mathbf{M}_d \left(\mathbf{x}-\mathbf{x}_o\right) = 1 \quad . \tag{C4.9}$$

The positive-definite matrix $\mathbf{M}_d$ can be decomposed as:

$$\mathbf{T}_n \mathbf{D}_n \mathbf{T}_n^T = \mathbf{M}_d \tag{C4.10}$$

where $\mathbf{D}_n$=diag(d_1, …, d_{n_φ}) is a diagonal matrix of eigenvalues of $\mathbf{M}_d$, and $\mathbf{T}_n$ is a matrix of orthonormal eigenvectors of $\mathbf{M}_d$. Define now

$$\mathbf{y} = \mathbf{T}_n^T \mathbf{x},\ \mathbf{y}_o = \mathbf{T}_n^T \mathbf{x}_o \quad . \tag{C4.11}$$

The first-order optimality conditions are then transformed:

$$\left(\lambda \mathbf{D}_n - \mathbf{I}\right)\mathbf{y} = \lambda \mathbf{D}_n \mathbf{y}_o \tag{C4.12}$$

$$\mathbf{y}^T \mathbf{D}_n^{-1} \mathbf{y} = \lambda^2 \Rightarrow \sum_{i=1}^{n} \frac{1}{d_i} y_i^2 = \lambda^2 \tag{C4.13}$$

and the objective function is transformed:

$$g(\mathbf{y}) = \sum_{i=1}^{n} y_i^2 \quad . \tag{C4.14}$$

Two cases need to be considered next, depending on whether $\lambda\mathbf{D}_n$-$\mathbf{I}$ is invertible or not.

Case (1): Assume $\lambda \neq 1/d_i \ \forall i$, then ($\lambda\mathbf{D}_n$-$\mathbf{I}$) is invertible and the solution for λ will be converted to an eigenvalue problem. Equation (C4.12) is transformed to:

$$\mathbf{y} = \lambda \left(\lambda \mathbf{D}_n - \mathbf{I} \right)^{-1} \mathbf{D}_n \mathbf{y}_o \quad . \tag{C4.15}$$

Plugging this value into (C4.13) leads to:

$$\mathbf{y}_o^T \mathbf{D}_n \left(\lambda \mathbf{D}_n - \mathbf{I} \right)^{-1} \mathbf{D}_n^{-1} \mathbf{y} = \lambda \ \Rightarrow \mathbf{y}_o^T \mathbf{w} = \lambda \tag{C4.16}$$

where:

$$\mathbf{w} = \mathbf{D}_n \left(\lambda \mathbf{D}_n - \mathbf{I} \right)^{-1} \mathbf{D}_n^{-1} \mathbf{y} \Rightarrow \left(\lambda \mathbf{D}_n - \mathbf{I} \right) \mathbf{D}_n^{-1} \mathbf{w} = \mathbf{D}_n^{-1} \mathbf{y} \Rightarrow \lambda \mathbf{w} = \mathbf{D}_n^{-1} \mathbf{w} + \mathbf{D}_n^{-1} \mathbf{y} \quad . \tag{C4.17}$$

Then (C4.12) is transformed:

$$\left(\lambda \mathbf{D}_n - \mathbf{I} \right) \mathbf{y} = \mathbf{D}_n \mathbf{y}_o \mathbf{y}_o^T \mathbf{w} \Rightarrow \lambda \mathbf{y} = \mathbf{y}_o \mathbf{y}_o^T \mathbf{w} + \mathbf{D}_n^{-1} \mathbf{y} \tag{C4.18}$$

and we end up with the eigenvalue problem

$$\begin{bmatrix} \mathbf{D}_n^{-1} & \mathbf{y}_o \mathbf{y}_o^T \\ \mathbf{D}_n^{-1} & \mathbf{D}_n^{-1} \end{bmatrix} \begin{bmatrix} \mathbf{y} \\ \mathbf{w} \end{bmatrix} = \lambda \begin{bmatrix} \mathbf{y} \\ \mathbf{w} \end{bmatrix} \quad . \tag{C4.19}$$

This problem has at most 2*n* real solutions, corresponding to potential 2*n* local extrema given by:

$$\mathbf{y}_j = \frac{\lambda_i d_j}{\lambda_i d_j - 1} \mathbf{y}_{o,j} \quad . \tag{C4.20}$$

The distance from the origin for each one of them is then:

$$g(\mathbf{y}) = \sum_{i=1}^{n} y_i^2 = \sum_{i=1}^{n} \frac{\left(\lambda_i d_j\right)^2}{\left(\lambda_i d_j - 1\right)^2} \left(\mathbf{y}_{o,j}\right)^2 \quad . \tag{C4.21}$$

Case (2): Assume $\lambda = 1/d_i$. Let the multiplicity of eigenvalue d_i be n_k, $\{k\}$ corresponding to the index for all eigenvalues of $\mathbf{M}_d$ that are equal to d_i and $\{j\}$ to the index of the rest n-n_k eigenvalues. Equation (C4.12) leads to

$$\mathbf{y}_j = \frac{d_j}{\left(d_j - d_i\right)} \mathbf{y}_{o,j} \text{ if } d_j \neq d_i \tag{C4.22}$$

also

$$y_{o,k} = 0 \text{ if } d_k = d_i \tag{C4.23}$$

has to hold. Then (C4.13) leads to:

$$\sum_k y_k^2 = \frac{1}{d_i} - d_i \sum_j \frac{1}{d_j} y_j^2 \tag{C4.24}$$

and thus the distance from the origin will be

$$g(\mathbf{y}) = \sum_{i=1}^{n} y_i^2 = \sum_j y_j^2 + \sum_k y_k^2 = \sum_{j=1} \frac{d_j - d_i}{d_j} y_j^2 + \frac{1}{d_i} = \sum_{j=1} \frac{d_j}{(d_j - d_i)} y_{o,j}^2 + \frac{1}{d_i} \quad . \tag{C4.25}$$

Note that calculation of the exact coordinates for **y** was not necessary. The necessary and sufficient conditions for the case (2) to be true are that equations (C4.23) and (C4.24) have a solution which is equivalent to:

$$y_{o,k} = 0 \text{ and } \frac{1}{d_i^2} \geq \sum_j \frac{1}{d_j} y_j^2 \Rightarrow \frac{1}{d_i^2} > \sum_j \frac{d_j}{\left(d_j - d_i\right)^2} \mathbf{y}_{o,j}^2 \quad . \tag{C4.26}$$

The potential extremal distances are finally given by equations (C4.21) ($2n_\varphi$ potential solutions) or (C4.25) (n_φ potential solutions) with Lagrange multipliers for the first case given by the real eigenvalues of (C4.19) and additional constraints for the second case by (C4.26). If the maximum of these distances is smaller than 1 then we have that $I \subset \chi_2$.

CHAPTER 5

Stochastic System Design: Stochastic Optimization Framework

Chapter 4 presented SSO, a novel algorithm for efficiently exploring the sensitivity with respect to the design variables in stochastic optimization problems and iteratively identifying a subset of the original design space that has high plausibility of containing the optimal design variables. This chapter initially discusses topics related to stochastic optimization algorithms that are appropriate for the design problems considered in this study. An efficient two-stage framework is then suggested combining SSO with such algorithms. Topics related to the combination of the two different stages for overall enhanced efficiency and accuracy of the optimization process are discussed.

5.1 Stochastic Optimization

The original formulation of the stochastic objective function, i.e., (2.1), is used herein. In principle, though, the techniques discussed here are applicable to the case that the loss function $h(\boldsymbol{\theta},\boldsymbol{\varphi})$ is replaced by $h_s(\boldsymbol{\theta},\boldsymbol{\varphi})$ used in the SSO setting (given by (4.1)).

5.1.1 Common random numbers

The efficiency of stochastic optimizations such as (2.6) can be enhanced by the reduction of the absolute and/or relative importance of the estimation error $e_N(\boldsymbol{\varphi},\boldsymbol{\Omega}_N)$. The absolute

importance may be reduced by obtaining more accurate estimates of the objective function, i.e., by reducing the variance of the estimates. This can be established in various ways, for example, by using importance sampling (see Section 5.2.2) or by selecting a larger sample size N in (2.4); but these methods typically involve extra computational effort. It is more efficient to seek a reduction in the relative importance of the estimation error. This means reducing the variance of the difference of the estimates $\hat{E}_{\boldsymbol{\theta},N}[h(\boldsymbol{\varphi}^1,\boldsymbol{\Omega}_N^1)]$ and $\hat{E}_{\boldsymbol{\theta},N}[h(\boldsymbol{\varphi}^2,\boldsymbol{\Omega}_N^2)]$ that correspond to two different design choices $\boldsymbol{\varphi}^1$ and $\boldsymbol{\varphi}^2$. This variance can be decomposed as:

$$\begin{aligned}\operatorname{var}\left(\hat{E}_{\boldsymbol{\theta},N}[h(\boldsymbol{\varphi}^1,\boldsymbol{\Omega}_N^1)]-\hat{E}_{\boldsymbol{\theta},N}[h(\boldsymbol{\varphi}^2,\boldsymbol{\Omega}_N^2)]\right)&=\operatorname{var}\left(\hat{E}_{\boldsymbol{\theta},N}[h(\boldsymbol{\varphi}^1,\boldsymbol{\Omega}_N^1)]\right)\\&+\operatorname{var}\left(\hat{E}_{\boldsymbol{\theta},N}[h(\boldsymbol{\varphi}^2,\boldsymbol{\Omega}_N^2)]\right)-2\operatorname{cov}\left(\hat{E}_{\boldsymbol{\theta},N}[h(\boldsymbol{\varphi}^1,\boldsymbol{\Omega}_N^1)],\hat{E}_{\boldsymbol{\theta},N}[h(\boldsymbol{\varphi}^2,\boldsymbol{\Omega}_N^2)]\right)\end{aligned}\quad . \tag{5.1}$$

If $\hat{E}_{\boldsymbol{\theta},N}[h(\boldsymbol{\varphi}^1,\boldsymbol{\Omega}_N^1)]$ and $\hat{E}_{\boldsymbol{\theta},N}[h(\boldsymbol{\varphi}^2,\boldsymbol{\Omega}_N^2)]$ are evaluated independently, their covariance is zero; deliberately introducing dependence, increases the covariance (i.e., increases their correlation) and thus decreases their variability (the variance on the left). This decrease in the variance improves the efficiency of the comparison of the two estimates; it may be considered as creating a consistent estimation error. In the stochastic simulation-based context this task is achieved by adopting common random number streams (CRN), i.e., $\boldsymbol{\Omega}_N^1=\boldsymbol{\Omega}_N^2$, in the simulations generating the two different estimates. Figure 5.1 shows the influence of such a selection: the curves that correspond to CRN are characterized by consistent estimation error and are smoother. Also note that the absolute influence of the estimation error for the case that corresponds to larger N (curve (iii)) is, as expected, smaller.

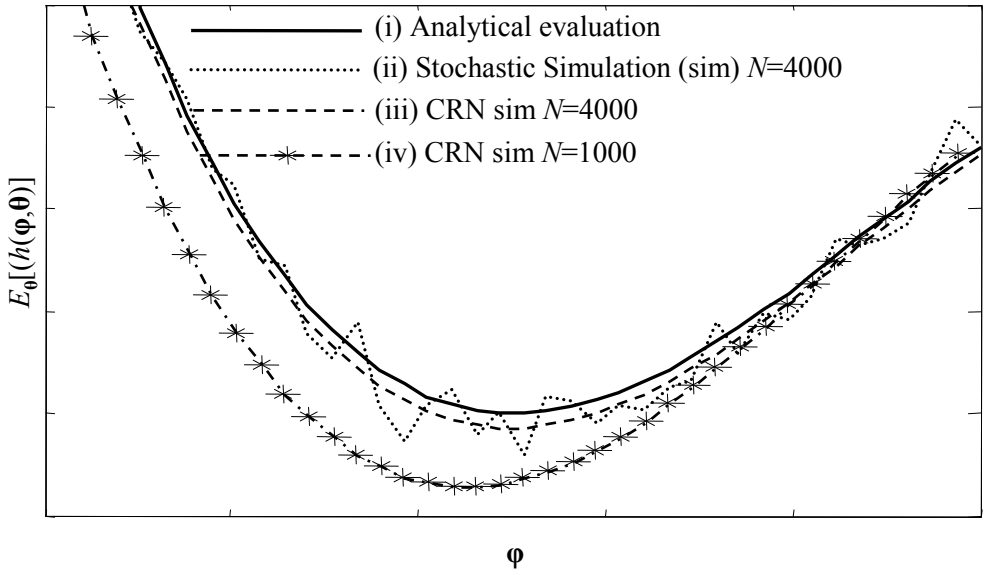

Figure 5.1: Evaluation of objective function using common random numbers (CRN)

Two important questions regarding the use of CRN are: Will the variance be reduced (efficiency)? Is this the best one can do (optimality)? The answer to both these questions depends on the way the random sample $\boldsymbol{\theta}$ (input) influences the sample value of the loss function $h(\boldsymbol{\varphi},\boldsymbol{\theta})$ (output) in each simulation. Optimality can be proved only in special cases, but efficiency can be guaranteed under mild conditions (Glasserman and Yao, 1992). Continuity and monotonicity of the output with respect to the random number input are key issues for establishing efficiency. If $h(\boldsymbol{\varphi},\boldsymbol{\theta})$ is sufficiently smooth then the two aforementioned requirements for CRN-based comparisons can be guaranteed, as long as the design choices compared are not too far apart in the design variable space. In such cases it is expected that use of CRN will at least be advantageous (if not optimal). If the systems compared are significantly different, i.e., correspond to $\boldsymbol{\varphi}$ that are not close, then CRN does not necessarily guarantee a consistent estimation error. This might occur if the regions of Θ that contribute most to the integral of the expected value for the two systems are drastically different and the CRN streams selected do not efficiently represent both of these regions. This feature is also indicated in curve (iv) in Figure 5.1; the estimation error is not consistent along the whole range of $\boldsymbol{\varphi}$ for the CRN curves (compare the objective function

for curve (iv) for large and small values of $\boldsymbol{\varphi}$), but for local comparisons it appears to be consistent.

For ROP, CRN does not necessarily have a similar effect on the calculated output if formulation (2.8) is adopted, since the indicator function $I_F(\boldsymbol{\varphi},\boldsymbol{\theta})$ is discontinuous. Thus the aforementioned requirements for establishing efficiency of CRN application cannot be guaranteed. It is, thus, beneficial to use the formulation (2.12) for the probability of failure in CRN-based optimizations. For design problems where no prediction error in the model response is actually assumed, a small fictitious error should be chosen so that the optimization problems with and without the model prediction error are practically equivalent, i.e., correspond to the same optimum. Figure 5.2 illustrates this concept. In Figure 5.2(a) the two performance measures for ROP are compared when ε is modeled as a Gaussian variable with mean 0 and standard deviation 0.01. In Figure 5.2(b) the influence on P_F of these two different choices and the advantage of selecting $P_\varepsilon(\tilde{g}(\boldsymbol{\varphi},\boldsymbol{\theta}))$ for establishing a consistent prediction error is clearly demonstrated.

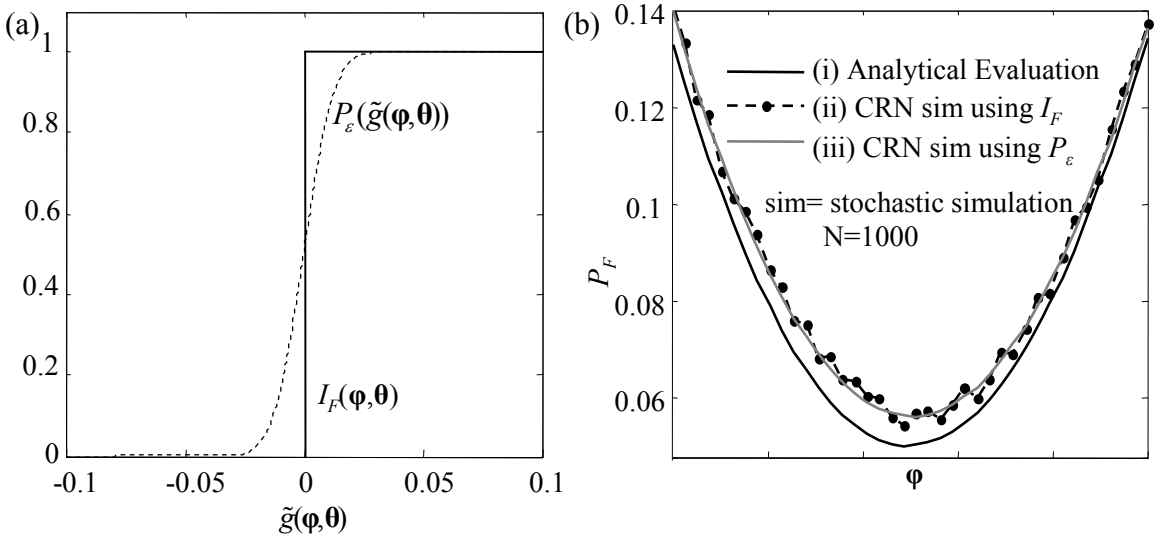

Figure 5.2: Illustration of CRN application in ROP: (a) the two possible performance measures and (b) comparison between the estimated objective functions using these two choices

5.1.2 Exterior sampling approximation

Solution approaches to optimization problems using stochastic simulation are based on either interior or exterior sampling techniques (Ruszczynski and Shapiro, 2003). Interior sampling methods resample $\mathbf{\Omega}_N$ at each iteration of the optimization algorithm. On the other hand, exterior sampling approximation (ESA) adopts the same stream of random numbers throughout all iterations in the optimization process, thus transforming problem (2.6) into a deterministic one, which can be solved by any appropriate routine. These methods are also commonly referred to as sample average approximations (Royset and Polak 2004) and they are closely related to CRN. The CRN cases in Figure 5.1 correspond actually to ESA. Several asymptotic results are available for ESA and their rate of convergence under weak assumptions. For finite sample sizes, the optimal solution depends on the sample $\mathbf{\Omega}_N$ selected. Figure 5.1 clearly demonstrates this issue (compare the optimum values in the CRN curves (iii) and (iv)). Usually ESA is implemented by selecting N "large enough", typically much higher than it would be for interior sampling methods, in order to get better quality estimates for the objective function and thus more accurate solutions to the optimization problem. See Ruszczynski and Shapiro (2003) for more details and Royset and Polak (2007) for a computationally efficient iterative approach that adaptively implements higher accuracy estimates as the algorithm converges to the optimal solution. The quality of the solution obtained through ESA is commonly assessed by solving the optimization problem multiple times, for different independent random sample streams. Even though the computational cost for the ESA deterministic optimization is typically smaller than that of the original stochastic search problem, the overall efficiency may be worse because of the requirement to perform the optimization multiple times.

5.1.3 Appropriate stochastic optimization algorithms

Both gradient-based and gradient-free algorithms can be used in conjunction with CRN or ESA and can be appropriate for stochastic optimizations.

Gradient-based algorithms: they use derivative information to iterate in the direction of steepest descent for the objective function. Only local designs are compared in each iteration, which makes the implementation of CRN efficient and allows for application of stochastic approximation, which can significantly improve the computational efficiency of stochastic search methods (Kushner and Yin 2003). The latter approximation is performed by establishing through proper recursive formulas an equivalent averaging across the iterations of the optimization algorithm, instead of getting higher accuracy estimates for the objective function at each iteration (that is, averaging over one single iteration). In simple examples, the performance measure $h(\boldsymbol{\varphi},\boldsymbol{\theta})$ (or even the limit state function $\tilde{g}(\boldsymbol{\varphi},\boldsymbol{\theta})$ in ROP) are such that the gradient of the objective function with respect to $\boldsymbol{\varphi}$ can be obtained through a single stochastic simulation analysis (Spall 2003; Royset and Polak 2004). In many structural design problems, though, the models used are generally complex and it is difficult, or impractical, to develop an analytical relationship between the design variables and the objective function. Finite difference numerical differentiation is often the only possibility for obtaining information about the gradient vector but this involves a computational cost which increases linearly with the dimension of the design parameters. Simultaneous-perturbation stochastic approximation (SPSA) (Spall 1992; Spall 2003) is an efficient alternative search method. It is based on the observation that one properly chosen simultaneous random perturbation in all components of $\boldsymbol{\varphi}$ provides as much information for optimization purposes in the long run as a full set of one at a time changes of each component. Thus, it uses only two evaluations of the objective function, in a direction randomly chosen at each iteration, to form an approximation to the gradient vector.

Gradient-free optimization methods: include approaches, such as evolutionary algorithms, direct search and objective function approximation methods (OAM). They are based on comparisons of design choices that are distributed in large regions of the design space. They require information only for the objective function, which makes them highly appropriate for stochastic optimizations (Au and Beck 1999; Lagaros et al. 2002; Jensen and Catalan 2007) because they avoid the difficulty of obtaining derivative information.

They involve, though, significant computational effort if the dimension of the design variables is high. Use of CRN in these algorithms may only improve the efficiency of the comparisons in special cases; for example, if the size (volume) of the design space is "relatively small" and thus the design variables being compared are always close to each other.

More detailed discussion of algorithms for stochastic optimization can be found in Spall (2003) and Ruszczynski and Shapiro (2003). Also algorithms suggested for simulation-based optimizations (see, for example, Gosavi (2003)) can be appropriate for the class of problems considered here. Two approaches, SPSA and OAM, are briefly summarized here.

5.1.4 Simultaneous-perturbation stochastic approximation using common random numbers

The implementation of SPSA using CRN for stochastic design problems take the iterative form (Kleinmann et al. 1999):

$$\begin{aligned} \boldsymbol{\varphi}_{k+1} &= \boldsymbol{\varphi}_k - \alpha_k \mathbf{g}_k\left(\boldsymbol{\varphi}_k, \boldsymbol{\Omega}_N^k\right) \\ \boldsymbol{\varphi}_{k+1} &\in \Phi \end{aligned} \tag{5.2}$$

where $\boldsymbol{\varphi}_1$ corresponds to the chosen point to initiate the algorithm, and the j^{th} component for the CRN simultaneous perturbation approximation to the gradient vector in the k^{th} iteration, $\mathbf{g}_k(\boldsymbol{\varphi}_k, \boldsymbol{\Omega}_N^k)$, is given by:

$$g_{k,j} = \frac{\hat{E}_{\boldsymbol{\theta},N}\left(\boldsymbol{\varphi}_k + c_k \boldsymbol{\Delta}_k, \boldsymbol{\Omega}_N^k\right) - \hat{E}_{\boldsymbol{\theta},N}\left(\boldsymbol{\varphi}_k - c_k \boldsymbol{\Delta}_k, \boldsymbol{\Omega}_N^k\right)}{2c_k \Delta_{\kappa,j}} \tag{5.3}$$

where $\mathbf{\Delta}_k \in \mathbb{R}^{n_\varphi}$ is a vector of mutually independent random variables that defines the random direction of simultaneous perturbation for $\boldsymbol{\varphi}_k$ and that satisfies the statistical properties given in (Spall, 2003). A symmetric Bernoulli ±1 distribution is typically chosen for the components of $\mathbf{\Delta}_k$. A detailed discussion about other possible distributions is provided in Hutchison (2002). The selection for the sequences $\{c_k\}$ and $\{\alpha_k\}$ is discussed in detail in Spall (1998) and Kleinmann et al. (1999). A choice that guarantees asymptotic convergence to $\boldsymbol{\varphi}^*$ is $\alpha_k=\alpha/(k+w)^\beta$ and $c_k=c_1/k^\zeta$, where $4\zeta-\beta>0$, $2\beta-2\zeta>1$, with $w,\zeta>0$ and $0<\beta<1$. This selection leads to a rate of convergence that asymptotically approaches $k^{-\beta/2}$ when CRN is used (Kleinmann et al. 1999). The asymptotically optimal choice for β is, thus, 1. In applications where efficiency using a small number of iterations is sought after, use of smaller values for β are suggested in Spall (2003). For complex structural design optimizations, where the computational cost for each iteration of the algorithm is high, the latter suggestion should be adopted. Implementation of CRN contributes to reducing the variance of the gradient approximation in (5.3) and thus the variability in estimating $\boldsymbol{\varphi}_\kappa$; for example, the rate of convergence is $k^{-\beta/3}$ when CRN is not used.

Regarding the rest of the parameters for the sequences $\{c_k\}$ and $\{\alpha_k\}$: w is typically set to 10% of the number of iterations selected for the algorithm and the initial step c_1 is chosen "close" to the standard deviation of the measurement error $e_N(\mathbf{\Omega}_N,\boldsymbol{\varphi}_1)$. This last selection prevents the finite difference gradient from getting excessively large in magnitude but might be inefficient if the standard deviation of the error changes dramatically with $\boldsymbol{\varphi}$. The value of α can be determined based on the estimate of $\mathbf{g}_1$ and the desired step size for the first iteration. Some initial trials are generally needed in order to make a good selection for α, especially when little prior insight is available for the sensitivity of the objective function to each of the design variables. Typically SPSA is implemented adopting interior sampling techniques. Convergence of the iterative process is judged based on the value $\|\boldsymbol{\varphi}_{k+1}-\boldsymbol{\varphi}_k\|$ in the last few steps for an appropriate selected vector norm. Note that since the progress of the algorithm at each step depends on the sample $\mathbf{\Omega}_N^k$ and the randomly chosen perturbation direction, convergence cannot be judged based on the value of

$|\hat{E}_{\boldsymbol{\theta},N}\left(\boldsymbol{\varphi}_{k+1},\boldsymbol{\Omega}_N^{k+1}\right)-\hat{E}_{\boldsymbol{\theta},N}\left(\boldsymbol{\varphi}_k,\boldsymbol{\Omega}_N^{k}\right)|$ (because the two estimates are evaluated using different steams of random samples and thus include different estimation error) or the value of $\|\boldsymbol{\varphi}_{k+1}-\boldsymbol{\varphi}_k\|$ at the last step only (because this value depends on the random search direction chosen). This notion of convergence, though, depends on the selection of the sequence $\{\alpha_k\}$; for example, selection of small step sizes might in some cases give a false impression that convergence has been established, even though this is not true. Such problems can be avoided by restarting the SPSA algorithm at the converged optimal solution to monitor the behavior for some small number of iterations. Additionally, iterate averaging can be applied for selecting the optimal solution (Maryak 1997); instead of selecting the optimal design configuration to correspond to the solution identified at the last iteration of the algorithm, a weighted average is chosen over the last few iterations. Blocking rules can also be applied in order to avoid potential divergence of the algorithm, especially in the first iterations (Spall 2003).

5.1.5 Objective function approximation methods

Objective function approximation methods (OAM) sequentially approximate the optimization objective using interpolating functions dependent on the design variables. They belong to the larger class of response surface methods that are commonly used for global approximations of functions that are costly to evaluate, particularly in terms of simulation-based analyses. Since response surface methodologies are not limited to optimization problems, the terminology OAM is preferred here to describe this optimization approach.

Various applications of OAM have been presented in the optimization literature, implementing different kinds of interpolating functions, for example, radial basis functions or polynomials (Husain et al. 2002), and rules for convergence to the optimal solution, see, for example, Neddermeijer et al. (2000). The basic idea is to first perform several evaluations of the objective function at some interpolating points in a region $\Phi_a \subset \Phi$ and

then build an “approximation surface” describing the local behavior of it. This surface is used to move toward a better candidate for the optimal design variables.

There are two main approaches for creating the approximation surface in OAM. The first approach uses radial basis functions; at each iteration the objective function is evaluated at the location identified at the previous step as potential optimal solution, and this information is used in order to sequentially establish a more accurate approximation and progress to the next step (Jones et al. 1998). The second approach uses polynomial interpolation functions to approximate the objective function at each point, with coefficients that are determined by means of a regression analysis. Most commonly the number of interpolation points is selected larger than the number of the polynomial coefficients. The minimization of a weighted least-squares norm is then implemented for choosing the coefficients; this norm is typically related to the approximation error at the interpolation points. The weighting functions can be selected according to the location of the interpolation points relative to the point at which the objective function is approximated. This methodology aims at reducing the approximation error at each point by performing a weighted local averaging of the information obtained by the interpolation points that are closer to it. It is typically referred to as moving least-squares method, e.g., Choi et al. (2001), and leads to coefficients for the polynomial approximation that are functions of the design variables. Global methodologies have also been proposed; in this case the polynomial coefficients are set to constant values, i.e., they are assumed independent of the design variables, e.g., Gasser and Schueller (1997). These methodologies are referred to as global least-squares method. After establishing the approximate surfaces for the objective function, a secondary optimization problem is solved to locate the potential local minima. The process progresses then to the next iteration.

For stochastic design problems these two approaches can be implemented by adopting either exterior or interior sampling. For exterior sampling the optimization problem is

equivalent to deterministic optimization using OAM. For interior sampling the existence of estimation error, because of the evaluation of the objective function using stochastic simulation, must be additionally taken into account. The importance of this error can be reduced by establishing a local averaging; this idea is similar to the reduction of the approximation error discussed earlier. For this purpose the weights in the least-squares minimization problem can be scaled according to the c.o.v. of the estimate of the objective function, given by (2.5). Estimates that have smaller c.o.v. should be given higher weight. For converging to the optimal solution a moving iterative approach has also been suggested; in this case the set Φ_α is adjusted within the search space Φ , e.g., Jensen (2005); this way a better local approximation for the objective function around the optimal point can be established. Typically Φ_α is centered on the location identified as the optimal solution in the previous step.

Similar convergence criteria, as in SPSA, can be adopted. The efficiency of this methodology for stochastic optimization problems depends, ultimately, on the insight available for the characteristics of the optimization objective inside the search space Φ; for example, in terms of selecting the form of interpolating functions.

5.2 Framework for Stochastic Optimization Using Stochastic Simulation

5.2.1 Outline of the framework

As already mentioned, a two-stage framework for stochastic system design may be established by combining some stochastic optimization algorithm, like the ones presented in the previous section, with the SSO algorithm developed in Chapter 4. In the first stage, SSO is implemented in order to efficiently explore the sensitivity of the objective function and adaptively identify a subset $I_{SSO} \subset \Phi$ containing the optimal design variables. In the second stage, any appropriate stochastic optimization algorithm is implemented in order to pinpoint the optimal solution within I_{SSO}. The specific algorithm selected for the second stage determines the level of quality that should be established in the SSO identification. If

a method is chosen that is restricted to search only within I_{SSO} (typically characteristic of gradient-free methods), then better quality is needed. The iterations of SSO should stop at a larger size set, and establish greater plausibility that the identified set includes the optimal design point. If, on the other hand, a method is selected that allows for convergence to points outside the identified set, lower quality may be acceptable in the identification. A value 0.75–0.80 for $\hat{H}(\hat{I}_k)$ with a c.o.v. of 4% for that estimate, indicates high certainty, in the applications examined so far, that $\hat{I}_k$ includes the optimal solution. Of course, this depends on the characteristics of the problem too, and particularly on the selection of the shape of admissible subsets, but this guideline has proved to be robust in the applications considered so far.

The efficiency of the stochastic optimization considered in the second stage is influenced by (a) the size of the design space Φ defined by its volume V_Φ, and, depending on the characteristics of the algorithm chosen, by (b) the initial point $\boldsymbol{\varphi}_1$ at which the algorithm is initiated, and (c) the knowledge about the local behavior of the objective function in Φ. For example, topic (b) is important for gradient-based algorithms whereas topic (c) is relevant for iterative algorithms that require user insight for selecting appropriate step sizes (like SPSA). The SSO stage gives valuable insight for all these topics and can, therefore, contribute to increasing the efficiency of convergence to the optimal solution $\boldsymbol{\varphi}^*$. The set I_{SSO} has smaller size (volume) than the original design space Φ. Also, it is established that the sensitivity of the objective function with respect to all components of $\boldsymbol{\varphi}$ is small. This allows, for example, for efficient normalization of the design space (in selecting step sizes) and choice of interpolating functions (for OAM). With respect to the two algorithms discussed in detail in Section 5.1.5 the following guidelines are suggested for fine-tuning their parameters using information from SSO:

For SPSA: $\boldsymbol{\varphi}_1$ should be selected as the center of the set I_{SSO}. Parameter α can be chosen so that the initial step for each component of $\boldsymbol{\varphi}$ is smaller than a certain fraction (chosen as 1/10) of the respective size of I_{SSO}, based on the estimate for $\mathbf{g}_1$ from (5.3). This estimate

should be averaged over n_g (chosen as 6) evaluations because of its importance in the efficiency of the algorithm. Also no movement in any direction should be allowed that is greater than a quarter of the size of the respective dimension of I_{SSO} (blocking rule). For greater efficiency the optimization can be performed in the normalized search space, as discussed in Section 4.2.1.

For OAM: since set I_{SSO} corresponds to a region close to the optimal solution that is characterized by small sensitivity with respect to all design variables, a global least-squares second-order polynomial approximation to the objective function should be efficient. Thus $E_{\boldsymbol{\theta}}[h(\boldsymbol{\varphi},\boldsymbol{\theta})]$ can be approximated as:

$$E_{\boldsymbol{\theta}}[h(\boldsymbol{\varphi},\boldsymbol{\theta})] \approx c_a + \mathbf{B}_a\boldsymbol{\varphi} + \boldsymbol{\varphi}^{\mathrm{T}}\mathbf{M}_a\boldsymbol{\varphi} \tag{5.4}$$

where $c_a \in \mathbb{R}$, $\mathbf{B}_\alpha \in \mathbb{R}^{n_\varphi}$, and $\mathbf{M}_a \in \mathbb{R}^{n_\varphi x n_\varphi}$ are the polynomial coefficients to be estimated. In reliability optimizations, such polynomial approximations are typically applied with respect to the log of the probability of failure (Gasser and Schueller 1997; Jensen 2005). The candidate stationary point for the approximation in (5.4) is finally:

$$\boldsymbol{\varphi} = \frac{1}{2}\mathbf{M}_a^{-1}\mathbf{B}_a \quad . \tag{5.5}$$

If this point does not satisfy the optimization constraints, then the candidate stationary point can be identified by solving a constrained optimization problem with objective function that has the analytical form in (5.4). The computational effort for solving the latter problem is minimal.

This OAM approach has the relative disadvantage that it cannot benefit from usage of CRN, unless exterior sampling is chosen. That is why SPSA is preferred in the applications considered in the current study. Still, the formulation suggested here for OAM, in particular combined with a local averaging scheme for reducing the influence of the estimation error,

as discussed earlier, seems a promising idea for stochastic optimization problems and deserves further consideration in future research.

Additionally, the information from the SSO stage can be exploited in order to reduce the variance of the estimate $E_{\boldsymbol{\theta}}[h(\boldsymbol{\varphi},\boldsymbol{\Omega}_N)]$ in the second stage of the framework by using importance sampling. This choice is discussed next.

5.2.2 Importance sampling

Importance sampling (IS) is an efficient variance reduction technique. It is based on choosing an importance sampling density $p_{is}(\boldsymbol{\theta}|\boldsymbol{\varphi})$ to generate samples in regions of Θ that contribute more to the integral of $E_{\boldsymbol{\theta}}[h(\boldsymbol{\varphi},\boldsymbol{\theta})]$. An alternative representation of this integral is utilized:

$$E_{\boldsymbol{\theta}}\left[h(\boldsymbol{\varphi},\boldsymbol{\theta})\right] = \int_{\boldsymbol{\Theta}} h(\boldsymbol{\varphi},\boldsymbol{\theta}) \frac{p(\boldsymbol{\theta}\,|\,\boldsymbol{\varphi})}{p_{is}(\boldsymbol{\theta}\,|\,\boldsymbol{\varphi})}\, p_{is}(\boldsymbol{\theta}\,|\,\boldsymbol{\varphi}) d\boldsymbol{\theta} = E_{\boldsymbol{\theta},is}\left[h(\boldsymbol{\varphi},\boldsymbol{\theta}) R(\boldsymbol{\theta}\,|\,\boldsymbol{\varphi})\right] \tag{5.6}$$

where $E_{\boldsymbol{\theta},\text{is}}[.]$ denotes expectation under distribution $p_{is}(.)$ and

$$R(\boldsymbol{\theta}\,|\,\boldsymbol{\varphi}) = \frac{p(\boldsymbol{\theta}\,|\,\boldsymbol{\varphi})}{p_{is}(\boldsymbol{\theta}\,|\,\boldsymbol{\varphi})} \tag{5.7}$$

is the importance sampling quotient. The estimate for $E_{\boldsymbol{\theta}}[h(\boldsymbol{\varphi},\boldsymbol{\theta})]$ is given in this case by:

$$\hat{E}_{\boldsymbol{\theta},N}[h(\boldsymbol{\varphi},\boldsymbol{\Omega}_N)] = \frac{1}{N}\sum_{i=1}^{N} h(\boldsymbol{\varphi},\boldsymbol{\theta}_i) R(\boldsymbol{\theta}_i\,|\,\boldsymbol{\varphi}) \tag{5.8}$$

where the samples $\boldsymbol{\theta}_i$ are simulated according to $p_{is}(\boldsymbol{\theta}\,|\,\boldsymbol{\varphi})$.

The main problem is how to choose a good IS density. The optimal density is simply the PDF that is proportional to the absolute value of the integrand of $E_{\boldsymbol{\theta}}[h(\boldsymbol{\varphi},\boldsymbol{\theta})]$, $|h(\boldsymbol{\varphi},\boldsymbol{\theta})|p(\boldsymbol{\theta}|\boldsymbol{\varphi})$ (Robert and Casella 2004) leading to a selection:

$$p_{is,opt}(\boldsymbol{\theta} \mid \boldsymbol{\varphi}) = \frac{\left|h(\boldsymbol{\varphi},\boldsymbol{\theta})\right| p(\boldsymbol{\theta} \mid \boldsymbol{\varphi})}{E_{\boldsymbol{\theta}}[\left|h(\boldsymbol{\varphi},\boldsymbol{\theta})\right|]} \quad . \tag{5.9}$$

Use of this IS density is infeasible (it requires information that is not available a priori) or impractical (too difficult to sample from). Still this discussion shows that an efficient IS scheme should generate conditional samples from an IS density similar to $|h(\boldsymbol{\varphi},\boldsymbol{\theta})|p(\boldsymbol{\theta}|\boldsymbol{\varphi})$.

Samples for $\boldsymbol{\theta}$ that are distributed proportional to $h_s(\boldsymbol{\varphi},\boldsymbol{\theta})p(\boldsymbol{\theta}|\boldsymbol{\varphi})$ when $\boldsymbol{\varphi} \in I_{SSO}$ are available from the last iteration of the SSO stage. They simply correspond to the $\boldsymbol{\theta}$ component of the available sample pairs $[\boldsymbol{\varphi},\boldsymbol{\theta}]$. Re-sampling can be performed within these samples, using weighting factors $|h(\boldsymbol{\varphi}_i,\boldsymbol{\theta}_i)|/\ h_s(\boldsymbol{\varphi}_i,\boldsymbol{\theta}_i)$ for each sample, in order to approximately simulate samples proportional to $|h(\boldsymbol{\varphi},\boldsymbol{\theta})|p(\boldsymbol{\theta}|\boldsymbol{\varphi})$ when $\boldsymbol{\varphi} \in I_{SSO}$. The efficiency of this re-sampling procedure depends on how different $h_s(\boldsymbol{\varphi}_i,\boldsymbol{\theta}_i)$ and $h(\boldsymbol{\varphi}_i,\boldsymbol{\theta}_i)$ are. In most cases the difference will not be significant and good efficiency can be established. Alternatively, $h_s(\boldsymbol{\varphi}_i,\boldsymbol{\theta}_i)$ can be used as loss function in the second stage of the optimization. In this case there is no need to modify the samples from SSO. This choice would be inappropriate if s was negative because it makes the loss function less sensitive to the uncertain parameters $\boldsymbol{\theta}$, thus possibly reducing the efficiency of IS. In such design problems it is better to use the original loss function $h(\boldsymbol{\varphi},\boldsymbol{\theta})$.

The samples simulated from the density proportional to $|h(\boldsymbol{\varphi},\boldsymbol{\theta})|p(\boldsymbol{\theta}|\boldsymbol{\varphi})$ can be finally used to create an importance sampling density $p_{is}(\boldsymbol{\theta}|\boldsymbol{\varphi})$ to use in (5.7), since the set I_{SSO} is small. Various strategies have been discussed in the literature for such an adaptive importance sampling (see for example Au and Beck (1999)).

For problems with high-dimensional vector $\boldsymbol{\theta}$, the efficiency of IS can be guaranteed only under strict conditions (Au and Beck 2003). An alternative approach can be applied for such cases: the uncertain parameter vector is partitioned into two sets, Θ_1 and Θ_2. Θ_1 is comprised of parameters that individually do not significantly influence the loss function (they have significant influence only when viewed as a group)–for example, the white noise sequence modeling the stochastic excitation in dynamic reliability problems–while Θ_2 is comprised of parameters that have individually a strong influence on $h(\boldsymbol{\varphi},\boldsymbol{\theta})$. The latter set typically corresponds to a low-dimensional vector. IS is applied for the elements of Θ_2 only. This approach is similar to the one discussed in Pradlwater et al. (2007) and circumvents the problems that may appear when applying IS to design problems involving a large number of uncertain parameters.

CHAPTER 6

Stochastic System Design: Structural Engineering Applications

In the preceding chapters a stochastic design methodology was developed for problems that might involve complex system models. Chapter 2 presented the general characteristics of the design problem formulation. Then an efficient optimization framework was presented in Chapters 4 and 5. This methodology is illustrated in this chapter in the context of two structural engineering applications. The first considers the design of a base-isolation system for improving the reliability of a three-story structure against near-field earthquakes. The efficiency of SSO and the suggested combined optimization framework, discussed in the previous two chapters, are examined in detail in the context of this example. The second example discusses the retrofitting of a four-story structure with viscous dampers. The expected lifetime cost is adopted as the design objective in this case. Instead of approximating the damages from future earthquakes in terms of the reliability of the structure, as typically performed in RBDO problems, an accurate methodology is presented for estimating this cost; this methodology uses the nonlinear response of the structure under a given time-history (generated according to some stochastic excitation model) to estimate the damages in a more-detailed, component level.

The intention of the studies presented here is to illustrate the efficiency of the suggested stochastic optimization framework and to bring forward some issues pertaining to

stochastic system design. Some idealizations are made in terms of the non-linear structural behavior in order to avoid unnecessary complexities and to strike a balance between computational tractability and realism. Additionally, specific structural sites are not considered for determining the probabilistic characteristics of the seismic hazard. The seismological parameters that define this hazard are set to typical values that should be considered, in general, reasonable in terms of the applications considered. These characteristics do not reduce the validity of the conclusions drawn in the examples, at least with respect to the topics intended to be examined (which were outlined above).

6.1 Optimal Reliability Design of a Base Isolation Protection System

This example considers the design of a base-isolation system, with lead-rubber bilinear isolators and supplemental viscous dampers at the base level, for the protection of a three-story symmetric building. The pre-yield, K_{pr}, and post-yield, K_p, stiffness and the yield force, F_y, are the design variables $\boldsymbol{\varphi}$ for the isolators, along with the damping coefficient, c_d, for the dampers. A simplified problem with only two design variables is also formulated by setting the post-yield stiffness equal to 15% of the pre-yield stiffness and the viscous dampers to 5% critical damping, assuming a nominal period of 2.25 sec for the isolated structure (thus only K_{pr} and F_y are design variables in this case). The simplified problem is denoted by D_1 and the full one by D_2. Note that the simplified problem has been simply formulated as a means of investigating the influence of the number of design variables to the stochastic optimization framework. In actual design applications, the simultaneous optimization of all characteristics of the isolation system should be performed. The design objective is the reliability of the base-isolated system given that a seismic event occurs (with characteristics as described by the seismicity of the structural site).

6.1.1 Probabilistic system and excitation models

The three-story superstructure is modeled (Figure 6.1) as a planar (because of the symmetry) shear building with uncertain inter-story stiffness and uncertain classical modal

damping. The lumped mass of the top story is 636 ton while it is 817 ton for the bottom two. The mass of the base is m_b=999 ton. The inter-story stiffnesses k_i of all the stories are parameterized by $k_i = \theta_{k,i}\hat{k}_i$, i=1,2,3, where $[\hat{k}_i]$=[633.9, 443.7, 253.6] MN/m are the most probable values for the inter-story stiffness, and $\theta_{k,i}$ are nondimensional uncertain parameters, assumed to be correlated Gaussian variables with mean value one and covariance matrix with elements

$$\mathrm{E}\left[\left(\boldsymbol{\theta}_{k,i}-1\right)\left(\boldsymbol{\theta}_{k,j}-1\right)^{T}\right]=\left(0.1\right)^{2}\exp\left[-\left(i-j\right)^{2}/2^{2}\right] \tag{6.1}$$

that roughly imply significant correlation between inter-story stiffness' within two stories apart and c.o.v. of 10%. The damping ratios for the modes are modeled as independent Gaussian variables with mean value 5% and coefficient of variation 10%.

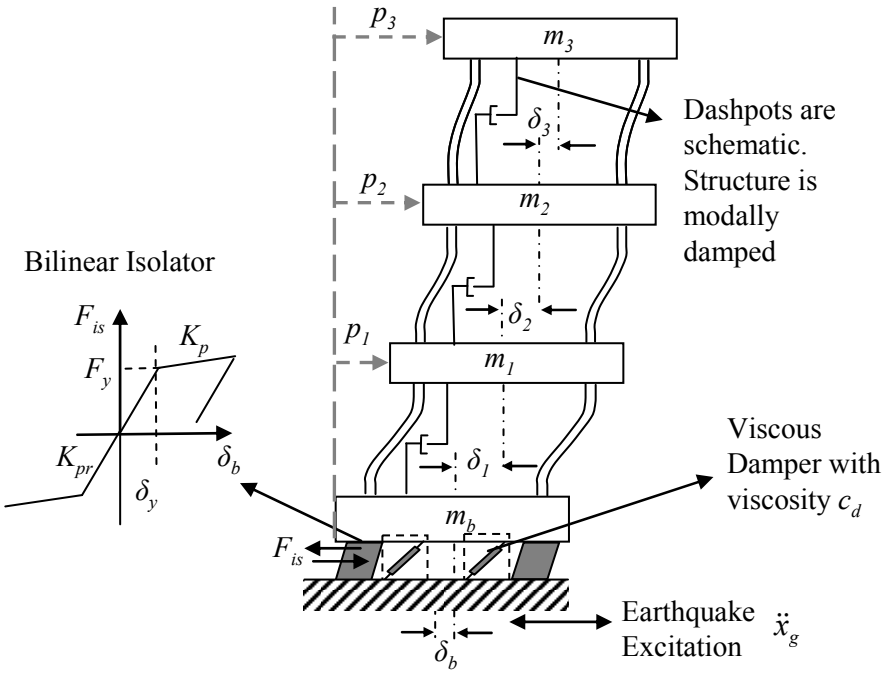

Figure 6.1: Base-Isolated structure

Under these assumptions, the superstructure is a linear system with mass, damping, and stiffness matrices $\mathbf{M}_s$, $\mathbf{C}_s$, and $\mathbf{K}_s$. The differential equation for structural the model is:

$$\begin{bmatrix} \mathbf{M}_s & \mathbf{M}_s\mathbf{R}_s \\ \mathbf{R}_s^T\mathbf{M}_s & \mathbf{R}_s^T\mathbf{M}_s\mathbf{R}_s + m_b \end{bmatrix}\begin{bmatrix} \ddot{\mathbf{p}}(t) \\ \ddot{\delta}_b(t) \end{bmatrix} + \begin{bmatrix} \mathbf{C}_s & \mathbf{0}_{3\times1} \\ \mathbf{0}_{1\times3} & c_b \end{bmatrix}\begin{bmatrix} \dot{\mathbf{p}}(t) \\ \dot{\delta}_b(t) \end{bmatrix} + \begin{bmatrix} \mathbf{K}_s & \mathbf{0}_{3\times1} \\ \mathbf{0}_{1\times3} & 0 \end{bmatrix}\begin{bmatrix} \mathbf{p}(t) \\ \delta_b(t) \end{bmatrix} = + \begin{bmatrix} \mathbf{0}_{3\times1} \\ 1 \end{bmatrix}\mathbf{F}_{is}(t) + \begin{bmatrix} \mathbf{M}_s\mathbf{R}_s \\ \mathbf{R}_s^T\mathbf{M}_s\mathbf{R}_s + m_b \end{bmatrix}\ddot{x}_g(t) \tag{6.2}$$

where $\mathbf{p}(t) \in \mathbb{R}^3$ is the vector of floor displacements relative to the base, $\delta_b(t)$ is the base displacement, $F_{is}(t) \in \mathbb{R}$ is the isolator bilinear restoring force, $\mathbf{R}_s \in \mathbb{R}^3$ is the vector of earthquake influence coefficients, and $\ddot{x}_g(t)$ is the acceleration of the ground.

In order to estimate the structural system reliability, a probability model needs to be established for the seismicity of the structural site, which corresponds to potentially damaging future near-fault ground motions. The model discussed in detail in Section 2.4 is adopted. The uncertainty in moment magnitude for seismic events, M, is modeled by the Gutenberg-Richter relationship (2.14) truncated on the interval $[M_{min}, M_{max}]=[6, 8]$, with the regional seismicity factor selected as $b=0.7\log_e(10)$. For the uncertainty in the event location, the logarithm of the epicentral distance, r, for the earthquake events is assumed to follow a Gaussian distribution with mean log(20) km and standard deviation 0.5. Figure 6.2(a) illustrates the PDFs for M and r. The magnitude and the frequency of the pulse are chosen according to the probabilistic models for near-field pulses at rock sites given by (2.17) and Table 2.1. The probability models for the near-field pulse parameters are chosen as: Gaussian with mean 1.8 and standard deviation 0.3 for γ_p, uniform in the range $[-\pi/2, \pi/2]$ for v_p, and Gaussian with mean zero and standard deviation as shown in Table 2.1 for ε_f and ε_v.

The uncertain parameter vector in this design problem consists of the structural model parameters, $\boldsymbol{\theta}_s$, the seismological parameter $\boldsymbol{\theta}_g=[M, r]$, the additional parameters for the

near-fault pulse $\boldsymbol{\theta}_p=[\gamma_p, \nu_p, \varepsilon_f, \varepsilon_v]$, and the white-noise sequence, $\mathbf{Z}_w$, so $\boldsymbol{\theta}=[\boldsymbol{\theta}_s, \boldsymbol{\theta}_g, \boldsymbol{\theta}_p, \mathbf{Z}_w]$. Note that $\mathbf{Z}_w$ corresponds to a 5001-dimensional vector in this case (partitioning of a 50 sec time window into intervals of 0.01sec).

The reliability of the system given that an earthquake occurs is the design objective. Failure is defined to be that any of the inter-story drifts, base displacement, or shear force at the first story exceeds the thresholds 0.0105m, 0.25 m, and 0.24 of the superstructure weight, respectively. The limit state function $\tilde{g}(\boldsymbol{\varphi},\boldsymbol{\theta})$ is defined as the logarithm of the maximum over the excitation duration of these performance variables (normalized by their respective threshold):

$$\mathbf{z}(t;\boldsymbol{\varphi},\boldsymbol{\theta}) = \left[\frac{\delta_i(t)}{0.0105} i=1,2,3 \quad \frac{\delta_b(t)}{0.25} \quad \frac{1^{st} \text{ story shear}(t)}{0.24g \cdot \sum_{i=1}^{3} m_i} \right]^{\mathrm{T}} \tag{6.3}$$

$$\tilde{g}(\boldsymbol{\varphi},\boldsymbol{\theta}) = \log\left(\max_{t\in T} \left\{ \left\| \mathbf{z}(t;\boldsymbol{\varphi},\boldsymbol{\theta}) \right\|_\infty \right\} \right)$$

where $\mathbf{z}(t;\boldsymbol{\varphi},\boldsymbol{\theta})$ corresponds to the (normalized) response vector for the system, $\|.\|_\infty$ to the largest magnitude component, and T to the duration of the excitation event defined by $\boldsymbol{\theta}_g$. A small prediction-error ε is assumed and is modeled as a Gaussian random variable with mean 0 and standard deviation 0.05. This selection for the limit state function and the prediction error agrees with the usual choice of probability models in performance-based engineering, i.e., that the engineering demand parameters, such as maximum drifts, are modeled as log-normally distributed variables. Note that the relationship between the model response $z(t;\boldsymbol{\varphi},\boldsymbol{\theta})$ and the actual system response $\mathbf{z}_s(t;\boldsymbol{\varphi},\boldsymbol{\theta})$ is:

$$\mathbf{z}_s(t;\boldsymbol{\varphi},\boldsymbol{\theta}) = \mathbf{z}(t;\boldsymbol{\varphi},\boldsymbol{\theta}) \exp(\varepsilon) \quad . \tag{6.4}$$

Thus a multiplicative relationship exists between the two responses with scaling parameter exp(ε) that follows a log-normal distribution with median value 1 and coefficient of variation 0.05. This connection between (a) the definition of the limit state function along with the probabilistic model assumed for the prediction error, and (b) the relationship between the assumed model and the actual system responses is important and requires some special attention. Special care is always needed so that the first definition leads to a reasonable relationship for the latter, in the context of the specific application. The relevant probability models chosen in this study seem reasonable.

6.1.2 Optimization algorithm characteristics

The two-stage framework discussed in Chapter 5 is used, combining SSO with SPSA. For the SSO algorithm (Section 4.4), the parameter selections are: ρ=0.2, N=3000. The shape for the admissible sets I is selected as a hyper-ellipse and the adaptive identification is stopped when $\hat{H}(\hat{I}_k)$ becomes larger than 0.8. For the non-smooth optimization of (4.33) an algorithm based on direct-search is chosen (Holmstrom et al. 2007).

SPSA with CRN (Section 5.3) is adopted for the second stage of the optimization, with parameter selection: β=0.71, ζ=0.25, N=1500. Convergence is judged by looking at the norm $\left\|\boldsymbol{\varphi}_{k+1}-\boldsymbol{\varphi}_k\right\|_\infty$ for each of the five last iterations. If that norm is less than 0.2% (normalized by the dimension of the initial design space), then we assume that convergence to the optimal solution has been established. Formulation (2.12) is used for the probability of failure in the SPSA optimization in order to improve the efficiency of CRN comparisons, as discussed earlier. The guidelines discussed in Section 5.2 are adopted for selection of step sizes and blocking rules for SPSA. To implement these guidelines, normalization of the search space is performed so that the hyper-ellipse I_{SSO} is transformed into a unit radius hyper-sphere.

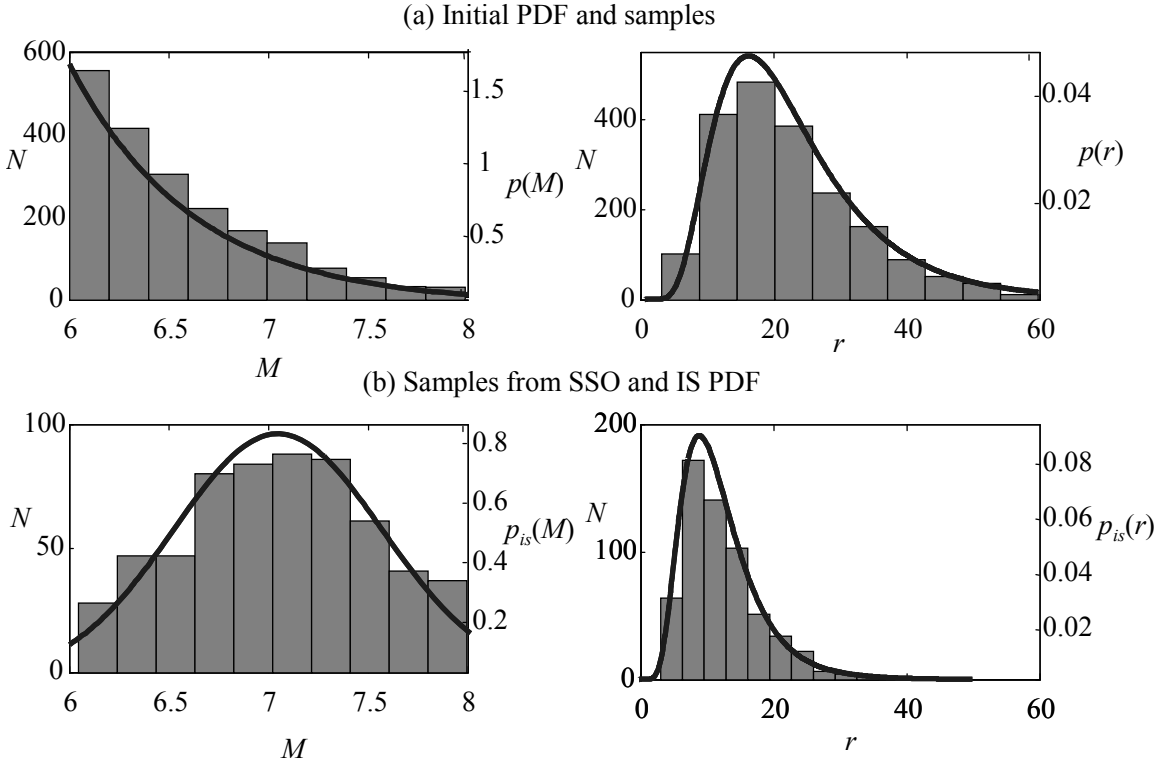

Figure 6.2: Details about importance sampling densities formulation

For the second optimization stage (SPSA), following the discussion in Section 5.2, importance sampling densities are established for the structural, near-field pulse model parameters and the seismological parameters, but not for the high-dimensional white-noise sequence $\mathbf{Z}_w$. Apart from the phase of the near-field pulse, v_p, for which the samples from $\pi(v_p)$ were found to be distributed similar to $p(v_p)$ (indicating that this model parameter has small influence on the response of the model), for the rest of the parameters, the IS PDFs were approximated by Gaussian distributions, like the prior distributions $p(\boldsymbol{\theta}_i)$, but with a shifted mean value and variance, selected as the mean and variance of the samples from the SSO stage that are distributed according to $\pi(\boldsymbol{\varphi})$. Figure 6.2(b) illustrates this concept for M and r for problem D_1. Note that the IS PDF for M and r are significantly different from their initial distribution; since these seismological parameters are expected to have a strong influence on the model response, the difference between the distributions is expected to have a big effect on the accuracy of the estimation. The same remark holds for the near-

field pulse model parameter ε_f and ε_v and only to a small degree for all other parameters. This behavior according to the discussion in Section 4.1.8 yields information to address the question: what is expected to happen when the system fails? It ultimately indicates that the influence on the system failure of the structural model parameters and the number of half-cycles of the near-field pulse is relatively small compared to the influence of the other parameters for the excitation model (moment magnitude, epicentral distance, uncertainty about the pulse frequency and amplitude).

For problem D_1 the c.o.v. for $\hat{P}_F(\boldsymbol{\varphi}\,|\,\Theta)$ for a sample size N=1500 is 12.5% without using IS and 4.4% when IS is used. This c.o.v. is of the same level for all values of $\boldsymbol{\varphi} \in I_{SSO}$ (since the I_{SSO} set is relatively small). Note that the c.o.v. varies according to $1/\sqrt{N}$ (Robert and Casella 2004); thus, the sample size for direct estimation (i.e., without use of IS) of $\hat{P}_F(\boldsymbol{\varphi}\,|\,\Theta)$ with the same level of accuracy as in the case when IS is applied would be approximately 8 times larger. This illustrates the efficiency increase that can be established by the IS scheme discussed earlier. Similarly, for problem D_2 the c.o.v. is 4.9% when IS was used and 16.2% when not. In this case a sample size that is 11 times larger is needed for direct estimation of $\hat{P}_F(\boldsymbol{\varphi}\,|\,\Theta)$ for establishing the same accuracy as with the IS scheme.

6.1.3 Results and discussion for a sample optimization run

Results for a sample run are presented in Table 6.2 for the SSO, and in Table 6.3, Figure 6.3 and Figure 6.4 for the combined optimization framework using SPSA in the second stage. The SSO algorithm converged in 3 iterations for problem D_1, and in 6 iterations for problem D_2 to sets that are characterized by small sensitivity to the objective function (I_{sso} in Figure 6.3 and Figure 6.4 with center $\boldsymbol{\varphi}_{SSO}$). SPSA was then used to pinpoint the optimal solution, $\boldsymbol{\varphi}^*$, within these sets (point X in the aforementioned figures). The results of this sample optimization run are discussed in greater detail next, focusing on the aspects related to the novel SSO algorithm.

Table 6.1 Results from a sample run of the SSO algorithm for two design problems

Problem D_1 $n_\varphi=2$, $\hat{I}_{SSO}=\hat{I}_3$	Iteration of SSO 1	2	3	Problem D_2 $n_\varphi=4$, $\hat{I}_{SSO}=\hat{I}_6$	Iteration of SSO 1	2	3	4	5	6
$V_{\hat{I}_k} / V_{\hat{I}_{k-1}}$	0.381	0.265	0.241	$V_{\hat{I}_k} / V_{\hat{I}_{k-1}}$	0.286	0.345	0.305	0.271	0.259	0.230
$\sqrt[n_\varphi]{V_{\hat{I}_k} / V_{\hat{I}_{k-1}}}$	0.617	0.514	0.491	$\sqrt[n_\varphi]{V_{\hat{I}_k} / V_{\hat{I}_{k-1}}}$	0.731	0.7676	0.743	0.722	0.713	0.693
$\hat{H}(\hat{I}_k)$	0.525	0.754	0.830	$\hat{H}(\hat{I}_k)$	0.698	0.580	0.657	0.738	0.772	0.865
$V_{\hat{I}_{SSO}} / V_{\Phi}$	0.0243			$V_{\hat{I}_{SSO}} / V_{\Phi}$	$4.85\ 10^{-4}$					
$\sqrt[n_\varphi]{V_{\hat{I}_{SSO}} / V_{\Phi}}$	0.156			$\sqrt[n_\varphi]{V_{\hat{I}_{SSO}} / V_{\Phi}}$	0.149					

Table 6.2 Cumulative results from a sample run of the optimization framework

		$\hat{P}_F(\boldsymbol{\varphi} \in \Phi)$	$\boldsymbol{\varphi}_{SSO}$	$\hat{P}_F(\boldsymbol{\varphi} \in I_{SSO})$	$\hat{P}_F(\boldsymbol{\varphi}_{SSO} \mid \Theta)$	$\boldsymbol{\varphi}^*$	$\hat{P}_F(\boldsymbol{\varphi}^* \mid \Theta)$
D_1	K_{pr}	0.0896	98.05	0.0371	0.0366	92.75	0.0361
	F_y		2.35			2.44	
D_2	K_{pr}	0.1186	68.2	0.0250	0.0241	53.2	0.0228
	F_y		1.76			1.92	
	K_p		15.56			13.93	
	c_d		4.21			4.24	

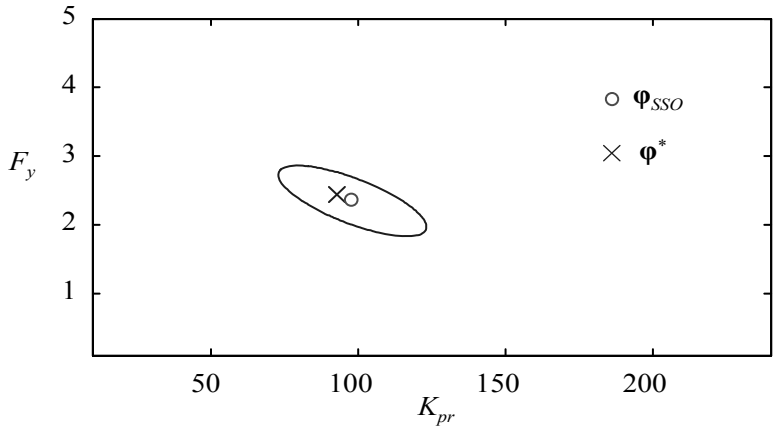

Figure 6.3: Sets I_{SSO} (ellipse) and Φ (rectangle) for problem D_1

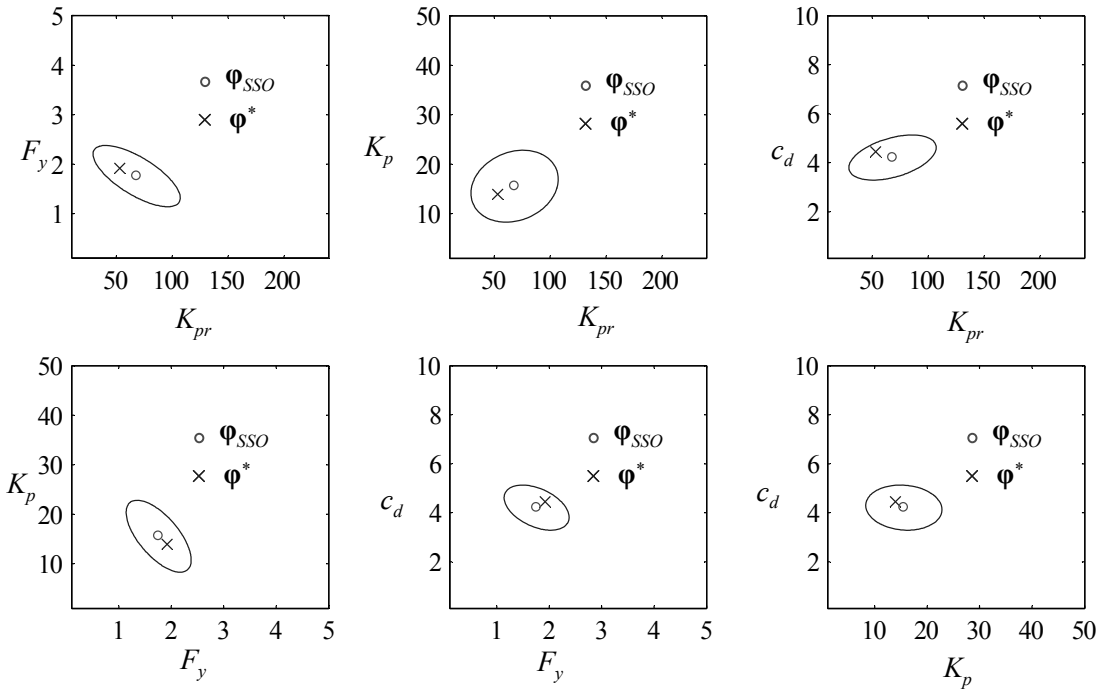

Figure 6.4: Projections of sets I_{SSO}(ellipse) and Φ(rectangle) onto the planes of all pairs for the design parameters for problem D_2

SSO leads to a significant reduction of the size (volume) of the search space for both design problems; this is evident in both Table 6.3 (last two rows) as well as Figure 6.3 and Figure 6.4. These two figures and Table 6.2 also illustrate that SSO efficiently identifies a subset for the optimal design variables; the converged optimal solution in the second stage, $\boldsymbol{\varphi}^*$, is close to the center of the set that is identified by SSO, $\boldsymbol{\varphi}_{SSO}$; also the objective function at that center point $\hat{P}_F(\boldsymbol{\varphi}_{SSO} \mid \Theta)$ is not significantly different than the optimal value $\hat{P}_F(\boldsymbol{\varphi}^* \mid \Theta)$ (Table 6.2). Thus, selection of $\boldsymbol{\varphi}_{SSO}$ as the design choice leads to a sub-optimal design but close to the true optimum in terms of both the design vector selection and its corresponding performance. The comparison between the average value of the objective function in sets Φ and I is also important. $\hat{P}_F(\boldsymbol{\varphi} \in I_{SSO})$ and $\hat{P}_F(\boldsymbol{\varphi} \in \Phi)$ are significantly different, but $\hat{P}_F(\boldsymbol{\varphi} \in I_{SSO})$ and $\hat{P}_F(\boldsymbol{\varphi}^* \mid \Theta)$ are very close for both design problems (Table 6.2). These comparisons illustrate the efficiency of SSO for identifying subsets that are

characterized by small sensitivity for the probability of failure: the design choices in set I_{SSO} correspond to reliability that is not far away from the optimal one, especially when compared to the reliability of other choices in the admissible space.

All these characteristics illustrate the effectiveness and quality of the set identification in SSO. Note that as the algorithm evolves, this quality, expressed by $\hat{H}(\hat{I}_k)$, decreases (Table 6.2). Within I_{SSO}, the small sensitivity of the objective function to $\boldsymbol{\varphi}$ cannot be easily captured by samples obtained by stochastic simulation, unless a large number of them are available. Instead, SPSA is chosen here for pinpointing the optimal design variables.

For the design problem D_2 the difference of the shapes of the initial design space and the admissible subsets is considerable (difference in volumes of four-dimensional hyper-rectangles and the inscribed hyper-ellipses). As discussed earlier, this leads to some small loss of quality for the first stage of the identification; $\hat{H}(\hat{I}_k)$ in the first iteration is larger than the second one, though typically, as discussed in detail in Section 4.2.2, it is expected to be a decreasing function of the iteration number. This feature does not influence, though, the overall quality of the SSO identification, as evident by the rest of the results.

The ability of SSO to estimate contours of the objective function and capture the correlation between the design variables is illustrated in Figure 6.3 and Figure 6.4. This correlation can be demonstrated also by looking at the normalized positive definite matrix, $\mathbf{M}_n$, that defines the ellipses:

$$\left(\boldsymbol{\varphi}-\boldsymbol{\varphi}_{SSO}\right)^T \mathbf{D}_e^{1/2}\mathbf{M}_n^{-1}\mathbf{D}_e^{1/2}\left(\boldsymbol{\varphi}-\boldsymbol{\varphi}_{SSO}\right)=1 \tag{6.5}$$

where normalization is used in order to make all diagonal elements of $\mathbf{M}_n$ be unity. The off-diagonal elements of $\mathbf{M}_n$ show the correlation between the different design variables (similar to the concept of correlation for a Gaussian PDF); the larger the absolute values of

these elements the more important the correlation between the design variables. For the sample run of SSO discussed in this section, these matrices are respectively:

$$\mathrm{D}_1 : \mathbf{M}_n = \begin{matrix} \\ K_{pr} \\ F_y \end{matrix} \begin{matrix} \begin{matrix} K_{pr} & F_y \end{matrix} \\ \begin{bmatrix} 1 & -0.74 \\ -0.74 & 1 \end{bmatrix} \end{matrix} \tag{6.6}$$

$$\mathrm{D}_2 : \mathbf{M}_n = \begin{matrix} \\ K_{pr} \\ F_y \\ K_p \\ c_d \end{matrix} \begin{matrix} \begin{matrix} K_{pr} & F_y & K_p & c_d \end{matrix} \\ \begin{bmatrix} 1 & -0.71 & 0.19 & 0.45 \\ -0.71 & 1 & -0.66 & -0.43 \\ 0.19 & -0.66 & 1 & -0.09 \\ 0.45 & -0.43 & -0.09 & 1 \end{bmatrix} \end{matrix} . \tag{6.7}$$

The correlation between pairs of design variables indicated by these matrices can be visually verified in Figure 6.3 and Figure 6.4; the highly-correlated variables are K_{pr} and F_y in design problem D_1 and pairs of variables K_{pr}-F_y , K_{pr}-c_d, F_y-K_p, and F_y-c_d in problem D_2. These higher correlations mean that these pairs of design variables can be traded off (in the normalized space) without significantly changing the objective function. Note, also, that the correlation relationship between K_{pr} and F_y is the same in both design problems.

The influence of the number of the design variables in the efficiency of SSO, is now evident when comparing the results in Table 6.2 between the two design cases. For D_2 the average reduction of the size for each design variable (second row of Table 6.2) is much smaller, which leads to more iterations, until a set with small sensitivity to the objective function is identified. The proportionality dependence on the number of design variables with regard to the computational cost of SSO that was argued in Section 4.1.6 is also verified in the context of the example discussed here: the mean total length reduction over all iterations for D_1 and D_2, corresponding to the quantity in (4.21), is similar (look at

$\sqrt[n_\varphi]{V_{I_{SSO}} / V_{\Phi}}$ in Table 1) but the number of required iterations for convergence to the I_{sso} set for D_2 (which has twice as many design variables) is only double.

The small average probability $\hat{P}_F(\boldsymbol{\varphi} \in I_{SSO})$ of the sets that the SSO algorithm gradually converges to shows also the efficiency of the MCMC approach suggested for simulating failed samples within each identified subset. For example, for design case D_2, $1/\hat{P}_F(\boldsymbol{\varphi} \in I_{SSO})$=1/0.025=40 simulations are needed on the average in order to obtain one failed sample inside set I_{SSO} if direct MCS is used. This means that about 120,000 simulations would be needed in order to obtain 3000 failed samples if the SSO algorithm was to be warm-started at this level. In the suggested MCMC simulation approach, only [3000(1+γ_s)-600] additional simulations would be needed (since already 600 samples are retained from previous step of the algorithm) in order to obtain the same effective number of failed samples inside this set. The efficiency of this approach depends, of course, on the efficiency of the MCMC simulation, which defines the value of γ_s. A value close to 2 is common for this parameter. Additionally note that since $\hat{P}_F(\boldsymbol{\varphi} \in \Phi)$ is larger, at least in the examples considered in this study, failed samples can be obtained more efficiently in Φ using MCS. These failed samples populate towards regions with lower probability content in the iterative identification process.

6.1.4 Efficiency of optimization framework

The efficiency of the suggested optimization framework is judged by performing the same optimization by applying only SPSA. No information from the SSO stage is used. The optimization in this case is performed with respect to the initial design space, Φ, by randomly selecting the starting point for the algorithm. In this case IS is not implemented; since a search inside the whole design space Φ is considered, it is unclear how samples of $\boldsymbol{\theta}$ can be obtained to form the IS densities, and separately establishing an IS density for each design choice $\boldsymbol{\varphi}$ is computationally too expensive. Larger values for the sample size, N, are

chosen in order to establish a similar c.o.v. near the optimal solution, as in the case that IS is implemented; according to previous discussion the selection for N is 8 times larger than in the two-stage approach for problem D_1 and 11 for D_2. In 10 runs of the optimization algorithm, the average number of iterations (and its standard deviation) for convergence to the optimal solution was (a) for D_1: with SSO 20.42 (4.5) and without 59.5 (21.4), and (b) for D_2: with SSO 30.5 (9.4) and without 98.4 (36.9). In order to evaluate the effectiveness of the two-stage framework discussed, note that the computational cost of one iteration of SSO, in terms of system simulations needed, is equal to the computational cost of one iteration of SPSA; thus, one can simply add three and six additional iterations to the means for problems D_1 and D_2 in (a) and (b), respectively, when SSO is used.

This discussion illustrates the effectiveness of the proposed two-stage optimization framework to enhance the efficiency of stochastic optimization. It should also be noted that use of SSO leads to greater consistency in the optimization efficiency (smaller variation). The better starting point of the algorithm, as well as the smaller size of the search space which allows for better normalization, that SSO can provide, are the features that contribute to this improvement in efficiency. If we consider the added efficiency because of the use of IS when the combined framework is chosen, then the computational advantages from using this framework are even higher: in this example the computational cost of each iteration of SPSA is 8 and 11 times smaller for problems D_1 and D_2, respectively, in the setting of the combined framework.

Similar increase in efficiency has been reported in Taflanidis and Beck (2007a) when combining SSO with gradient-based (SPSA) or gradient-free algorithms. An OAM was selected in that study as the gradient-free algorithm in the second stage of the optimization framework. The approach adopted there used radial basis functions for approximating the objective function and exterior sampling techniques for handling the estimation error, not the quadratic global approximation suggested in Section 5.2.

6.1.5 *Accuracy of design identified by SSO*

A second study is also performed in order to investigate the quality of the identification established by SSO. Only the first stage for the optimization framework is considered in this study, thus $\boldsymbol{\varphi}_{SSO}$ is considered as the optimal design choice. Similar characteristics are assumed for SSO as previously, but 3 different cases are considered for the number of samples, N=2000, N=4000, and N=8000. The c.o.v. of the set probability for these three cases (assuming direct Monte Carlo simulation) is 4.5%, 3.1%, and 2.2%, respectively (for r=0.2), decreasing as $1/\sqrt{N}$. Also the iterative identification stops in this case when $\hat{H}(\hat{I}_k)$ becomes larger than 0.9. This was selected in order to further reduce the size of the subset identified by SSO by performing more iterations. It was found that on the average 1–2 more steps were needed in order to establish this stopping criteria (compared to the previous study where $\hat{H}(\hat{I}_k) > 0.80$ was selected).

Table 6.3 Efficiency for identification of optimal design using SSO only

Shape of admissible subsets	N	D_1			D_2		
		$\hat{P}_F(\boldsymbol{\varphi}_{SSO}\mid\Theta)$		$\frac{\hat{P}_F(\boldsymbol{\varphi}_{SSO}\mid\Theta)}{\hat{P}_F(\boldsymbol{\varphi}^*\mid\Theta)}$	$\hat{P}_F(\boldsymbol{\varphi}_{SSO}\mid\Theta)$		$\frac{\hat{P}_F(\boldsymbol{\varphi}_{SSO}\mid\Theta)}{\hat{P}_F(\boldsymbol{\varphi}^*\mid\Theta)}$
		Mean	c.o.v.		mean	c.o.v.	
Hyper-ellipse	2000	0.0384	4.4%	1.065	0.0252	5.8%	1.095
	4000	0.0373	2.4%	1.032	0.0243	3.1%	1.061
	8000	0.0367	1.7%	1.021	0.0236	1.9%	1.032
Hyper-rectangle (no rotations)	2000	0.0388	4.7%	1.076	0.0258	6.3%	1.111
	4000	0.0380	3%	1.054	0.025	4.8%	1.085
	8000	0.0373	1.9%	1.033	0.023	3.2%	1.051

The identification was performed 10 times and the average results are reported in Table 6.3. A comparison between selection of admissible subsets as hyper-ellipses and hyper-rectangles is also performed. The results show that the reliability of the design choice

identified by SSO is close to the true optimal. Increase of the number of simulated samples from $\pi(\boldsymbol{\varphi})$ improves, as expected, the quality of the estimate: both the average $\hat{P}_F(\boldsymbol{\varphi}_{SSO} \mid \Theta)$ and its c.o.v. decrease; this means that design choices closer to the optimum one are identified and there is better consistency in the identification process. For design case D_2, the associated greater challenges (optimal choice close to the boundary, larger number of design variables) contribute so that the identification is less efficient. Still the design $\boldsymbol{\varphi}_{SSO}$ can be considered quite efficient if the number of samples is sufficiently large. Comparison between the two different shapes of subsets illustrates that selection of hyper-ellipses improves the efficiency of the SSO identification. This is again an anticipated result since this choice is associated with greater versatility for selection of the optimal subset I and thus can provide a better fit to the contours of the optimization objective. This feature leads to better quality in the SSO identification.

Note that in this study we were able to directly characterize the quality of the identified solution because $\hat{P}_F(\boldsymbol{\varphi}^* \mid \Theta)$ was a priori known. As discussed in Section 4.4, for problems where knowledge of the true optimum is important and no insight is available for the objective function value that corresponds to the optimal choice, the two-stage approach presented earlier is more reliable.

6.1.6 Efficiency of stochastic design

A comment with respect to the effectiveness of the base isolation protection system in this example is warranted. Design D_2 involves much larger versatility in the selection of the characteristics of the isolation system, and thus leads to smaller failure probability, as expected. The period of the base isolated structures for a displacement of base displacement of 25 cm is 2.40 sec for D_1 and 2.47 sec for D_2. These selections seem reasonable based on common design practice for base isolation systems, and verify the validity of the stochastic framework chosen (system and excitation models, modeling uncertainty, and objective function formulation).

6.1.7 Sensitivity of design to model prediction error

The concept of the existence of a prediction error between the responses of the actual system and the assumed system model has been considered in numerous reliability analyses, see for example Papadimitriou et al. (2001). No studies though exist that examine the influence of this error within an optimal stochastic system design framework. Such an analysis is presented here in the context of example D_1. In particular, the influence of the standard deviation of the model prediction error, σ_ε, is investigated. Figure 6.5 presents the location of the optimal solution and the reliability performance under optimal design for different values for σ_ε. Note that larger values for σ_ε are equivalent to greater potential differences between the model and the system responses.

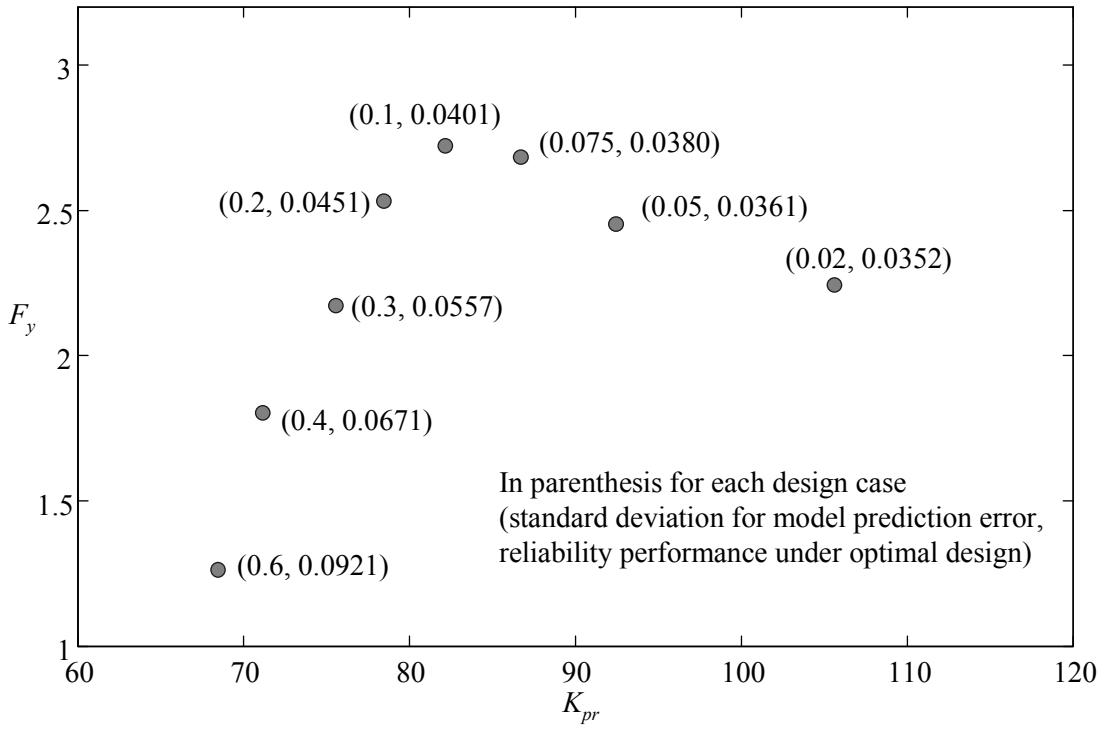

Figure 6.5: Optimal design variables and performance for various instances of the model prediction error for design problem D_1

The results illustrate that there is indeed an influence on the optimal design configuration by the selection of σ_ε. The path of the optimal design variables, as a function of σ_ε, does not correspond to a simple pattern, which indicates a complex relationship between the model prediction error and the model performance. Also, as σ_ε becomes larger the reliability performance, under optimal design, decreases. This is attributed to the fact that the uncertainty in the model description increases, which creates greater difficulties in regulating the performance in the whole region of the Θ space that is important (the region that leads to unacceptable performance and has non-negligible probability of occurrence).

This discussion reveals, more generally, an important sensitivity of the optimal system design to (a) our available knowledge about the system and excitation properties and (b) the utility function selected to quantify the model performance. The model prediction error can be equivalently considered to represent either of the latter two characteristics. This remark brings forward the importance of all details of the system modeling for the efficient stochastic design.

6.1.8 Objective function approximation application

A simple example is finally presented about the implementation of the OAM approach discussed in Section 5.2. The example is merely intended to illustrate the potential capabilities of the method in the context of design problem D_2, not to investigate in depth the efficiency and robustness properties of it. Thirty interpolation points have been used for developing the approximation surface but no relative weighting has been chosen between them. The evaluation of the objective function at these points follows the same guidelines as for the SPSA algorithm discussed earlier. Figure 6.6 shows the interpolation points along with the contours of the objective function, the set I_{SSO} identified at the SSO stage and the optimal design variables. The design configuration corresponding to the minimum of the approximation surface (center of the contours) is close to the optimal solution identified earlier. Note, additionally, that the contours of the objective function have similar shape to the I_{SSO}. This latter agreement verifies (a) the capabilities of SSO for capturing the

sensitivity of the objective function as well as (b) the efficiency of the approximation of that function established by OAM.

This discussion shows the potential of the proposed OAM methodology. Still, further research is needed in order to explore the robustness properties of this optimization approach and improve its efficiency by providing guidelines for iterative convergence to the optimal solution. The reduction of the influence of the model prediction error when interior sampling is used also needs to be explicitly addressed. Note that even though similar techniques have been considered before for stochastic optimization problems, e.g., Bailey et al. (1999), no special attention has been given on reducing the influence of the estimation error in the evaluation of the performance objective. The importance of this error can be quite significant though when the approximation of the objective function is established in regions close to the true optimal solution, that is, in regions that are characterized by small sensitivity.

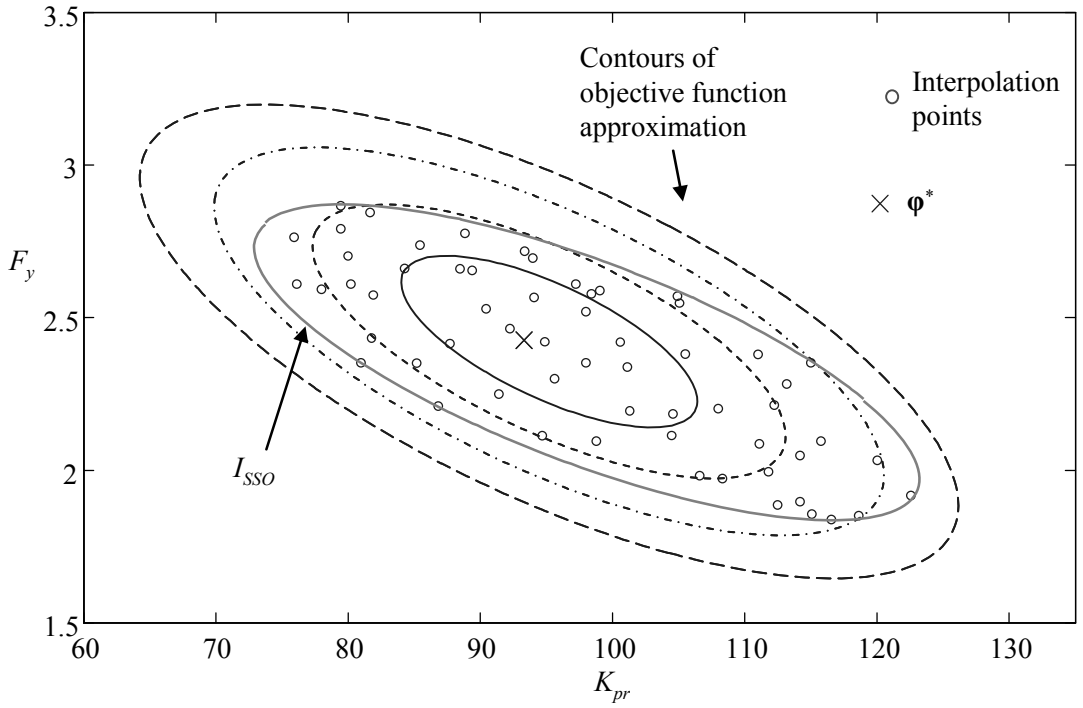

Figure 6.6: Illustration of OAM application for design problem D_1

6.2 Optimal Life-Cycle Cost-Based Retrofitting of a Four-Story Structure

The retrofitting of a symmetric, four-story, office building with linear viscous dampers is considered. The building is a non-ductile reinforced concrete, perimeter moment-frame structure, similar to the one discussed in Mitrani (2007) . The dimension of the building is 45 m x 45 m and the height of each story is 3.9 m. The perimeter frames in the two building directions are separated from each other, which allows structural analysis in each direction to be done separately. Because of the symmetry of the building, analysis of only one of the directions is necessary. The objective function in the stochastic design problem in this case is the expected life-cycle cost of the structure.

A methodology for a detailed estimation of the life-cycle cost is adopted. In traditional RBDO problems this cost is typically approximated in terms of the reliability of the structure, see, for example, Sorensen et al. (1994), Kong and Frangopol (2003). Recent advances in performance-based engineering (most recently the ATC-58 project developed by the Applied Technology Council) quantify, more accurately, economical losses, casualties, and downtime in relation to the structural response, using fragility curves to develop such a relationship. Although currently fragility curves are available only for a limited number of elements, it is expected that in the future more general standard fragility curves will be developed.

In this context, many approaches have been suggested, the most popular being the well known HAZUS model (see, for example, Kircher et al. (2006)) that use pushover methods to analyze the structural performance and a categorization of buildings into different groups to estimate earthquake losses. Other researchers (e.g., Porter et al. (2001)) have developed analytical tools to evaluate seismic vulnerability using non-linear time-history analyses, characterizing the structure as a unique building and estimating damage on a more-detailed level. The reference by Mitrani (2007) includes a more detailed discussion on recent advances in earthquake loss estimation. In this study, the earthquake losses are estimated adopting the methodology described in Porter et al. (2004a) and Goulet et al. (2007) which

belongs in the latter category; the nonlinear response of the structure under seismic excitation is used to calculate the damages in a component level.

6.2.1 Probabilistic structural model

A class of shear-building frame models with hysteretic behavior and deteriorating stiffness and strength is assumed. Figure 6.7 illustrates some of the characteristics of the model. The hysteretic behavior is assumed to have bilinear characteristics with a maximum strength capacity. A distributed element model assumption is used for the deteriorating part of the restoring force for each story, as discussed in Iwan and Cifuentes (1986). According to this assumption the reduction of the strength during the loading of a story is attributed to the failure of a fraction of the structural elements of the story (that fraction is proportional to the fractional strength reduction). These failed elements no longer contribute to the stiffness and strength of the story for future unloading and loading cycles. Additionally, a residual strength is assumed equal to 10% of the maximum strength.

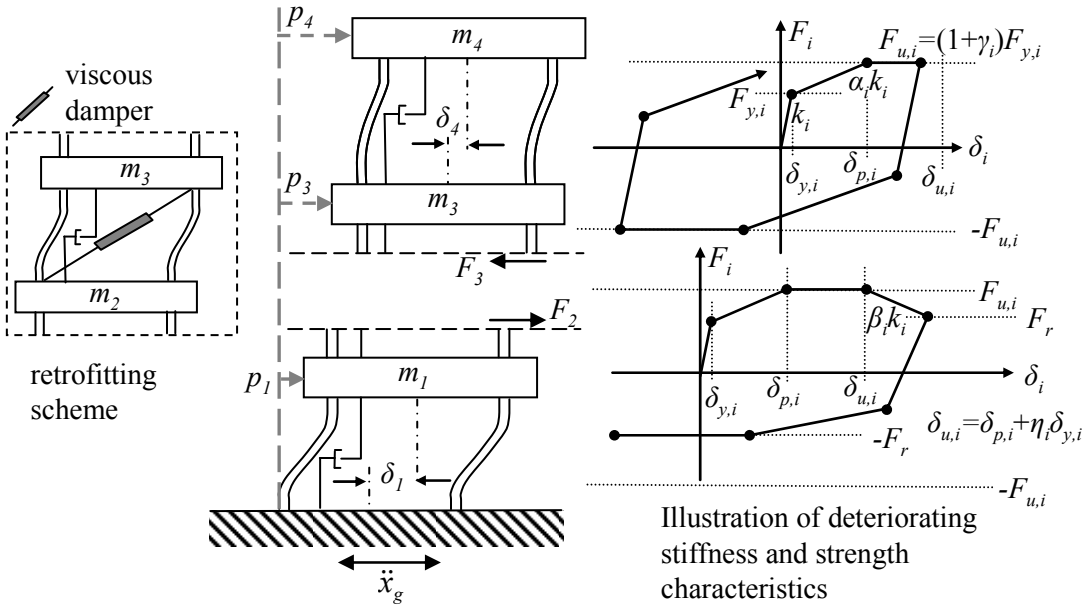

Figure 6.7: Structural model assumed in the study

In this study, the parameters that define the backbone curve for the restoring force of the i^{th} story are: the elastic inter-story stiffness k_i, the strain-hardening coefficient α_i, the over-strength factor γ_i, the yield displacement $\delta_{y,i}$, the displacement coefficient η_i and the stiffness deterioration coefficient β_i (see also Figure 6.7). Based on these parameters, the following resultant characteristics can be defined: yielding force $F_{y,\mathrm{i}}$ ultimate force $F_{u,i}$, displacement when restoring force reaches maximum strength $\delta_{p,i}$, capping displacement $\delta_{u,i}$, which is defined as the maximum ductility at peak strength, strain-hardening stiffness $k_{h,i}$, and the initial post-capping stiffness $k_{p,i}$. These characteristics are given, respectively, by the following relationships:

$$
\begin{aligned}
&F_{y,i} = \delta_{y,i} k_i,\ F_{u,i} = (1+\gamma_i)\delta_{y,i} k_i \\
&\delta_{p,i} = \left(1+\frac{\gamma_i}{\alpha_i}\right)\delta_{y,i},\ \delta_{u,i} = \left(1+\frac{\gamma_i}{\alpha_i}+\eta_i\right)\delta_{y,i} \\
&k_{h,i} = \alpha_i k_i,\ k_{p,i} = \beta_i k_i \qquad .
\end{aligned}
\tag{6.8}
$$

The lumped mass of the top story is 935 ton while it is 1215 ton for the bottom three. The initial inter-story stiffnesses k_i of all the stories are parameterized by $k_i = \hat{k}_i \theta_{k,i}$, i=1,2,3, where $[\hat{k}_i]$=[700.0, 616.1, 463.6, 281.8] MN/m are the most probable values and $\theta_{k,i}$ are nondimensional uncertain parameters, modeled as correlated Gaussian variables with mean value one and covariance matrix with elements given by (6.1). For each story, the post-yield stiffness coefficient α_i, stiffness deterioration coefficient β_i, over-strength factor γ_i, yield displacement $\delta_{y,i}$, and displacement coefficient η_i have mean values 0.1, 0.2, 0.3, 0.22% of story height and 2, respectively. All these parameters are treated as independent Gaussian variables with coefficient of variation (c.o.v.) 10%. The structure is assumed to be modally damped. The damping ratios for all modes are treated similarly as Gaussian variables with mean values 5% and c.o.v. 10%. Note that the main variables identified in Porter et al. (2002) to influence the earthquake loss estimation are probabilistically taken into account here.

Under these assumptions the differential equation for the structural model is:

$$\mathbf{M}_s\ddot{\mathbf{p}}(t)+\mathbf{C}_s\dot{\mathbf{p}}(t)+\mathbf{F}(t)=\mathbf{M}_s\mathbf{R}_s\ddot{x}_g(t) \tag{6.9}$$

where $\mathbf{M}_s$ and $\mathbf{C}_s$ are mass and damping matrices, $\mathbf{F}(t)$ is the vector or restoring forces for each story, $\mathbf{p}(t)\in\mathbb{R}^3$ is the vector of floor displacements relative to the ground, $\mathbf{R}_s\in\mathbb{R}^3$ is the vector of earthquake influence coefficients and $\ddot{x}_g(t)$ is the acceleration of the ground. The nominal, i.e., most probable, fundamental period for the linear structural model is calculated as 0.76 sec.

6.2.2 Probabilistic site seismic hazard and ground motion model

In order to estimate the earthquake losses, probability models are established for the seismic hazard at the structural site and for the ground motion. Seismic events are assumed to occur following a Poisson distribution and so are independent of previous occurrences. The uncertainty in moment magnitude M is modeled by the Gutenberg-Richter relationship truncated on the interval $[M_{min}, M_{max}]=[5.5, 8]$, leading to the PDF in (2.14) and expected number of events per year (Kramer 2003):

$$\nu=\exp(a-bM_{\min})-\exp(a-bM_{\max}) \quad . \tag{6.10}$$

The regional seismicity factors are selected as $b=0.9\log_e(10)$ and $a=4.35\log_e(10)$, leading to $\nu=0.25$. For the uncertainty in the event location, the logarithm of the epicentral distance, r, for the earthquake events is assumed to follow a normal distribution with mean log(20) km and standard deviation 0.4. Figure 6.13(a) illustrates the PDFs for M and r.

For modeling the ground motion, the methodology described in detail in Section 2.3 is adopted. Near-fault effects are not expected to be important for this structure and site combination; the building has a relatively small fundamental period, 0.76 sec, based on the

nominal model and the ground motions (M>6, r<15 Km) that might have near-field characteristics consist of only a small portion of the set of potential future excitations. Additionally it is unclear how the relationships suggested for modeling the characteristics of near-fault pulses can be extended to the whole range of moment magnitudes considered here. For these reasons near-fault characteristics are not included in the stochastic excitation model. The ground motion time history is modeled simply by the methodology presented in Section 2.4.1.

According to these seismicity and ground motion models, the mean total rate of seismic events corresponding to some intensity measure IM that exceeds some threshold im, $IM \geq im$, is:

$$v_{IM}(im) = v \int\int P\left[IM \geq im \mid M, r\right] p(M)\, p(r) dM\, dr \tag{6.11}$$

and the probability that at least one seismic event of interest will occur over time t_{dur} which has $IM \geq im$ is (because of the Poisson model for earthquake occurrences);

$$P\left[IM \geq im \mid t_{dur}\right] = 1 - e^{v_{IM}(im) t_{dur}} \quad . \tag{6.12}$$

Figure 6.8 shows the mean rate for $IM \geq im$ (Figure 6.8(a)) and the probability of occurrence for t_{dur}=1 year (Figure 6.8(b)) and t_{dur}=60 years (Figure 6.8(c)) for two families of intensity measures. The first family corresponds to the peak ground acceleration and the second to the peak spectral acceleration for a SDOF oscillator with damping ratio 5% and four different periods, 1 sec, 0.76 sec (which equals to the period of the linear structural model), 0.5 sec, and 0.25 sec. These plots constitute a representation in civil engineering terminology, rather than the abstract PDF and ground motion model characterization, of the mean seismic hazard considered for the structural site. Stochastic simulation has been used for evaluating the integral in (6.11).

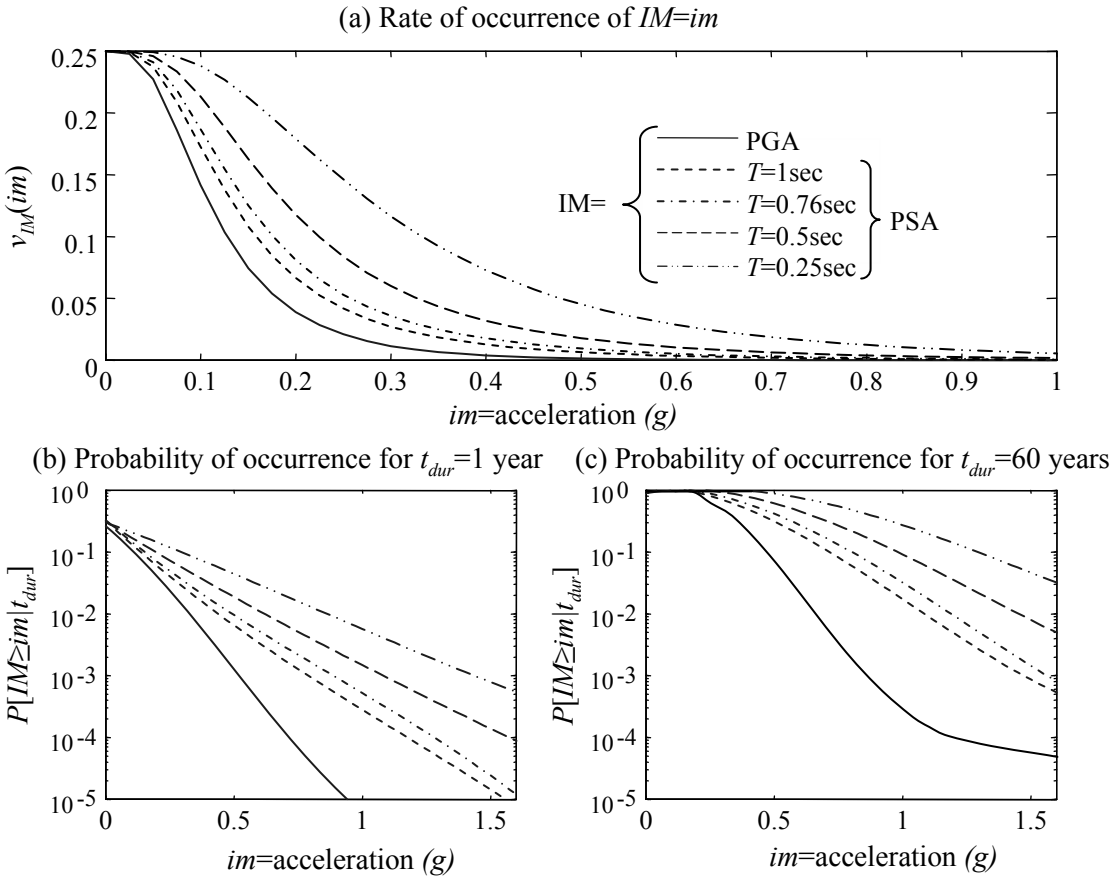

Figure 6.8: (a) Mean occurrence rate, and probability of occurrence for (b) t_{dur}=1 year and (c) t_{dur}=60 years, for PGA (peak ground acceleration) and PSA (peak spectral acceleration)

6.2.3 Expected life-cycle cost

The uncertain parameter vector in this design problem consists of the structural model parameters, $\boldsymbol{\theta}_s$, the seismological parameter $\boldsymbol{\theta}_g=[M, r]$, and the white noise sequence, $\mathbf{Z}_w$, so $\boldsymbol{\theta}=[\boldsymbol{\theta}_s, \boldsymbol{\theta}_g, \mathbf{Z}_w]$. The objective function in the stochastic design problem is the expected life-cycle cost of the structure for a life-time of t_{life}=60 years after the retrofit. This cost, $C(\boldsymbol{\varphi})$, as a function of the design variables is given by (Porter et al. 2004a):

$$C(\boldsymbol{\varphi}) = C_d(\boldsymbol{\varphi}) + \int_{\Theta} L(\boldsymbol{\varphi},\boldsymbol{\theta}) \left[vt_{life} \frac{1-e^{-r_d t_{life}}}{r_d t_{life}} \right] p(\boldsymbol{\theta}) d\boldsymbol{\theta} \tag{6.13}$$

where $C_d(\boldsymbol{\varphi})$ is the cost of the viscous dampers, r_d equals the discount rate (taken here as 2.5%), and $L(\boldsymbol{\varphi},\boldsymbol{\theta})$ is the expected cost given the earthquake event and the system specified by the pair $[\boldsymbol{\varphi},\boldsymbol{\theta}]$. The term in the brackets in (6.13) is the present worth factor, which is used in order to calculate the present value of the expected future earthquake losses (Porter et al. 2004a). The earthquake damage and loss are calculated assuming that after each event the building is quickly restored to its undamaged state. The cost of the dampers at each floor is estimated based on their maximum force capacity $F_{ud,i}$ as $C_{d,i}(\boldsymbol{\varphi})=\$80(F_{ud,i})^{0.8}$. This simplified relationship comes from fitting a curve to the cost of some commercially-available dampers. The viscosity of the dampers is selected assuming that the maximum force capacity is established at a velocity of 0.2 m/sec.

The earthquake losses are estimated adopting the methodology described in Porter et al. (2004a) and Goulet et al. (2007). The components of the structure are grouped into n_{as} damageable assemblies. For each assembly j, $n_{d,j}$ different damage states are designated and a fragility function is established for each damage state $d_{k,j}$. These functions quantify the probability that the component has reached or exceeded that damage state, conditional on some engineering demand parameter (EDP_j). Damage state 0 always corresponds to an undamaged condition. Each fragility function is a conditional cumulative log-normal distribution with median x_m and logarithm standard deviation b_m, as presented in Table 6.4. Indirect losses because of (a) fatalities and (b) building downtime, i.e., loss of revenue while the building is being repaired, are ignored in this study. The expected losses in the event of the earthquake are given by:

$$L(\boldsymbol{\varphi},\boldsymbol{\theta}) = \sum_{j=1}^{n_{as}} \sum_{k=1}^{n_{d,j}} P[d_{k,j} \mid \boldsymbol{\varphi},\boldsymbol{\theta}] C_{k,j} \tag{6.14}$$

where $P[d_{k,j}|\boldsymbol{\varphi},\boldsymbol{\theta}]$ is the probability that the assembly j will be in its k^{th} damage state and $C_{k,j}$ is the corresponding expected repair cost.

Table 6.4 Characteristics of fragility functions and expected repair cost for each story

$d_{k,j}$	Structural Components				$d_{k,j}$	Partitions			
	x_m	b_m	n_{el}	\$/n_{el}		x_m	b_m	n_{el}	\$/n_{el}
1 (light)	$1.4\delta_{y,i}$	0.2	22	2000	1 (patch)	0.33%	0.2	500	180
2 (moderate)	$(\delta_{y,i}+\delta_{p,i})/2$	0.35	22	9625	2 (replace)	0.7%	0.25	500	800
3 (significant)	$\delta_{p,i}$	0.4	22	18200	$d_{k,j}$	Acoustical Ceiling			
4 (severe)	$\delta_{u,i}$	0.4	22	21600		x_m	b_m	n_{el}	\$/n_{el}
5 (collapse)	3%	0.5	22	34300	1 (damage)	1g	0.7	10^3m^2	25
$d_{k,j}$	Contents				$d_{k,j}$	Paint			
	x_m	b_m	n_{el}	\$/n_{el}		x_m	b_m	n_{el}	\$/n_{el}
1 (damage)	0.6g	0.3	100	3000	1 (damage)	0.33%	0.2	3500m^2	25

Table 6.4 summarizes the characteristics for the fragility functions (x_m, β_m) and the expected cost per element \$/n_{el}. The n_{el} in this table corresponds to the number of elements that belong to each damageable assembly in each direction of each floor. For the structural contents and the acoustical ceiling, the maximum story absolute acceleration is used as EDP and for all other assemblies the maximum inter-story drift ratio is used. For estimating the total wall area requiring a fresh coat of paint, the simplified formula developed in (Goulet et al. 2007) is adopted. According to this formula a percentage of the undamaged wall area is also repainted, considering the desire of the owner to achieve a uniform appearance. This percentage depends on the extent of the damaged area and is chosen here based on a lognormal distribution with median 0.25 and logarithmic standard deviation 0.5.

The fragility curves adopted are similar to the ones selected in Mitrani (2007) and Goulet et al. (2007) for all damageable assemblies apart from the structural components. For the latter, the fragility curves have been chosen in the current study according to the characteristics of the backbone curve for the restoring force in each story. In this setting, a

direct link is established between the fragility curves and the stiffness and strength characteristics of the corresponding structural model, considering their associated uncertainties. Figure 6.9 illustrates this concept for the nominal values of the structural model parameters.

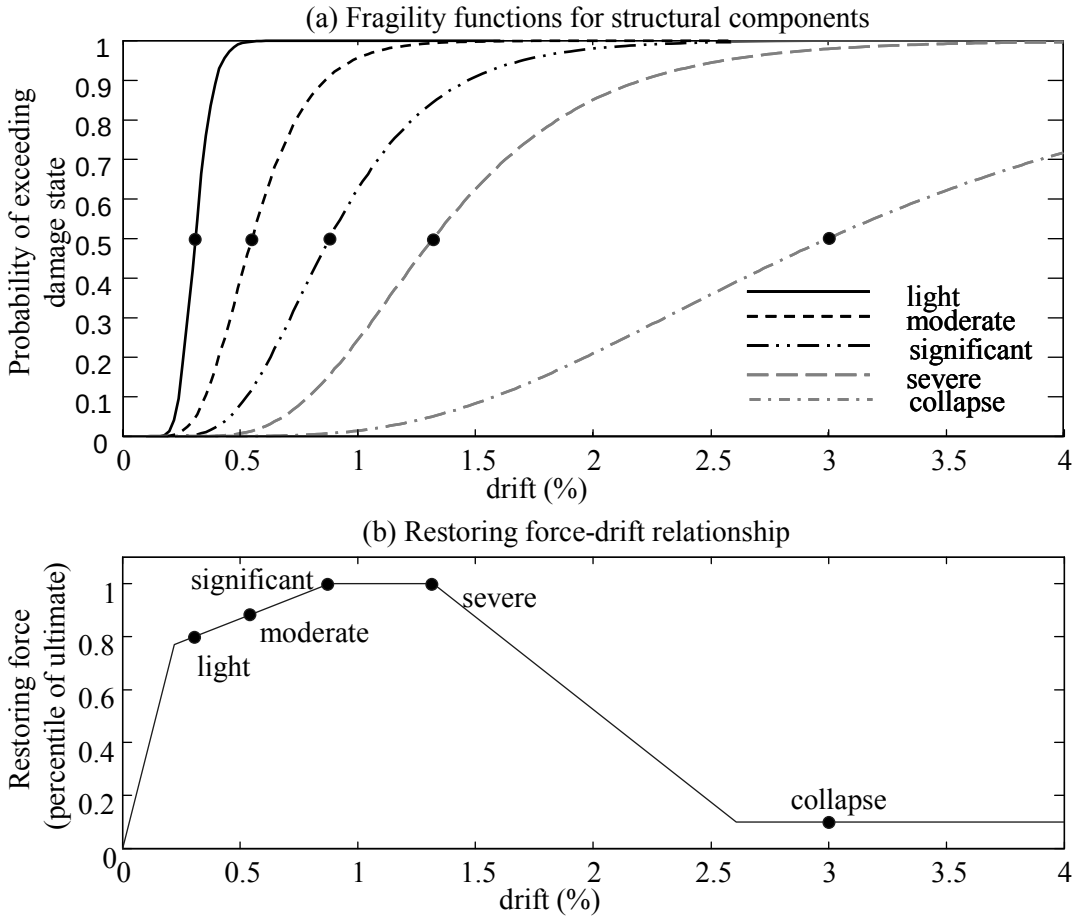

Figure 6.9: (a) Fragility functions for structural components and (b) restoring force-drift relationship

Figure 6.9(a) shows the fragility curves for each damaged state of the structural components, with characteristics the ones reported in Table 6.4. Figure 6.9(b) indicates the location of the median for each damaged state in the backbone curve for the restoring force at each story. The comparison between the two curves reveals the connection between the

fragility of the structural components and the strength/stiffness characteristics of each story. Such a link of the damaged states of the structural components to strength and stiffness model characteristics has not been established in most other studies that use similar methodologies for estimating repair damages from earthquakes (for example, in Goulet et al. (2007)).

The expected repair cost for all damageable assemblies is selected based on the repair-cost characteristics reported in Mitrani (2007) and Beck, Porter et al. (2002). In particular, for the "structural components" damageable assembly the frame at each story is assumed to consist of beams and column that have possible repair methods [epoxy injection, jacketed repair, replacement] (depending on the extend of the damage) and associated repair cost [$ 8000, $ 22500, $ 34300], as discussed in detail in Beck, Porter et al. (2002). For each of the damage states of the "structural components" damageable assembly that are reported in Table 6.4, the expected repair cost has been estimated assuming that a specific portion (chosen based on engineering judgment) of the beams and columns will need one of the three aforementioned repair methods. The chosen relationship between the damaged state for the structural components and the percentage of the beams and columns that need some repair method is shown in Table 6.5.

Table 6.5 Relationship between damage states for "structural components" damageable assembly and type of repair needed for the beams and columns

Damaged states for "structural components" assembly	Percentage of beams and columns of the frame that needs each type of repair			
	no repair	epoxy injection	jacketed repair	replacement
1 (light)	80%	20%	0%	0%
2 (moderate)	25%	50%	25%	0%
3 (significant)	0%	50%	25%	25%
4 (severe)	0%	33.3%	33.3%	33.3%
5 (collapse)	0%	0%	0%	100 %

Figure 6.10 illustrates the fragility curves adopted in this study for the partitions and the damaged state probabilities $P[d_{kj}|\boldsymbol{\varphi},\boldsymbol{\theta}]$ estimated according to these curves. Then Figure 6.11 shows the mean cost for the drift sensitive (Figure 6.11(a)) and acceleration sensitive (Figure 6.11(b)) components of the structure. These two plots in Figure 6.11 correspond ultimately to the utility functions (performance measure) that are used to evaluate the favorability of the dynamic response of the structure, either maximum inter-story drift or absolute acceleration, under the given ground motion excitation.

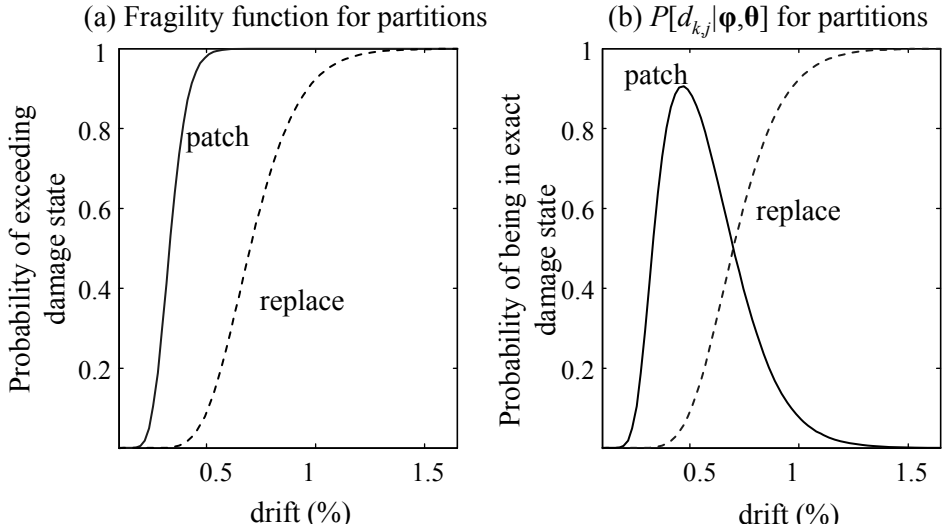

Figure 6.10: (a) Fragility function and (b) damage state probabilities for partitions

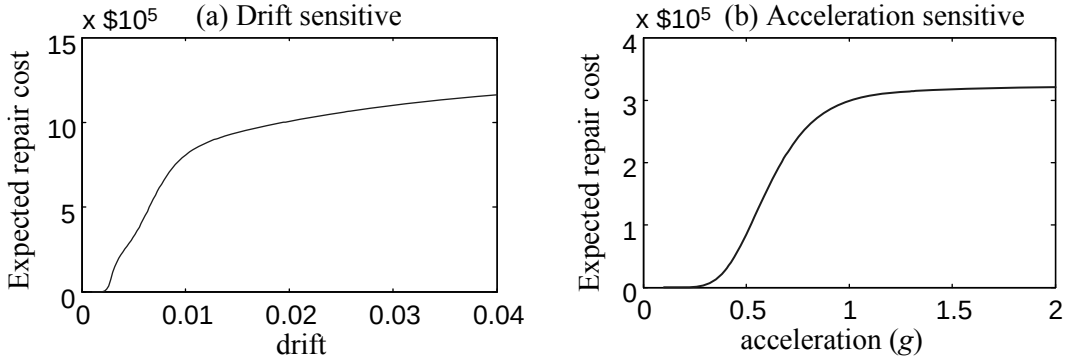

Figure 6.11: Total expected repair cost for the (a) drift and (b) acceleration sensitive components (per story)

Finally in Figure 6.12 the expected repair cost for each of the different drift-sensitive damageable assemblies is plotted. The acceleration-sensitive assemblies have much smaller contribution to the total cost, as will be demonstrated later, and thus presentation of a similar plot for them was deemed unnecessary. Figure 6.12 shows that the repair cost for the paint is more important for smaller drifts but converges to a plateau fast. On the contrary, the repair cost for the structural components is small for lower drifts but monotonically increases and becomes dominant for large drifts. For medium drifts the repair cost for the partitions is relatively more important. Also the maximum expected repair cost for the paint is significantly smaller that the repair cost for the other drift-sensitive components. These remarks illustrate that under smaller excitations the cost of repainting the damaged rooms will be the major contributor to the total expected cost, possibly because of the assumption used that the owner will desire to achieve a uniform appearance and repaint greater wall area than the one actually damaged. For moderate excitations the total repair cost increases considerably, due to the cost of primarily replacing the damaged partitions and secondarily repairing the structural components. The cost of the structural components dramatically contributes to the total repair cost for large excitations which lead to nonlinear structural behavior and thus to large inter-story drifts.

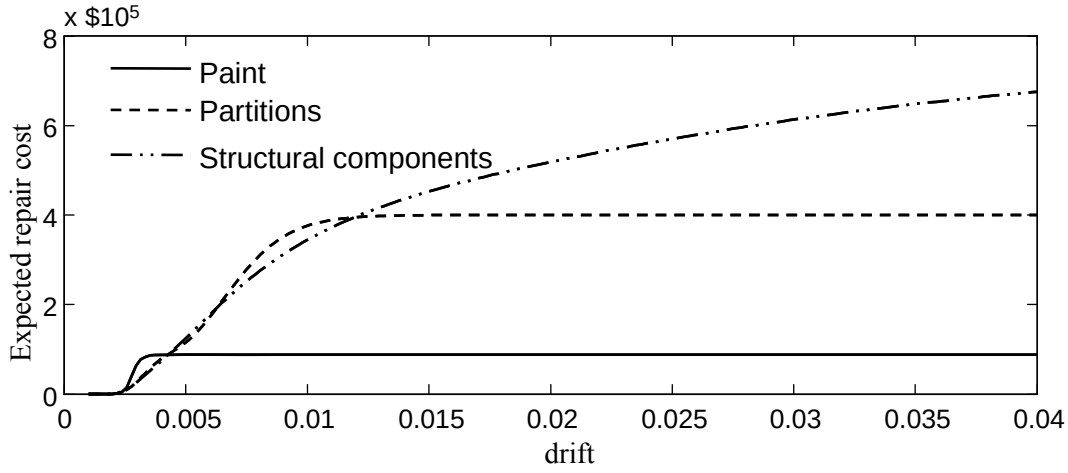

Figure 6.12: Expected repair cost for the drift sensitive damageable assemblies (per story)

6.2.4 Optimal damper design

The maximum force capacities of the dampers in each floor are the four design variables $\boldsymbol{\varphi}=[F_{ud,i}: i=1,...,4]$. The initial design space for each variable is set to [0, 13000] kN for $F_{ud,1}$ and $F_{ud,2}$ and [0, 8000] kN for $F_{ud,3}$ and $F_{ud,4}$. Results for a sample run of the optimization algorithm are presented in Table 6.6. For the SSO stage only the sets I_3 (after three iterations of the algorithm) and I_{SSO} (at the final stage of the algorithm, which in this case corresponded to the sixth iteration) are reported here. Also l_I^i denotes the length of set I in the direction of the i^{th} design variable.

Table 6.6 Optimization results

$\boldsymbol{\Phi}$	I_3 (kN)	I_{SSO} (kN)	$\boldsymbol{\varphi}_{SSO}$ (kN)	$\boldsymbol{\varphi}^*$ (kN)	$\hat{E}_\theta[h(\boldsymbol{\varphi}^*,\boldsymbol{\theta})]$ $\hat{E}_\theta[h(\boldsymbol{\varphi}_{SSO},\boldsymbol{\theta})]$	l_{SSO}^i / l_{Φ}^i	$\sqrt[n_\varphi]{V_{I_{SSO}} / V_{\Phi}}$
$F_{ud,1}$	[3610, 7657]	[5857, 6980]	6418	6420	$0.430\text{x}10^6$ \$	0.094	0.131
$F_{ud,2}$	[3557, 7756]	[4539, 6045]	5292	5195		0.126	
$F_{ud,3}$	[4034, 7095]	[4085, 5517]	4801	4481	$0.438\text{x}10^6$ \$	0.179	
$F_{ud,4}$	[1566, 4751]	[1841, 2959]	2400	2060		0.139	

6.2.5 Details for stochastic subset optimization

The objective function (6.13) can be written as:

$$C(\boldsymbol{\varphi}) = E_{\boldsymbol{\theta}}[h_s(\boldsymbol{\varphi},\boldsymbol{\theta})] = \int_{\Theta}\left(C_d(\boldsymbol{\varphi}) + L(\boldsymbol{\varphi},\boldsymbol{\theta})\left[vt_{life}\frac{1-e^{-r_d t_{life}}}{r_d t_{life}} \right] \right) p(\boldsymbol{\theta}) d\boldsymbol{\theta} \quad . \tag{6.15}$$

Thus, the loss function used in the SSO stage of the optimization is:

$$h_s(\boldsymbol{\varphi},\boldsymbol{\theta}) = C_d(\boldsymbol{\varphi}) + L(\boldsymbol{\varphi},\boldsymbol{\theta})\left[vt_{life}\frac{1-e^{-r_d t_{life}}}{r_d t_{life}} \right] \quad . \tag{6.16}$$

The parameter selections for SSO are: ρ=0.2, N=2000, s=0. The shape for the sets I is selected as a hyper-rectangle and the adaptive identification is stopped when $\hat{H}(\hat{I}_k)$ becomes larger than 0.80. In total, 6 iterations of the SSO algorithm are performed. After 3 iterations the loss functions $h_s(\boldsymbol{\varphi},\boldsymbol{\theta})$ is reformulated by choosing s=\$200,000 . Algorithm 1 (Appendix 4A) is used for sampling in the 1st and 4th iterations, and Algorithm 2 in all others. For the MCMC simulation a global proposal PDF equal to $p(\mathbf{Z}_w)$ is chosen for the white noise sequence, to avoid the problems with the high-dimensionality of the uncertain parameter vector, and local random walk proposal PDFs are chosen for all other parameters.

The results in Table 6.6 show that SSO efficiently identifies a smaller subset for the optimal design variables that leads to a significant reduction of the size (volume) of the search space (look at the last two columns of Table 6.6). The converged optimal solution in the second stage, $\boldsymbol{\varphi}^*$, is close to the center $\boldsymbol{\varphi}_{SSO}$ of the set that is identified by SSO; also the objective function at that center point $E_{\boldsymbol{\theta}}[h(\boldsymbol{\varphi}_{SSO},\boldsymbol{\theta})]$ is not significantly different from the optimal value $E_{\boldsymbol{\theta}}[h(\boldsymbol{\varphi}^*,\boldsymbol{\theta})]$. Thus, selection of $\boldsymbol{\varphi}_{SSO}$ as the design choice leads to a sub-optimal design that is, however, close to the true optimum in terms of both the design vector selection and its corresponding performance. This agrees with the findings of the previous study in this chapter and indicates that sole use of SSO might be adequate for many problems.

6.2.6 Details for simultaneous-perturbation stochastic approximation with common random numbers

For the second stage of the optimization framework the formulation of the objective function in (6.13) is adopted. Stochastic simulation is used in order to estimate only the second part, since the cost of the dampers can be deterministically evaluated, so:

$$h(\boldsymbol{\varphi},\boldsymbol{\theta}) = L(\boldsymbol{\varphi},\boldsymbol{\theta})\left[vt_{life}\frac{1-e^{-r_d t_{life}}}{r_d t_{life}} \right] \quad . \tag{6.17}$$

Following the discussion in Section 5.2, importance sampling densities are established for the structural model parameters and the seismological parameters, M and r, but not for the high-dimensional white-noise sequence. Figure 6.13(b) illustrates this concept for M and r. A truncated lognormal distribution is selected for the IS PDF for M (with median 7 and logarithmic standard deviation 0.1) and a lognormal for r (with median 15 and logarithmic standard deviation 0.4). Note that the IS PDF for M is significantly different from its initial distribution; since M is expected to have a strong influence on $h(\boldsymbol{\theta},\boldsymbol{\varphi})$, the difference between the distributions is expected to have a big effect on the accuracy of the estimation. The respective difference between the PDFs for r is much smaller. For the structural model parameters this difference is negligible, and the IS PDFs were approximated to be Normal distributions, like $p(\boldsymbol{\theta}_s)$, with a slightly shifted mean value but the same variance. According to the discussion in section 4.1.7, these remarks show that the sensitivity of the loss estimation to the seismological parameters, that is, to the stochastic excitation characteristics, is much more important than to the structural model characteristics.

The c.o.v. for $\hat{E}_{\boldsymbol{\theta},N}[h(\boldsymbol{\varphi},\boldsymbol{\Omega}_N)]$ for a sample size N=1000 is 16% without using IS and 4% when IS is used. Since this c.o.v. varies according to $1/\sqrt{N}$, the sample size for direct estimation (i.e., without use of IS) of the objective function with the same level of accuracy as in the case when IS is applied would be approximately 16 times larger. This illustrates again the efficiency increase that can be established by the IS scheme discussed earlier. The converged optimal solution in the second stage is included in Table 6.6. Forty iterations were needed in the second stage of the framework using a sample size of N=1000. This computational cost can be characterized as small. Convergence is judged by looking at the norm $\|\boldsymbol{\varphi}_{k+1}-\boldsymbol{\varphi}_k\|_\infty$ for each of the last five iterations. If that norm is less than 0.2% (normalized by the dimension of the initial design space), then we assume that convergence to the optimal solution has been established.

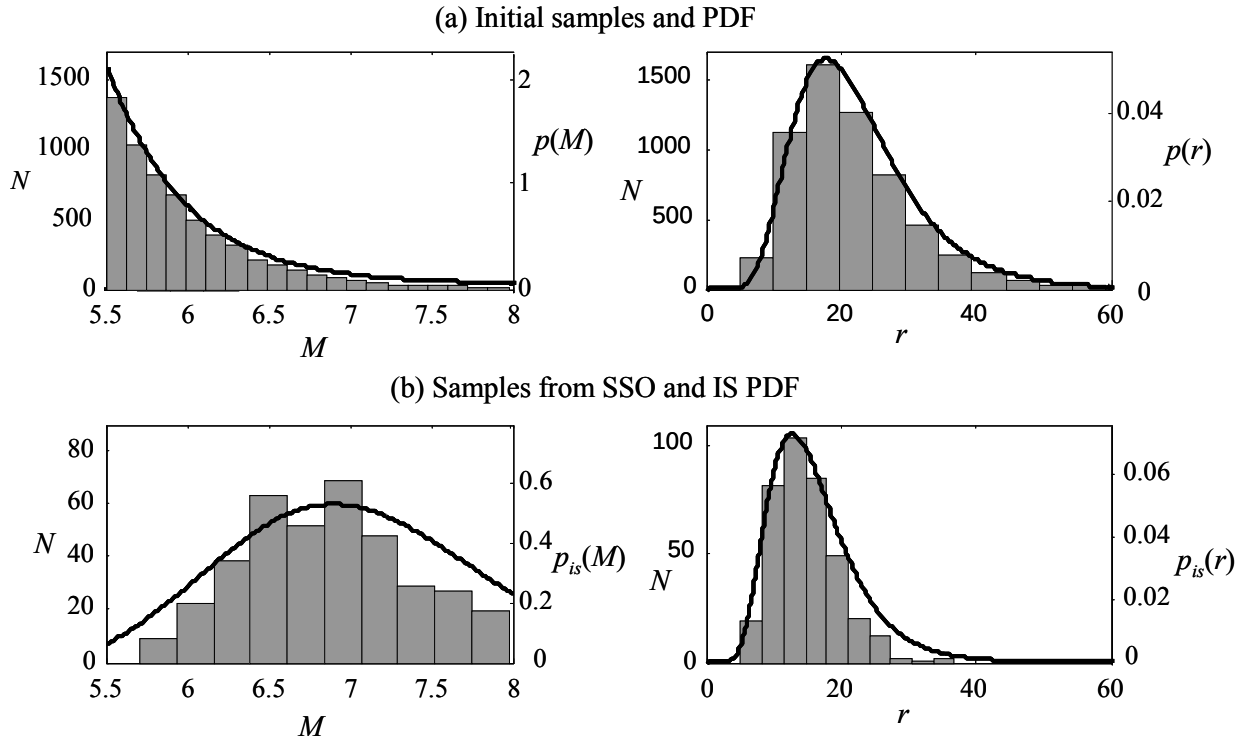

Figure 6.13: Details about importance sampling densities formulation

6.2.7 Efficiency of the two-stage optimization framework

To evaluate the efficiency of the optimization framework, the same optimization was performed without the use of SSO in the first stage. In this case the starting point for SPSA was selected as the center of the design space Φ, and α was chosen so that in the first iteration the movement for any design variable is not larger than 5% of the respective dimension of the design space. In this case IS is not implemented; since search inside the whole design space Φ is considered, it is unclear how samples of $\boldsymbol{\theta}$ can be obtained to form the IS densities and separately establishing an IS density for each design choice $\boldsymbol{\varphi}$ is too computationally expensive. The larger variability of the estimates caused the gradient-based algorithm diverge in the first couple of iterations. Thus a larger value for the sample size (N=3000) was used. The required number of iterations for convergence of the algorithm in a sample run and the total number of system simulations was 102 and

612,000, respectively. When the combined framework was used, the corresponding numbers were 40 and 80,000, respectively. This comparison illustrates the efficiency of the proposed two-stage optimization framework. The better starting point of the algorithm, as well as the smaller size of the search space, which allows for better normalization, that the SSO subset identification can provide are the features that contribute to this improvement of efficiency.

6.2.8 Efficiency of seismic protection system

The expected lifetime cost for the structure in each direction without the dampers is estimated as $1.1 million. The expected lifetime cost of the retrofitted system is $430,000, so the addition of the viscous dampers improves significantly the performance of the structural system. Of this amount, $267,000 corresponds to the cost for the installation of the viscous dampers and $163,000 to the present worth of the expected repair cost for damage from future earthquakes. The maximum force capacities for the dampers at each story under optimal design have been reported in Table 6.6. They are also illustrated later in Figure 6.16. These values seem reasonable compared to current commercial applications of viscous dampers.

Figure 6.14 shows the decomposition of the expected lifetime repair cost into its different components for both the initial structure (Figure 6.14(a)) and the retrofitted structure (Figure 6.14(c)). Only minor changes occur in the distribution of the total cost over its different components. Note that the relative importance of the repair cost for acceleration-sensitive assemblies (for example the building contents) increases by the addition of the dampers, as expected, but still the importance of this cost remains small and it is practically negligible. Figure 6.14(b) shows the expected lifetime cost for the structure with dampers. The improvement of the performance of the structure is clearly evident in these charts. Also the comparison between the plots in Figure 6.14(a) and Figure 6.14(c), taking additionally into account the distribution of the repair cost in Figure 6.12, clearly show that for the retrofitted structure the larger drift response accounts for the smaller amount of the total

repair cost, since the relative importance of the repair cost for the paint becomes larger and for the structural components smaller.

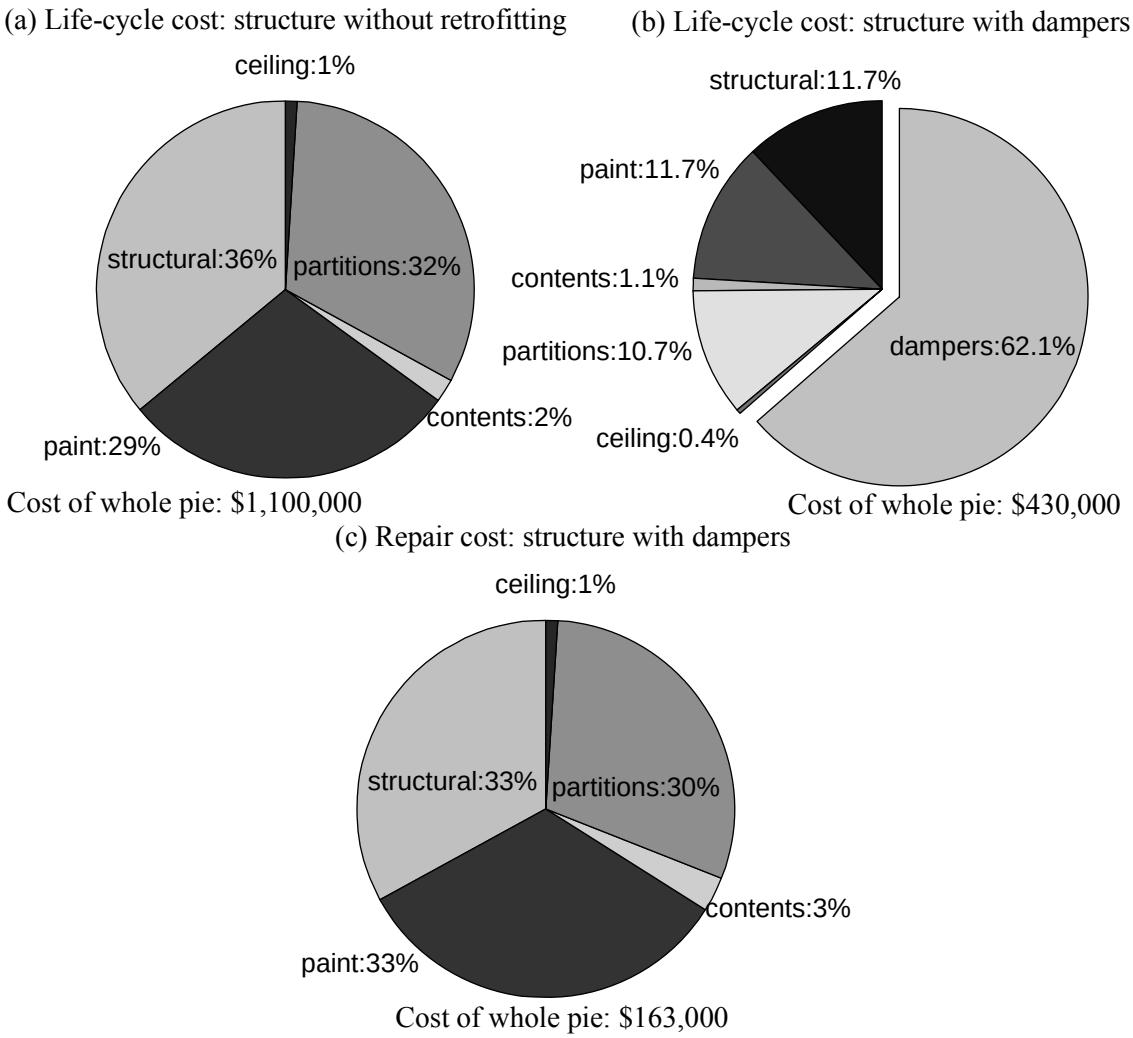

Figure 6.14: Details about expected life-cycle cost

Finally Figure 6.15 and Figure 6.16 show the decomposition of the repair cost into the four different stories for both the initial structure (Figure 6.16(a), Figure 6.15(a)) and the retrofitted structure (Figure 6.16(b), Figure 6.15(c)) as well as the life-cycle cost for the retrofitted structure (Figure 6.16(b), Figure 6.15(b)). For the initial structure the earthquake damages are slightly larger in the first story but in general are characterized by an almost

uniform distribution along the height of the building. This is not the case for the retrofitted structure, where the earthquake damages are concentrated in the lower part of the structure, primarily the first story. If the additional cost of the dampers is considered, then the distribution along the height gets more regular but is still higher for the lower parts of the building. This may be attributed, ultimately, to the fact that the earthquake forces at the higher floors are smaller (smaller shear force), thus smaller size dampers are able to alleviate the undesirable performance easier and prevent yielding at these floors without reaching their ultimate forcing capacity, which would reduce their efficiency. Of course, this behavior is also connected to the distribution of nonlinear phenomena along the height of the building. Apparently, nonlinear phenomena appear much stronger at the lower floors; the energy dissipation that is provided by this hysteretic behavior reduces the forces acting on the higher floors for the retrofitted structure.

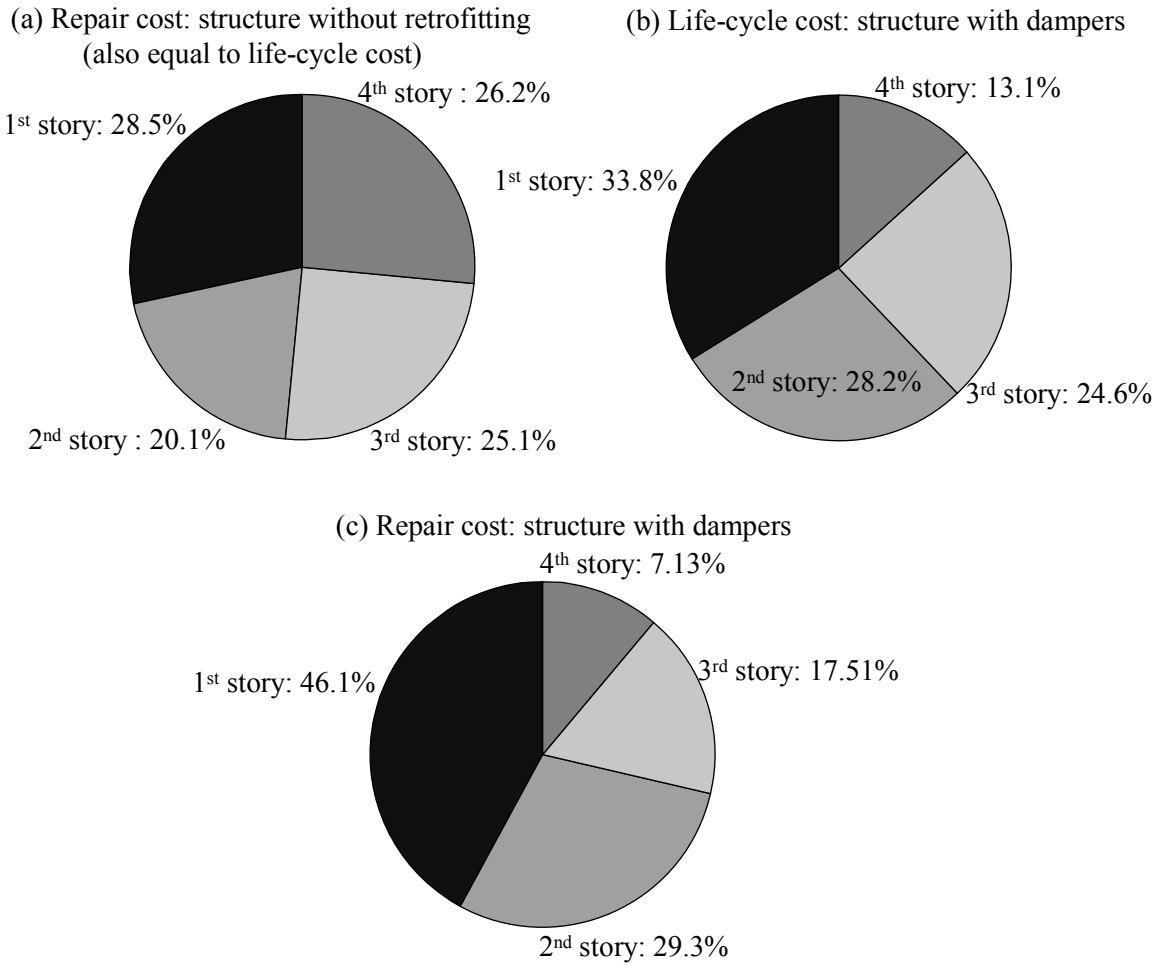

Figure 6.15: Distribution of repair and life-cycle cost between different stories

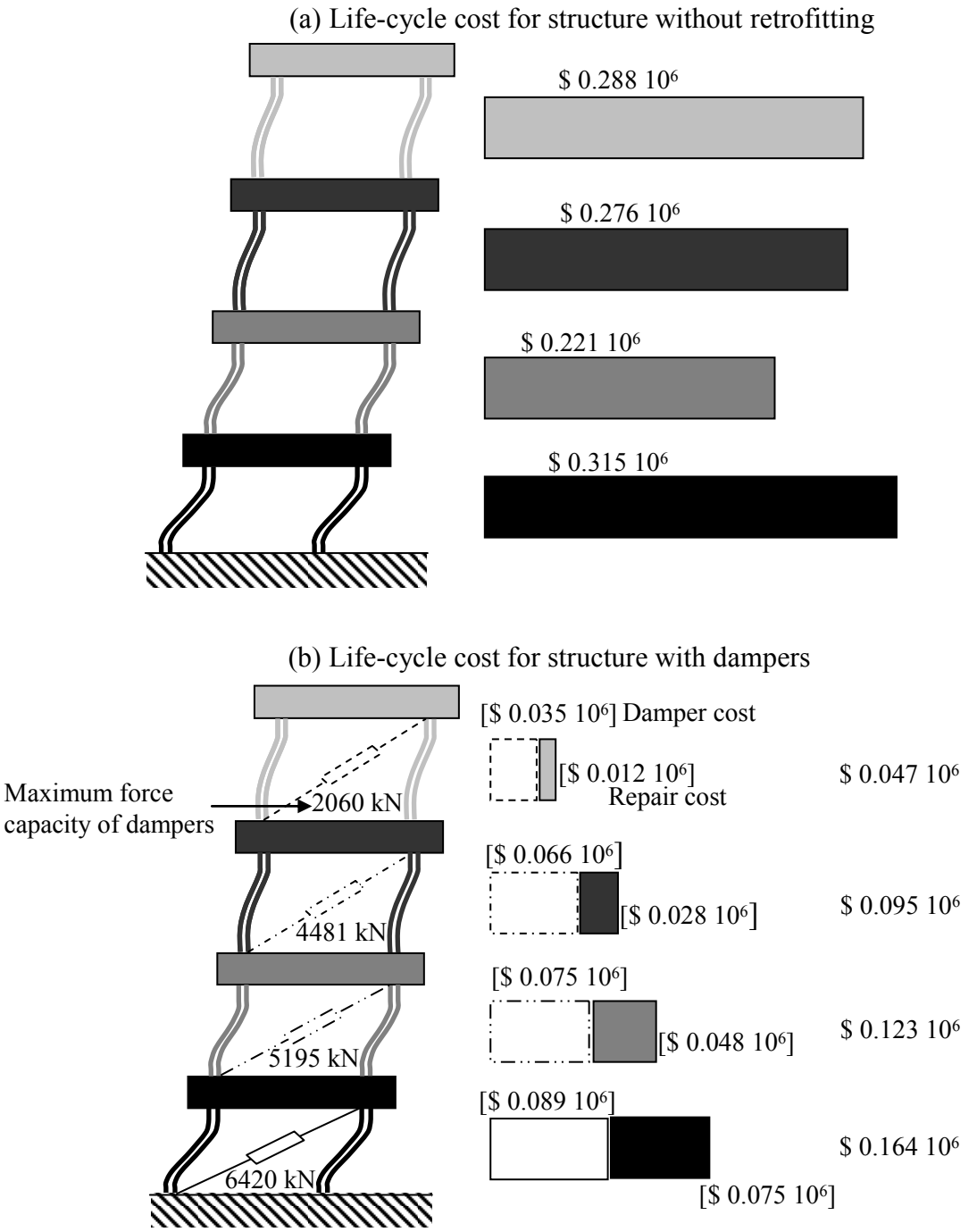

Figure 6.16: Distribution of repair, damper and life-cycle cost between different stories. Maximum force capacity of the dampers for each story is also illustrated

CHAPTER 7

Stochastic System Design: Structural Control Applications

This chapter presents applications of the general stochastic system design framework to the specific field of structural control. It can also be considered as an extension of the controller design discussed in Chapter 3 for linear systems, to design problems that involve nonlinear system and excitation models. The general model formulation illustrated in Figure 2.3 is adopted and the robust-to-uncertainties nonlinear controller design that was discussed in Section 2.3 is implemented, using simulation techniques to evaluate the model performance. In this simulation-based framework, all nonlinear characteristics of the controlled system can be potentially incorporated into the assumed system model at the design stage. Additionally, of course, uncertainty about the model parameters can be treated using a probabilistic description. Compared to the approach presented in Chapter 3, this more general controller design methodology has the potential to be more effective, i.e., lead to a control system that accomplishes more favorably the designated performance objectives, because it does not impose hard restrictions on the models selected to represent the true system. Ultimately, the efficiency of this design methodology depends on the ability of the adopted model to represent (a) the structural system, and (b) future excitations. If the representation is accurate and the uncertainty about the model parameters is quantified properly, the proposed methodology provides a powerful tool for designing the controlled system by taking into account all of its important (linear or nonlinear)

characteristics and their uncertainties, and this can provide significant improvement in the system performance. The only consideration for the complexity in the system description is the available computational power for efficiently performing multiple simulation analyses. The stochastic optimization framework, based on SSO, developed earlier provides a powerful tool for performing the associated controller optimization, as long as the controller structure is not overly complex and, thus, the number of design variables is relatively small. For structural control applications, which involve systems whose dynamic response is dominated by frequencies in a few narrow bands, the latter requirement can be easily satisfied in most applications by careful consideration of the characteristic of the control application. Such characteristics involve, for example, the dynamics of the facility to be controlled, the type of motion that needs to be regulated, the type of actuators used, the available measurements for designing the control law and so forth.

Two applications are considered for illustrating the efficiency of the controller nonlinear stochastic design methodology. The first involves the Base-Isolated ASCE Benchmark structure under near-fault earthquake excitation and the second a Tension Leg Platform under random sea excitation. The system reliability is adopted in both cases as the design objective. This selection was dictated by the fact that little information is currently available for developing different utility functions for evaluating the dynamic performance of the facilities considered in the studies, particularly with respect to monetary quantification of the performance. Still, the reliability-based design suggested is adequate for developing robust-to-uncertainties controllers. The following studies will demonstrate, though, that this is not always sufficient for evaluating the efficiency of the control system in structural applications and that there is a need for comparing, or even designing, such systems using socio-economic criteria to establish a direct cost-benefit quantification of the control implementation merits.

The TLP application has been also published in Taflanidis, Angelides, and Beck (2007).

7.1 Protection of Base-Isolated ASCE Benchmark Structure

The increasing attention that structural control applications have received in the last couple of decades has motivated the recent proposal by the ASCE Structural Control Committee of the Base-Isolation Benchmark Control Problem (Nagarajaiah and Narasimhan 2006; Narasimhan et al. 2006; Narasimhan et al. 2008). It consists of an eight-story irregular structure, as illustrated in Figure 7.1, equipped with a passive isolation system, which may be fitted with different actuators (both active and semi-active devices may be considered) and controlled through various feedback laws, to further reduce seismic response beyond that of the passive isolation system alone. In addition to a specified structural dynamic model, the problem statement imposes specific constraints on the actuators, sensors, and control laws that may be used, and requires that different approaches be compared under a single set of performance measures. As such, comparisons of different base-isolation strategies becomes more straight-forward.

One of the main challenges in controlling base-isolated buildings has been the explicit consideration of the nonlinear behavior of the isolators in the controller design stage. Another challenge has been the development of forcing systems which yield effective control of the dynamic response under near-fault ground motions. Such motions frequently include a strong longer-period pulse that has important implications for flexible structures, such as base-isolated systems (Hall et al. 1995). A third challenge, which is relevant to all structural control seismic applications, concerns the characterization and inclusion of the variability of future ground motions in the feedback controller design process. Typically a nominal model is assumed for stochastic representation of the ground motion and iterative procedures are applied for fine tuning the selected controller structure (such as weighting matrices in LQR design or linearization parameters for nonlinear models (Erkus and Johnson 2006)) based on the response of the system to a few recorded ground motions. What would be desirable is an approach which more systematically incorporates all available probabilistic knowledge of the character of future ground motions into the controller design.

The stochastic system design methodology proposed in this study addresses all these challenges. Uncertainty in the model parameters and future excitations is treated through the incorporation of a probabilistic description for them. Since stochastic simulation techniques are used for evaluation of the structural response, the controller can be optimized based on the non-linear characteristics of the base isolation system. Additionally, the probabilistic model for the realistic description of near-fault ground motions presented in Section 2.4 can be incorporated into the system model in the design stage to adequately characterize future excitations.

This methodology is illustrated in the context of the base-isolated benchmark structure equipped with linear and nonlinear (friction pendulum) bearings. A Regenerative Force Actuation (RFA) network with eight actuators in each direction operating in tandem with the passive isolation system is considered. The feedback controller designed for this application accepts noisy measurements of the absolute base accelerations, and implements a three-degree-of-freedom "skyhook" control law using estimates of the absolute velocities of the center of mass of the base. An efficient approach is presented for clipping the control forces to satisfy the RFA network actuator constraints. Comparison to the performance of an array of passive viscous dampers with the same characteristics (position, actuator capacities) is also presented.

7.1.1 Benchmark structure

The Base-Isolation Benchmark Problem (Narasimhan et al. 2006; Narasimhan et al. 2008) concerns a base-isolated structure with n_f =8 floors. The base and floor slabs are assumed to be infinitely rigid in plane, and are modelled by three master degrees of freedom located at the centres of mass of each floor. The superstructure is assumed to be a linear system with mass, damping, and stiffness matrices $\mathbf{M}_s$, $\mathbf{C}_s$, and $\mathbf{K}_s$. The natural periods and participation factors for the first couple of modes are shown in Table 7.1. Modal damping equal to 5% is assumed for all modes for determining $\mathbf{C}_s$.

Table 7.1 Periods and participation factors for superstructure

Mode	Period	Participation Factors		
		North-South	East-West	Torsion
1st	0.89	0.0 %	72.9 %	5.7 %
2nd	0.77	74.9 %	0.0 %	0.2 %
3rd	0.66	0.2 %	0.0 %	67.9 %
4th	0.28	17.2 %	0.0 %	0.0 %
5th	0.27	0.0 %	17.3 %	0.1 %
6th	0.21	0.0 %	0.2 %	16.72 %
7th	0.15	4.3 %	0.0 %	0.0 %
8th	0.15	0.0 %	5.3 %	0.3 %
9th	0.12	0.0 %	0.1 %	4.68 %

Below the base, the isolation system consists of a variety of 92 isolation bearings. In this study, the isolators are selected as 31 linear elastomeric rubber bearings and 61 nonlinear friction pendulum bearings (Figure 7.1). The properties of all isolators are set to the nominal parameters considered for the benchmark problem. The linear bearings are modelled as a spring-dashpot system with stiffness 919.42 kN/m^2 and viscous damping 27.17 kN/m/sec. For the frictional bearings the biaxial hysteretic behaviour is modelled using the biaxial interaction equations of the Bouc-Wen model proposed by Park et al. (1986) as follows:

$$U^y \begin{bmatrix} \dot{z}_x \\ \dot{z}_y \end{bmatrix} = \alpha_{is} \begin{bmatrix} \dot{U}_x \\ \dot{U}_y \end{bmatrix} - \mathbf{Z}_W \begin{bmatrix} \dot{U}_x \\ \dot{U}_y \end{bmatrix}$$

$$Z_W = \begin{bmatrix} z_x^2(\gamma_{is}\,\mathrm{sgn}(\dot{U}_x z_x) + \beta_{is}) & z_x z_y(\gamma_{is}\,\mathrm{sgn}(\dot{U}_y z_y) + \beta_{is}) \\ z_x z_y(\gamma_{is}\,\mathrm{sgn}(\dot{U}_x z_x) + \beta_{is}) & z_y^2(\gamma_{is}\,\mathrm{sgn}(\dot{U}_y z_y) + \beta_{is}) \end{bmatrix} \tag{7.1}$$

where z_x and z_y are dimensionless hysteretic variables that are bounded by values ±1, U_x, U_y; $\dot{U}_x$, $\dot{U}_y$ represent the displacements and velocities in the x and y directions, respectively, at the isolation bearing; and U^y is the yield displacement, selected as 0.3 cm. Also α_{is}, β_{is}, and γ_{is} are dimensionless quantities that characterize the properties of the

biaxial hysteretic behavior. The values suggested in Gavin (2002) are adopted in this study: α_{is}=1, β_{is}=0.1, and γ_{is}=0.9. The force of the bearing is finally given by:

$$f_{x,is} = K_p U_x + c_v \dot{U}_x + \mu \mathrm{N} z_x$$
$$f_{y,is} = K_p U_y + c_v \dot{U}_y + \mu \mathrm{N} z_y \tag{7.2}$$

where K_p is the post yield stiffness, c_v the viscous damping coefficient, N the average normal force at the bearing (normal force variation is neglected), and μ is the coefficient of friction. The first two quantities are chosen equal to the respective values of the linear isolators, N is calculated as 3137.8 kN and the coefficient of friction is selected as 6%. Figure 7.8 later presents the displacement-force relationship, in both x and y directions, for a sample earthquake ground motion in terms of the specific control implementation considered in this study.

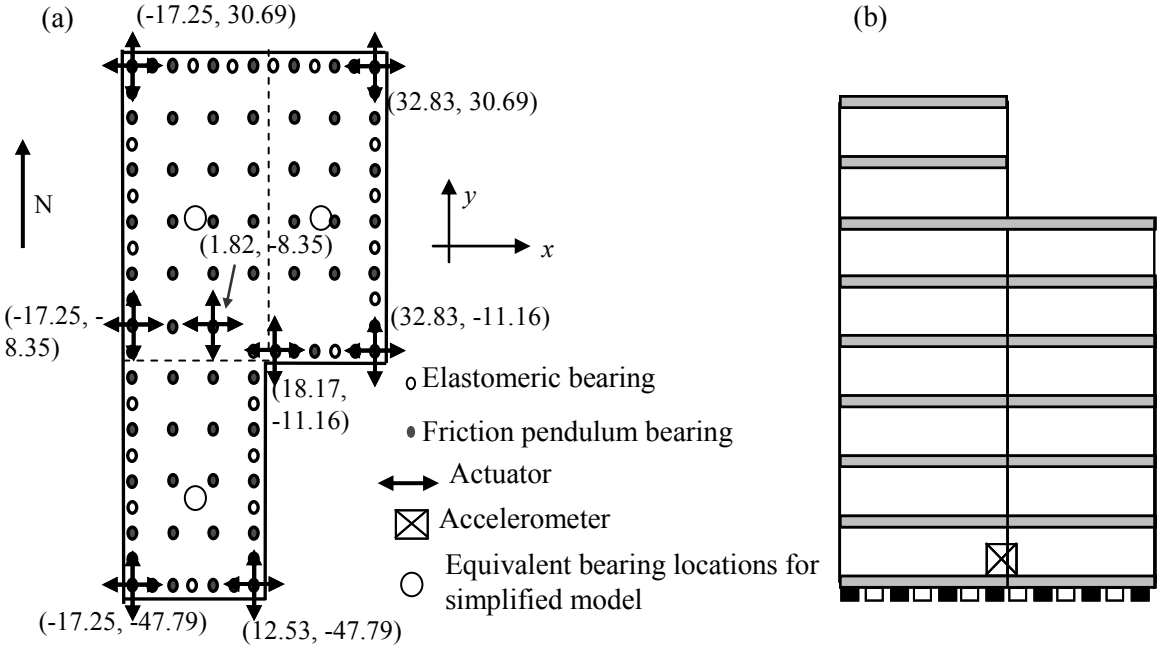

Figure 7.1: (a) Base plan of the benchmark structure and (b) side view

Let $\mathbf{M}_b$, $\mathbf{C}_b$, and $\mathbf{K}_b$ denote the mass and damping matrices for the base and the stiffness matrix of the linear isolators, respectively. The differential equation for the coordinate vector $\mathbf{p}$ (consisting of lateral and rotational displacements for each floor relative to the base and the lateral and rotational displacements for the base relative to the ground) can be expressed as:

$$\begin{bmatrix} \mathbf{M}_s & \mathbf{M}_s\mathbf{R}_s \\ \mathbf{R}_s^T\mathbf{M}_s & \mathbf{R}_s^T\mathbf{M}_s\mathbf{R}_s + \mathbf{M}_b \end{bmatrix}\ddot{\mathbf{p}}(t) + \begin{bmatrix} \mathbf{C}_s & \mathbf{0}_{3n_f\times 3} \\ \mathbf{0}_{3n\times 3_f} & \mathbf{C}_b \end{bmatrix}\dot{\mathbf{p}}(t) + \begin{bmatrix} \mathbf{K}_s & \mathbf{0}_{3n_f\times 3} \\ \mathbf{0}_{3n\times 3_f} & \mathbf{K}_b \end{bmatrix}\mathbf{p}(t) = \begin{bmatrix} \mathbf{0}_{3n_t\times 3} \\ \mathbf{I} \end{bmatrix}\mathbf{f}_c(t) + \begin{bmatrix} \mathbf{0}_{3n_t\times 3} \\ \mathbf{I} \end{bmatrix}\mathbf{F}_{is}(t) + \begin{bmatrix} \mathbf{M}_s\mathbf{R}_s \\ \mathbf{R}_s^T\mathbf{M}_s\mathbf{R}_s + \mathbf{M}_b \end{bmatrix}\begin{bmatrix} \ddot{\mathbf{x}}_g(t) \\ 0 \end{bmatrix} \tag{7.3}$$

where $\ddot{\mathbf{x}}_g(t) \in \mathbb{R}^2$ is the acceleration of the ground in the x and y directions and $\mathbf{R}$ is the $3n_f\times 3$ matrix of earthquake influence coefficients. Vector $\mathbf{f}_c(t)$ contains the total control on the base in the x and y directions and the total control torque about the base center of mass. This vector and the vector of forces produced by each individual device, $\mathbf{f}$, are related by:

$$\mathbf{f}_c = \mathbf{R}_c\mathbf{f} \text{ where } \mathbf{R}_c = \begin{bmatrix} \mathbf{r}_c^1 & \dots & \mathbf{r}_c^{n_c} \end{bmatrix},$$
$$\text{with } \mathbf{r}_c^i = \begin{cases} \begin{bmatrix} 1 & 0 & -y_c^i \end{bmatrix}^T & \text{(actuator in the } x\text{-direction)} \\ \begin{bmatrix} 0 & 1 & x_c^i \end{bmatrix}^T & \text{(actuator in the } y\text{-direction)} \end{cases}. \tag{7.4}$$

Vector $\mathbf{F}_{is}(t)$ in (6.2) contains the total forces produced by the nonlinear hysteretic isolators at the base center of mass. A relationship similar to (7.4) holds between $\mathbf{F}_{is}(t)$ and the force provided by each individual isolator in each direction given by (7.2).

7.1.2 Control implementation details

Noisy acceleration measurements are available at the center of mass of each floor level and the base for control applications. According to the definition of the Benchmark problem,

the A/D and D/A converters for the digitally implemented controller have a 16-bit precision and a span of ±10 Volts. Small RMS noise (0.05 Volts) is added to all measured outputs and the sampling time should be between 0.001 and 0.01 sec (the latter is chosen here).

7.1.3 RFA Network

In this study a Regenerative Force Actuation (RFA) network, similar to the one in Figure 1.1(b), but with more actuators, is implemented at the base level for the protection of the benchmark structure.

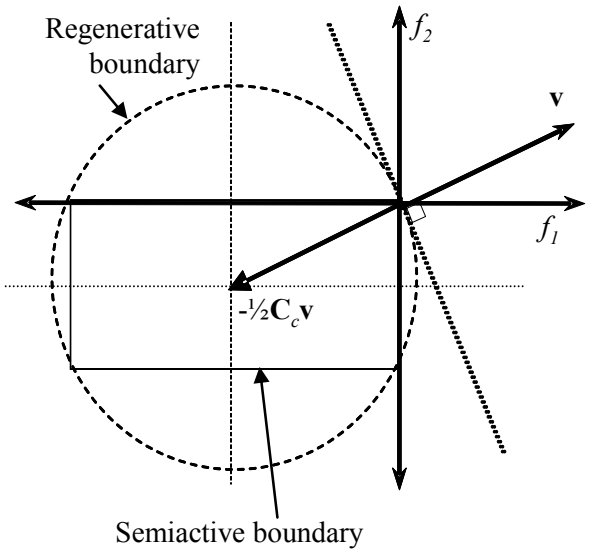

Figure 7.2: Feasible force region for regenerative and semi-active two actuator system

Consider a network of m actuators and define $\mathbf{f}=[f_1 \ldots f_m]^T$ as the vector of actuator forces. Define $\mathbf{v} = [v_1 \ldots v_m]^T$ as the corresponding vector of actuator velocities. Let c_{ci} be the maximum effective viscous damping of each device (related to electrical characteristics) and define the matrix $\mathbf{C}_c$=diag$[c_{c1} \ldots c_{cm}]$. The velocity-dependent force constraints for the device system operating in regenerative mode or semi-active mode (i.e, with or without, respectively, connecting the electrical networks of different actuators) are (Scruggs et al., 2007a):

$$\text{Regenerative}: \mathbf{f}^T \mathbf{C}_c^{-1} \mathbf{f} + \mathbf{f}^T \mathbf{v} \le 0 \quad . \tag{7.5}$$

$$\text{Semiactive: } f_i \in \left[-c_{ci} v_i, 0\right] \Leftrightarrow c_{ci}^{-1} f_i^2 + f_i v_i \le 0 \quad . \tag{7.6}$$

These feasible force regions are illustrated in Figure 7.2 for a two-device system. The regenerative constraint is less restrictive than the semi-active constraint because a single constraint is imposed on the entire network, whereas for semi-active systems the *same* constraint is imposed on *each device separately.*

In practice, if an RFA network is commanded to realize a force which lies outside its feasible force region, (i.e., a force for which constraint (7.5) is violated), this will result in a kind of saturation which is coupled in all the forces. In Scruggs and Iwan (2005) it was shown that the manner in which this saturation, or "clipping" occurs, can be controlled through proper design of the power-electronic control system.

7.1.4 Control law selection

An array of eight regenerative force actuators is considered in each direction, working in tandem with the isolation system (Figure 7.1). In this configuration, energy is transmitted between the actuators at different locations in the base, as well as between the two translational directions of motion. The maximum viscosity of all actuators is set to 2.0×10^6 kg/s. The control law is assumed to be of a "skyhook" form; i.e., the total control forces at the center of mass of the base are determined as a static feedback function of the absolute velocities of the respective degrees of freedom. Because the only feedback measurements are from accelerometer data, the absolute velocities must be estimated by filtering the accelerometer measurements through a second-order bandpass filter, with transfer function:

$$H_f = \frac{s}{s^2 + 2\zeta_f \omega_f s + \omega_f^2}, \quad \zeta_f = \sqrt{2}/2, \quad \omega_f = 0.15 \text{ rad/sec} \quad . \tag{7.7}$$

For frequencies significantly above ω_f, this filter resembles pure integration.

The control law designates the optimal force vector $\mathbf{f}_c$ at the center of mass of the base. Since more than three actuators, not aligned with each other, are used, $\mathbf{R}_c$ in (7.4) has a nontrivial null space. Thus, there are an infinite number of choices for $\mathbf{f}$ which will produce a desired $\mathbf{f}_c$. These solutions can be expressed as:

$$\mathbf{f} = \mathbf{T}\mathbf{f}_c + \mathbf{a} \tag{7.8}$$

where $\mathbf{T} = \mathbf{C}_c\mathbf{R}_c\left(\mathbf{R}_c^T\mathbf{C}_c\mathbf{R}_c\right)^{-1}$ and $\mathbf{a}$ belongs in the nullspace of $\mathbf{R}_c$. As such, the particular choice of $\mathbf{a}$ does not affect $\mathbf{f}_c$. This constitutes a redundancy in the actuator configuration. The selection for $\mathbf{a}$ should be related to constraint (7.5) and how it is transformed for the resultant control forces at the center of mass. Let $\mathbf{v}_c$ denote the relative velocities at the center of mass of the base, satisfying:

$$\mathbf{v} = \mathbf{R}_c\mathbf{v}_c \tag{7.9}$$

Substituting (7.8) and (7.9) in (7.5) and using $\mathbf{R}_c\mathbf{a}=\mathbf{0}$ we end up with a constraint in terms of the control forces and the relative velocities at the center of mass of the base:

$$\mathbf{f}_c^T\left(\mathbf{R}_c\mathbf{C}_c\mathbf{R}_c\right)^{-1}\mathbf{f}_c + \mathbf{a}^T\mathbf{C}_c^{-1}\mathbf{a} + \mathbf{f}_c{}^T\mathbf{v}_c \le 0 \quad . \tag{7.10}$$

Thus, for any $\mathbf{a}\neq\mathbf{0}$, the feasible region for $\mathbf{f}_c$ is unnecessarily restricted. As such, the most efficient control is achieved with $\mathbf{a}=\mathbf{0}$. This choice produces the minimum-Euclidean-norm for $\mathbf{f}$ given $\mathbf{f}_c$ (i.e., produces minimal control effort in a mean square sense).

In the example discussed in this work, the control system formulates a desired force for $\mathbf{f}_c$, which will be denoted by $\mathbf{f}_d$ and is given by the "skyhook" control law:

$$\mathbf{f}_{d,i} = K_{s,i} v_{c,i} \tag{7.11}$$

where $v_{c,i}$ is the absolute velocity at the center of mass of the base along the i^{th} degree of freedom, where i=x, y, θ, and $K_{s,i}$ is the corresponding element of the gain vector $\mathbf{K}_s \subset \mathbb{R}^3$ for the skyhook control law.

The control intelligence which produces this force does not explicitly impose constraint (7.10) on $\mathbf{f}_d$. If an $\mathbf{f}_d$ is formulated which does not adhere to this constraint, then the vector $\mathbf{f}_d$ must somehow be adjusted, or "clipped" to accommodate the constraint. There are a number of ad-hoc ways in which this adjustment might be accomplished. The approach taken here is to find an $\mathbf{f}_c$ which gets "as close as possible" to $\mathbf{f}_d$ under some norm; i.e., the idea is to make $\mathbf{f}_c$ track $\mathbf{f}_d$ as closely as possible, given the physical constraints on the actuation system. Here, we define "closeness" in the Euclidean sense; i.e.,

$$\mathbf{f}_c = \underset{\tilde{\mathbf{f}} \text{ feasible}}{\operatorname{argmin}} \left\| \tilde{\mathbf{f}} - \mathbf{f}_d \right\|_{\mathbf{R}} \tag{7.12}$$

where $\|.\|_{\mathbf{R}}$ is a Euclidean vector norm using a weighting matrix $\mathbf{R}$. Thus $\mathbf{f}_c$ tracks the feedback signal $\mathbf{f}_d$ if it is feasible, and if not is "clipped" to the feasible region in such a way that the tracking error is instantaneously minimized. This is similar to a problem investigated in Scruggs et al. (2007a). Figure 7.9 later presents the time histories for $\mathbf{f}_d$ and $\mathbf{f}_c$ in the context of the example considered.

It remains to determine the weighting matrix $\mathbf{R}$, which prioritizes how closely the control system will try to match the various components of $\mathbf{f}_c$ to those of $\mathbf{f}_d$. In Scruggs et al. (2007a) the performance objective was the optimization of the mean-square stationary performance. In that case the optimal weighting matrix $\mathbf{R}$ in (7.12) was derived to be time invariant and related to the correlation between the actuators and the selected performance variables. Contrary to the performance objectives of the Scruggs et al. (2007a) study, for earthquake excitation we are concerned with optimizing the maximum response; this can

be established by trying to regulate the instantaneous performance, rather than the average performance. This implies a selection for the weighting matrix **R** that should be time-varying, as the relative importance of tracking each force changes from one instance to the other, depending on which performance quantity is larger, i.e., closer to its failure threshold. Denoting the components of $\mathbf{f}_d$ as $[f_{d,x} f_{d,y} f_{d,\theta}]^T$, the nonlinear weighting matrix is adopted:

$$\mathbf{R} = diag\left[f_{d,x}{}^{k_1} \quad k_2 f_{d,y}{}^{k_1} \quad k_3 f_{d,\theta}{}^{k_1} \right] \tag{7.13}$$

where the parameters k_1, k_2, and k_3 are to be optimized. This weighting prioritizes larger force signals at the center of mass of the base, assuming that they have greater importance in regulating the instantaneous response. A nonlinear dependence is introduced by the parameter k_1. A scaling is also introduced for the relative importance between the different forces by parameters k_2 and k_3. A more detailed analysis of the influence of the specific parameterization of **R** is left for future work.

Given **R**, optimization (7.12) can be accomplished analytically, through the solution of an associated polynomial root equation (degree of polynomial equal to six), which can be performed computationally efficiently. Details regarding this solution can be found in Scruggs (2004).

In summary, the nonlinear control law $\mathbf{K}_c$ implemented in this study consists of (a) a three-dimensional linear feedback gain vector $\mathbf{K}_s \subset \mathbb{R}^3$ for the skyhook control law, (b) the weighting matrix **R** parameterized by the vector $\mathbf{K}_r=[k_1\ k_2\ k_3]^T$ as in (7.13), and (c) the filter for obtaining estimates of the absolute base velocities. The controller parameters to be optimized consist of the six dimensional vector $\mathbf{K}=\{\mathbf{K}_s, \mathbf{K}_r\}$.

To facilitate a more straightforward comparison to studies that use different types of control devices, a maximum force capacity for each electromechanical actuator equal to

2200 kN is assumed. This additional constraint could, in principle, be incorporated in the tracking problem (7.13) (Scruggs 2004). For simplicity of the controller design and since the actuators typically operate far away from the maximum force threshold, this constraint is ignored in (7.12); it is simply enforced as force saturation on each actuator.

7.1.5 Controller design

The reliability of the base isolated structure given that a seismic event has occurred is adopted as the design objective. The vector of performance variables for the controller design consists of the next four groups of response quantities:

(a) The inter-story drifts of all floors measured at the outermost corners, $\delta_{i,j}$, i=1, …, 8, j=x,y.

(b) The base displacement, again measured at the outermost corners $\delta_{b,j}$.

(c) The absolute accelerations at the center of mass of all floors and the base in x and y directions, $a_{i,j}$, i=1, …, 8,b, where b denotes the structure's base.

(d) The structural shear force at the first-story level in x and y directions.

Failure is defined for the system if any of these quantities exceeds its respective threshold. The failure thresholds are chosen to be, respectively, (a) 0.3% of the story height (4.04 m), (b) 0.45 m, which is comparable to the clearance adopted in many base-isolated buildings (Hall et al. 1995), (c) 0.6g, and (d) 0.2 of the structural weight (202,000 kN). The limit state function $\tilde{g}(\boldsymbol{\varphi}, \boldsymbol{\theta})$ is defined as:

$$\mathbf{z}(t;\boldsymbol{\varphi},\boldsymbol{\theta}) = \left[\frac{\delta_{i,j}(t)}{0.012} i = 1,...,8 \quad \frac{\delta_{b,j}(t)}{0.45} \quad \frac{a_{i,j}(t)}{0.6g} i = b,1,...,8 \quad \frac{1^{st}\ \text{story shear}_j(t)}{0.20g \cdot \sum_{i=1}^{8} m_i} \right]_{j=x,y}^{T} \tag{7.14}$$

$$\tilde{g}(\boldsymbol{\theta},\boldsymbol{\varphi}) = \max_{t \in T} \left\{ \left\| \mathbf{z}(t;\boldsymbol{\varphi},\boldsymbol{\theta}) \right\|_{\infty} \right\} - 1 \qquad .$$

where $\mathbf{z}(t;\boldsymbol{\varphi},\boldsymbol{\theta})$ corresponds to the (normalized) response vector for the system, $\|.\|_{\infty}$ to the largest magnitude component, and T to the duration of the seismic event in consideration.

The controller design framework discussed here requires a probabilistic model for describing the stochastic input, i.e., the earthquake excitation. The model discussed in Section 2.4 is used. The suggestions by Somerville in (2.16) are used here to scale the characteristics of the near-fault pulse. The excitation model parameter vector $\boldsymbol{\theta}_s$ consists of the seismological parameters (moment magnitude, M, and epicentral distance, r), the additional parameters for the near-fault pulse (phase angle, v_p, and oscillatory character, γ_p), as well as two parameters that address the bi-directional characteristics of the ground motion. These parameters are (a) a reduction factor, A_n, for the fault-parallel component of the ground motion, and (b) the angle, δ, at which the ground motion shakes the structure. Note that the base isolated-structure is a torsionally asymmetric building and thus its dynamic performance needs to be evaluated under bi-directional loading. Since there is no well-defined method for modeling the characteristics of the fault-parallel component of near-fault ground motions using the stochastic method, an approximation based on engineering judgment is adopted. The same model is used for both fault parallel and fault normal components but a reduction factor is introduced for the fault parallel component. Also, the white-noise sequences that are used to generate the time histories for the two components are chosen to be different. This agrees with the observation in Jangid and Kelly (2001) that the two orthogonal components of near-fault motions have incoherent characteristics.

The structural properties in this study are set to their nominal values, i.e., no uncertainty is taken into account in the structural model. The variability of future excitations is addressed by assigning a PDF to the uncertain seismological and ground motion model parameters. We consider only severe seismic events, so the uncertainty in M is modeled by the Gutenberg-Richter relationship in (2.14) truncated on the interval $[M_{min}, M_{max}]=[6.5, 8]$, with seismicity factor $b=\log_e(10)$, which is a typical value. For the uncertainty in the event location, earthquakes are assumed to be equally likely to occur in a circular area of radius $r_{max}=15$ km centered at the structural site, leading to a triangular distribution for r on [0, 15] km and a uniform distribution for δ on $[-\pi, \pi]$. Figure 7.3 illustrates the seismological model for the site along with the resultant probability models for M, r and δ. The selection for r_{max} and M_{min} was based on the observation that events at larger distances or smaller magnitude could rarely lead to failure of the system and thus have no significance for the controller design.

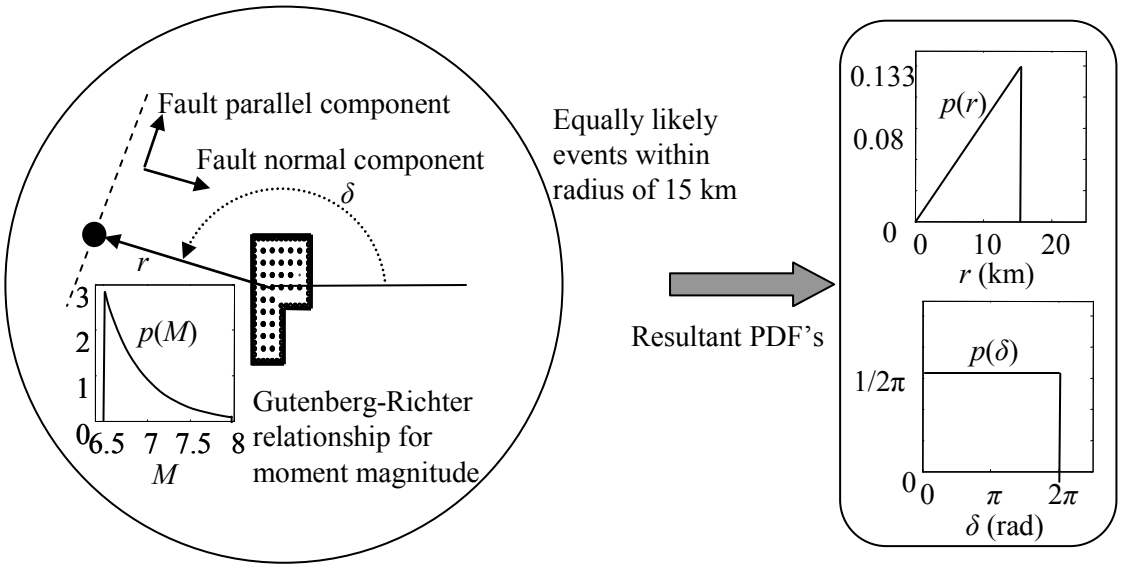

Figure 7.3: Seismological model for the site of the structure and resultant probability models

The probability distribution for the velocity pulse characteristics are selected as uniform on $[-\pi/2, \pi/2]$ for v_p, and Gaussian with mean 1.8 and standard deviation 0.4 for γ. The

uncertainty in the reduction factor for the fault parallel component of the ground motion is modeled by a uniform distribution on the range [0.6, 0.9], selected according to engineering judgment. Finally, a model prediction-error ε is assumed. This error is taken to be Gaussian with mean zero and standard deviation 0.05.

7.1.6 Controller design optimization

The response of the base-isolated structure is evaluated through a computer-based simulation using the SIMULINK toolbox of MATLAB. Figure 7.4 presents a simple schematic. It was found that by modeling each nonlinear isolator separately the computational cost for evaluating the response of the structure was significant (because biaxial interaction through the dynamical model in Park et al. (1986) needs to be taken into account). In order to reduce the computational effort in the design stage, since many simulations of the structural performance are needed, a simplification of the model for the base isolators is assumed by grouping the 61 nonlinear bearings into 3 groups. Figure 7.1(a) illustrates these three groups (dotted lines) and the location of the equivalent isolator for each of the groups. It was that found the response of this simplified model does not significantly differ from the response of the actual model because the rotational motion of the base, especially for the controlled structure, is not large; differences smaller than 1% for the base corner displacement for the uncontrolled structure were estimated. As such the simplified representation is considered adequate for the controller design stage. The model prediction error ε might be considered to partially address the discrepancies in response caused by the simplified model representation. The computer model used for the controller design incorporates additionally all control implementation characteristics discussed in Section 7.1.2 and the clipping action described in Section 7.1.4.

Note that the simplified model is assumed only for the design stage; for the performance evaluation, the nonlinear isolators are distributed according to the benchmark problem definition.

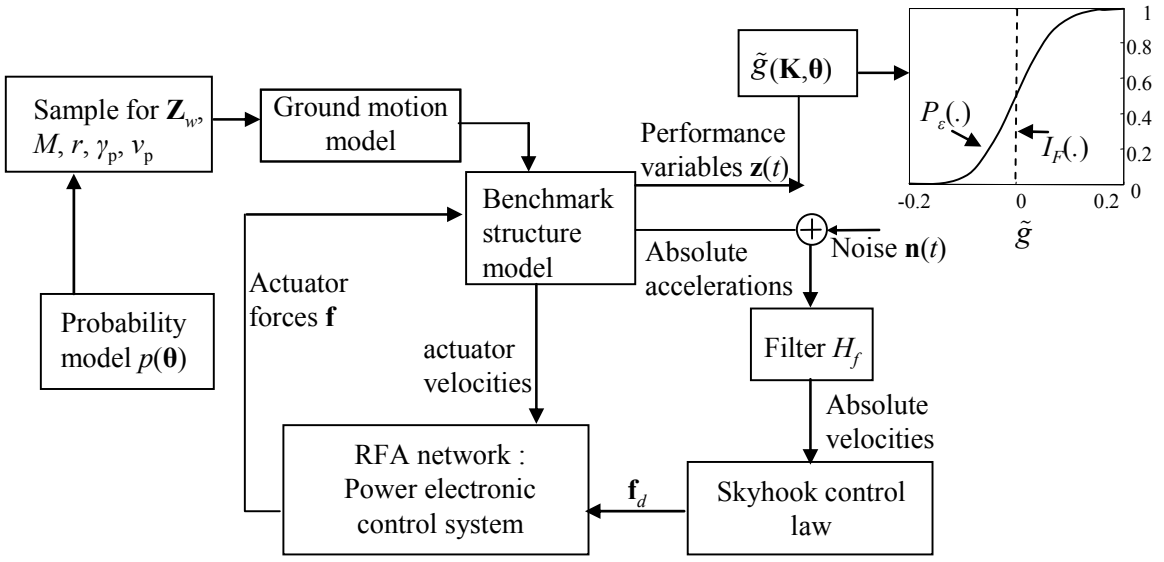

Figure 7.4: Block diagram of simulated controlled system at design stage

The optimization is finally performed using the SSO framework discussed earlier. Of particular interest are the optimal parameters for the weighting matrix **R**. The optimal values for these parameters were found to be k_1=3.16, k_2=1.3, k_3=2.2 10^{-4}, leading to:

$$\mathbf{R} = diag\left[f_{d,x}{}^{3.16} \quad 1.3 f_{d,y}{}^{3.16} \quad 2.2 \cdot 10^{-4} f_{d,\theta}{}^{3.16} \right] \quad . \tag{7.15}$$

Thus the desired signals are prioritized according to a nonlinear, almost cubic, law. The importance of the forces on the two lateral directions is almost the same. A smaller weighting is given to the moments, but that is typically compensated for by the fact that the desirable moment is at least an order of magnitude larger than the desirable forces in the lateral directions.

Passive network: An equivalent network is considered in which the electromechanical actuators are replaced by viscous dampers. In this case the actuators function as passive devices, i.e., no sensors and no control intelligence is needed. The viscosity of each of the dampers is optimized using the same reliability and performance setting as for the RFA network, assuming a maximum capacity that is the same as for the electromechanical

actuators, 2.0×10^6 kg/s. For all of the dampers the optimal viscosity was found to be close to the maximum capacity. The maximum force for the dampers is set equal to that of the electromechanical actuators (2200 kN). This network of viscous dampers may be equivalently considered to correspond to the RFA network operating in passive mode.

7.1.7 Performance evaluation

Reliability performance: In the probabilistic setting considered in this study, the probability of failure of the base-isolated structure, given a severe seismic event, is 0.378 without the control system, 0.119 under the optimal design with the RFA network, and 0.125 under the optimal passive configuration. Table 7.2 shows additionally the individual probabilities of failure for each of the four groups of performance variables discussed in Section 7.1.5.

Table 7.2 Reliability-related statistics for various controller designs

Case	$P_F(\mathrm{K}^*)$	Failure probabilities for each group of response quantities			
		Base displacement	Inter-story drift	Absolute acceleration	Structural shear at 1st story
Uncontrolled	0.378	0.372	0.09	0.001	0.18
RFA	0.119	0.104	0.034	0.009	0.072
Passive	0.125	0.090	0.071	0.035	0.077

The results indicate that the RFA network contributes significantly to increasing structural reliability under the criteria considered. The passive application provides an overall comparable performance, i.e., reliability level similar to the one of the RFA network, but this is established with a different balance between the various groups of performance variables. For both the uncontrolled structure and the structure equipped with an RFA network, the probability of failure of the base displacement is much greater, compared to the other response quantities. The RFA network application provides an overall balanced reduction of the relative failure probabilities for all performance variables, apart from absolute accelerations. This is not the case for the passive application though, for which the

performance enhancement is achieved by prioritization of the reduction of the base deformation. It is interesting to note that even though $P_F(\mathbf{K}^*)$ is smaller for the RFA network application, the probability of failure for the base displacement, which is the larger among the performance variables considered here, is smaller for the passive application. This trend is further examined in the next section.

Performance under recorded earthquake excitations: The control design is further evaluated through the seven near-fault earthquake sample ground motions suggested in the benchmark problem statement. These ground motions are assumed to represent future earthquakes. The acceleration time-histories for all off them are shown in Figure 7.5.

Table 7.3 and Table 7.4 show ten performance criteria for the seven earthquake records under consideration for either a regenerative network of actuators (RFA) or an equivalent network of passive viscous dampers (PAS). For each of these records, separate results are shown for the cases with the fault parallel to the *x*-axis (i.e., FP-*x*) and parallel to the *y* axis (i.e., FP-*y*). Nine evaluation criteria which represent measures of different RMS and maximum responses of the buildings are part of the Benchmark problem definition: evaluation criteria J_1 and J_2 represent the peak base shear at the isolation level and the structure shear force at the first story level; J_3 is the peak base displacement, J_4 is the peak inter-story drift, and J_5 is the peak absolute floor acceleration; J_7 and J_8 are the RMS values of base displacement and interstory drift. In all of the above cases, the performance measures are normalized by the corresponding quantities in the uncontrolled structure. In contrast, J_6 represents the force generated by all control devices normalized by the peak base shear in the controlled structure, and J_9 is the total energy absorbed by all control devices normalized by the energy input to the controlled structure. In addition to these nine criteria, a tenth criterion J_{10} is included in the results for this study. This additional criterion is equal to the maximum *corner* drift for the controlled structure, normalized by the maximum for the uncontrolled case. Comparisons with J_4 give an indication of the total reduction in the twisting of the building.

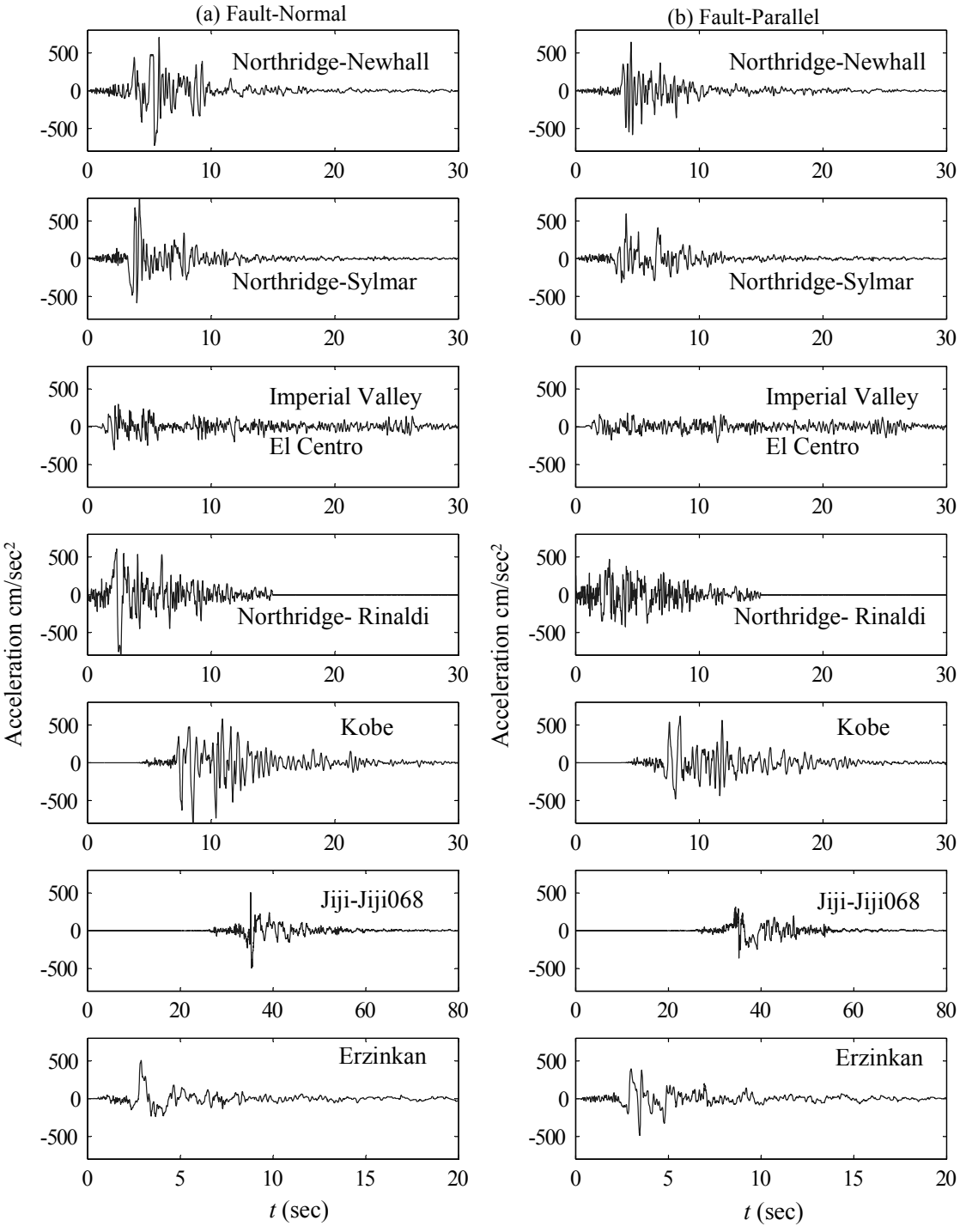

Figure 7.5: Time-histories for recorded earthquake records used in this study

Table 7.3 Performance evaluation criteria for recorded excitations; FX-*x* case

Simulation case		J_1	J_2	J_3	J_4	J_5	J_6	J_7	J_8	J_9	J_{10}
Newhall	RFA	0.999	0.999	0.925	0.904	1.043	0.296	0.783	1.046	0.186	0.902
	PAS	1.012	1.017	0.840	1.200	1.088	0.362	0.749	1.139	0.303	1.242
Sylmar	RFA	0.879	0.906	0.762	0.911	1.098	0.314	0.647	0.996	0.295	0.817
	PAS	0.930	0.909	0.733	0.965	1.212	0.371	0.625	1.062	0.393	0.972
El Centro	RFA	0.973	1.047	0.683	1.049	1.054	0.168	0.861	1.026	0.077	1.013
	PAS	1.062	1.052	0.792	1.125	1.107	0.234	0.869	1.041	0.133	1.108
Rinaldi	RFA	1.009	0.987	0.942	0.983	1.265	0.271	0.811	1.144	0.256	1.000
	PAS	1.152	1.118	0.866	1.142	1.508	0.407	0.786	1.223	0.398	1.272
Kobe	RFA	0.919	0.951	0.727	0.942	1.123	0.248	0.720	1.057	0.147	0.945
	PAS	0.990	1.245	0.740	1.477	1.262	0.433	0.709	1.203	0.311	1.473
Jiji	RFA	0.786	0.787	0.667	0.800	0.799	0.220	0.675	0.861	0.296	0.789
	PAS	0.747	0.769	0.686	0.806	0.869	0.261	0.620	0.844	0.332	0.784
Erzikan	RFA	0.952	0.987	0.726	1.076	1.113	0.306	0.628	0.947	0.289	0.993
	PAS	0.939	0.944	0.688	1.023	0.972	0.310	0.622	0.953	0.378	1.032

Table 7.4 Performance evaluation criteria for recorded excitations; FP-*y* case

Simulation case		J_1	J_2	J_3	J_4	J_5	J_6	J_7	J_8	J_9	J_{10}
Newhall	RFA	0.970	0.903	0.950	0.919	1.102	0.289	0.857	1.035	0.183	0.887
	PAS	0.998	0.997	0.862	1.250	1.282	0.305	0.739	1.153	0.294	1.214
Sylmar	RFA	0.808	0.814	0.753	0.834	1.111	0.302	0.615	0.911	0.287	0.817
	PAS	0.920	0.963	0.785	0.961	1.302	0.373	0.635	0.991	0.394	1.044
El Centro	RFA	1.033	1.051	0.821	1.033	1.037	0.168	0.831	1.002	0.075	1.020
	PAS	1.062	1.052	0.792	1.125	1.107	0.234	0.869	1.041	0.133	1.108
Rinaldi	RFA	0.980	0.961	0.967	0.949	1.005	0.253	0.820	1.095	0.251	0.949
	PAS	1.140	1.105	0.833	1.149	1.108	0.395	0.777	1.202	0.395	1.329
Kobe	RFA	0.886	0.906	0.635	1.008	1.026	0.215	0.727	1.049	0.140	1.025
	PAS	0.997	1.127	0.668	1.275	1.185	0.427	0.748	1.190	0.309	1.338
Jiji	RFA	0.747	0.739	0.603	0.723	0.770	0.266	0.620	0.809	0.309	0.727
	PAS	0.753	0.738	0.632	0.757	0.871	0.247	0.588	0.797	0.335	0.776
Erzikan	RFA	0.942	0.908	0.672	0.907	1.099	0.303	0.578	0.874	0.287	0.906
	PAS	0.936	0.901	0.596	0.944	0.955	0.314	0.516	0.919	0.386	0.961

Before discussing these results in Table 7.3 and Table 7.4 in more detail, a comment about the characteristics and the anticipated efficiency of the implemented control scheme is warranted. In this study, the objective is the regulation of the performance of a base-isolated structure by using a network of actuators that (i) has globally strictly dissipative capability and (ii) is placed at the base level. Engineering judgment and experience (Nagarajaiah and Narasimhan 2006; Nagarajaiah et al. 2006; Taflanidis et al. 2007b) indicate that it is easier to control the motion of the base rather than the vibration of the superstructure and that displacement response quantities can be more efficiently regulated compared to absolute accelerations. In particular, efficient suppression of both displacement and acceleration quantities in such a setting is recognized as a challenging task. The degree to which the different performance quantities are reduced depends, ultimately, on the characteristics of the control system (capabilities of actuators and control law) and the objectives set at the controller design stage. In the context of the design framework suggested in this study, the latter corresponds to dependence on the specific performance variables selected and, more importantly, on the failure threshold that is assigned to each of them, since these thresholds ultimately designate the relative importance of the different response quantities.

For this reason, and to further distill the extensive amount of data in Table 7.3 and Table 7.4 to a few general observations, it is instructive to examine the *failure data* for each earthquake; i.e., the normalized-by-the-failure-thresholds response for each group of performance variables. Because the performance metrics J_i in the Table 7.3 and Table 7.4 are all normalized by the uncontrolled values for the structure, these performance variable ratios are difficult to determine from the information in these tables. Trends for these ratios are illustrated in Figure 7.6 which includes scatter plots for the failure data for the uncontrolled and controlled structure. For the uncontrolled structure, accelerations and base shear stay below their failure thresholds, apart from a couple of cases for the base shear (corresponding to the Jiji earthquake). Base-displacement and inter-story drifts are characterized by larger performance variable ratios, with the first one exhibiting greater

departure from the acceptable threshold. This pattern agrees with the behavior of the uncontrolled system reported in Table 7.2 and indicates that reduction of the displacement-based performance quantities should have greater importance.

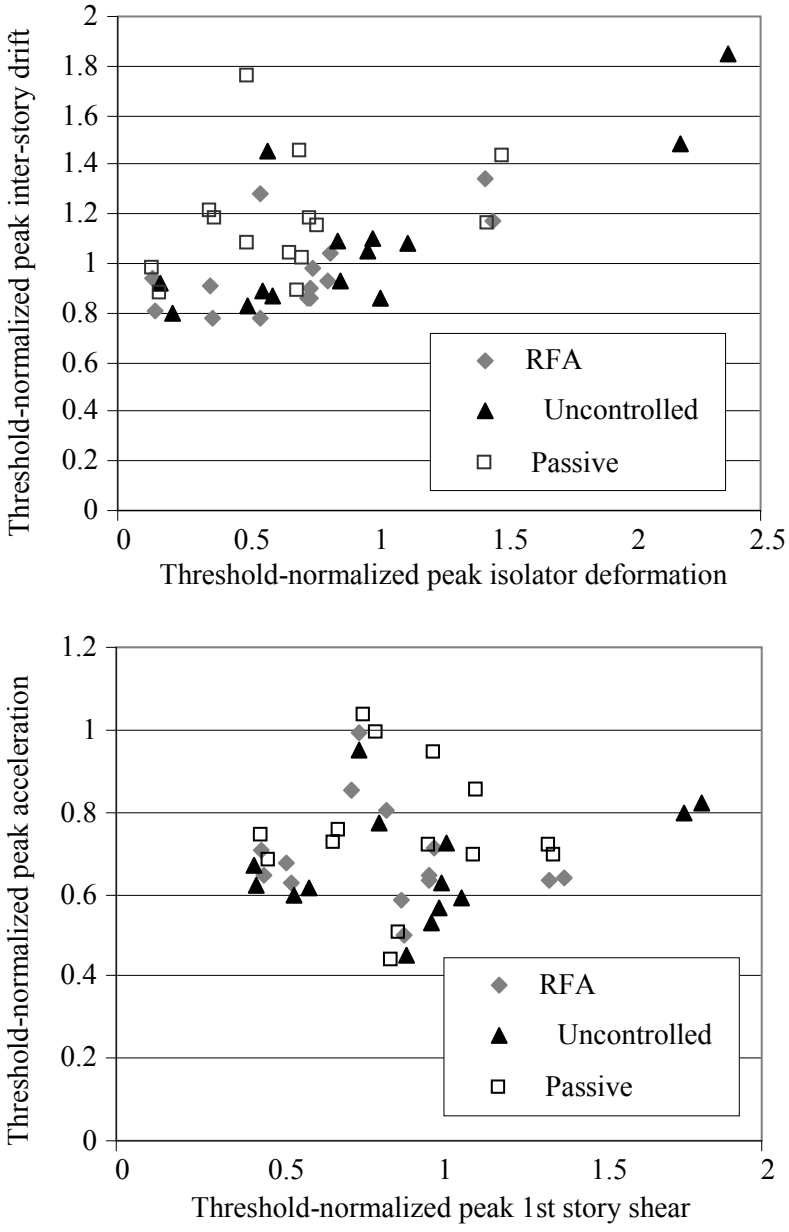

Figure 7.6: Scatter plots of threshold-normalized response for the four groups of performance variables for the 14 ground motion cases

Now the discussion returns to the data in the tables and focus on the RFA network performance. The maximum base deformation (J_3) is characterized by the biggest reduction for all cases. This feature can be attributed to the goals set at the design stage and the characteristics of the control application. The improvement in performance for the inter-story drift, base or structural shear is smaller but in only a few cases is there a degradation of performance, compared to the uncontrolled structure, reported (for example, for El Centro). A small increase of the accelerations of the structure occurs (J_5), but this behavior is expected because of the characteristics of the control application (regenerative actuators and skyhook control). These trends are also depicted in the scatter diagrams of Figure 7.6. The RMS performance quantities (J_7 and J_8) follow similar patterns as their maximum response counterparts (J_3 and J_5, respectively). Comparison between J_{10} (corner drift) and J_4 (drift at center of mass) gives some indication of the degree to which twisting of the superstructure has been suppressed by the control. The results are mixed but the underlying observation is that J_{10} is usually a bit smaller than J_4, implying that the controller aims at suppressing the twisting of the superstructure more than the lateral drift.

Overall, the performance obtained seems to be in good agreement with the objectives set at the design stage, taking into account the capabilities of the actuator network. This illustrates the efficiency of the simulation-based controller design scheme suggested. It also indicates that the probabilistic model adopted for the ground motion at the design stage can appropriately characterize future ground motions.

Now comparison to the passive control case verifies the trend discussed previously. The passive application provides similar reduction for the peak isolator deformation but at the same time it leads to significant performance deterioration for all other metrics. It is interesting to note that the average energy dissipated by the viscous dampers (J_9) and the maximum control force (J_6) is much larger in the passive application. The RFA network with skyhook control manages to establish more efficient regulation of the structural response with smaller control forces.

A further assessment of the overall performance can be established by considering the special characteristics of base-isolated buildings. These structures are constructed with a clearance gap at the base level, separating them from the surrounding environment. Under current design practice this gap is typically close to 40 cm and rarely exceeds 60 cm. Base deformations that are larger than these thresholds have severe implications for the response of the superstructure (Hall et al. 1995), due to the impact of the base against the surrounding walls. Thus, regulation of the base deformation should be considered of greater importance. For the earthquakes considered here, apart from Jiji, the peak base displacement of the controlled structure is kept below 45 cm. For Jiji, the peak displacement was 71 cm for the RFA network and 75 cm for the passive application. The passive control application efficiently regulates the base deformation. Still, it leads to significant increase in peak inter-story drifts and peak absolute accelerations which can cause, respectively, (a) nonlinear deformations of the superstructure and (b) failure of the contents of the building. It is a matter of debate as to whether these characteristics justify the extra cost associated with sensor and control intelligence for application of an RFA network. This discussion illustrates that comparisons of control systems based on socio-economic criteria is warranted. In such a setting, the characteristics of the controlled system, in terms of number of actuators, sensor cost, force capacities and control law synthesis should be optimized using a cost-benefit analysis, as demonstrated in Section 6.2 for viscous dampers. This, of course, requires appropriate quantification of fragility and cost information for the building considered, which is not available for the base-isolated benchmark structure.

The design presented here can also be compared to the results by Nagarajaiah et al. (2006) who considered a network of eight semi-active actuators (MR-dampers) and used a Lyapunov-based nonlinear controller. Direct comparison is difficult because actuators with different characteristics are used here. Still, some interesting comments can be made: the total energy absorbed by the devices (J_9) in this study is significantly smaller than the quantities reported in Nagarajaiah et al. (2006) and the maximum force (J_6) is at

comparable levels; this indicates that the capabilities of the actuator network used here should be considered equivalent (or somewhat smaller) to the ones considered in Nagarajaiah et al. (2006). The performance established here is considerably improved for all criteria, apart from J_3. For the maximum base deformation the performance here is better for some earthquakes (for example, Jiji and Sylmar) and worse for others (for example, El Centro). Thus, the control implementation in Nagarajaiah et al. (2006) simply strikes a different balance between the different performance quantities, prioritizing the reduction of the isolator deformations. Note, though, that, contrary to the design methodology discussed here, the approach adopted in Nagarajaiah et al (2006) cannot explicitly specify the importance of the different performance goals. Also, it is interesting to note that in Nagarajaiah et al. (2006) an increase of structural drifts was reported for almost all cases for the controlled structure. Such a degradation of performance was avoided here. This comparison further verifies the efficiency of the RFA network and the control design methodology.

Finally some indicative time histories are included in Figure 7.7, Figure 7.8, and Figure 7.9. These time histories are presented only for illustrative purposes. They cover only a minimal portion of the earthquake excitations and structural responses considered in this study. Figure 7.7 shows the base displacement at the southeast corner for the uncontrolled structure and RFA-equipped structure. The performance improvement is obvious. Figure 7.8 includes the displacement-force plot for the friction pendulum bearing at the same corner. The energy dissipation by the nonlinear isolator is evident. This dissipation is proportional to the area inscribed by the force-displacement relationship. Note that for the RFA-equipped structure the additional energy dissipation provided by the control application leads to reduction of the requirements for the passive protection system. The energy dissipation contributed by the nonlinear isolators is obviously smaller in this case. Finally, Figure 7.9 shows the desired and applied resultant control forces at the center of mass of the base. The inability of the RFA network to track the desired control forces at all

times is evident in this plot; the applied forces can be different from the desired ones. Thus the control implementation remains far from an ideal skyhook law.

In general, the results discussed in this section illustrate significant reduction in important response quantities that shows the efficiency of both the controller design methodology and the capabilities of the regenerative force actuators. More detailed quantification of the uncertainty for the ground motion model parameters, which will be possible when a specific site is considered, can further improve this efficiency. The comparison to the performance of a passive viscous damping system showed that the RFA network yielded superior performance, in the sense that it reduced the overall probability of failure of the uncertain system and provides better trade-offs in the reductions of failure probabilities of the various individual failure modes. The response of the base-isolated structure under recorded near-fault ground motions verified these trends.

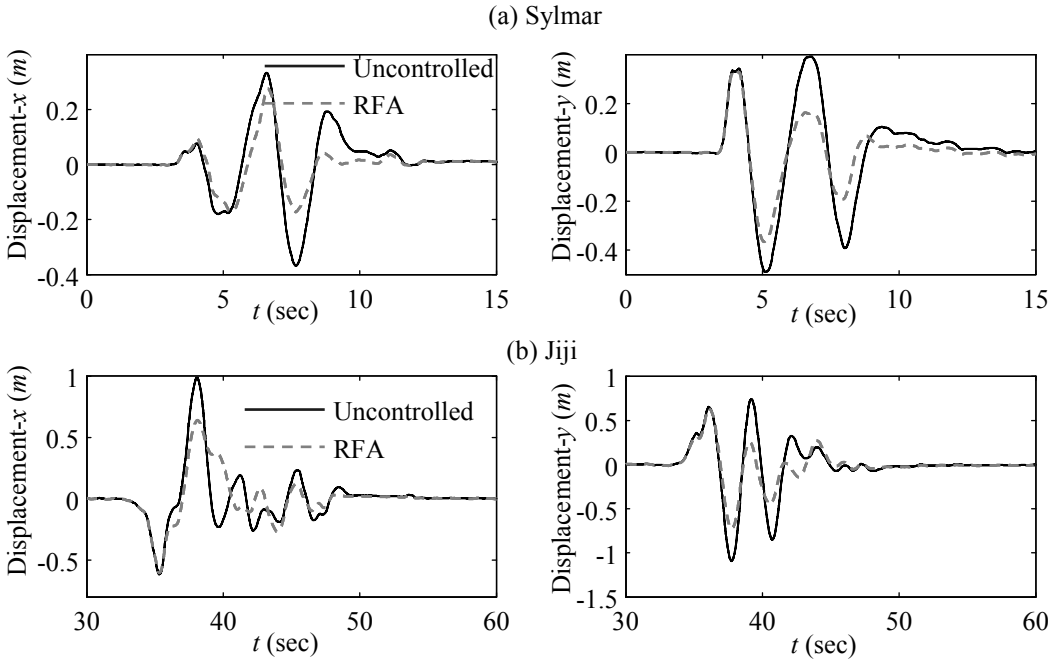

Figure 7.7: Base displacement at southeast corner for (a) Sylmar and (b) Jiji earthquakes acting in FP-*y* direction

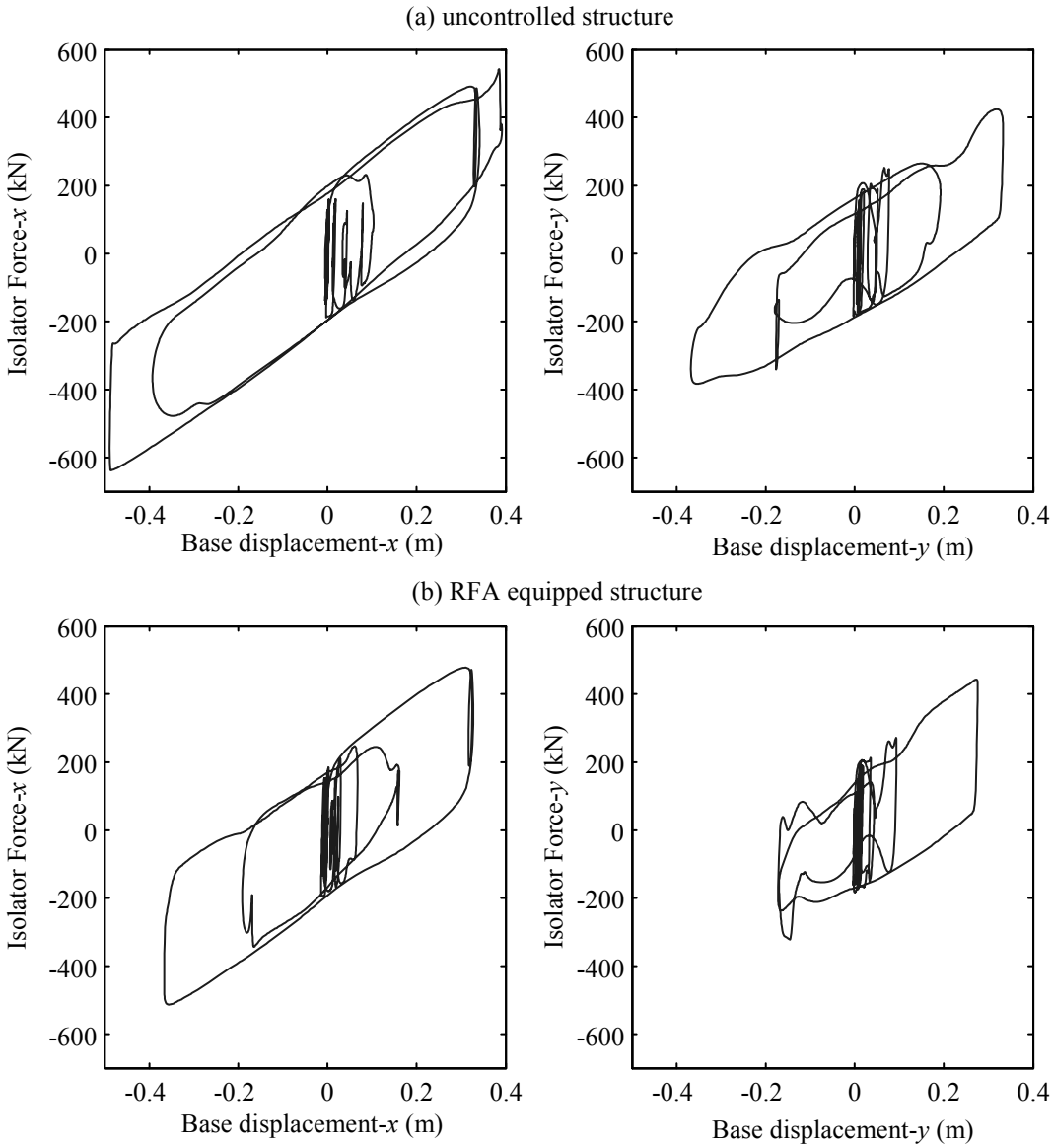

Figure 7.8: Displacement-force plot for the friction pendulum isolator at southeast corner for (a) uncontrolled and (b) RFA equipped structure for the Sylmar earthquake acting in FP-*y* direction

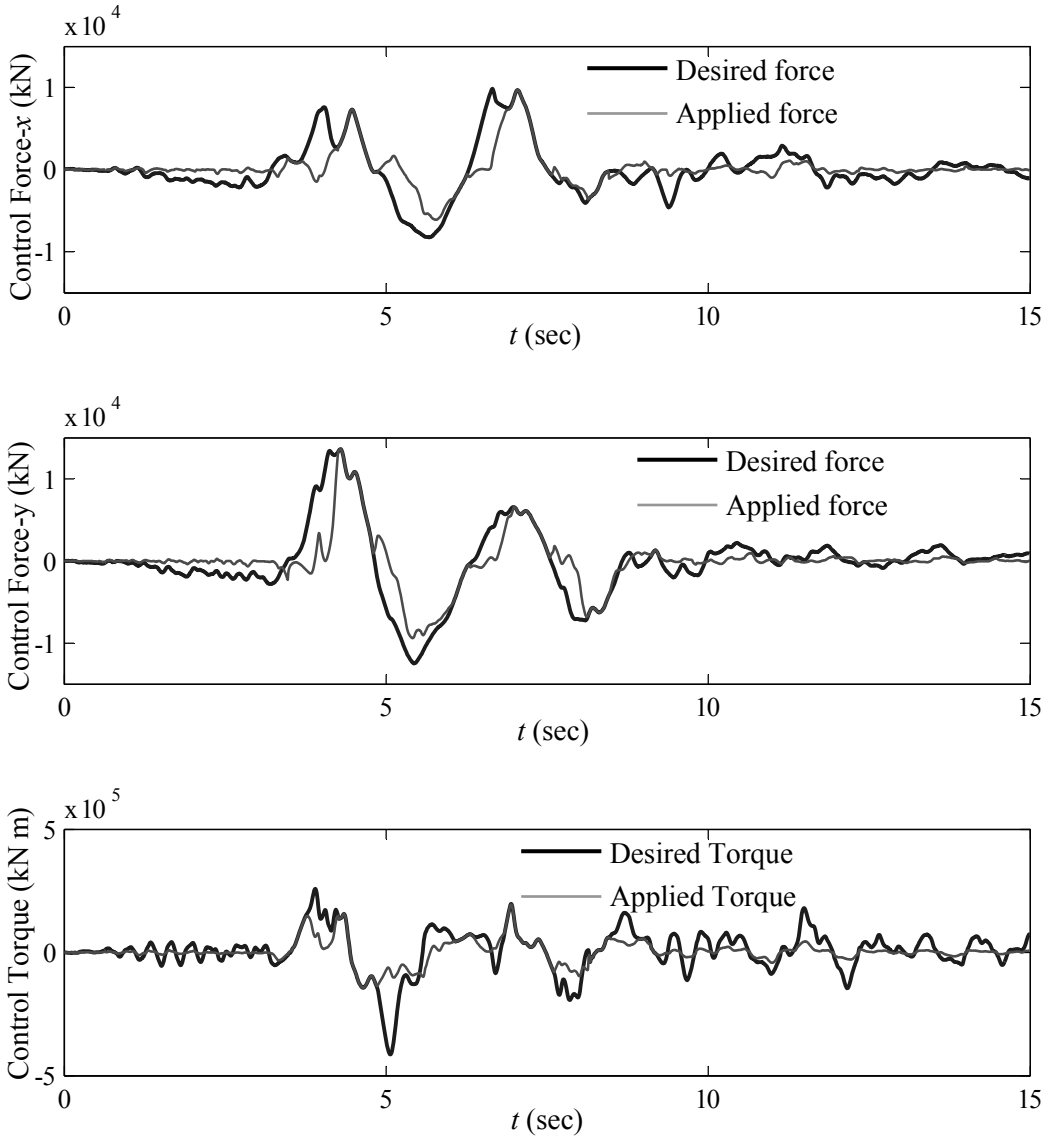

Figure 7.9: Desired and feasible resultant forces at the center of mass of the base for the Sylmar earthquake acting in FP-*y* direction

7.2 Controller Design for Offshore Platforms

Under severe sea and wind conditions, offshore structures, such as jacket-type or tension leg platforms, may experience large response amplitudes that affect their serviceability and structural integrity. Active and passive control techniques have been considered for

reduction of the effects of such dynamic loadings (Nakamura et al. 1997; Ahmad and Ahmad 1999; Alves and Batista 1999; Suhardjo and Kareem 2001). Most of the studies in offshore structure control have adopted linear methodologies for the controller design, typically $\mathcal{H}_2$ control. The models, though, that are used for the prediction of the behavior of offshore structures typically involve various types of nonlinearities. In particular, nonlinearities may come from (a) modeling the dynamic response of the structure (for example, in the case of Tension Leg Platforms, as discussed in Angelides et al. (1982)) and also from (b) characterizing the excitation forces acting on the structure (for example, the spectrum for random sea environment or the wave particle kinematics (Goda 2000)). One of the main challenges in controller design for offshore applications has been the explicit consideration of these nonlinearities.

Enhanced linearization techniques have been suggested for addressing the excitation nonlinearity when applying linear control methodologies (Suhardjo and Kareem 2001). This approach has the potential to adequately capture important nonlinear characteristics of the response; but for complex systems the application is usually not straightforward. The structural response nonlinearity, which is more important, is commonly ignored. The controlled system is usually designed based on a linear model that does not take into account nonlinear characteristics (Ahmad and Ahmad 1999; Alves and Batista 1999). Only the performance of the system is evaluated using, at a later stage, a nonlinear model (Ahmad and Ahmad 1999). This approach leads to a sub-optimal design in terms of the actual system performance.

Another challenge related to offshore structure control has been the efficient description of the uncertainties involved in the system model. In maritime applications, like most other engineering applications, there are model properties that involve some level of uncertainty (for example the characteristics of the sea environment). This uncertainty can be quantified by a probabilistic description of the model parameters (Mathisen and Bitner-Gregersen 1990). Such an approach logically incorporates the available knowledge about the system

into the model and allows for a robust-to-uncertainty design. Typically, though, a nominal model is adopted when designing the controlled system, using the most probable values for the model parameters. No uncertainty for these values is taken into account.

The stochastic system design methodology proposed earlier addresses all these challenges. Simulation is used for evaluation of the model response at the controller design stage, which allows for *explicitly* taking into account nonlinear characteristics of the system. Uncertainty about the model parameters is treated by assigning probability density functions to them. The methodology is illustrated in an example involving the control of a Tension Leg Platform (TLP) in an uncertain sea environment. The control force is provided by tuned mass dampers placed inside the columns of the platform's hull. Both passive and active applications are discussed. A realistic setting is considered for the latter, with actuator saturation, availability of only noisy acceleration measurements, and time delays in the control loop being assumed. Multiple nonlinearities are taken into account for the platform's response and a probabilistic description is adopted for the system model.

7.2.1 Model for Tension Leg Platform

TLPs (Figure 7.10) are floating structures of semi-submersible type, moored by vertical tendons under initial pretension, T_o, imposed by excess buoyancy. Several TLPs have been used for oil exploration and drilling operations in deep waters. They can be modeled as a rigid body having six degrees of freedom, which includes three translations (surge, x, sway, y, and heave, z) and three rotations (roll, φ, pitch, θ, and yaw, ψ). The natural period in surge, sway and yaw are in the range 80–120 sec, and well above the range of dominant waves, which typically have periods 6–18 sec. On the other hand the heave, pitch, and roll periods are in the range 2–4 sec, and below the period of the exciting waves. Thus, forces at the dominant wave frequencies do not excite the TLP at its natural frequencies. Still, higher-order nonlinear forces at the sum and difference of the wave frequencies can produce significant resonant excitations at the TLP natural frequencies because of the small amount of damping available at these frequencies (Mekha et al. 1996). Passive and active

control techniques have been investigated for reducing the effects of these excitations (Ahmad and Ahmad 1999; Alves and Batista 1999).

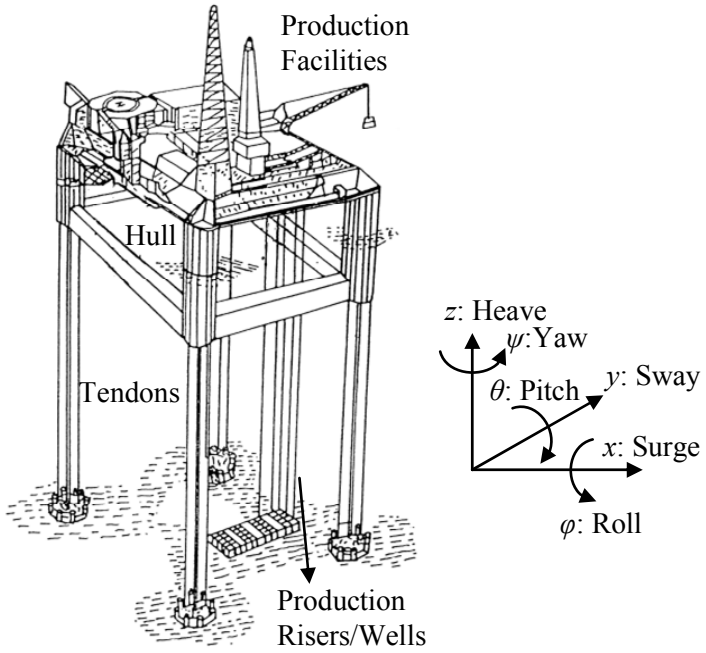

Figure 7.10: Tension Leg Platform with degrees of freedom

In this study, we assume that the direction of wave propagation coincides with one of the axes of symmetry of the platform (Figure 7.11). Thus, only 3 degrees of freedom are excited (surge, heave, pitch). Additionally, wave diffraction effects are neglected. Structural damping is also neglected because it can be considered small compared to the hydrodynamic damping (Mekha et al. 1996) and the damping provided by the control application.

Various types of nonlinearities are present in the analysis of a TLP (Zeng et al. 2006). The influence of the change in the submerged TLP surface because of the wave passage and the coupling between the different degrees of freedom in evaluating the tendon stiffness are two of the more important ones. The TLP model assumed here incorporates the most

important nonlinearities. The formulation follows closely the one presented in Angelides et al. (1982) which considers large translations and large rotations for the TLP response. The main characteristics are briefly summarized next.

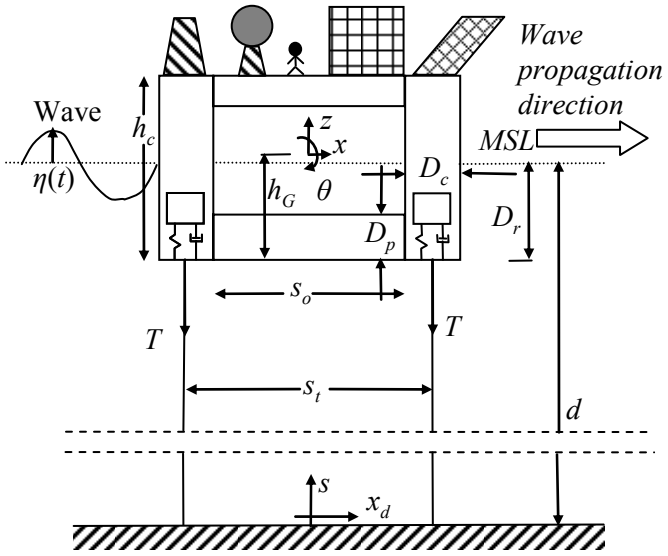

Figure 7.11: Tension Leg Platform model considered in the study

Hydrodynamic and hydrostatic Forces: The hydrodynamic force of the submerged TLP portion is calculated using the Morrison equation. For a cylinder with diameter *D*, the force in the normal direction, per unit length *dl,* is given by:

$$df(t) = \frac{1}{2}\rho_w D C_D \left(\dot{U}_{wn} - \dot{U}_{sn}\right)\left|\dot{U}_{wn} - \dot{U}_{sn}\right| dl + \frac{1}{4}\rho_w \pi D^2 C_M \ddot{U}_{wn} dl - \frac{1}{4}\rho_w \pi D^2 \left(C_M - 1\right)\ddot{U}_{sn} dl \tag{7.16}$$

where ρ_w is the density of the sea water, $\ddot{U}_{wn}$ and $\dot{U}_{wn}$ are the wave particle acceleration and velocity normal to the cylinder, $\ddot{U}_{sn}$ and $\dot{U}_{sn}$ are the structural element normal acceleration and velocity, C_D is the drag coefficient, and C_M is the inertia coefficient. Both coefficients

are assumed here to be same for columns and pontoons, constant along the water depth and frequency independent. The last term in (7.16) is referred to as the added-mass. For evaluation of the total hydrodynamic forces, the total length of the structural elements (columns and pontoons) is divided into equal length segments. The structural and wave kinematics are then calculated at the centroid of each segment. Based on these values, the hydrodynamic forces are calculated and then multiplied by the segment length to yield the forces at the center of the segment. These forces are then transferred to the center of gravity of the hull to obtain the resultant forces and moments. For the TLP columns the instantaneous submerged depth, accounting for wave passage and structural motion, is considered in the evaluation of the hydrodynamic forces. In addition, the hydrostatic pressures acting on the submerged part of the TLP geometry are integrated at each time instant up to the instantaneous free surface sea level to yield a vertical buoyancy force and moment at the center of gravity of the TLP.

Tendon restoring forces: The tendon stiffness is derived with reference to the instantaneous position of the platform, i.e., displacements in all degrees of freedom are simultaneously considered. The tension on each tendon is:

$$T = \frac{EA}{L} \Delta L + T_o \tag{7.17}$$

where E is Young's modulus, A is the cross-sectional area of the tendon, L is the initial length of the tendon, and ΔL is the instantaneous change in length. This force is applied along the instantaneous axial direction of the tendon and transformed into the center of gravity of the hull to obtain resultant forces and moments. This formulation introduces a nonlinear coupling between the different degrees of freedom.

7.2.2 Stochastic sea model

Water particle kinematics are modeled according to Airy wave theory. The sea is modeled as a Gaussian process following a modified Pierson-Moskowitz (PM)-type spectrum for the free-surface elevation (Goda 2000):

$$S(\omega) = \frac{H_s^2 T_z}{8\pi^2}\left(T_z \frac{\omega}{2\pi}\right)^{-5} \exp\left[\frac{1}{\pi}\left(T_z \frac{\omega}{2\pi}\right)^{-4}\right] \tag{7.18}$$

where ω is the frequency, H_s the significant wave height, and T_z the zero up-crossing period. To implement this spectrum, the free-surface wave elevation is represented in the time domain by a superposition of a large number of harmonic waves corresponding to different frequencies ω_i:

$$\eta(t) = \sum_{i=1}^{k} A_i \cos(\kappa_i x - \omega_i t + \varphi_i) \tag{7.19}$$

$$A_i = \sqrt{\left(\alpha_i^2 + \delta_i^2\right) S(\omega_i)\Delta\omega_i}\,,\ \varphi_i = \operatorname{atan}\left(\delta_i / \alpha_i\right) \tag{7.20}$$

where α_i and δ_i are standard Gaussian variables and $\Delta\omega_i$ is the bandwidth that each harmonic represents. The number of component waves, k, in (7.19) is a compromise between realizing the Gaussian distribution for the surface elevation and establishing computational efficiency for the simulation of the model response. For determining the sequence $\{\omega_i\}$, the frequency range of interest is divided into sub-ranges and ω_i is chosen as the middle of each one. The bandwidth $\Delta\omega_i$ equals the width of the respective sub-range. The frequencies ω_i should be chosen so that (a) they do not constitute harmonics with each other, and (b) describe adequately the whole frequency range of significant excitation. The procedure described in Chandrasekaran and Jain (2002) is adopted here. Let $[\omega_{\min}, \omega_{\max}]$

denote the frequency range that is important and consider the division into k-1 sub-ranges by:

$$\omega_1^{'} = \frac{\omega_{\max} - \omega_{\min}}{k-1},\ \omega_i^{'} = \omega_1^{'}\left(\frac{\omega_{\max}}{\omega_1^{'}}\right)^{\frac{i-1}{k-2}} \tag{7.21}$$

then select at random (following a uniform distribution), the dividing frequencies $\omega_1^{"},...,\omega_{\kappa-1}^{"}$ in each of these sub-ranges and set $\omega_0^{"} = \omega_{\min}$ and $\omega_{\kappa}^{"} = \omega_{\max}$. This new sequence $\{\omega^{"}\}$ defines finally the sub-ranges for the selection of ω_i :

$$\omega_i = \frac{1}{2}\left(\omega_i^{"} + \omega_{i-1}^{"}\right),\ \ \Delta\omega_i = \omega_i^{"} - \omega_{i-1}^{"} \quad . \tag{7.22}$$

This methodology leads to selection of uncorrelated frequencies ω_i. Also, it efficiently describes, in a stochastic simulation setting, the energy content in the whole range of the spectrum that is considered important for the response, even for small number of component waves, k. This is established by the randomness in the selection of the frequencies $\omega_i^{"}$ in the different simulation runs. Note that alternative methods have been suggested for cases where k is large (for example, partitioning the spectrum into equal areas without employing any randomness, as discussed in Goda (2000)). In this application, the above methodology was preferred because k was selected "relatively" small.

In (7.19), κ_i is the wave number, related to the frequency and the water depth, d, through the well-known dispersion relationship:

$$\omega_i^2 = g\kappa_i \tanh(\kappa_i d) \tag{7.23}$$

The water particle kinematics are computed according to Airy linear wave theory with the modification discussed by Chakrabarti (1971) in order to incorporate the effect of variable

free surface sea level. The velocity of the water particles in the horizontal and vertical direction is given respectively by:

$$\dot{u}(t) = \sum_{i=1}^{k} A\omega_i \cos(\kappa_i x_d(t) - \omega_i t + \varphi_i) \frac{\cosh\left(\kappa_i s(t)\right)}{\sinh\left(\kappa_i \left(d + \eta(t)\right)\right)} \tag{7.24}$$

$$\dot{v}(t) = \sum_{i=1}^{k} A\omega_i \cos(\kappa_i x_d(t) - \omega_i t + \varphi_i) \frac{\sinh\left(\kappa_i s(t)\right)}{\sinh\left(\kappa_i \left(d + \eta(t)\right)\right)} \tag{7.25}$$

where $s(t)$ and $x_d(t)$ are the vertical and horizontal distance, respectively, at which the wave kinematics are evaluated (see Figure 7.11). The acceleration may be obtained by differentiation of these relationships.

This model fully characterizes the excitation vector. In the context of Figure 2.3, the excitation model parameters are represented by the vector $\boldsymbol{\theta}_s$=[H_s, T_z, $\{\alpha_i\}$, $\{\delta_i\}$, $\{\omega_i\}$]. The excitation vector $\mathbf{q}(t)$ is composed of the free surface elevation and the orthogonal components (horizontal and vertical) of the wave particles' velocity and acceleration. The latter quantities are resolved to give $\dot{U}_{wn}$ and $\ddot{U}_{wn}$ in (7.16) according to the instantaneous rotation of the TLP. The free surface elevation is used for estimation of the submerged portion of the TLP hull.

7.2.3 Control implementation for Tension Leg Platform

Various devices have been proposed for control of offshore structures (for example, passive or active tuned mass dampers (TMD), active thrusters, active tendons, and pneumatic actuators) depending on the application characteristics (for example, properties of the motion that is controlled). For TLPs, of particular interest is the control of the coupled heave/pitch motion, since large displacements in the vertical direction may lead to unacceptable strain for both pre-stressed tendons and production risers. This can be

established by TMDs placed in all columns of the hull, as suggested in Alves and Batista (1999) and illustrated in Figure 7.11. Both passive and active application of TMDs is considered in this study. A simplified schematic is given in Figure 7.12. We assume that the TMDs are allowed to vibrate in the vertical only direction. This control implementation allows for directly controlling the heave and pitch response of the structure. The surge response may only indirectly be influenced (through the coupling with the other two degrees of freedom).

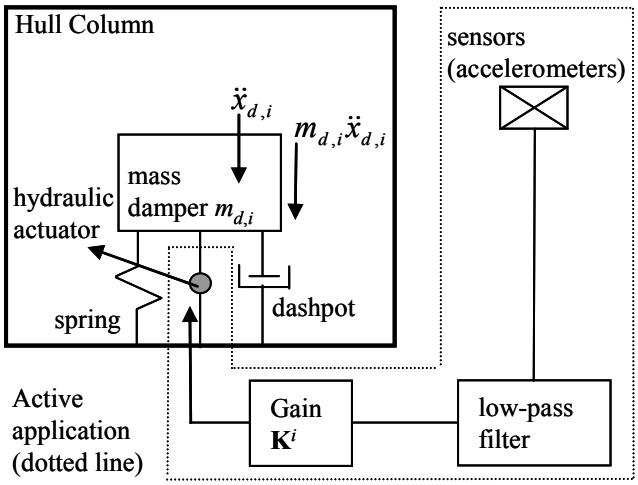

Figure 7.12: Schematic of passive and active TMD implementation

Passive TMD: A TMD consists of a mass attached to the primary structure through a spring and a dashpot. The motion of this mass counteracts the motion of the platform, thereby providing energy dissipation to the platform's vibration (inertia force of the damper acting on the structure). The controller parameters **K** in this case consist of the spring and dashpot coefficient or, equivalently, the frequency $\omega_{d,i}$ and the damping ratio $\zeta_{d,i}$ for each damper i, assuming that the mass $m_{d,i}$ of the damper has been already selected (based on consideration about the maximum feasible or allowable additional mass). Excessive vibrations of the TMD can be prevented (due to space limitations) by appropriately placed stoppers.

Active TMD: The effectiveness of TMDs can be enhanced by application of active control forces through hydraulic actuators (Figure 7.12). In this study, only noisy acceleration measurements are assumed to be available for the active control implementation. Because of the nonlinear characteristics and the complexity of the system model, estimating its states (velocities and displacements) based on the acceleration measurements cannot be performed accurately (Anderson and Moore 2005) and is avoided here. Also, because of the presence of noise, double integration of the accelerations to obtain displacement measurements might be unstable and unreliable. Velocity or acceleration feedback are practically the only feasible choices for feedback control design. The latter is selected here, and the control force on each damper, u_i, is designated as a feedback function of the heave and pitch filtered accelerations; the acceleration measurements are filtered by a low-pass filter in order to reduce the influence of the noise in the signal (May and Beck 1998; Chu et al. 2006). The transfer function of the filter is:

$$H_f(s) = \frac{\omega_f^2}{s^2 + 2\zeta_f \omega_f s + \omega_f^2} \tag{7.26}$$

where $\zeta_f = \sqrt{2}/2$ and ω_f should be selected higher than the natural frequencies of the system. If $\ddot{z}_f$ and $\ddot{\theta}_f$ are the filtered accelerations, $\mathbf{K}^i$ the feedback gain for the i^{th} damper, and K_k^i its k^{th} element, then

$$u_i = \mathbf{K}^i \begin{bmatrix} \ddot{z}_f & \ddot{\theta}_f \end{bmatrix}^T = \begin{bmatrix} K_1^i & K_2^i \end{bmatrix} \begin{bmatrix} \ddot{z}_f & \ddot{\theta}_f \end{bmatrix}^T \quad . \tag{7.27}$$

7.2.4 Equation of motion for controlled system

The model for the dynamic response of the controlled system is finally:

$$
\begin{aligned}
m\ddot{x} + F_{r,x} &= F_{d,x} \\
m\ddot{z} + F_{r,z} &= F_{d,z} + F_b - w - \sum_{i=1}^{4} m_d \ddot{x}_{d,i} \\
I_\theta \ddot{\theta} + F_{r,\theta} &= F_{d,\theta} + M_b + \sum_{i=1}^{4} l_i m_d \ddot{x}_{d,i} \\
m_{d,i}\left(\ddot{x}_{d,i} + \ddot{z} - l_i \ddot{\theta}\right) + 2\omega_{d,i}\zeta_{d,i} m_{d,i}\dot{x}_{d,i} + \omega_{d,i}^2 m_{d,i} x_{d,i} &= u_i \quad \text{i=1,...,4}
\end{aligned}
\tag{7.28}
$$

where $x_{d,i}$ is the relative displacement of the i^{th} mass damper, m is the total mass of the platform (including the TMDs), I_θ is the mass moment of inertia at the center of gravity of the hull (again including the TMDs), $F_{r,j}$ is the resultant restoring force (or moment in the center of mass of the hull) generated by the tendon system in degree of freedom j (j=x,y,θ), $F_{d,j}$ is the similar quantity for the hydrodynamic forces, w is the weight of the structure, F_b is the buoyancy force, M_b is the moment created by that force (again calculated at the center of mass of the TLP), and l_i is the instantaneous horizontal position of damper i with respect to the center of gravity of the hull. In (7.28), the coupling between the TMD motion and the rotation of the platform is directly taken into account. This coupling was neglected in previous investigations (for example in Alves and Batista (1999)).

Table 7.5 Details of TLP

Column diameter (D_c)	18 m	Pontoon diameter (D_p)	12 m
Radius of gyration (pitching motion)	39 m	Mass	40 kton
Total pre-tension (T_o)	165 10^3 kN	Structural damping	0%
E of tendons	200 kN/cm^2	Tendon diameter	0.3 m
Water depth	640 m	Draft (D_r)	33.5 m
C_D	1	C_M	2
Distance between columns (s_o)	77 m	Column height (h_c)	75 m
Position of center of mass (h_G)	38 m above keel	Tendons per leg	3

The characteristics of the platform considered in this study are shown in Table 7.5. The natural frequencies of the platform are: heave 3.16 sec, pitch 3.13 sec, and surge 117 sec.

Four mass dampers with individual mass equal to 0.5% of the hull mass are considered, one on each hull column. When considering the total apparent mass of the platform (structural mass+added mass up to mean sea level), this ratio drops to 0.3%. For the active control application, the actuators are modeled as ideal forcing systems (no dynamics) with maximum force capability of 500 kN (saturation of actuator forces). A time delay equal to 5 ms is also assumed in the control loop. The maximum allowable displacement for the damper is set to 2 m and ω_f in (7.26) is equal to 8 rad/sec.

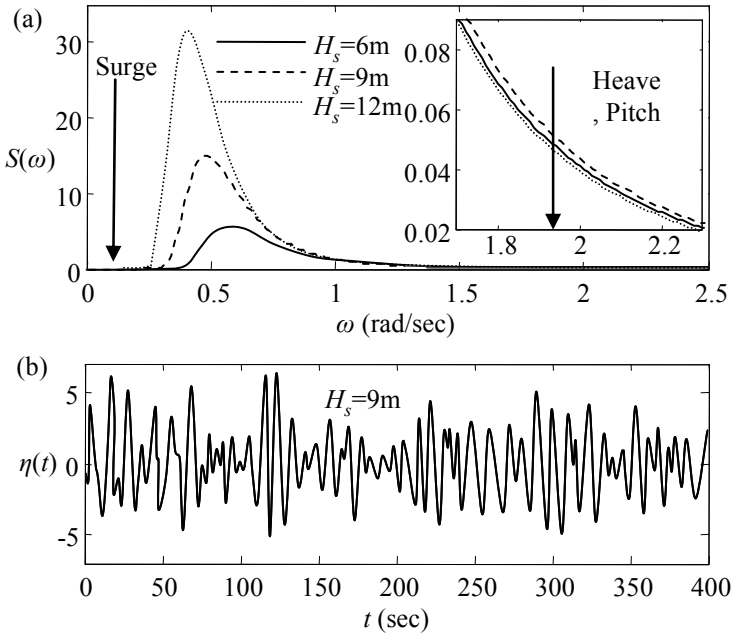

Figure 7.13: (a) PM spectrum and eigenfrequencies of TLP (arrows) and (b) a sample realization of $\eta(t)$

7.2.5 Controller Design

Model Uncertainty: The biggest sources of uncertainty in the TLP and excitation models are the characteristics of the PM spectrum, H_s and T_z. The joint distribution of H_s and T_z has been discussed in numerous studies (for example, in Mathisen and Bitner-Gregersen

(1990)) and a variety of statistical descriptions have been suggested. In this study, we adopt a three-parameter marginal Weibull distribution for H_s:

$$p(H_s) = \frac{\beta_w}{\alpha_w}\left(\frac{H_s - \gamma_w}{\alpha_w}\right)^{\beta_w - 1} \exp\left(-\left(\frac{H_s - \gamma_w}{\alpha_w}\right)^{\beta_w}\right) \tag{7.29}$$

and a conditional log-normal for the zero up-crossing period, T_z. The parameters selected for the Weibull distribution are α_w=1.41, β_w=1.2, and γ_w=1, whereas the median, e^{μ}, and logarithmic standard deviation, σ, for the log-normal are (Mathisen and Bitner-Gregersen 1990):

$$\exp(\mu) = \exp(a_1 + a_2 H_s^{a_3}), \;\; \sigma = b_1 + b_2 \exp\left(b_3 H_s\right) \tag{7.30}$$

where a_1=1.22, a_2=0.32, a_3=0.52, b_1=0.075, b_2=0.04, and b_3=-0.6. Figure 7.13(a) shows the PM spectrum for various H_s and Figure 7.13(b) shows a sample realization of the free surface elevation for H_s=9 m. In these figures, T_z is set to its conditional mean value.

The uncertain model parameters, finally, correspond to the PM spectrum characteristics, T_z and H_s, and the stochastic sequences $\{\alpha_i\}$, $\{\delta_i\}$, and $\{\omega_i\}$] used to a realize a sample time history for the sea state, so $\boldsymbol{\theta}$=[H_s, T_z, $\{\alpha_i\}$, $\{\delta_i\}$, $\{\omega_i\}$].

Controller design: The platform reliability is adopted as the design objective. The controller optimization is performed under the framework described earlier, using nonlinear simulations. The time duration for each simulation run is set to T_t=10 min. The number of component waves, k, is set to 60 in order to reduce the computational time needed for each simulation run.

The performance criteria considered for the controller design are the structural integrity of the risers, the yielding and snapping of the tendons, and the comfort of the crew. The

corresponding performance variables used are the maximum heave displacement, maximum and minimum dynamic stress of the tendons, and the root mean square acceleration in vertical and horizontal directions at the deck of the platform. The thresholds for each one are 0.25 m, 450 MPa (assumed yielding stress of steel), 0 (no compressive stress allowed), 0.15 g, and 0.07 g. The latter two quantities are adopted based on the survey by Stevens and Parson (2002). Note that under the initial pretension, the stress on the tendons is 195 MPa.

Applying SSO, the design yielded the optimal passive damper parameters: period 3.1 sec and damping ratio 0.08 (same for all dampers because of symmetry). For the active case, the damper parameters for the active application were set fixed to the corresponding values from the passive case.

7.2.6 Performance evaluation

The evaluation of the controlled system is performed with respect to (a) reliability criteria (similar to the ones considered in the design stage) and (b) the response characteristics for 12 different sea states. These sea states ultimately represent potential future excitations. They are simulated, here, according to the model presented earlier for four different significant wave heights selections; (i) H_s=12 m, (ii) H_s=9 m, (iii) H_s=6 m, and (iv) H_s=3 m. For each H_s three different up-crossing periods are considered, corresponding to (a) the mean value and to values that are one standard deviation (b) higher or (c) lower than the mean value. These values are calculated according to the probabilistic model presented earlier, conditioned on the selection of H_s.

The reliability is evaluated for three different cases, in terms of the minimum significant wave height considered, (i) H_s>1 m, (ii) H_s>4 m, and (iii) H_s>6 m. The first case corresponds to the nominal probabilistic description for the site (the one assumed in the controller design stage), but the latter two cases correspond to conditioning on moderate or significant excitation events (H_s is set higher than some threshold). The efficient Subset

Simulation algorithm (Au and Beck 2001b) was used for the reliability evaluations. The results are reported in Table 7.6. The control application significantly increases the reliability of the platform. Implementation of active control provides a considerable margin of improvement over the passive application. These comments are true for all excitation cases. Even for significant excitation events (H_s>6 m), the probability of failure of the controlled system is kept small.

Table 7.6 Evaluation of control implementation under reliability criteria

Case	Estimated probability of failure		
	No control	Passive TMD	Active TMD
H_s>1 m	0.038	0.0017	0.0006
H_s>4 m	0.121	0.0071	0.0024
H_s>6 m	0.201	0.0188	0.0093

Table 7.7 Evaluation of control implementation for simulated sea states

		No control	Passive	Active
(i)H_s=9, T_z=9.3	Max(|z|)	0.35 m	0.27 m	0.23 m
	Max(|θ|)	0.0091 rad	0.0074 rad	0.0061 rad
	Max(stress)	381 MPa	327 MPa	291 MPa
	Min(stress)	-1.18 MPa	50 MPa	82 MPa
	aRMSv	0.032 g	0.019 g	0.011 g
	aRMSh	0.054 g	0.035 g	0.028g
(ii)H_s=9, T_z=8.5	Max(|z|)	0.39 m	0.31 m	0.30 m
	Max(|θ|)	0.0101 rad	0.0083 rad	0.0079 rad
	Max(stress)	404 MPa	336 MPa	312 MPa
	Min(stress)	-3.18 Mpa	47 MPa	43 MPa
	aRMSv	0.032 g	0.021 g	0.012 g
	aRMSh	0.054 g	0.039 g	0.031 g

The results for the sea states are discussed next. The simulation of the response is performed over 10 min. The response quantities reported are the ones used for evaluation of the reliability performance in the controller design stage, plus the maximum pitch rotation. In Figure 7.8 some results are reported for two cases. For both of them the significant height is equal to H_s=9 m, but T_z is set (i) for the first case to its conditional mean value, T_z=9.3 sec, and (ii) for the second to a value one standard deviation lower, T_z=8.5 sec (this corresponds to excitation closer to resonance). aRMSv and aRMSh denote the RMS deck acceleration in the vertical and horizontal directions, respectively. Figure 7.15 shows some comparative scatter diagrams of the response for all cases. Some indicative time histories are illustrated in Figure 7.14.

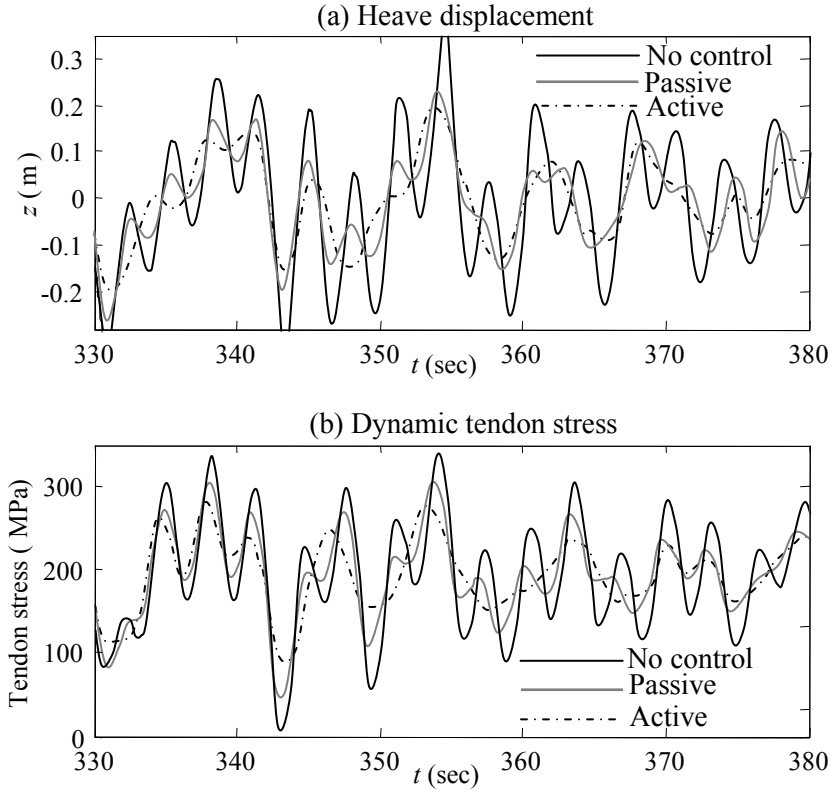

Figure 7.14: Sample time histories for heave displacement and tendon stress for simulated sea state with properties H_s=9 m, T_z=10.6 sec

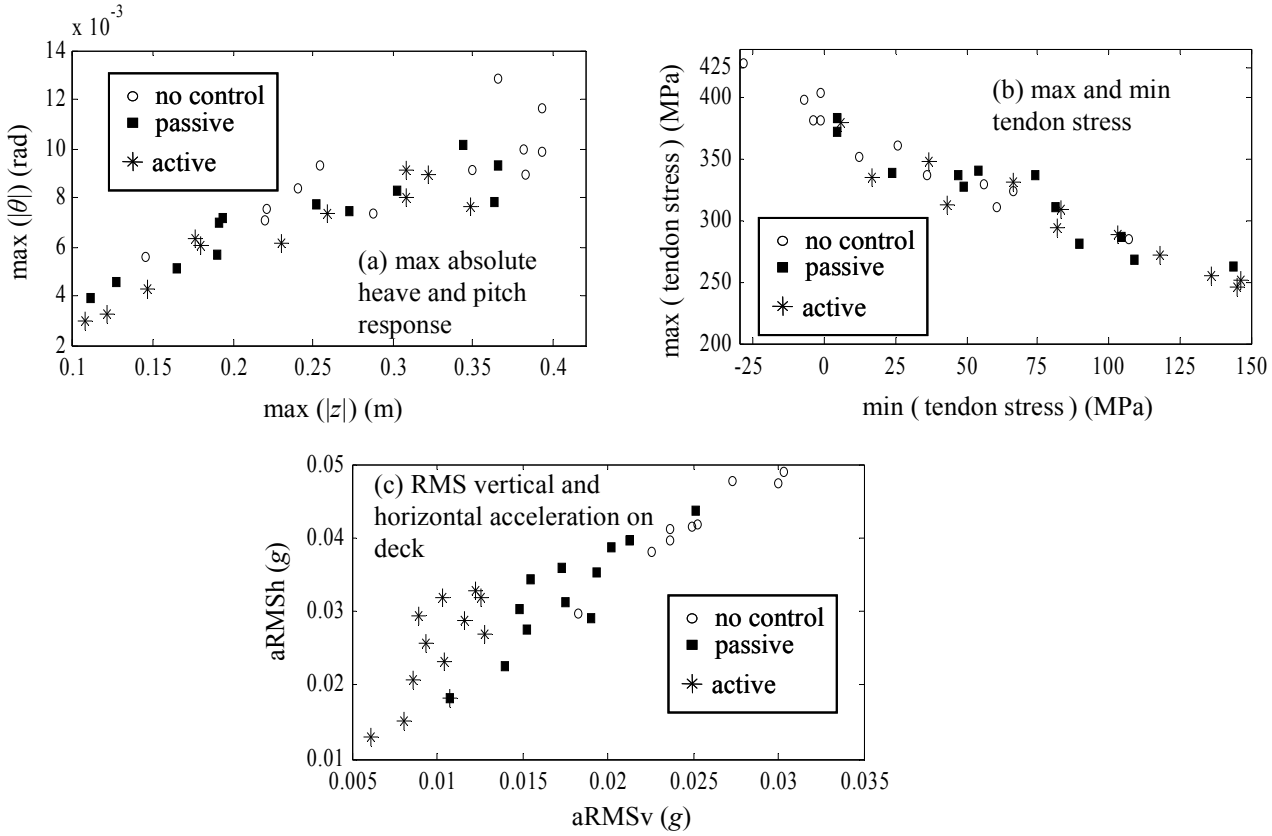

Figure 7.15: Scatter diagrams of response for 12 simulated sea states

The results further verify the effectiveness of the control application. It is important to note that the dynamic strain of the uncontrolled system in some of the excitations cases becomes negative (Figure 7.15(b)).Under most quantifications of acceptable performance, i.e. even if one did not use the thresholds assumed in the controller design stage, such response may cause failure because it leads to snapping of the tendons. This unacceptable performance is eliminated in the TMD-equipped platform. This shows the effectiveness of the control application in protecting the integrity of the platform under severe weather conditions. Overall the response of the controlled system, as indicated in the scatter diagrams of Figure 7.15, illustrates a significant improvement over the uncontrolled one. This holds for both the pitch and heave responses separately, as indicated in Figure 7.15(a), as well as for their coupled effect, which is represented by the tendon stress in Figure 7.15(b). Since the

average performance is easier to regulate than the extreme one, the improvement in terms of the RMS acceleration is even greater (compare Figure 7.15(c) to Figure 7.15(b) or Figure 7.15(a)).

Finally, a comparison between the passive and active control implementations is warranted. In terms of both the reliability evaluation (Table 7.6) and the simulated sea states (Table 7.7 and Figure 7.15), the active control application provides an improvement over the passive one. For the simulated sea states, this improvement is more evident for the RMS response (Figure 7.15(c)), for similar reasons to these explained above. The margin of improvement over the passive control application is of course smaller when compared to the margin between the "passive control" and "no control" cases. This is expected since the passively controlled system represents a system that is considerably enhanced over the uncontrolled one. Thus further improvement of its performance is more challenging. Note, also, that the setting for the active control application assumed here incorporates many practical constraints that reduce the control effectiveness. This is apparent from the results of Table 7.7. Recall that case (ii) represents excitation conditions closer to resonance. This leads to operation of the actively controlled system closer to its constraints in terms of both (a) actuator saturation and (b) allowable damper displacement, and consequently to some degradation of performance (the constraints are actually violated in this case). This is why a smaller improvement over the passive control applications appears for the extreme response quantities, when compared to case (i) of Table 7.7. Overall, the improvement in performance, in particular with respect to the system reliability, shows that the application of active control techniques should be considered as an attractive extension in control of Tension Leg Platforms when Tuned Mass Dampers are used. The fact that the setting considered for the active control implementation in this study takes into account most practical constraints and may be considered feasible, based on current actuator, sensor, and software capabilities, further supports this conclusion.

Ultimately, the results illustrate significant reduction in important response quantities for both (a) the integrity of the oil risers and the tendons of the platform, as well as (b) the comfort of the crew. This shows the efficiency of both the controller design methodology and the capabilities of the suggested control implementation for TLPs, especially if one considers that the total mass of the damper was kept to a feasible level. Both passive and active TMD implementations were considered. A realistic setting was considered for the control application: actuator saturation, availability of only noisy acceleration measurements, constraints in the maximum damper displacements, and time delay in the control loop were taken into account. For the active application, acceleration feedback was chosen, which is easy to implement and corresponds to a reliable controller structure selection. The active control case illustrated improvement over the passive one, which justifies further exploration of such techniques when considering control applications to TLPs. In future work, evaluation of the performance of the passively and actively controlled TLP based on socio-economic criteria—that is, life-cycle cost—is desirable to establish a direct cost-benefit comparison between the two types of control application.

CHAPTER 8

Conclusions

8.1 Summary and Main Contributions

This thesis discusses the robust-to-uncertainties design of engineering systems when a probability logic approach is adopted for quantifying the partial knowledge about the characteristics of the system under consideration and its environment. This design methodology is called *stochastic system design*. This section summarizes all the chapters of the current study and emphasizes the main contributions. The latter are presented in bullet form.

8.1.1 Chapter 2

Chapter 2 outlined the stochastic system design problem. The system modeling in a stochastic setting was initially addressed; a probability-logic approach was demonstrated for incorporating the available knowledge about the system into its model. The performance quantification in this stochastic framework was then discussed; the design objective was expressed as a stochastic integral over the possible values for the model parameters. Some special attention was given to design problems that involve the system reliability as performance objective. Topics related to the application of the general stochastic system design methodology to the specific field of structural control were also addressed. The following topics constitute novel contributions in this chapter:

- For systems whose design has been traditionally interpreted in a deterministic framework, the potential extension of the deterministic performance quantifications to account for a probabilistic modeling characterization was discussed. Various approaches were suggested for such an extension.
- For reliability-based design problems attention was given to the influence of the model prediction error when quantifying the system model performance. An equivalent formulation of the objective function (probability of failure) was derived that clearly illustrates this influence.
- A probabilistic model for characterizing the system excitation in earthquake engineering applications was developed. In contrast to previous research efforts the model discussed here efficiently describes both far-fault and near-fault characteristics of earthquake ground motions, and also establishes a direct link between the probabilistic seismic hazard of a site and future excitations.

8.1.2 Chapter 3

In Chapter 3, design problems were addressed that involve models for which the system performance can be analytically evaluated and the uncertain parameter vector is low dimensional. An efficient approximation for the stochastic integrals and the associated design optimization was presented.

The focus was initially on the reliability-based design of linear controlled systems under stochastic stationary excitation. The novel contributions are:

- Accurate analytical approximations were presented for all reliability performance measures. These approximations allowed for theoretical discussions on topics related to the characteristics of optimal reliability controllers and to the associated controller optimization procedure.

- For system with certain model parameters, the relationship of reliability-based design to minimum variance controller synthesis was examined in detail. The theoretical discussions and the examples presented showed that significant differences are expected between optimal reliability and optimal $\mathcal{H}_2$ controllers. Smaller differences were shown to exist between optimal reliability and optimal multi-objective $\mathcal{H}_2$ controllers. Still, it was demonstrated that these differences can be quite important, even for a system with simple dynamics and a scalar control law.
- For systems that involve model uncertainty, the influence of the time duration T on the optimal robust controller design was considered, and a probabilistic treatment for T was investigated. It was demonstrated that there is some sensitivity of the control system optimization to the time duration, but only small differences in controller design and respective performance were observed between deterministic and probabilistic treatments of the time duration.

The influence of probabilistic model uncertainty on classical controller synthesis methods, such as $\mathcal{H}_2$ and multi-objective $\mathcal{H}_2$ designs, was also considered in this chapter. Two different approaches were presented for the extension of the deterministic performance quantification to a probabilistic one, the average robustness, and the reliability robustness. The novel contributions are:

- The sensitivity of the performance objective around the optimal solution was examined in detail for the various design approaches and it was illustrated that it is particularly high when the design objective is the reliability robustness and the focus is on rare events, that is, where there are large thresholds for the acceptable system performance.
- Controllers optimized by explicitly considering modeling uncertainties were demonstrated to yield considerable improvement in performance compared to controllers optimized using only a nominal model or the usual control robustness notion of worst-case scenario.

- The examples considered in this chapter also examined the connection between the reliability and average robustness quantifications for the stochastic performance, as well as the influence on the design of the specific probability models adopted for quantifying the available knowledge. The results illustrated that if the focus of the design is on rare events, then there are important differences between the designs based on the reliability and the average robustness performance, and that a significant influence exists on the design characteristics of (a) the level of the uncertainty and (b) the specific PDFs selected for quantifying the missing information about the system model.

Even though the methods discussed in Chapter 3 involve a challenging nonlinear optimization, the potential performance improvement, either in a reliability or general stochastic design setting, demonstrated in this study justify the additional computational cost that is involved in the design process and motivate further theoretical studies of this topic.

8.1.3 Chapter 4

The focus in Chapters 4, 5, 6 and 7 was shifted to design problems which might involve complex models for the system under consideration and its environment. The methods developed for studying these systems are general; specialized assumptions were avoided. To address the potential complexity in the model description, stochastic simulation was used for evaluating the system performance. In this context, the response of the system model can be also calculated using computer simulation. This simulation-based approach allows for explicit consideration of (a) nonlinearities in the models assumed for the system and its future excitation, and (b) complex failure modes. Chapters 4 and 5 addressed the challenging design optimization problem involved in such cases.

- Chapter 4 presented a novel algorithm called Stochastic Subset Optimization (SSO), for efficiently exploring the sensitivity of the objective function to the design variables and iteratively identifying a subset of the original design space that has high plausibility of

containing the optimal design variables. Implementation issues for the algorithm were discussed in detail, including: appropriate advanced stochastic simulation algorithms for complex system models, essential normalization and coordinate transformation techniques for computational efficiency, as well as statistical properties along with stopping criteria for the iterative approach.

SSO leads, ultimately, to an adaptive exploration of the design space for the optimal design configuration. A single stochastic analysis is used at each iteration; thus, the whole process is highly efficient. Also, the computational cost of SSO increases linearly with the dimension of the design variables, which makes it appropriate candidate for problems involving a large number of design variables. This algorithm represents one of the most important contributions of this work.

The efficiency of SSO in accurately converging to the optimal solution depends on the sensitivity of the design problem. For problems that are characterized by small sensitivity around the optimal design choice, a combination of SSO with other stochastic optimization algorithms may be chosen for enhanced overall efficiency.

8.1.4 Chapter 5

Chapter 5 further discussed topics in stochastic optimization.

- An efficient two-stage framework for the simulation-based stochastic optimization problem was discussed by combining SSO with another appropriate stochastic optimization algorithm. Characteristics of these algorithms, as well as to the combination of the two different stages for overall improved computational efficiency and accuracy of the optimization process, were discussed.

Special attention was given to the following issues which represent significant new contributions to the field of stochastic optimization:

- Guidelines for the combination of SSO with the highly efficient Simultaneous Perturbation Stochastic Approximation (SPSA) algorithm were presented. These guidelines allow for better normalization of the search space and for automatic selection of step sizes, blocking rules and stopping criteria for SPSA.
- Topics related to the adaptation of common random numbers in reliability-based design problems were discussed. A necessary transformation of the performance measure was suggested for establishing computational efficiency. This transformation is based on the equivalent formulation of the probability of failure when a model prediction error is assumed.
- The implementation of importance sampling for the second stage of the optimization framework was also discussed. Guidelines for the development of importance sampling densities based on the information directly available from the SSO stage were presented. Special focus was given on cases that involve system models with uncertain parameter vectors of large dimension.

8.1.5 Chapter 6

Chapter 6 presented applications of the stochastic system design methodology to structural engineering applications. The first application considered the design of a base-isolation system for improving the reliability of a three-story shear structure against near-fault earthquakes. The efficiency of SSO and the suggested combined optimization framework was examined in detail in the context of this example.

- It was demonstrated that SSO can efficiently identify a set that contains the optimal design variables, and also can improve the efficiency of SPSA when combined as in the suggested optimization framework. The implementation of importance sampling using the information for SSO was shown to be highly efficient. Use of SSO on its own was shown to lead to a design that is sub-optimal but close to the optimal one. Additionally, SSO was demonstrated to be able to describe the correlation between the design variables in terms of the contours for the objective function.

- The influence on the design of the model prediction error was also examined. This last study revealed an important sensitivity of the optimal system design to (a) our available knowledge about the system and excitation properties and (b) the utility function selected to quantify the model performance.

The second application discussed the retrofitting of a four-story structure with viscous dampers. The expected lifetime cost was adopted as the design objective in this case.

- Instead of approximating the damages from future earthquakes in terms of the reliability of the structure, as typically performed in previous design optimization studies, an accurate loss-estimation methodology was adopted for estimating this cost, using the nonlinear response of the structure under seismic excitation to estimate the damage at a more-detailed, component level. For the structural components a direct link was established between their fragility (in terms of damage states) and their strength and stiffness characteristics.
- All important sources of uncertainty were considered in the formulation of the structural and excitation models, and a significant reduction of the expected life-cycle cost was demonstrated by the suggested retrofitting scheme. The decomposition of the total cost with respect to the various building components, as well as the distribution of this cost along the height of the structure, were presented. This analysis was then used to draw conclusions about the level of nonlinear behavior of the initial and retrofitted structure.

Both base-isolation and retrofitted-structure examples show the following: If the representation for the system and excitation models is adequate and the uncertainty about the model properties is quantified properly, the proposed methodology leads to an efficient design that takes into account all of the important characteristics and can yield significant improvement in the system performance.

- Additionally, the sensitivity of the stochastic performance to the various model parameters was examined. It was demonstrated that the excitation characteristics have

bigger influence on the system performance, compared to the structural model parameters.

8.1.6 Chapter 7

Finally, Chapter 7 discussed structural control applications of the suggested stochastic system design framework. This approach can be considered as an extension of the controller design discussed in Chapter 3 for linear systems, to applications that involve nonlinear system and excitation models. The first application discussed the Base-Isolated ASCE Structural Control Benchmark problem. The design of the controlled system for improvement of the structural reliability against near-fault earthquakes was adopted as the design objective. A Regenerative Force Actuation (RFA) network with eight actuators in each direction was suggested for this purpose. The novel contributions are:

- Two important issues were addressed for the RFA network: (a) the redundancy of the actuator configuration with respect to the resultant control forces, and (b) the clipping of the control forces for optimal reliability performance when trying to satisfy the RFA network constraints.
- Comparison to the performance of a passive viscous damping system was also discussed. It was also shown that the design with the RFA network yielded better overall performance and better trade-offs in the reductions of failure probabilities of the various individual failure modes. The marginal improvement was small, however. The response of the base-isolated structure under recorded near-fault ground motions verified these trends and the overall design efficiency.

The second application discussed the protection of an off-shore Tension Leg Platform in an uncertain sea environment. Implementation of both passive and active tuned mass dampers was considered for realization of the control force on the structure. Significant performance improvement was established with respect to (a) the integrity of the oil risers and the tendons of the platform, as well as (b) the comfort of the crew.

- In both applications, all important nonlinearities of the system, excitation, and actuator models were explicitly accounted for when *designing* the controller. Most other popular structural control design approaches either (a) neglect these characteristics or (b) try to approximately consider them by designing the controller using linear methodologies and an iterative approach, that is by trial and error, to try to establish adequate performance for the nonlinear model.
- The studies considered here also brought forward an important topic: that ultimately socio-economic criteria need to be implemented for evaluating the efficiency of structural control systems. The stochastic design framework discussed here has the potential to address this need, as long as proper monetary-oriented utility functions are developed for evaluating the model performance for each specific application.

8.1.7 Conclusions

In general, the suggested simulation-based stochastic system design approach developed in this study provides a powerful tool for robust-to-modeling uncertainty design while, at the same time, explicitly accounting for all important system characteristics, linear or nonlinear. The stochastic optimization framework developed for solving the associated design optimization problem was shown to be highly efficient. Especially the SSO algorithm was demonstrated to provide a computationally-efficient method for performing a global sensitivity analysis with respect to the design variables as well as the model parameters.

8.2 Future Work

There are a couple of avenues that constitute the next logical developments for the stochastic design approach discussed here.

First of all, the stochastic optimization framework can be further improved. The criteria for quality of the SSO identification needs to be examined in more detail. The guidelines

suggested in this study, in terms of stopping criteria relevant to this quality, stem from personal experience. The development of a thorough theoretical basis for this aspect of SSO is warranted. Also the application of objective function approximation methods should be examined in more detail. The example presented in this study illustrated that the combination of SSO with objective function approximation methods has a lot of potential. Still, further research is needed in order to explore the robustness properties of this optimization approach and to improve its efficiency by providing guidelines for iterative convergence to the optimal solution.

For linear controlled systems the analysis presented here for extending the ideas of probabilistic robustness to classical control methodologies was based on solving nonlinear optimization problems, which can be a challenging task when higher-order controllers are considered. A more thorough analytical approach is warranted, if possible, to allow for in-depth theoretical comparisons and for extension of the design methodology to complex controller structures. Certain simplifications with respect to the probability models for the parametric uncertainty could be employed as a first step towards developing these approaches.

In terms of structural engineering applications, more realistic models can be considered. For example, three-dimensional effects in the structural response and in the performance of the structural and non-structural building components can be taken into account. Additionally, more accurate methodologies can be used to evaluate the dynamic nonlinear response of the models adopted. Also, since the studies here illustrated that there is a higher sensitivity of the stochastic performance to the excitation characteristics than to the structural model properties, further attention is warranted for the probabilistic modeling of earthquake ground motions, especially near-fault ones. Additionally, a similar improved probabilistic modeling could be considered for other dynamic excitations, such as sea waves.

Also, in the structural control applications discussed in this study, the focus was on the reliability performance. In order to fully evaluate the benefits from control application and compare the different actuator configurations, a cost-benefit analysis needs to be developed. This analysis will lead to a clear characterization of the benefits coming from control implementation and will help to justify future control applications to civil engineering structures.

References

Acevedo, J., and Pitsikopoulos, E.N., 1988. Stochastic optimization based algorithm for process synthesis under uncertainty, *Computers and Chemical Engineering*, 22, 647–671.

Ahmad, S.K., and Ahmad, S., 1999. Active control of non-linearly coupled TLP response under wind and wave environments, *Computers and Structures*(72), 735–747.

Alavi, B., and Krawinkler, H., 2000. Consideration of near-fault ground motion effects in seismic design, *Proceedings of the 12th World Conference on Earthquake Engineering*, January 30–February 4, Auckland, New Zealand.

Alves, R.M., and Batista, C.R., 1999. Active/Passive control of heave motion for TLP type of offshore platforms, *Proceedings of the 9th International Offshore and Polar Engineering Conference*, May 30–June 4 Brest, France, pp. 332–338.

Anderson, B.D.O., and Moore, J.B., 2005. *Optimal filtering*. Dover Publications, Mineola, New York.

Ang, H.-S.A., and Lee, J.-C., 2001. Cost optimal design of R/C buildings, *Reliability Engineering and System Safety*, 73, 233–238.

Angelides, D.C., Chen, C.-Y., and Will, S.A., 1982. Dynamic response of tension leg platform, *Proceedings of the 3rd International Conference on Behaviour of Off-shore Structures*, pp. 100–120.

Atkinson, G.M., and Silva, W., 2000. Stochastic modeling of California ground motions, *Bulletin of the Seismological Society of America*, 90(2), 255–274.

Au, S.K., and Beck, J.L., 1999. A new adaptive importance sampling scheme, *Structural Safety*, 21, 135–158.

Au, S.K., Papadimitriou, C., and Beck, J.L., 1999. Reliability of uncertain dynamical systems with multiple design points, *Structural Safety*, 21, 113–133.

Au, S.K., and Beck, J.L., 2001a. Estimation of small failure probabilities in high dimensions by subset simulation, *Probabilistic Engineering Mechanics*, 16, 263–277.

Au, S.K., and Beck, J.L., 2001b. First-excursion probabilities for linear systems by very efficient importance sampling, *Probabilistic Engineering Mechanics*, 16, 193–207.

Au, S.K., and Beck, J.L., 2003. Subset simulation and its applications to seismic risk based on dynamic analysis, *Journal of Engineering Mechanics, ASCE*, 129(8), 901–917.

Au, S.K., 2005. Reliability-based design sensitivity by efficient simulation, *Computers and Structures*, 83, 1048–1061.

Bailey, T.G., Jensen, P.A., and Morton, D.P., 1999. Response surface analysis of two-stage stochastic linear programming with recourse, *Naval Reasearch Logistics*, 46, 753–776.

Beck, J.L., and Katafygiotis, L.S., 1998. Updating models and their uncertainties. I: Bayesian statistical framework, *Journal of Engineering Mechanics*, 124(4), 455–461.

Beck, J.L., and Au, S.K., 2002. Bayesian updating of structural models and reliability using Markov Chain Monte Carlo simulation, *Journal of Engineering Mechanics*, 128(4), 380–391.

Beck, J.L., Porter, K.A., Shaikhutdinov, R.V., Au, A.K., Mizukoshi, K., Miyamura, H., Ishida, H., Moroi, T., Tsukada, Y., and Masuda, M., 2002. Impact of seismic risk on lifetime property values, *Earthquake Engineering Research Library Report No. 2002–4*, California Institute of Technology, Pasadena. California.

Beck, J.L, and Yuen, K.V., 2004. Model selection using response measurements: Bayesian probabilistic approach, *Journal of Engineering Mechanics*, 130(2), 192–203.

Belyaev, Y., 1968. On the number of exits across the boundary of a region by a vector stochastic process, *Theory of Probabilistic Applications*, 13(2), 320–324.

Boers, Y., Weiland, S., and Damen, A.A.H., 1997. Expected H_2 performance control for systems with statistical uncertainty, *Proceedings of the American Control Conference*, Albuquerque, New Mexico, pp. 1225–1229.

Boers, Y., 2002. Average performance control by static output feedback, *IEE Proceedings in Control Theory and Applications*, 149(3), 188–192.

Boore, D.M., and Joyner, W.B., 1997. Site amplifications for generic rock sites, *Bulletin of the Seismological Society of America*, 87, 327–341.

Boore, D.M., 2003. Simulation of ground motion using the stochastic method, *Pure and Applied Geophysics*, 160, 635–676.

Boyd, S., Ghaoui, L.E., Feron, E., and Balakrishnan, V., 1994. *Linear Matrix Inequalities in systems and control theory*. SIAM, Philadelphia.

Bray, J.D., and Rodriguez-Marek, A., 2004. Characterization of forward-directivity ground motions in the near-fault region, *Soil Dynamics and Earthquake Engineering*, 24, 815–828.

Chakrabarti, S.K., 1971. Discussion of dynamics of single point moorings in deep water, *Journal of Waterways, Harbour and Coastal Engineering*, 97, 558–590.

Chandrasekaran, S., and Jain, A.K., 2002. Triangular configuration tension leg platform behaviour under random sea wave loads, *Ocean Engineering*, 29, 1895–1928.

Ching, J., and Hsieh, Y.-H., 2007. Local estimation of failure probability function and its confidence interval with maximum entropy principle, *Probabilistic Engineering Mechanics*, 22, 39–49.

Choi, K.K., Youn, B., and R.J, Y., 2001. Moving least squares method for reliability-based design optimization, *Proceedings of the 4th World Congress of Structural and Multidisciplinary Optimization*, June 4–8, Dalian, China.

Chu, S.Y., Soong, T.T., and Reinhorn, A.M., 2006. *Active, hybrid and semi-active structural control: A design and implementation handbook*. John Wiley & Sons, Chichester, England.

Clough, R.W., and Penzien, J., 1993. *Dynamics of structures*. McGraw-Hill Inc., New York.

Cox, R.T., 1961. *Algebra or Probable Inference*. The Johns Hopkins University Press, Baltimore, Rhode Island.

Dullerud, G.E., and Paganini, F., 1999. *A course in robust control theory: A convex approach*. Springer-Verlag, New York.

Dyke, S.J., Spencer, B.F.J., Sain, M.K., and Carlson, J.D., 1996. Modeling and control of magnetorheological dampers for seismic response reduction, *Smart Materials and Structures*, 5, 565–575.

Dyke, S.J., 2005. Current directions in structural control in the US, *Proceedings of the 9th World Seminar in Seismic Isolation, Energy Dissipation and Active Vibration Control of Structures*, June 13–16, Kobe, Japan.

Enevoldsen, I., and Sorensen, J.D., 1994. Reliability-based optimization in structural engineering, *Structural Safety*, 15(3), 169–196.

Erkus, B., and Johnson, E.A., 2006. Smart base isolated benchmark building Part III: a sample controller for bilinear isolation, *Journal of Structural Control and Health Monitoring*, 13, 605–625.

Field, R.V., and Bergman, L.A., 1998. Reliability-based approach to linear covariance control design, *Journal of Engineering Mechanics, ASCE*, 124(2), 193–199.

Fishman, G., 1996. *Monte Carlo: Concepts, algorithms and applications*. Springer Verlag, New York.

Friedman, J.H., Kabamba, P.T., and P.P, K., 1995. Worst-case and average H_2 performance analysis against real constant parametric uncertainty, *Automatica*, 31(4), 649–657.

Gasser, M., and Schueller, G.I., 1997. Reliability-based optimization of structural systems, *Mathematical Methods of Operations Research*, 46, 287–307.

Gavin, H.P., 2001. Control of seismically excited vibration using electrorheological materials and Lyapunov methods, *IEEE Transactions on Control Systems Technology*, 9(1), 27–36.

Gavin, H.P., 2002. Control of torsionally asymmetric structures, *Proceedings of the American Control Conference*, May 8–10, Anchorage.

Genz, A., 1992. Numerical computation of multivariate Normal probabilities, *Journal of Computational and Graphical Statistics*, 1, 141–149.

Glasserman, P., and Yao, D.D., 1992. Some guidelines and guarantees for common random numbers, *Management Science*, 38, 884–908.

Goda, Y., 2000. *Random seas and design of maritime structures*. World Scientific Publishing, Singapore.

Gosavi, A., 2003. *Simulation-based optimization: Parametric optimization techniques and reinforcement learning*. Kluwer Academic Publishers, Norwell, Massachusetts.

Goulet, C.A., Haselton, C.B., Mitrani-Reiser, J., Beck, J.L., Deierlein, G., Porter, K.A., and Stewart, J.P., 2007. Evaluation of the seismic performance of code-conforming reinforced-concrete frame building—From seismic hazard to collapse safety and economic losses, *Earthquake Engineering and Structural Dynamics*, 36(13), 1973–1997.

Gupta, A., and Maranas, C.D., 2000. A two-stage modeling and solution framework for multisite midterm planning under demand uncertainty, *Industrial and Engineering Chemistry Research*, 39, 3799–3813.

Hall, F.F., Heaton, T.H., Halling, M.W., and Wald, D.J., 1995. Near-source ground motion and its effects on flexible buildings, *Earthquake Spectra*, 11(4), 569–605.

Holmstrom, K., Goran, A.O., and Edvall, M.M., 2007. *User's guide for TOMLAB 5.8*. Tomlab Optimization Inc., San Diego, California. www.TOMLAB.biz.

Housner, G.W., Bergman, L.A., Caughey, T.K., Cassiakos, A.G., Claus, R.O., Masri, S.F., Skelton, R.E., Soong, T.T., Spencer, B.F.J., and Yao, J.T.P., 1997. Structural Control: Past, Present and Future, *Journal of Engineering Mechanics*, 123(9).

Husain, M.F., Barton, R.R., and Joshi, S.B., 2002. Metamodeling: Radial basis functions versus polynomials, *European Journal of Operational Research*, 138, 142–154.

Hutchison, D.W., 2002. On an efficient distribution of perturbations for simulation optimization using simultaneous perturbation stochastic approximation, *Proceedings of the IAESTED International Conference on Applied Modeling and Simulation*, November 4–6, Cambridge, Massachusetts, pp. 440–445.

Iwan, W.D., and Cifuentes, A.O., 1986. A model for system identification of degrading structures, *Earthquake Engineering and Structural Dynamics*, 14, 877–890.

Iwasaki, T., Skelton, R.E., and Geromel, J.C., 1994. Linear Quadratic suboptimal control with static output feedback, *Systems & Control Letters*, 23, 421–430.

Iwasaki, T., and Skelton, R.E., 1995. A unified approach to fixed-order controller design via linear matrix inequalities, *Mathematical Problems in Engineering*, 1, 59–75.

Jangid, R.S., and Kelly, J.M., 2001. Base isolation for near fault motions, *Earthquake Engineering and Structural Dynamics*, 30, 691–707.

Jaynes, E.T., 2003. *Probability Theory: The logic of science*. Cambridge University Press, Cambridge, UK.

Jensen, H.A., 2005. Structural synthesis of non-linear stochastic dynamical systems, *Proceedings of the 6th European Conference on Structural Dynamics*, 4–7 September, Paris, France, pp. 729-734.

Jensen, H.A., and Catalan, M.A., 2007. On the effects of non-linear elements in reliability-based optimal design of stochastic dynamical systems. *International Journal of Non-Linear Mechanics*, 42, 802-816.

Johnson, R.A., and Wichern, D.W., 2002. *Applied multivariate statistical analysis*. Prentice Hall, Upper Saddle River, New Jersey.

Jones, D., Schonlau, M., and Welch, W., 1998. Efficient global optimization of expensive black-box functions, *Journal of Global optimization*, 13, 455–492.

Katafygiotis, L.S., and Cheung, J.S.H., 2002. A new efficient MCMC based simulation methodology for reliability calculations, *Proceedings of the Fifth World Congress on Computational Mechanics*, Vienna, Austria.

Kim, Y.S., and Wang, K.W., 1993. On the sliding mode control of structural vibrations via variable damping, *Mechanical Systems and Signal Processing*, 7(4), 335–347.

Kircher, C.A., Whitman, R.V., and Holmes, W.T., 2006. Hazus earthquake loss estimation methods, *Natural Hazards*, 7(2), 45–59.

Kleinmann, N.L., Spall, J.C., and Naiman, D.C., 1999. Simulation-based optimization with stochastic approximation using common random numbers, *Management Science*, 45(11), 1570–1578.

Kong, J.S., and Frangopol, D.M., 2003. Life-cycle reliability-based maintenance cost optimization of deteriorating structures with emphasis on bridges, *Journal of Structural Engineering*, 129(6), 818–828.

Kouwenberg, R., and Zenios, S.A., 2001. *Stochastic programming models for asset liability management*, HERMES Center of Excellence on Computational Finance and Economics, University of Cyprus, Nicosia, Cyprus.

Kramer, S.L., 2003. *Geotechnical earthquake engineering*. Prentice Hall, Upper Saddle River, New Jersey.

Krstic, M., Kanellakopoulos, I., and Kokotovic, P., 1995. *Nonlinear and adaptive control design*. John Wiley & Sons, Inc., New York.

Kushner, H.J., and Yin, G.G., 2003. *Stochastic approximation and recursive algorithms and applications*. Springer-Verlag, New York.

Lagaros, N.D., Papadrakakis, M., and Kokossalakis, G., 2002. Structural optimization using evolutionary algorithms, *Computers and Structures*, 80(7–8), 571–589.

Laguna, 1998. Applying robust optimization to capacity expansion of one location in telecommunications with demand uncertainty, *Management Science*, 44, S101–S110.

Lutes, L.D., and Sarkani, S., 1997. *Stochastic analysis of structural and mechanical vibrations*. Prentice Hall, Upper Saddle River, New Jersey.

Marti, K., 2005. *Stochastic optimization methods*. Springer-Verlag, Berlin, Germany.

Maryak, J.L., 1997. Some guidelines for using iterate averaging in stochastic approximation, *Proceedings of the IEEE Conference on Decision and Control*, December 10–12, San Diego, California, pp. 2287-2290.

Mathisen, J., and Bitner-Gregersen, E., 1990. Joint distributions for significant wave height and wave zero up-crossing period, *Applied Ocean Research*, 12(2), 93–103.

Mavroeidis, G.P., and Papageorgiou, A.P., 2003. A mathematical representation of near-fault ground motions, *Bulletin of the Seismological Society of America*, 93(3), 1099–1131.

May, B., and Beck, J., 1998. Probabilistic control for the active mass driver benchmark structural model, *Earthquake Engineering and Structural Dynamics*, 27(11), 1331–1346.

Mekha, B.B., Johnson, C.P., and Roesset, J.M., 1996. Implications of tendon modeling on nonlinear response of TLP, *Journal of Structural Engineering*, 122(2), 142–149.

Mitrani, J., 2007. *An ounce of prevention: Probabilistic loss estimation for performance-based earthquake engineering*. California Institute of Technology, Pasadena, California.

Morton, D.P., 1996. An enhanced decomposition algorithm for multistage stochastic hydroelectric scheduling, *Annals of Operations Research*, 64, 211–235.

Moses, F., 1977. Structural system reliability and optimization, *Computers and Structures*, 7, 283–290.

Muto, M.M, and Beck, J.L., 2007. Bayesian updating and model class selection for hysteretic structural models using stochastic simulation. *Journal of Vibration and Control*, in press.

Nagarajaiah, S., and Narasimhan, S., 2006. Smart base isolated benchmark building. Part II —phase I sample controllers for linear isolation system., *Journal of Structural Control and Health Monitoring* 13(2–3), 589–604.

Nagarajaiah, S., Narasimhan, S., and Johnson, E.A., 2006. Phase II Smart base isolated benchmark building with nonlinear isolation systems, *Proceedings of the 4th World Conference on Structural Control and Monitoring*, 11–13 July, San Diego, California.

Nakamura, M., Kajiwara, H., Koterayama, W., and Hyakudome, T., 1997. Control system design and model experiments on thruster assisted mooring system, *Proceedings of the 7th International Offshore and Polar Engineering Conference*, 25–30 May, Honolulu, Hawai, pp. 641–648.

Narasimhan, S., Nagarajaiah, S., and Johnson, E.A., 2008. Smart Base Isolated Benchmark Building Part IV: Phase II Problem Definition and Sample Controllers for Nonlinear Isolation Systems, *Journal of Structural Control and Health Monitoring* (in press).

Narasimhan, S., Nagarajaiah, S., Johnson, E.A., and Gavin, H.P., 2006. Smart base isolated benchmark building part I: Problem definition, *Journal of Structural Control and Health Monitoring*, 13(2–3), 573–588.

Neddermeijer, H.G., Van Oortmarsen, G.J., Piersma, N., and Dekker, N., 2000. A framework for response surface methodology for simulation optimization *Proceedings of the 2000 Winter Simulation Conference*, Orlando, Florida, pp. 129–136.

Papadimitriou, C., Beck, J.L., and Katafygiotis, L., 1997. Asymptotic expansions for reliabilities and moments of uncertain dynamic systems, *Journal of Engineering Mechanics*, 123, 1219–1229.

Papadimitriou, C., Beck, J.L., and Au, S.K., 2000. Entropy-based optimal sensor location for structural model updating., *Journal of Sound and Control*, 6, 781–800.

Papadimitriou, C., Beck, J.L., and Katafygiotis, L.S., 2001. Updating robust reliability using structural test data, *Probabilistic Engineering Mechanics*, 16, 103–113.

Pardalos, P.M., and Resende, M.G.C., 2002. *Handbook of applied optimization*. Oxford University Press.

Park, Y.J., Wen, Y.K., and Ang, A.H.S., 1986. Random vibration of hysteretic systems under bi-directional ground motions, *Earthquake Engineering and Structural Dynamics*, 14(4), 543–557.

Porter, K.A., Kiremidjian, A.S., and LeGrue, J.S., 2001. Assembly-based vulnerability of buildings and its use in performance evaluation, *Earthquake Spectra*, 18(2), 291–312.

Porter, K.A., Beck, J.L., and Shaikhutdinov, R.V., 2002. Sensitivity of building loss estimates to major uncertain variables, *Earthquake Spectra*, 18(4), 719–743.

Porter, K.A., Beck, J.L, and Shaikhutdinov, R.V., 2004. Simplified estimation of economic seismic risk for buildings, *Earthquake Spectra*, 20(4), 1239–1263.

Porter, K.A., Beck, J.L., Shaikhutdinov, R.V., Au, S.K., Mizukoshi, K., Miyamura, M., Ishida, H., Moroi, T., Tsukada, Y., and Masuda, M., 2004. Effect of seismic risk on lifetime property values, *Earthquake Spectra*, 20, 1211–1237.

Pradlwater, H.J., Schueller, G.I., Koutsourelakis, P.S., and Champris, D.C., 2007. Application of line sampling simulation method to reliability benchmark problems, *Structural Safety*, 29(3), 208–221.

Rice, S.O., 1944. Mathematical analysis of random noise, *Bell System Technical Journal*, 23, 282–332.

Rice, S.O., 1945. Mathematical analysis of random noise, *Bell System Technical Journal*, 24, 46–152.

Robert, C.P., and Casella, G., 2004. *Monte Carlo statistical methods*. Springer-Verlag, Upper Saddle River, New York.

Roberts, G.O., Gelman, A., and Gilks, W.R., 1997. Weak convergence and optimal scaling of random walk metropolis algorithms, *The Annals of Applied Probability*, 7(1), 110–120.

Roberts, G.O., and Rosenthal, J.S., 2001. Optimal scaling for various Metropoplis-Hastings algorithms, *Statistical Science*, 16, 351–367.

Roberts, G.O., and Rosenthal, J.S., 2004. General state-space Markov chains and MCMC algorithms, *Probability Surveys*, 1, 20–71.

Roberts, J.B., and Spanos, P.D., 2003. *Random vibration and statistical linearization*. Dover, Mineola, New York.

Royset, J.O., and Polak, E., 2004. Reliability-based optimal design using sample average approximations, *Probabilistic Engineering Mechanics*, 19, 331–343.

Royset, J.O., and Polak, E., 2007. Efficient sample size in stochastic nonlinear programming, *Journal of Computational and Applied Mathematics* (in press).

Ruszczynski, A., and Shapiro, A., 2003. *Stochastic programming*. Elsevier, New York.

Sahinidis, N.V., 2004. Optimization under uncertainty: state-of-the-art and opportunities, *Computers and Chemical Engineering*, 28, 971–983.

Sakawa, M., Nishizaki, I., and Uemura, Y., 2002. A decentralized two-level transportation problem in a housing material manufacturer: Interactive fuzzy programming, *European Journal of Operational Research*, 141, 167–185.

Scruggs, J.T., and Iwan, W.D., 2003. Control of a Civil Structure Using an Electric Machine with Semiactive Capability, *ASCE Journal of Structural Engineering*, 129(7), 951–959.

Scruggs, J.T., 2004. *Structural Control Using Regenerative Force Actuation Networks* (Ph.D. dissertation), Division of Engineering & Applied Science, Caltech, Pasadena, California.

Scruggs, J.T., and Iwan, W.D., 2005. Structural Control Using Regenerative Force Actuation Networks, *Journal of Structural Control and Health Monitoring*, 12, 25–45.

Scruggs, J.T., Taflanidis, A.A., and Beck, J.L., 2006. Reliability-based control optimization for active base isolation systems, *Journal of Structural Control*, 13, 705–723.

Scruggs, J.T., 2007. Multi-objective performance-guaranteed control of semiactive and regenerative systems, *Proceedings of the 18th Engineering Mechanics Division Conference of the ASCE*, June 3–6 Blacksburg, Virginia.

Scruggs, J.T., Taflanidis, A.A., and Iwan, W.D., 2007a. Non-linear stochastic controllers for semmiactive and regenerative systems with guaranteed quadratic performance bounds-Part 1:State feedback control, *Structural Control and Health Monitoring*, 14(8), 1101–1120.

Scruggs, J.T., Taflanidis, A.A., and Iwan, W.D., 2007b. Non-linear stochastic controllers for semmiactive and regenerative systems with guaranteed quadratic performance bounds-Part 2:Output feedback control, *Structural Control and Health Monitoring*, 14(8), 1121–1137

Shannon, C.E, 1948. A mathematical theory of communications, *Bell System Technical Journal*, 27, 379–343 and 623–656.

Somerville, P., 1998. Development of an improved representation of near-fault ground motions, *Proceedings of the SIMP98-CDMG*, Oakland, California, pp. 1–20.

Sorensen, J.D., Kroon, I.B. and Faber, M.H., 1994. Optimal reliability-based code calibration, *Structural Safety*, 15, 197–208.

Spall, J.C., 1992. Multivariate stochastic approximation using a simultaneous perturbation gradient approximation, *IEEE Transactions on Automatic Control*, 37, 332–341.

Spall, J.C., 1998. Implementation of the simultaneous perturbation algorithm for stochastic optimization, *IEEE Transactions on Aerospace and Electronic Systems*, 34, 817–823.

Spall, J.C., 2003. *Introduction to stochastic search and optimization*. Wiley-Interscience, New York.

Spencer, B.F.J., Sain, M.K., Won, C.-H., Kaspari, D.C., and Sain, P.M., 1994. Reliability-based measures of control robustness, *Structural Safety*, 15, 111–129.

Spencer, B.F., Jr., and Nagarajaiah, S., 2003. State of the Art in Structural Control, *ASCE Journal of Structural Engineering*, 129(7), 845–856.

Stengel, R., 1994. *Optimal Control and Estimation*. Dover Publications, Inc., New York.

Stevens, S.C., and Parson, M.G., 2002. Effects of motion at sea on crew performance: a survey, *Marine Technology*, 39(1), 29–47.

Suhardjo, J., and Kareem, A., 2001. Feedback-feedforward control of offshore platforms under random waves, *Earthquake Engineering and Structural Dynamics*, 30, 213–235.

Symans, M.D., and Constantinou, M.C., 1999. Semiactive Control of Systems for Seismic Protection of Structures: A State-of-the-Art Review, *Engineering Structures*, 21(6), 469–487.

Taflanidis, A.A., and Beck, J.L., 2005. Analytical approximation for stationary reliability calculation of linear dynamic systems, *Earthquake Engineering Research Library Report No. 2005–3*, California Institute of Technology, Pasadena. California.

Taflanidis, A.A., and Beck, J.L., 2006a. Analytical approximation for stationary reliability of certain and uncertain linear dynamic systems with higher dimensional output, *Earthquake Engineering and Structural Dynamics*, 35, 1247–1267.

Taflanidis, A.A., and Beck, J.L., 2006b. Reliability-based optimal design by efficient stochastic simulation, *Proceedings of the 5th International Conference on Computational Stochastic Mechanics*, June 14–16, Rhodes, Greece.

Taflanidis, A.A., Scruggs, J.T., and Beck, J.L., 2006. Reliability-based performance objectives and probabilistic model uncertainty in optimal structural control, *Proceedings of the 4th World Conference on Structural Control and Monitoring*, July 11–13, San Diego, California.

Taflanidis, A.A., Angelides, D.C, and Beck, J.L., 2007. Probabilistically robust nonlinear control of offshore structures, *Proceedings of the 19th International Conference of Offshore and Polar Engineering*, July 1–6 Lisbon, Portugal

Taflanidis, A.A., and Beck, J.L., 2007a. Efficient simulation-based optimization for optimal reliability problems, *Proceedings of the 10th International Conference on Applications of Statistics and Probability in Civil Engineering*, July 31–August 3, Tokyo, Japan.

Taflanidis, A.A., and Beck, J.L., 2007b. Stochastic subset optimization for stochastic design, *Proceedings of the ECCOMAS Thematic Conference on Computational Methods in Structural Dynamics and Earthquake Engineering*, June 13-16 Rethymno, Greece.

Taflanidis, A.A., Beck, J.L., and Angelides, D.C., 2007. Robust reliablity-based design of liquid column mass dampers under earthquake excitation using an analytical reliability approximation, *Engineering Structures*, 27, 3525–3537.

Taflanidis, A.A., Scruggs, J.T., and Beck, J.L., 2007a. Probabilistic model uncertainty in control applications, *Proceedings of the 18th Engineering Mechanics Division Conference of the ASCE*, June 3–6 Blacksburg, Virginia.

Taflanidis, A.A., Scruggs, J.T., and Beck, J.L., 2007b. Smart base isolation design including model uncertainty in ground motion characterization, *Proceedings of the 4th International Conference on Earthquake Geotechnical Engineering*, June 25–28 Thessaloniki, Greece.

Taflanidis, A.A., Scruggs, J.T., and Beck, J.L., 2008. Reliability-based performance objectives and probabilistic robustness in structural control applications, *Journal of Engineering Mechanics*, in press.

Vanmarcke, E.H., 1975. On the distribution of the first passage time for Normal stationary processes, *Journal of Applied Mechanics*, 42, 215–220.

Vietor, T., 1997. Stochastic optimization for mechanical structures, *Mathematical Methods of Operations Research*, 46, 377–408.

Wang, Q., and Stengel, R.F., 2002. Robust control of nonlinear systems with parametric uncertainty, *Automatica*, 38, 1591–1599.

Winterstein, S.R., and Cornell, C.A., 1985. Energy fluctuation scale and diffusion models, *Journal of Engineering Mechanics*, 111(2), 125–42.

Yuen, K., and Beck, J., 2003. Reliability-based robust control for uncertain dynamical systems using feedback of incomplete noisy response measurements, *Earthquake Engineering and Structural Dynamics*, 32(5), 751–770.

Zeng, X., Liu, Y., Shen, X., and Wu, Y., 2006. Nonlinear dynamic response of tension leg platform, *Proceedings of the 16th International Offshore and Polar Engineering Conference*, San Francisco, California pp. 94–100.

Zhang, Y.F., and Iwan, W.D., 2002. Protecting base isolated structures from near-field ground motion by tuned interaction damper, *Journal of Engineering Mechanics, ASCE*, 128(3), 287–295.